

การแปลงเฟสโดยเหนี่ยวนำด้วยความร้อนของโนเด็กซ์โคพอลิเมอร์
ตรวจสอบโดยอินฟราเรดสเปกโทรสโกปีแบบสองมิติ



นางสาวอัจฉรา เผลิมโชค

สถาบันวิทยบริการ
จุฬาลงกรณ์มหาวิทยาลัย

วิทยานิพนธ์นี้เป็นส่วนหนึ่งของการศึกษาตามหลักสูตรปริญญาวิทยาศาสตรดุษฎีบัณฑิต

สาขาวิชาปิโตรเคมี

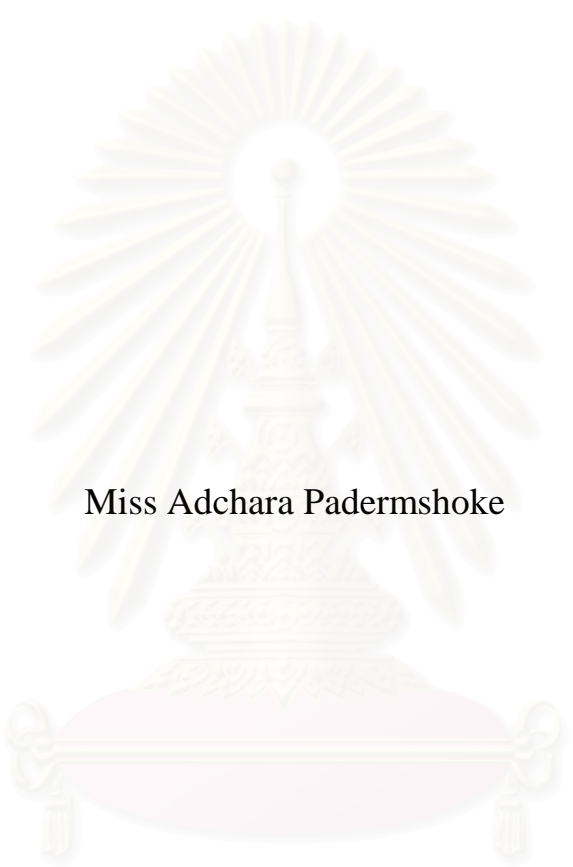
คณะวิทยาศาสตร์ จุฬาลงกรณ์มหาวิทยาลัย

ปีการศึกษา 2547

ISBN 974-17-5960-6

ลิขสิทธิ์ของจุฬาลงกรณ์มหาวิทยาลัย

THE THERMALLY INDUCED PHASE TRANSFORMATION OF
NODAX COPOLYMER MONITORED BY
TWO-DIMENSIONAL INFRARED SPECTROSCOPY



Miss Adchara Padermshoke

สถาบันวิทยบริการ
จุฬาลงกรณ์มหาวิทยาลัย

A Dissertation Submitted in Partial Fulfillment of the Requirements
for the Degree of Doctor of Philosophy in Petrochemistry

Faculty of Science
Chulalongkorn University
Academic Year 2004
ISBN 974-17-5960-6

Thesis Title The Thermally Induced Phase Transformation of Nodax Copolymer
 Monitored by Two-Dimensional Infrared Spectroscopy
By Miss Adchara Padermshoke
Field of Study Petrochemistry
Thesis Advisor Assistant Professor Sanong Ekgasit, Ph.D.
Thesis Co-advisor Professor Yukihiro Ozaki, Ph.D.

Accepted by the Faculty of Science, Chulalongkorn University in Partial Fulfillment of
the Requirements for the Doctor's Degree

.....Dean of the Faculty of Science
(Professor Piamsak Menasveta, Ph.D.)

THESIS COMMITTEE

.....Chairman
(Associate Professor Supawan Tantayanon, Ph.D.)

.....Thesis Advisor
(Assistant Professor Sanong Ekgasit, Ph.D.)

.....Member
(Assistant Professor Warinthorn Chavasiri, Ph.D.)

.....Member
(Assistant Professor Vipavee P. Hoven, Ph.D.)

.....Member
(Assistant Professor Toemsak Srikhirin, Ph.D.)

อัจฉรา เติมโชค: การแปลงเฟสโดยเหนี่ยวนำด้วยความร้อนของโนเด็กซ์โคพอลิเมอร์ตรวจ
 สอบโดยอินฟราเรดสเปกโทรสโกปีแบบสองมิติ (THE THERMALLY INDUCED PHASE
 TRANSFORMATION OF NODAX COPOLYMER MONITORED BY TWO-
 DIMENSIONAL INFRARED SPECTROSCOPY) อาจารย์ที่ปรึกษา: ผศ. ดร. สนอง เอกสิทธิ์,
 อาจารย์ที่ปรึกษาร่วม: PROFESSOR DR. YUKIHIRO OZAKI, 144 หน้า. ISBN 974-17-
 5960-6.

จากการศึกษาพฤติกรรมการแปลงเฟสของไบโอพอลิเมอร์ชนิดใหม่คือพอลิ(3-ไฮดรอกซีบิวที-
 เรต-โค-3-ไฮดรอกซีเฮกซาโนเอต) และหน่วยพื้นฐานคือพอลิ(3-ไฮดรอกซีบิวทีเรต) ด้วยอินฟราเรด
 สเปกโทรสโกปีแบบสองมิติ โดยตรวจสอบแบบทั้งปริมาตรและแบบเฉพาะพื้นผิวด้วยเทคนิค
 ทรานสมิซชันและแอทเทนนูเอทเทดโททัลรีเฟลกชัน รวมถึงการวิเคราะห์สมบัติเชิงอุณหภาพของ
 พอลิเมอร์ทั้งสองชนิดโดยเอกซ์เรย์ดิฟแฟรกชันและดิฟเฟอร์เรนเทียลสแกนนิ่งคาลอริเมตรี พบว่า
 พอลิเมอร์ทั้งสองชนิดมีส่วนประกอบที่เป็นผลึกอยู่สองรูปแบบได้แก่ ผลึกความเป็นระเบียบสูงและ
 ผลึกความเป็นระเบียบต่ำ และการแปลงเฟสของพอลิเมอร์ทั้งสองชนิดเกิดผ่านสภาวะอินเทอร์มีเดียต
 นอกจากนี้ยังพบว่าการกระจายตัวของผลึกพอลิเมอร์มีความแตกต่างกันระหว่างบริเวณพื้นผิวของฟิล์ม
 พอลิเมอร์และภายในปริมาตรของฟิล์มพอลิเมอร์ โดยบริเวณพื้นผิวของฟิล์มพอลิเมอร์มีความเป็นผลึก
 สูงกว่าภายในปริมาตรของฟิล์มพอลิเมอร์ทั้งสองชนิด จากการติดตามการเปลี่ยนแปลงที่ขึ้นกับเวลา
 ของอินฟราเรดสเปกตรัมของพอลิเมอร์ทั้งสองชนิด พบว่าพอลิ(3-ไฮดรอกซีบิวทีเรต-โค-3-ไฮดรอกซี-
 เฮกซาโนเอต) เกิดเป็นผลึกได้ช้ากว่าพอลิ(3-ไฮดรอกซีบิวทีเรต) มาก กล่าวคือหมู่ (3-ไฮดรอกซีเฮกซา-
 โนเอต) ที่เติมเข้าไปในพอลิ(3-ไฮดรอกซีบิวทีเรต-โค-3-ไฮดรอกซีเฮกซาโนเอต) นั้นไม่เพียงแต่ลดความ
 เป็นผลึกของโคพอลิเมอร์ที่ได้ แต่ยังลดอัตราเร็วของการเกิดเป็นผลึกของโคพอลิเมอร์อีกด้วย ผลึก
 ความเป็นระเบียบสูงและผลึกความเป็นระเบียบต่ำมีพฤติกรรมเกิดเป็นผลึกที่แตกต่างกัน ลำดับของ
 การเกิดผลึกจะตรงกันข้ามสำหรับกระบวนการแกรวูลูตลิ่งคริสตัลไลเซชันจากพอลิเมอร์หลอมเหลว
 และกระบวนการไอโซเทอร์มัลคริสตัลไลเซชันจากซูเปอร์คูลลิกวิดพอลิเมอร์

สาขาวิชา.....ปีโตรมณี.....ลายมือชื่อนิสิต.....
 ปีการศึกษา...2547.....ลายมือชื่ออาจารย์ที่ปรึกษา.....

4373872323 : MAJOR PETROCHEMISTRY

KEY WORD: POLYHYDROXYALKANOATES / PHASE TRANSFORMATION / CRYSTALLIZATION BEHAVIOR / 2D IR CORRELATION SPECTROSCOPY / SURFACE PHENOMENA

ADCHARA PADERMSHOKE: THE THERMALLY INDUCED PHASE TRANSFORMATION OF NODAX COPOLYMER MONITORED BY TWO-DIMENSIONAL INFRARED SPECTROSCOPY. THESIS ADVISOR: ASSISTANT PROFESSOR SANONG EKGASIT, PH.D., THESIS COADVISOR: PROFESSOR YUKIHIRO OZAKI, PH.D. 144 pp. ISBN 974-17-5960-6.

The crystalline/amorphous phase transformation behaviors monitored at the bulk and interface regions of a newly developed biopolymer, poly(3-hydroxybutyrate-*co*-3-hydroxyhexanoate) (P(HB-*co*-HHx)), and those of its basic unit, poly(3-hydroxybutyrate) (PHB), were investigated by using transmission and attenuated total reflection (ATR) infrared (IR) spectroscopy coupled with the generalized two-dimensional (2D) correlation analysis. Wide-angle X-ray diffraction (WAXD) and differential scanning calorimetry (DSC) were employed to study the thermal properties of the polymers. The asynchronous 2D correlation spectra generated from the dynamic IR spectra in the C=O stretching region for the two polymers reveal the coexistence of two crystalline components assignable to the highly ordered and less-ordered crystalline parts of the polymers. The phase transformation process of P(HB-*co*-HHx) and that of PHB take place through an intermediate state. The distributions of the crystalline phase detected by ATR and transmission techniques suggest that the population of polymer crystals at the surface is higher than that in the bulk for both polymers. The time-dependent IR spectral variations indicate that P(HB-*co*-HHx) crystallizes much slower than PHB. The HHx unit incorporated in P(HB-*co*-HHx) markedly reduce not only the degree of crystallinity but also the crystallization rate of PHB. The highly ordered and less-ordered crystalline parts of P(HB-*co*-HHx) exhibit different crystallization behaviors, and the orders of crystal growth steps are inverse between the gradual cooling crystallization of the melt and the isothermal crystallization of the supercooled liquid.

Field of study.....Petrochemistry..... Student's signature.....
Academic year.....2004..... Advisor's signature.....

ACKNOWLEDGEMENTS

The financial support via the Royal Golden Jubilee (RGJ) Ph.D. program, grant contract number: PHD/0066/2544, from the Thailand Research Fund (TRF) is gratefully acknowledged.

I would like to thank Associate Professor Dr. Supawan Tantayanon, Assistant Professor Dr. Warinthorn Chavasiri, Assistant Professor Dr. Toemsak Srihirin, and Assistant Professor Dr. Vipavee P. Hoven, for their substantial advice as thesis committee.

Deepest gratitude to my thesis co-advisor, Professor Dr. Yukihiro Ozaki, for years of excellent training, practicing, and encouragement throughout my research course. I have had tremendous support from him. Invaluable guidance, comments, and suggestions from my colleagues, Dr. Isao Noda, Dr. Harumi Sato, and Dr. Yukiteru Katsumoto, are sincerely appreciated. I am also grateful for their warm hospitality during my stay in Japan.

To my friends and colleagues, both at the Sensor Research Unit/Thailand and at the Ozaki Group/Japan, I wish to express my appreciation for sharing good times, surviving hard times together all the way through.

For all the strength, wisdom, and creativity, I am entirely indebted to my thesis advisor, Assistant Professor Dr. Sanong Ekgasit, who always keeps his eyes set on my success and believes in me. I learned so much from him and accumulated hands-on experiences and skills critical to my future. His untiring way of encouragement and support is so impressive that I will be forever thankful.

Finally, I am affectionately grateful to my father and mother for their wholehearted support, understanding, and unconditional love.

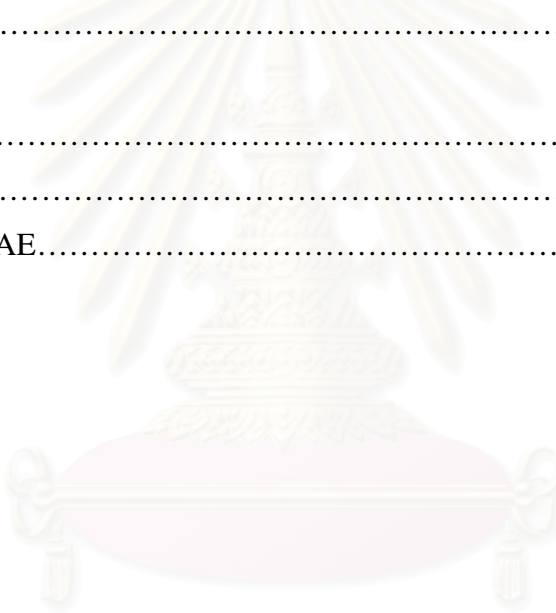
CONTENTS

	Pages
ABSTRACT IN THAI.....	iv
ABSTRACT IN ENGLISH.....	v
ACKNOWLEDGEMENTS.....	vi
LIST OF FIGURES.....	xi
LIST OF TABLES.....	xvi
LIST OF ABBREVIATIONS.....	xvii
LIST OF SYMBOLS.....	xviii
CHAPTER I INTRODUCTION.....	1
1.1 Biopolymers: Materials for a Sustainable Future.....	1
1.2 Development of Nodax Copolymer	3
1.3 Crystallinity and Phase Transformation of Nodax Copolymer	4
1.4 Two-dimensional Infrared Spectroscopy for Polymer Analysis.....	5
1.5 Scope of the Research.....	6
1.6 Objectives of the Research.....	6
CHAPTER II THEORETICAL BACKGROUND.....	8
2.1 Polyhydroxyalkanoate Copolymers	8
2.1.1 Material Background.....	8
2.1.2 Development of Polyhydroxyalkanoate Copolymers.....	9
2.2 Phase Transformation Behavior of Polymeric Materials.....	10
2.2.1 Polymer Crystallinity.....	10
2.2.2 Thermal Transition Phenomena.....	11
2.3 Differential Scanning Calorimetry.....	12
2.4 X-ray Diffraction.....	13
2.5 Infrared Spectroscopy for Polymer Analysis.....	14
2.6 Two-dimensional Infrared Correlation Spectroscopy.....	16

	Pages
2.6.1 General Concept.....	16
2.6.2 Two-dimensional Cross Correlation Function.....	17
2.6.3 Synchronous and Asynchronous Correlation Spectra.....	18
 CHAPTER III EXPERIMENTAL SECTION.....	 21
3.1 Materials and Equipments.....	21
3.1.1 Samples.....	21
3.1.2 Infrared Optical Elements.....	22
3.2 Instruments.....	22
3.2.1 Differential Scanning Calorimeters.....	22
3.2.2 X-ray Diffractometers.....	22
3.2.3 Infrared Spectrometers.....	22
3.2.4 Temperature Controllers for Infrared Measurements.....	23
3.3 Experimental Procedures.....	23
3.3.1 Differential Scanning Calorimetry Measurements.....	23
3.3.2 Wide-angle X-ray Diffraction Measurements.....	23
3.3.3 Infrared Measurements.....	24
3.3.3.1 Thermally Induced Phase Transformation of PHB.....	24
3.3.3.2 Thermally Induced Phase Transformation of P(HB-co-HHx)....	24
3.3.3.3 Surface Melting and Crystallization Behavior of PHB and P(HB-co-HHx).....	25
3.3.3.4 Crystallization Behavior of P(HB-co-HHx) under Different Crystallization Conditions.....	26
3.4 Two-dimensional Correlation Analysis.....	27
 CHAPTER IV RESULTS AND DISCUSSION.....	 29
4.1 Wide-angle X-ray Diffraction Study and Thermal Analysis of P(HB-co-HHx) and PHB.....	29

4.1.1 Wide-angle X-ray Diffraction.....	29
4.1.2 Differential Scanning Calorimetry.....	40
4.2 Thermally Induced Phase Transformation of PHB.....	43
4.2.1 Temperature-dependent Changes in the C=O Stretching Region.....	43
4.2.2 Temperature-dependent Changes in the C-O-C Stretching Region.....	48
4.2.3 Temperature-dependent Changes in the C-H Stretching Region.....	51
4.3 Thermally Induced Phase Transformation of P(HB- <i>co</i> -HHx).....	55
4.3.1 Temperature-dependent Changes in the C=O Stretching Region.....	55
4.3.2 Temperature-dependent Changes in the C-O-C Stretching Region.....	59
4.3.3 Temperature-dependent Changes in the C-H Stretching Region.....	62
4.3.4 Spectral Changes during the Cooling Down Process.....	66
4.3.5 Crystalline/Amorphous Phase Transformation Behavior of P(HB- <i>co</i> -HHx).....	68
4.3.6 Comparison between the Infrared Spectra of P(HB- <i>co</i> -HHx) and PHB.	68
4.4 Surface Melting and Crystallization Behavior of PHB and P(HB- <i>co</i> -HHx)...	70
4.4.1 Temperature-dependent Attenuated Total Reflection Spectra in the C=O Stretching Region of P(HB- <i>co</i> -HHx) during the Melting Process.	70
4.4.2 Time-dependent Infrared Spectra in the C=O Stretching Region of P(HB- <i>co</i> -HHx).....	73
4.4.3 Comparison between the Time-dependent Crystal Growth of P(HB- <i>co</i> -HHx) and PHB.....	80
4.5 Crystallization Behavior of P(HB- <i>co</i> -HHx) under Different Crystallization Conditions.....	82
4.5.1 Gradual Cooling Crystallization.....	82
4.5.2 Supercooled Melt Crystallization.....	85
4.5.3 Solvent-cast Film Crystallization.....	87
4.5.4 Comparison among the Three Types of Crystallization Processes.....	90

CHAPTER V CONCLUSIONS.....	92
5.1 Wide-angle X-ray Diffraction Study and Thermal Analysis of P(HB- <i>co</i> -HHx) and PHB.....	92
5.2 Thermally Induced Phase Transformation of PHB.....	92
5.3 Thermally Induced Phase Transformation of P(HB- <i>co</i> -HHx).....	93
5.4 Surface Melting and Crystallization Behavior of PHB and P(HB- <i>co</i> -HHx)...	94
5.5 Crystallization Behavior of P(HB- <i>co</i> -HHx) under Different Crystallization Conditions.....	94
REFERENCES.....	96
APPENDICES.....	102
CURRICULUM VITAE.....	144



สถาบันวิทยบริการ
จุฬาลงกรณ์มหาวิทยาลัย

LIST OF FIGURES

	Pages
1.1 Chemical structure (A) and the reported crystalline structure [9,10] (B) of PHB. (Reproduced from reference 9 with permission (B). Copy-right 1973 Elsevier Science.).....	2
1.2 Chemical structure of Nodax copolymer.	3
2.1 <i>Ralstonia eutropha</i> containing PHB granules (white fraction).....	8
2.2 Illustration for the coexistence of crystalline and amorphous regions in semi-crystalline polymers.....	11
2.3 Example of a DSC plot showing the thermal transitions occurring in the sample material as temperature increases (heating scan).....	13
2.4 Schematic diagram for obtaining an XRD pattern.....	14
2.5 IRE configurations commonly used in ATR experiments: single reflection variable-angle hemispherical crystal (left); and multiple reflection single-pass crystal (right).....	15
2.6 Transmission measurement experimental setup.....	16
2.7 Schematic illustration for the generation of 2D IR correlation spectra.....	16
2.8 Schematic contour map of a synchronous 2D correlation spectrum.....	18
2.9 Schematic contour map of an asynchronous 2D correlation spectrum.....	19
4.1 A WAXD pattern of the precipitated P(HB-co-HHx) sample measured at room temperature (A), and an XRD trace of P(HB-co-HHx) obtained by a radial microdensitometer scan of the diagram shown in (A).....	30
4.2 Temperature-dependent WAXD patterns of the precipitated P(HB-co-HHx) sample measured over a temperature range of 25-110 °C.....	31
4.3 Temperature-dependent peak areas and <i>d</i> spacings of the (110) reflection of the precipitated P(HB-co-HHx) sample.....	32
4.4 Temperature-dependent peak areas and <i>d</i> spacings of the (020) reflection of the precipitated P(HB-co-HHx) sample.....	33

4.5	Changes in the lattice parameters, a and b , of the precipitated P(HB- <i>co</i> -HHx) sample versus temperature.....	34
4.6	Temperature-dependent WAXD patterns of the chloroform solution-cast P(HB- <i>co</i> -HHx) sample measured over a temperature range of 30.1-105.8 °C....	35
4.7	Temperature-dependent peak areas and d spacings of the (110) reflection of the chloroform solution-cast P(HB- <i>co</i> -HHx) sample.....	36
4.8	Changes in the lattice parameters, a , of the chloroform solution-cast P(HB- <i>co</i> -HHx) sample versus temperature.....	37
4.9	Temperature-dependent WAXD patterns of PHB measured over a temperature range of 28.30-174.30 °C.....	38
4.10	Temperature-dependent peak areas and d spacings of the (110) reflection (A) and (020) reflection (B) of PHB.....	39
4.11	Changes in the lattice parameters, a and b , of PHB versus temperature.....	40
4.12	DSC curves of the first cooling scan (A) and second heating scan (B) of the precipitated P(HB- <i>co</i> -HHx) sample; heating and cooling rates were 10 °C min ⁻¹	41
4.13	DSC curves of the first cooling scan (A) and second heating scan (B) of the chloroform solution-cast P(HB- <i>co</i> -HHx) sample; heating and cooling rates were 20 °C min ⁻¹	42
4.14	IR spectra of PHB in the C=O stretching region (1800-1680 cm ⁻¹) collected over a temperature range of 40-180 °C.....	43
4.15	Synchronous (A) and asynchronous (B) correlation spectra of PHB in the C=O stretching region constructed from dynamic IR spectra in the melting process.....	46
4.16	A second derivative spectrum calculated from the IR spectrum of PHB in the C=O stretching region at 40 °C.....	47
4.17	IR spectra of PHB in the C-O-C stretching region (1320-1120 cm ⁻¹) collected over a temperature range of 40-180 °C.....	49

4.18 Synchronous (A) and asynchronous (B) correlation spectra of PHB in the C-O-C stretching region constructed from dynamic IR spectra in the melting process.....	50
4.19 IR spectra of PHB in the C-H stretching region (3100-2850 cm^{-1}) collected over a temperature range of 40-180 $^{\circ}\text{C}$	52
4.20 Second derivative spectra calculated from the IR spectra of PHB in the C-H stretching region at 40 and 180 $^{\circ}\text{C}$	53
4.21 Synchronous (A) and asynchronous (B) correlation spectra of PHB in the C-H stretching region constructed from dynamic IR spectra in the melting process..	54
4.22 Hetero-correlation synchronous spectrum of PHB between the C=O and C-H stretching regions constructed from dynamic IR spectra in the melting process.....	55
4.23 IR spectra of P(HB- <i>co</i> -HHx) in the C=O stretching region (1780-1680 cm^{-1}) measured over a temperature range of 30-140 $^{\circ}\text{C}$	56
4.24 Synchronous (A) and asynchronous (B) correlation spectra of P(HB- <i>co</i> -HHx) in the C=O stretching region generated from the temperature-dependent IR spectra measured over a temperature range of 30-140 $^{\circ}\text{C}$	57
4.25 A second derivative spectrum calculated from the IR spectrum of P(HB- <i>co</i> -HHx) in the C=O stretching region at 30 $^{\circ}\text{C}$	58
4.26 IR spectra of P(HB- <i>co</i> -HHx) in the C-O-C stretching region (1320-1160 cm^{-1}) measured over a temperature range of 30-140 $^{\circ}\text{C}$	59
4.27 Synchronous (A) and asynchronous (B) correlation spectra of P(HB- <i>co</i> -HHx) in the C-O-C stretching region generated from the temperature-dependent IR spectra measured over a temperature range of 30-140 $^{\circ}\text{C}$	61
4.28 Second derivative spectra calculated from the IR spectra of P(HB- <i>co</i> -HHx) in the C-O-C stretching region over a temperature range of 30-140 $^{\circ}\text{C}$	62
4.29 IR spectra of P(HB- <i>co</i> -HHx) in the C-H stretching region (3050-2850 cm^{-1}) measured over a temperature range of 30-140 $^{\circ}\text{C}$	63
4.30 Second derivative spectra calculated from the IR spectra of P(HB- <i>co</i> -HHx) in the C-H stretching region at 30 and 140 $^{\circ}\text{C}$	64

4.31 Synchronous (A) and asynchronous (B) correlation spectra of P(HB- <i>co</i> -HHx) in the C-H stretching region generated from the temperature-dependent IR spectra measured over a temperature range of 30-140 °C.....	65
4.32 IR spectra of P(HB- <i>co</i> -HHx) in the C=O stretching region measured over a temperature range of 140-30 °C (cooling down process).....	66
4.33 Synchronous (A) and asynchronous (B) correlation spectra of P(HB- <i>co</i> -HHx) in the C=O stretching region generated from the temperature-dependent IR spectra measured over a temperature range of 140-30 °C (cooling down process).....	67
4.34 Representative ATR spectra of P(HB- <i>co</i> -HHx) in the C=O stretching region (1780-1680 cm ⁻¹) measured over a temperature range of 30-140 °C.....	70
4.35 ATR (solid line) and transmission (dotted line) spectra of P(HB- <i>co</i> -HHx) in the C=O stretching region measured at 30 °C.....	71
4.36 Synchronous (A) and asynchronous (B) correlation spectra of P(HB- <i>co</i> -HHx) in the C=O stretching region generated from the temperature-dependent ATR spectra measured over a temperature range of 30-100 °C.....	73
4.37 Representative time-dependent ATR (A) and transmission (B) spectra of P(HB- <i>co</i> -HHx) in the C=O stretching region measured at room temperature...	74
4.38 ATR (solid line) and transmission (dotted line) spectra of P(HB- <i>co</i> -HHx) in the C=O stretching region: first (A) and last (B) spectra measured during the time-dependent IR measurements.....	76
4.39 ATR spectra of P(HB- <i>co</i> -HHx) in the C=O stretching region measured at 30 minutes after the solvent casting (dotted line) and when the crystal growth was completed (solid line) by using the Ge IRE.....	77
4.40 Synchronous (A) and asynchronous (B) correlation spectra of P(HB- <i>co</i> -HHx) in the C=O stretching region generated from the time-dependent ATR spectra shown in Figure 4.37 A.....	78
4.41 Synchronous (A) and asynchronous (B) correlation spectra of P(HB- <i>co</i> -HHx) in the C=O stretching region generated from the time-dependent transmission spectra shown in Figure 4.37 B.....	79

4.42	Representative time-dependent ATR (A) and transmission (B) spectra of PHB in the C=O stretching region measured at room temperature.....	81
4.43	Transmission spectra of P(HB- <i>co</i> -HHx) (solid line) and PHB (dotted line) in CHCl ₃ solution.....	82
4.44	IR spectra of P(HB- <i>co</i> -HHx) in the C=O stretching region measured during the gradual cooling crystallization of the melt over a temperature range of 140-30 °C.....	83
4.45	Synchronous (A) and asynchronous (B) correlation spectra of P(HB- <i>co</i> -HHx) in the C=O stretching region generated from the temperature-dependent IR spectra shown in Figure 4.44.....	84
4.46	IR spectra of P(HB- <i>co</i> -HHx) in the C=O stretching region measured during the isothermal crystallization of the supercooled liquid at room temperature....	85
4.47	Synchronous (A) and asynchronous (B) correlation spectra of P(HB- <i>co</i> -HHx) in the C=O stretching region generated from the time-dependent IR spectra shown in Figure 4.46.....	87
4.48	IR spectra of P(HB- <i>co</i> -HHx) in the C=O stretching region measured during the isothermal crystallization of the solvent-cast film at room temperature.....	88
4.49	Synchronous (A) and asynchronous (B) correlation spectra of P(HB- <i>co</i> -HHx) in the C=O stretching region generated from the time-dependent IR spectra shown in Figure 4.48.....	89

LIST OF TABLES

	Pages
3.1 Thermal properties and percentages of crystallinity of P(HB- <i>co</i> -HHx) and PHB.....	21
4.1 Assignments of IR bands in the C=O, C-O-C, and C-H stretching regions.....	48



สถาบันวิทยบริการ
จุฬาลงกรณ์มหาวิทยาลัย

LIST OF ABBREVIATIONS

1D	: one-dimensional
2D	: two-dimensional
3D	: three-dimensional
AFM	: atomic force microscopy
ATR	: attenuated total reflection
d_p	: penetration depth
DSC	: differential scanning calorimetry
FT-IR	: Fourier transform infrared
IRE	: internal reflection element
PE	: polyethylene
PHA	: polyhydroxyalkanoate
PHB	: poly(3-hydroxybutyrate)
P(HB- <i>co</i> -HHx)	: poly(3-hydroxybutyrate- <i>co</i> -3-hydroxyhexanoate)
P(HB- <i>co</i> -HV)	: poly(3-hydroxybutyrate- <i>co</i> -3-hydroxyvalerate)
PP	: polypropylene
RI	: refractive index
SEM	: scanning electron microscopy
T_c	: crystallization temperature
T_g	: glass transition temperature
T_m	: melting temperature
WAXD	: wide-angle X-ray diffraction
XPS	: X-ray photoelectron spectroscopy
XRD	: X-ray diffraction

LIST OF SYMBOLS

α	: alpha
β	: beta
γ	: gamma
Å	: angstrom



สถาบันวิทยบริการ
จุฬาลงกรณ์มหาวิทยาลัย

CHAPTER I

INTRODUCTION

1.1 Biopolymers: Materials for a Sustainable Future

Polymeric materials derived from petrochemicals are indispensable for modern human life. Their diverse applications range from a simple garbage bag to a medical device being used in human body. However, petrochemicals are limited in their abundances, and petroleum-based synthetic polymers cause tremendous environmental problems, especially at the waste disposal process. As a consequence, many researchers and manufacturers are driven towards consensus on materials that can be produced from renewable resources and would not persist in the environment.

At present, a number of truly biodegradable polymers are commercially available. Among several categories of those biopolymers, bacterially synthesized polyhydroxyalkanoates (PHAs) have received a great attention as a new family of environmentally friendly polymeric materials [1-7]. PHAs are a class of naturally occurring biodegradable polyesters accumulated as energy-storing inclusion body granules in the cells of certain microorganisms [1-4]. Despite their completely natural origin, PHAs bear a fairly close resemblance to some petroleum-based synthetic polymers in chemical structures and physical characteristics and possess an attractive combined set of end use properties. Poly(3-hydroxybutyrate) (PHB), the simplest bacterial PHA, is the most abundant polyester found in bacteria [1,4,6]. The chemical structure of PHB and its reported crystalline structure [9,10] are shown in Figure 1.1 A and B, respectively.

PHB bears similar glass transition temperature (T_g), melting temperature (T_m), and comparable ultimate tensile strength to those of polypropylene (PP) [1,4,6]. PHB is perfectly biocompatible, its medical use is therefore one of the important

potential applications being contemplated. However, due to the high stereoregularity of biologically produced macromolecules, PHB is a highly crystalline polymer that is stiff and brittle. It is also thermally unstable during processing [6]. The molecular weight of PHB decreases significantly at temperatures just above the T_m . This unfortunate aspect of properties poses a limitation of the application to a flexible film, which is one of the largest uses of biodegradable polymers. Consequently, various efforts have been made to copolymerize PHB with other comonomers to improve its mechanical properties [6].

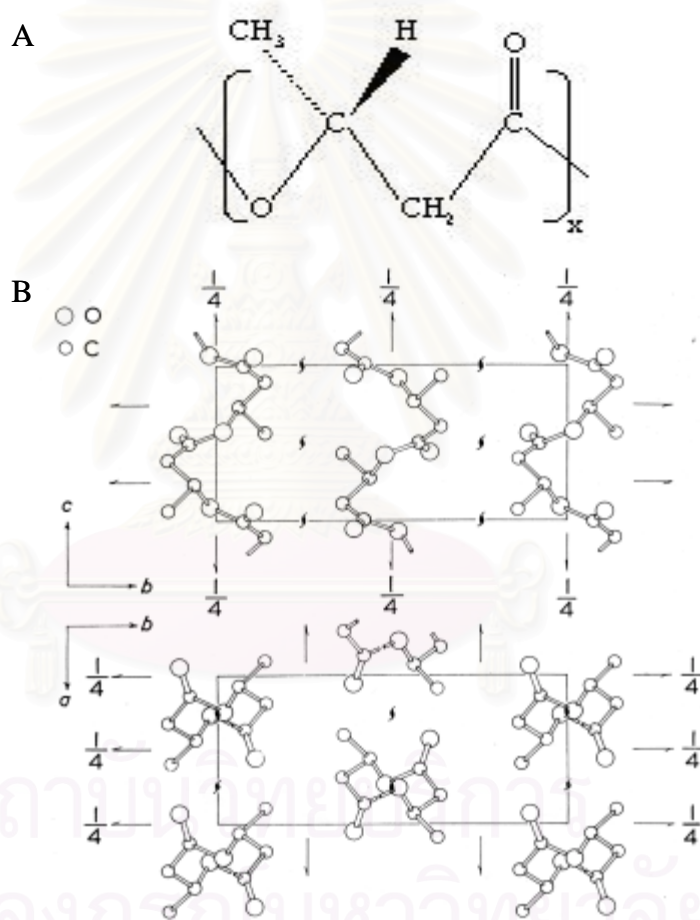


Figure 1.1 Chemical structure (A) and the reported crystalline structure [9,10] (B) of PHB. (Reproduced from reference 9 with permission (B). Copy-right 1973 Elsevier Science.)

One concept is to include a more bulky comonomer to reduce the crystallinity and presumably increase the flexibility of the resulting copolymers.

The copolymerization with 3-hydroxyvalerate (HV) was the first attempt performed by ICI (Billingham, UK), in the early 1980s [1,6]. However, the crystallinity of poly(3-hydroxybutyrate-*co*-3-hydroxyvalerate) (P(HB-*co*-HV)) never falls below 50% due to the isodimorphism of the P(HB-*co*-HV) copolymer [6]. It has been reported that poly(3-hydroxybutyrate-*co*-3-hydroxyhexanoate) (P(HB-*co*-HHx)) shows a greater T_m drop, at a given mol% comonomer, in comparison to P(HB-*co*-HV) [6]. Interestingly, hexanoate and larger comonomers depress T_m in the same manner regardless of their molecular sizes [6]. This feature indicates the break down of the isodimorphism occurring in the P(HB-*co*-HV) copolymer by the incorporation of comonomer units with three or more carbon unit side groups [6].

1.2 Development of Nodax Copolymer

The Procter and Gamble Company (Cincinnati, USA) has introduced a new family of commercial PHA copolymers under the trade name NodaxTM [8]. Nodax copolymer is comprised of 3-hydroxybutyrate and other longer side-chain 3-hydroxyalkanoates [6,8]. Poly(3-hydroxybutyrate-*co*-3-hydroxyhexanoate)s with the T_m of about 110 to 160 °C and approximately 35 to 45% crystallinity are typical available commercial grades of Nodax copolymer. The chemical structure of Nodax copolymer is shown in Figure 1.2

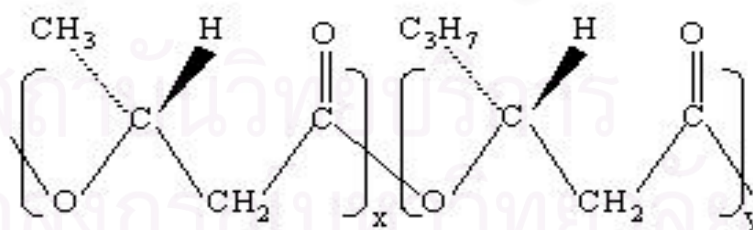


Figure 1.2 Chemical structure of Nodax copolymer.

The introduction of less crystallizable units, *i.e.*, HHx, into the molecular chains of PHB dramatically improves the physical and mechanical properties of the resulting copolymer [6,8]. As a consequence, Nodax copolymer possesses various attractive features, which are not only the notable physical and mechanical properties

but also the additional beneficial characteristics of polyesters. Nodax copolymer has excellent surface properties (*e.g.*, printability, dyeability, dispersibility, adhesion, etc.), and it is compatible with various additives and other polymers [8]. Examples of the potential applications of Nodax copolymer include flushable products, films and flexible packagings, coated papers, synthetic papers, and bioresorbable medical devices [8].

1.3 Crystallinity and Phase Transformation of Nodax Copolymer

Crystallinity is one of the most important key parameters for material applications of polymers and their further chemical or mechanical processing. The crystalline/amorphous phase transformation behavior of PHAs has gained keen interest recently [11-14]. A fundamental understanding of the crystallization and melting processes of this class of polymers is essential for improving their mechanical properties of biopolyesters.

Surface properties and surface phenomena of polymers are also of considerable interest from both fundamental and technological points of views. Crystallization behavior of macromolecules at surface and interface regions plays an important role in numerous properties, *e.g.*, mechanical strength, chemical compatibility, and biocompatibility, of polymeric materials [15]. In applications of polymers to thin films and coatings, for examples, it is often the interfacial behavior that governs the material performance rather than the bulk. For biocompatible objects such as a polymeric scaffold, the tissue/polymer interface where a cellular adhesion occurs is very important [16-18]. Kai *et al.* [16] investigated the effects of surface morphology on the biocompatibility of P(HB-*co*-HHx)/PHB blends by using scanning electron microscopy (SEM). It was found that the biocompatibility depends strongly on the surface crystallinity of the blending films [16]. As described above, the applications of Nodax copolymer have been expanded to a greater extent including biodegradable films, coatings, and bioresorbable medical devices. Therefore, the study on the surface properties of this class of polymers is crucial not only for improving the performances of existing film products but also for

developing new generation of biodegradable films.

1.4 Two-dimensional Infrared Spectroscopy for Polymer Analysis

Infrared (IR) spectroscopy has been successfully employed to investigate the conformational changes and local molecular environments of polymers during their phase transition process [19-24]. This is because the technique provides not only sensitivity to changes in molecular interactions and polymer crystallinity but also substantial advantages that allow the dynamic studies at the microscopic molecular level. IR spectra of polymers are often complicated, two-dimensional (2D) correlation analysis proposed by Noda [25-27] enables a more detailed interpretation of the IR spectral variations of polymers. The technique emphasizes spectral information not readily observable in conventional one-dimensional (1D) IR spectra. An asynchronous 2D spectrum is very powerful in differentiating highly overlapped bands that vary out of phase under the external perturbation [25-29]. The signs of synchronous and asynchronous cross peaks indicate the successive order of the events taking place in the system of interest under the applied perturbation [24-29]. These features make the technique ideally suitable for the study of polymer crystallization. The studies on the crystalline/amorphous phase transformation by using 2D IR correlation spectroscopy have been carried out for a number of polymers including PHAs [12-14].

As described previously, an insight into the surface phenomena of polymers is fundamentally essential for their various applications. In order to precisely extract the surface information, a non-destructive characterization technique capable of selectively probing surface molecules is required. There are various techniques applicable to polymer surface analysis [30], for examples, SEM, X-ray photoelectron spectroscopy (XPS), and atomic force microscopy (AFM). Attenuated total reflection (ATR) IR spectroscopy is known as one of the powerful surface characterization techniques that can provide information, *e.g.*, chemical reactions, functional groups, and molecular orientation, at the surface and interface regions of polymers [31-36]. Quantitative information of a sample can also be obtained from a

system with an optical contact between the sample and an internal reflection element (IRE) [32]. ATR IR spectroscopy possesses several advantages such as non-destructive nature, easy and fast operation, and little or no sample preparation [31-36].

1.5 Scope of the Research

The research aims at understanding the thermal behavior and crystalline/amorphous phase transformation of Nodax copolymer (P(HB-*co*-HHx), HHx = 12 mol%) and those of PHB, which is a basic unit for all other PHA polymers. 2D IR correlation spectroscopy, wide-angle X-ray diffraction (WAXD), and differential scanning calorimetry (DSC) were employed to investigate the thermal properties and temperature- and time-dependent phase behaviors of the polymers.

The surface phenomena of Nodax copolymer and those of PHB were studied by means of ATR IR spectroscopy coupled with 2D correlation analysis. The time-dependent ATR and transmission spectra of Nodax copolymer and those of PHB were monitored in order to follow the time-dependent crystal growth at the surface and in the bulk of the two polymers. The temperature-dependent IR spectral variations observed for the surface of Nodax copolymer during the melting process were also compared to those observed for the bulk sample.

Since the formation of an ordered structure during the crystallization of semi-crystalline polymers depends strongly on the crystallization conditions, the crystallization mechanisms of Nodax copolymer under different crystallization conditions were revealed by using 2D IR correlation analysis.

1.6 Objectives of the Research

1. To study the crystalline/amorphous phase transformation of Nodax copolymer and PHB by using transmission and ATR IR spectroscopy.

2. To compare the thermal behaviors and spatial distributions of crystals detected at bulk and film/ATR crystal interface of Nodax copolymer and PHB.

3. To apply 2D correlation analysis on the sets of the dynamic IR spectra for extracting additional information involved inter- and intra-molecular interactions, which is generally obscure in a conventional 1D IR spectrum.



สถาบันวิทยบริการ
จุฬาลงกรณ์มหาวิทยาลัย

CHAPTER II

THEORETICAL BACKGROUND

2.1 Polyhydroxyalkanoate Copolymers

2.1.1 Material Background

Poly(*(R)*-3-hydroxyalkanoates) (PHAs) are a class of bacterial storage compounds synthesized during unbalanced growth by many Gram-negative and Gram-positive bacteria [1-7]. PHAs are accumulated intracellularly in the form of inclusion bodies at levels up to 90% of the cellular dry weight [1,4]. PHAs can be isolated by breaking open the cells and using either an aqueous- or solvent-based extraction process to remove cell debris, lipid, nucleic acids, and proteins [1,4]. Traditionally, they have been produced by fermentation of renewable biomass such as sugars, fatty acids, or oils [1,4]. A schematic representation of the intracellularly deposited PHA granules is shown in Figure 2.1.

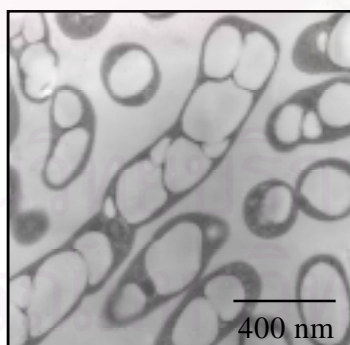


Figure 2.1 *Ralstonia eutropha* containing PHB granules (white fraction).

Poly(*(R)*-3-hydroxybutyrate) (PHB) was the first member of PHAs discovered by Lemoigne [1,4], and is the most abundant polyester found in bacteria. Bacterial copolymers containing randomly distributed (*(R)*-3-HB and (*(R)*-3-HV

units (P(HB-*co*-HV)) have been sold commercially for over a decade under the trade name Biopol®. About 150 hydroxyalkanoates other than HB have been identified as constituents of PHAs during the past three decades.

PHAs can be biodegraded to water and carbon dioxide or methane by a large variety of ubiquitous microorganisms present in many ecosystems. This fairly easy biodegradability came as a surprise given the inertness of the water-insoluble, hydrophobic, and partially crystalline polymers. The degradation mechanism of PHAs has been studied extensively and reported elsewhere [37-39].

2.1.2 Development of Polyhydroxyalkanoate Copolymers

PHAs offer a comprehensive design space with properties spanning a large range and extending the relatively narrow property range offered by existing absorbable synthetic polymers. The highly abundant PHB homopolymer, however, is a relatively stiff and rigid material. The introduction of a comonomer into the PHB backbone significantly increases the flexibility and toughness of the polymer. This is evident in P(HB-*co*-HV) and P(3HB-*co*-4HB) [6]. A progressive and substantial change in the mechanical properties of PHB also occurs when the pendant groups are extended from the polymer backbone [1,4,6]. Extending the distance between the ester groups in the PHA backbone can also dramatically affect the mechanical properties of PHAs. The thermal properties of PHAs vary with types and sizes of the comonomer units. In general, T_m decreases as the pendant groups become longer. This is particularly important in the melt processing of PHB, which is unstable at temperatures just above its T_m [1,4]. By incorporating other longer side-chain comonomers into the PHB backbone, lower-melting PHB-based copolymers, which are more readily processed, can be obtained.

As described in INTRODUCTION, the P(HB-*co*-HV) copolymer tends to form isodimorphic crystals [6]. The HB units fit in the crystal habit of the HV units, and vice versa. This effect results in a relatively low T_m depression of PHB as a function of the HV content. The question of when isodimorphism is dispelled is an important issue for inducing more flexibility of PHAs with moderate crystallinity. It was found

that a greater T_m drop, at a given mol% comonomer, can be achieved for P(HB-co-HHx) [6]. The HHx comonomer and other longer side-chain comonomers depress T_m in nearly the same pattern [6]. This is consistent with the theory of non-crystallizing comonomer T_m depression, which states that the T_m depression is only dependent on the non-crystallizing comonomer mol%. Further evidence for the break down of the isodimorphism is given by X-ray diffraction (XRD) [6].

Nodax copolymer being investigated in the present study is a member of the family of P(HB-co-HHx) copolymers recently developed by the Procter and Gamble Company (Cincinnati, USA) [8]. It is a semi-crystalline polyester with relatively similar mechanical and thermal properties to those of polyethylene (PE) and PP [6,8]. Key attributes and beneficial characteristics of Nodax copolymer are outlined as follows:

- available from renewable resources, biocompatible, and biodegradable,
- impervious to grease, water, and other liquids,
- excellent barrier for odor, oxygen, carbon dioxide, and moisture combined with heat-sealability and thermally processable,
- ideal surface properties, *i.e.*, adhesion, dispersibility, wettability, printability, and dyeability,
- compatible with various additives and fillers and blendable with many other polymers.

By modifying molecular weights and comonomer contents of Nodax copolymer, an extremely wide range of material forms and applications can be achieved. Potential applications of Nodax copolymer include fibers, foams, synthetic papers, injection molded articles, blow mold articles, films, coatings, adhesives, latex, etc.

2.2 Phase Transformation Behavior of Polymeric Materials

2.2.1 Polymer Crystallinity

Properties of polymeric materials depend strongly on their crystallinity. In general, macromolecules exist both in crystalline and amorphous states, which show

substantially different behaviors. Crystalline materials have their molecules arranged in repeating patterns. Consequently, they all tend to have highly ordered and regular structures. Amorphous materials, on the other hand, have their molecules arranged randomly and in long chains, which entangle around one-another, resulting in large regions of irregular conformations.

Most polymers assume semi-crystalline morphology. That is, parts of molecules are arranged in a regular order, composing the crystalline regions. In between these crystalline regions, the amorphous regions comprising of molecules in randomly disorganized state exist. The crystalline regions show a high degree of order formed by folding and stacking of the polymer chains. The amorphous regions show no long-range order, and the polymer chains are entangled as illustrated in Figure 2.2. Semi-crystallinity is a desirable characteristic for various applications of polymeric materials. Semi-crystalline polymers combine the strength of crystalline materials with the flexibility of amorphous substances.

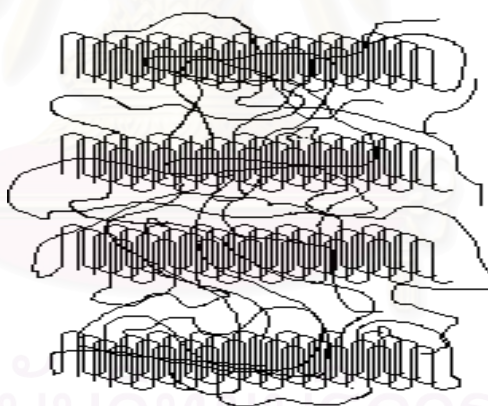


Figure 2.2 Illustration for the coexistence of crystalline and amorphous regions in semi-crystalline polymers.

2.2.2 Thermal Transition Phenomena

Polymers typically have small diffusion coefficients in the melt, and high-molecular weight polymers have a high degree of entanglement, which prevents the chains from reaching an equilibrium structure. At low temperatures, molecular motions in an amorphous region are restricted to molecular vibrations. The

entangled chains cannot rotate or move in space. This is the so-called “glassy state”. The glassy state can be considered as a supercooled liquid where the molecular motions have been frozen. A polymer in its glassy state is hard, rigid, and brittle like a crystalline solid but retains the molecular disorder of a liquid. When the polymer is heated until its T_g , segments of the entangled chains can then move, and the amorphous region becomes rubbery, which is soft and flexible. The glass transition is a property of only the amorphous portion of a semi-crystalline polymer. The crystalline portion remains crystalline during the glass transition. On the other hand, melting is the transition from a crystalline solid to a liquid. When a polymer melts, it slowly becomes liquid over a fairly broad temperature range. The crystalline portion of a polymer is a non-equilibrium distribution of a large number of crystallites of different sizes and in different environments. They all do not melt at exactly the same temperature. The melting is a property of only the crystalline portion of a polymer.

Crystalline structures in polymers form as a result of the kinetics of the crystallization process [15]. When a polymer melt is cooled to a temperature below its T_m , the crystallization occurs by nucleation and growth of spherulites. After completion of the primary crystallization at the first fixed temperature, it is a general phenomenon for polymers that crystallization does not come to an end but continues upon further cooling. The regions between the crystallites that remain amorphous after the primary isothermal crystallization still have the potential to crystallize. The secondary crystallization occurs in between the original existing crystalline lamellae. The temperature range where crystallization occurs, similar to the temperature range of melting, is always broad. Especially broad crystallization and melting ranges are observed for polymers with a small amount of non-crystallizable units [15].

2.3 Differential Scanning Calorimetry

DSC is a technique for measuring the energy necessary to establish a nearly zero temperature difference between a sample substance and an inert reference material, as the two specimens are subjected to identical temperature regimes in an environment heated or cooled at a controlled rate.

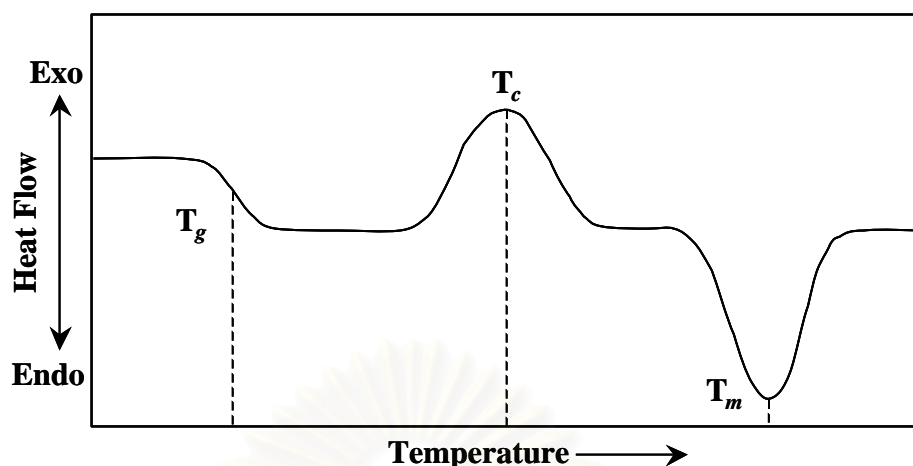


Figure 2.3 Example of a DSC plot showing the thermal transitions occurring in the sample material as temperature increases (heating scan).

When thermal transition occurs in the sample, DSC provides a direct calorimetric measurement of the transition energy at the temperature of the transition. The technique is commonly used to characterize the thermal transition temperatures such as the T_g , T_c , and T_m of polymers.

2.4 X-ray Diffraction

XRD is often used to study the nature and extent of crystallinity of polymers. A crystalline structure is a regular arrangement of atoms. As stated earlier, polymers generally contain both the crystalline and amorphous phases. Crystalline regions in a polymer seated in a well-defined manner act as diffraction grating. When the beam of X-ray passes through a polymer sample, the regularly arranged atoms reflect the X-ray beam constructively and produce an enhanced intense pattern. Therefore, the emerging diffracted pattern shows alternate dark and light bands on the screen. Figure 2.4 shows a schematic diagram for obtaining an XRD pattern.

An XRD pattern of a polymer contains both sharp as well as defused bands. Sharp bands correspond to crystalline regions and defused bands correspond to amorphous regions.

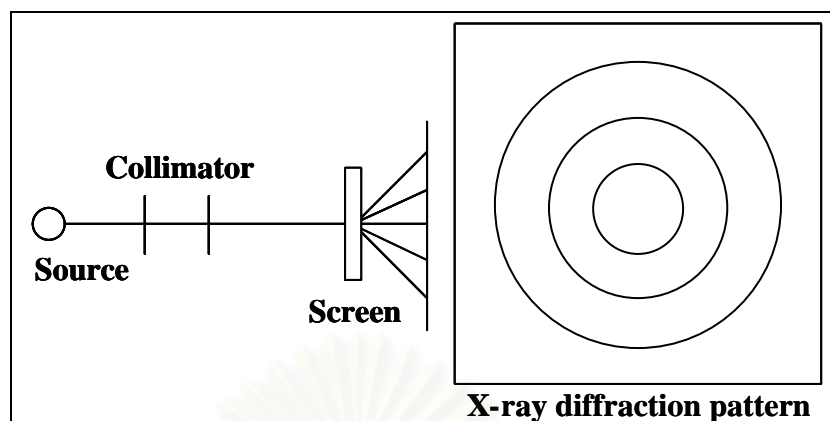


Figure 2.4 Schematic diagram for obtaining an XRD pattern.

Crystals and the crystalline state can be defined in a number of different ways, *e.g.*, density, enthalpy or free energy change on heating, spectroscopic associations, presence of certain planes of registry in microscopy. For XRD, a crystal is defined as a perfect three-dimensional (3D) order. For a semi-crystalline polymer, 100% crystallinity is never obtained by this definition since there are large interfacial regions where some degree of disorder is present. A perfect 3D order means that the structure repeats in all directions so that by describing the structure locally, *i.e.*, in a repeating 3D unit, the entire structure can be uniquely described.

2.5 Infrared Spectroscopy for Polymer Analysis

IR spectroscopy has been proven to be a powerful technique for studying the polymer crystallinity [19-24]. The technique is rapid and applicable to a number of samples with various forms. Many IR sampling techniques are generally available in common laboratories and easy to use.

In the study of polymer crystallinity, the IR absorption bands involved in the amorphous/crystalline phase transformation process are termed ‘amorphous bands’ and ‘crystalline bands’ according to their relative intensities present in each state of a polymer. The structural arrangement in a free amorphous state is different from that in a crystalline state. In a crystal field, a molecule usually has a lower symmetry

than in an amorphous state. As a result, certain types of vibrations that are inactive in an amorphous polymer may become active in a crystalline polymer, and therefore either new absorption bands or band splittings show up in an IR spectrum when polymers change from amorphous to crystalline phase.

Attenuated Total Reflection and Transmission Techniques

ATR is a spectroscopic technique utilizing an internal reflection phenomenon uniquely established when light traveling in an optically denser medium (IRE) impinges on surface of a rarer medium with an incident angle greater than the critical angle. It is the technique of recording the optical spectrum of a material that is in contact with an IRE. Therefore, ATR is considered as a surface-sensitive characterization technique.



Figure 2.5 IRE configurations commonly used in ATR experiments: single reflection variable-angle hemispherical crystal (left); and multiple reflection single-pass crystal (right).

ATR has been successfully employed to extract information, *e.g.*, chemical reactions, functional groups, molecular orientations, at the surface and interface regions of polymers [31-37]. The technique possesses several advantages such as non-destructive nature, easy and fast operation, and little or no sample preparation. Quantitative information can also be obtained from a system with an optical contact between the sample and an IRE [32].

Transmission technique is the most commonly used IR sampling technique. In transmission measurement, light propagates throughout a whole sample. Therefore, the information obtained is the average information coming from both the surface

and bulk of the sample.

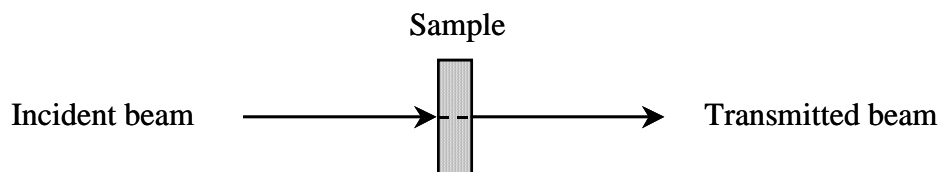


Figure 2.6 Transmission measurement experimental setup.

2.6 Two-dimensional Infrared Correlation Spectroscopy

2.6.1 General Concept

The basic concept of 2D IR correlation spectroscopy was first introduced by Noda [25]. 2D IR spectroscopy is a technique where the spectral intensity is plotted as a function of two independent IR wavenumbers. The general scheme for obtaining 2D IR correlation spectra is shown in Figure 2.7 [28]. There are various types of external perturbations used to stimulate the system of interest, for examples, electrical, thermal, chemical, and mechanical excitations. It is also very common to collect a set of dynamic spectra as a function of the system physical variable itself, such as temperature, concentration, and pressure.

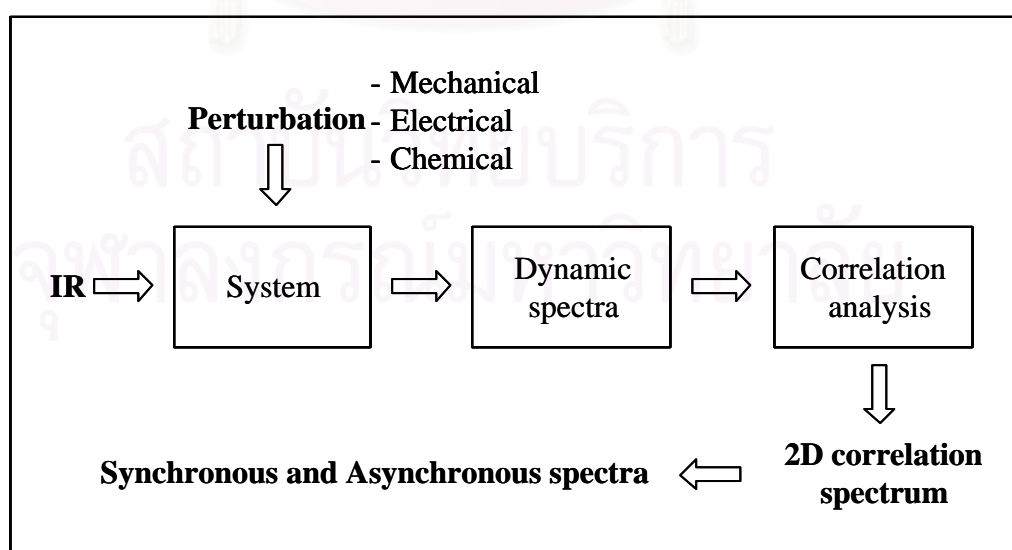


Figure 2.7 Schematic illustration for the generation of 2D IR correlation spectra.

2.6.2 Two-Dimensional Cross Correlation Function

To generate 2D IR correlation spectra, once a set of time-dependent spectral intensities is available, the mathematical procedure known as 2D cross correlation function is performed.

$$y(\nu, t) = \bar{y}(\nu) + \tilde{y}(\nu, t) \quad (2.1)$$

$$\tilde{Y}_1(\omega) = \int_{-\infty}^{\infty} \tilde{y}(\nu_1, t) e^{-i\omega t} dt \quad (2.2)$$

$$\tilde{Y}_2^*(\omega) = \int_{-\infty}^{\infty} \tilde{y}(\nu_2, t) e^{i\omega t} dt \quad (2.3)$$

$\tilde{Y}_1(\omega)$ is the Fourier transform of the time-dependent spectral intensity variations $y(\nu_1, t)$ observed at spectral variable ν_1 . The conjugate of the Fourier transform of the time-dependent spectral intensity variations $y(\nu_2, t)$ observed at spectral variable ν_2 is given by $\tilde{Y}_2^*(\omega)$. A 2D correlation intensity $X(\nu_1, \nu_2)$ is a complex number comprising two orthogonal (i.e., real, $\Phi(\nu_1, \nu_2)$, and imaginary, $i\Psi(\nu_1, \nu_2)$) components known as the synchronous and the asynchronous 2D correlation intensity. The cross correlation function is given in terms of Fourier transform of time-dependent signals by:

$$\begin{aligned} X(\nu_1, \nu_2) &= \frac{1}{\pi t} \int_0^{\infty} \tilde{Y}_1(\omega) \cdot \tilde{Y}_2^*(\omega) d\omega \\ &= \Phi(\nu_1, \nu_2) + i\Psi(\nu_1, \nu_2) \end{aligned} \quad (2.4)$$

The synchronous spectrum, $\Phi(\nu_1, \nu_2)$, represents the overall similarity between two spectral intensity variations measured at different spectral variables, as the moiety related to the spectral information changes as a function of time under external perturbation. The asynchronous spectrum, $\Psi(\nu_1, \nu_2)$, on the other hand, indicates the dissimilarity of the spectral intensity variations.

2.6.3 Synchronous and Asynchronous Correlation Spectra

Figure 2.8 shows a schematic example of a synchronous 2D correlation spectrum plotted as a contour map. A synchronous spectrum is a symmetric spectrum with respect to a diagonal line corresponding to coordinates $\nu_1 = \nu_2$. Correlation peaks appear at both diagonal and off-diagonal positions. The intensity of peaks located at diagonal positions corresponds to the autocorrelation function of spectral intensity variations. The diagonal peaks are, therefore, referred to as 'autopeaks'. In Figure 2.8, there are four autopeaks located at the spectral coordinates A, B, C, and D. The magnitude of an autopeak represents the overall extent of spectral intensity variation observed at the specific spectral variable ν during the observation interval. Thus, any regions of a spectrum that change intensity to a great extent under a given perturbation will show strong autopeaks. Those remaining near constant, on the other hand, develop weak or no autopeak.

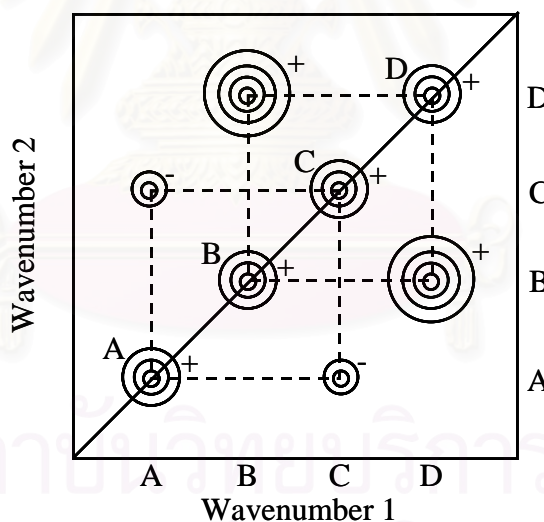


Figure 2.8 Schematic contour map of a synchronous 2D correlation spectrum.

Cross peaks located at the off-diagonal positions of a synchronous 2D spectrum represent simultaneous or coincidental changes of spectral intensities observed at two different spectral variables, ν_1 and ν_2 . In the example spectrum, bands A and C are synchronously correlated, as well as bands B and D. While the sign of autopeaks is always positive, the sign of cross peaks can be either positive or negative. The sign

of synchronous cross peaks becomes positive if the spectral intensities at the two correlated spectral variables are either increasing or decreasing together during the observation interval. On the other hand, a negative sign of cross peaks indicates that one of the spectral intensities is increasing while the other is decreasing. In Figure 2.8, the sign of cross peaks at the spectral coordinates A and C is negative, indicating that intensity at one band is increasing while the other is decreasing. The cross peak sign at the coordinates B and D is positive, indicating that both bands decrease or increase together.

Figure 2.9 shows an example of an asynchronous 2D correlation spectrum. The intensity of an asynchronous spectrum represents sequential, or successive, changes of spectral intensities measured at ν_1 and ν_2 . Unlike a synchronous spectrum, an asynchronous spectrum is antisymmetric with respect to a diagonal line. The asynchronous spectrum has no autopeak. It is consisting exclusively of cross peaks located at off-diagonal positions.

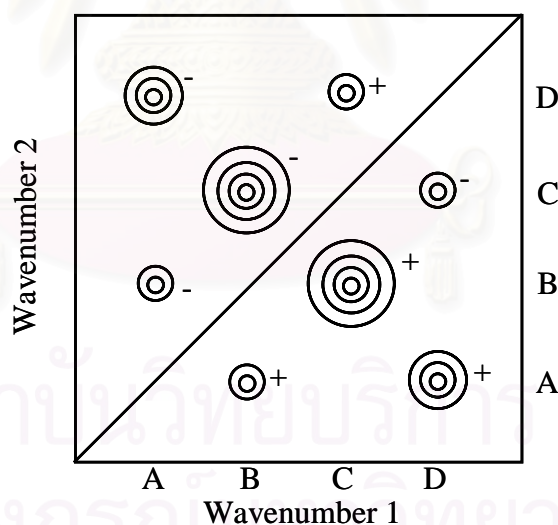
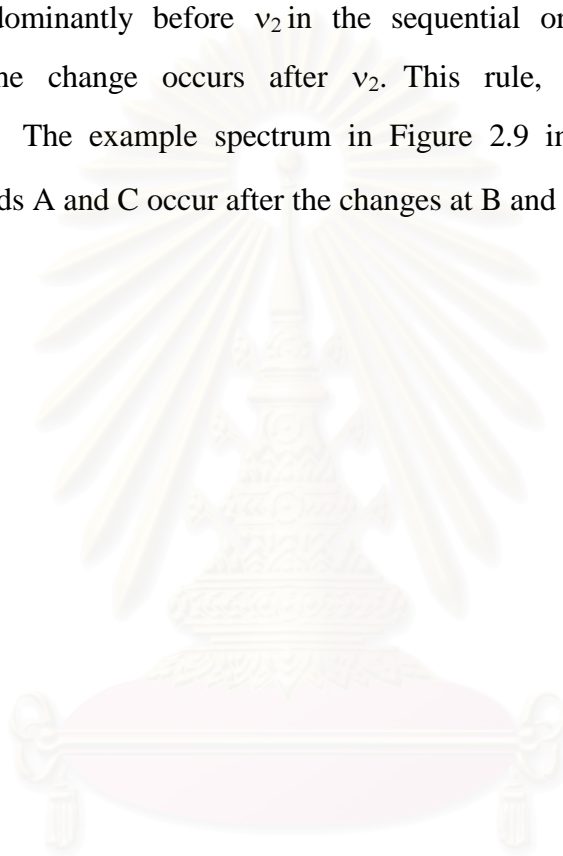


Figure 2.9 Schematic contour map of an asynchronous 2D correlation spectrum.

An asynchronous cross peak develops only if the intensities of two spectral bands change out of phase with each other. This feature is especially useful in differentiating overlapped bands arising from spectral signals of different origins. For example, different spectral intensity contributions from individual components of a complex mixture, chemical functional groups experiencing different effects from

some external fields, or inhomogeneous materials comprised of multiple phases may all be effectively discriminated. Even if bands are located close to each other, as long as the signatures or the pattern of sequential variations of spectral intensities are substantially different, asynchronous cross peaks will develop between their spectral coordinates. The sign of asynchronous cross peaks can be either negative or positive. The sign of an asynchronous cross peak becomes positive if the intensity change at ν_1 occurs predominantly before ν_2 in the sequential order of time. It becomes negative if the change occurs after ν_2 . This rule, however, is reversed if $\Phi(\nu_1, \nu_2) < 0$. The example spectrum in Figure 2.9 indicates that the intensity changes at bands A and C occur after the changes at B and D.



สถาบันวิทยบริการ
จุฬาลงกรณ์มหาวิทยาลัย

CHAPTER III

EXPERIMENTAL SECTION

3.1 Materials and Equipments

3.1.1 Samples

Bacterially synthesized P(HB-*co*-HHx) (HHx = 12 mol%) and PHB were provided by the Procter and Gamble Company (Cincinnati, USA). The crude P(HB-*co*-HHx) sample was refined by dissolving in hot chloroform (CHCl₃, Wako Pure Chemical Industries, Ltd., Osaka, Japan), vacuum-filtering the residual biomass, and precipitating with methanol (CH₃OH, Wako Pure Chemical Industries, Ltd., Osaka, Japan). The chloroform:methanol volume ratio for the precipitation was approximately 1:10. The precipitated P(HB-*co*-HHx) sample was vacuum-dried at 60 °C for 24 hours and then kept in a desiccator until used.

The PHB sample is a purified sample and thus was used as received. Chloroform was used as a solvent for re-dissolving the purified samples. The thermal properties and percentages of crystallinity of the samples are summarized in Table 3.1.

Table 3.1 Thermal properties and percentages of crystallinity of P(HB-*co*-HHx) and PHB

	P(HB- <i>co</i> -HHx)	PHB
Glass transition temperature, T_g , °C	2.4	4
Crystallization temperature, T_c , °C	51	100
Melting temperature, T_m , °C	110	170
Percentage of crystallinity, %	35	55

3.1.2 Infrared Optical Elements

1. Calcium fluoride (CaF_2) transmission windows ($\text{RI}_{\text{CaF}_2} = 1.4$)
2. Zinc selenide (ZnSe) transmission windows ($\text{RI}_{\text{ZnSe}} = 2.4$)
3. Germanium (Ge) transmission windows ($\text{RI}_{\text{Ge}} = 4.0$)
4. Multiple reflection ATR accessory with a 45° - ZnSe IRE (IRE dimension: $10 \times 75.5 \times 3$ mm, Spectra Tech)
5. Multiple reflection ATR accessory with a 45° - Ge IRE (IRE dimension: $10 \times 75.5 \times 3$ mm, Spectra Tech)

3.2 Instruments

3.2.1 Differential Scanning Calorimeters

1. Seiko EXDSTAR6000 apparatus with a DSC6200 module
2. Perkin-Elmer differential scanning calorimeter (Pyris 6 DSC)

3.2.2 X-ray Diffractometers

1. Rigaku R-Axis IV imaging plate diffractometer
X-ray source: $\text{CuK}\alpha$ radiation, wavelength 1.5418 \AA , from a Rigaku Ultra-X18 rotating anode X-ray generator, 40 kV, 100 mA.
2. Two-circle Rigaku X-ray diffractometer equipped with a scintillation detector (RINT2000/PC)
X-ray source: $\text{MoK}\alpha$ radiation, wavelength 0.71069 \AA , from a Rigaku Ultra-X18 rotating anode X-ray generator, 40 kV, 240 mA.

3.2.3 Infrared Spectrometers

1. Nicolet Magna-IRTM 550 spectrometer
2. Nicolet Nexus 670 spectrometer

Instrumental Setup

Source	Globar
Beam splitter	KBr
Detector	Mercury cadmium telluride (MCT)

Acquisition Parameters

Spectral resolution, cm^{-1}	2
Number of scans	512
Result spectrum	Absorbance

3.2.4 Temperature Controllers for Infrared Measurements

1. Transmission temperature controller unit (CHINO, model SU)
2. ATR temperature controller unit (CHINO, model LT230)

3.3 Experimental Procedures

3.3.1 Differential Scanning Calorimetry Measurements

A DSC measurement of the precipitated P(HB-*co*-HHx) sample was performed by using the Seiko EXDSTAR6000 apparatus with a DSC6200 module over a temperature range of -40 to 120 °C at heating and cooling rates of 10 °C min^{-1} .

For the chloroform solution-cast P(HB-*co*-HHx) sample, a DSC measurement was performed by using the Perkin-Elmer differential scanning calorimeter (Pyris 6 DSC) over a temperature range of -40 to 120 °C at heating and cooling rates of 20 °C min^{-1} .

3.3.2 Wide-angle X-ray Diffraction Measurements

A WAXD pattern and an XRD trace of the P(HB-*co*-HHx) sample were measured at room temperature (25 °C) in a scattering angle range of $2\theta = 5\text{-}35^\circ$ by

using the Rigaku R-Axis IV imaging plate diffractometer.

Temperature-dependent WAXD patterns of the P(HB-*co*-HHx) sample were measured over a temperature range of 25.0-110.0 °C in a scattering angle range of $2\theta = 5-13^\circ$ by using the two-circle Rigaku X-ray diffractometer. For comparison, the corresponding WAXD patterns of the PHB sample were collected over a temperature range of 28.3-174.3 °C in a scattering angle range of $2\theta = 2-13^\circ$ by using the two-circle Rigaku X-ray diffractometer.

XRD patterns of the chloroform solution-cast P(HB-*co*-HHx) sample were measured by using the two-circle Rigaku X-ray diffractometer and the imaging plate over a temperature range of 30.1-105.8 °C in a scattering angle range of $2\theta = 2-30^\circ$. Silicone powder was put in the samples for the calibration of the angles.

3.3.3 Infrared Measurements

3.3.3.1 Thermally Induced Phase Transformation of PHB

A film of the PHB sample was prepared by casting its chloroform solution on a CaF₂ window. The film was kept in a vacuum-dried oven at 60 °C for 12 hours and cooled down to room temperature before the measurements.

The CaF₂ window with the PHB film was placed in a home-made temperature-controlled transmission cell connected to the transmission temperature controller unit. IR spectra of the PHB film were collected by using the Nicolet Magna-IR™ 550 spectrometer. The spectral acquisitions were performed over a temperature range of 40-180 °C with an interval of 10 °C via both heating up and cooling down processes.

3.3.3.2 Thermally Induced Phase Transformation of P(HB-*co*-HHx)

A film of the P(HB-*co*-HHx) sample was prepared by casting its

chloroform solution on a CaF₂ window. The film was kept at 60 °C in a vacuum-dried oven for 12 hours and cooled down to room temperature before the measurements.

The temperature of the CaF₂ window with the P(HB-*co*-HHx) film was controlled by using the transmission temperature controller unit. IR spectra of the P(HB-*co*-HHx) film were measured by using the Nicolet Magna-IR™ 550 spectrometer. The temperature-perturbed dynamic IR spectra were collected throughout a temperature range of 30-140 °C with an interval of 10 °C via both heating up and cooling down processes.

3.3.3.3 Surface Melting and Crystallization Behavior of PHB and P(HB-*co*-HHx)

Temperature-Dependent Attenuated Total Reflection Measurements

The multiple reflection ATR accessory with a 45°-ZnSe IRE was employed for the temperature-dependent ATR measurements. The temperature of the attachment that holds the ZnSe IRE with the P(HB-*co*-HHx) film was controlled by using the ATR temperature controller unit. To assure the optical contact between the film and the IRE, the P(HB-*co*-HHx) film was prepared by casting its chloroform solution directly on the ZnSe IRE. The film was kept at 60 °C in a vacuum-dried oven for 12 hours and cooled down to room temperature before the measurements. Temperature-dependent ATR spectra of the film were collected by using the Nicolet Nexus 670 spectrometer. The measurements were carried out over a temperature range of 30-140 °C with an increment of 10 °C.

Time-Dependent Infrared Measurements

The same ATR experimental setup as described above without the ATR temperature controller unit was employed for the time-dependent ATR measurements of the P(HB-*co*-HHx) and PHB films. Time-dependent

transmission measurements were also performed for P(HB-*co*-HHx) and PHB. The films were prepared by casting their chloroform solutions on ZnSe transmission windows in the same manner as that for the ATR measurements.

All time-dependent measurements were conducted at room temperature. After the solvent castings, the films were air-dried for 30 minutes before the measurements. The time-dependent IR spectra were collected by using the Nicolet Nexus 670 spectrometer every 15 minutes until the crystal growth was by and large completed (*i.e.*, no significant spectral change was observed after prolonged measurement).

To minimize the effect of a localized anomalous refractive index dispersion results from absorption peaks, the Ge IRE was employed for comparison.

In order to directly compare the surface information obtained from the ATR technique with the bulk information obtained from the transmission technique, all ATR spectra were penetration depth-corrected to eliminate the artifact arising from the wavenumber-dependent sampling depth of the ATR technique. It should be noted that the inherent wavenumber-dependent ATR spectral intensity is eliminated by this operation. However, the corrected ATR spectra still carry the surface information of the polymer films since the actual sampling depth of the entire spectra is up to a few micrometers from the sample surface while the transmission spectra carry the bulk information of the whole films.

3.3.3.4 Crystallization Behavior of P(HB-*co*-HHx) under Different Crystallization Conditions

Gradual Cooling Crystallization

A film of the P(HB-*co*-HHx) sample was prepared by casting its chloroform solution on a CaF₂ window. After chloroform evaporated, the film

was heated to 140 °C and kept for 30 minutes. IR spectra of the film were measured by using the Thermo Nicolet Magna-IR™ 550 spectrometer. The temperature of the CaF₂ window with the P(HB-*co*-HHx) film was controlled by using the transmission temperature controller unit. The temperature-dependent dynamic IR spectra were collected throughout a temperature range of 140-30 °C with a decrement interval of 10 °C. The cooling rate was 2 °C/min. The sample film was kept at each temperature for 15 minutes before the measurement.

Supercooled Melt Crystallization

The sample film was prepared by casting its chloroform solution on a CaF₂ window in the same manner as that for the gradual cooling crystallization. After chloroform evaporated, the film was heated to 140 °C and kept for 30 minutes before rapidly quenched to room temperature. The time-dependent IR spectra were collected at room temperature by using the Thermo Nicolet Magna-IR™ 550 spectrometer with a time interval of 30 minutes until the crystal growth was by and large completed (*i.e.*, no significant spectral change was observed after prolonged measurement).

Solvent-cast Film Crystallization

The sample film was prepared by casting its chloroform solution on a CaF₂ window. After the solvent casting, the sample film was air-dried for 30 minutes before the measurements. The IR spectrum of the sample film measured after the solvent evaporated showed no spectroscopic evidence for the presence of chloroform. The time-dependent IR spectra were collected at room temperature by using the Thermo Nicolet Magna-IR™ 550 spectrometer with a time interval of 15 minutes until the crystal growth was by and large completed (*i.e.*, no significant spectral change was observed after prolonged measurement).

3.4 Two-dimensional Correlation Analysis

The IR spectra to be analyzed were preprocessed to minimize the effect of

baseline instability prior to the 2D correlation calculation. The spectral regions of interest were subjected to a linear baseline correction, followed by offsetting to the zero absorbance value. The calculations of 2D correlation spectra were performed by using the 2D-Pocha software composed by Daisuke Adachi (Kwansei-Gakuin University, Japan). Temperature-averaged and time-averaged IR spectra in the selected wavenumber regions were used as the reference spectra for the 2D correlation calculations of the temperature and time-dependent IR spectra, respectively.



สถาบันวิทยบริการ
จุฬาลงกรณ์มหาวิทยาลัย

CHAPTER IV

RESULTS AND DISCUSSION

4.1 Wide-angle X-ray Diffraction Study and Thermal Analysis of P(HB-*co*-HHx) and PHB

4.1.1 Wide-angle X-ray Diffraction

Figure 4.1 A and B shows the WAXD pattern and the XRD trace of the precipitated P(HB-*co*-HHx) sample measured at room temperature, respectively. It was reported that the unit cells of PHB and poly(hydroxyvalerate) (PHV) belong to the orthorhombic system ($\alpha = \beta = \gamma = 90^\circ$) with $a = 5.76 \text{ \AA}$, $b = 13.20 \text{ \AA}$, $c = 5.96 \text{ \AA}$ and $a = 9.52 \text{ \AA}$, $b = 10.08 \text{ \AA}$, $c = 5.56 \text{ \AA}$ [9,10,40]. The P(HB-*co*-HHx) sample also shows the orthorhombic system ($\alpha = \beta = \gamma = 90^\circ$) with $a = 5.76 \text{ \AA}$, $b = 13.20 \text{ \AA}$, $c = 5.96 \text{ \AA}$, which is the same as the PHB crystal system. The P(HB-*co*-HV) copolymers with the HV compositions from 0-37 mol % crystallize in the PHB lattice while those with the HV compositions from 53-95 mol % crystallize in the PHV lattice [41]. The (110) d spacing of P(HB-*co*-HV) apparently increases as the HV content increases to 37 mol % while the (020) and (002) d spacings remain unchanged. As described above, P(HB-*co*-HHx) shows only one crystalline form with the PHB lattice. One may expect that the propyl side chains of HHx units expand the (110) d spacing of the PHB lattice in P(HB-*co*-HHx) even more so than that in P(HB-*co*-HV) due to the steric effects of the propyl side chains. However, the (110) d spacing of P(HB-*co*-HHx) is smaller than that of P(HB-*co*-HV) [41]. It can be assumed that the propyl side chains of HHx have stronger inter- and intramolecular interactions than the ethyl side chains of HV since the propyl side chains are located closer to the C=O groups in the lattice constant a axis than the ethyl side chains. Another possibility is that the propyl side chains of HHx are protruded in the crystal structure while the ethyl side chains of HV can be fixed in the crystal with PHB. Therefore, the (110) d spacing of P(HB-*co*-HHx) may show the proximity value with that of PHB.

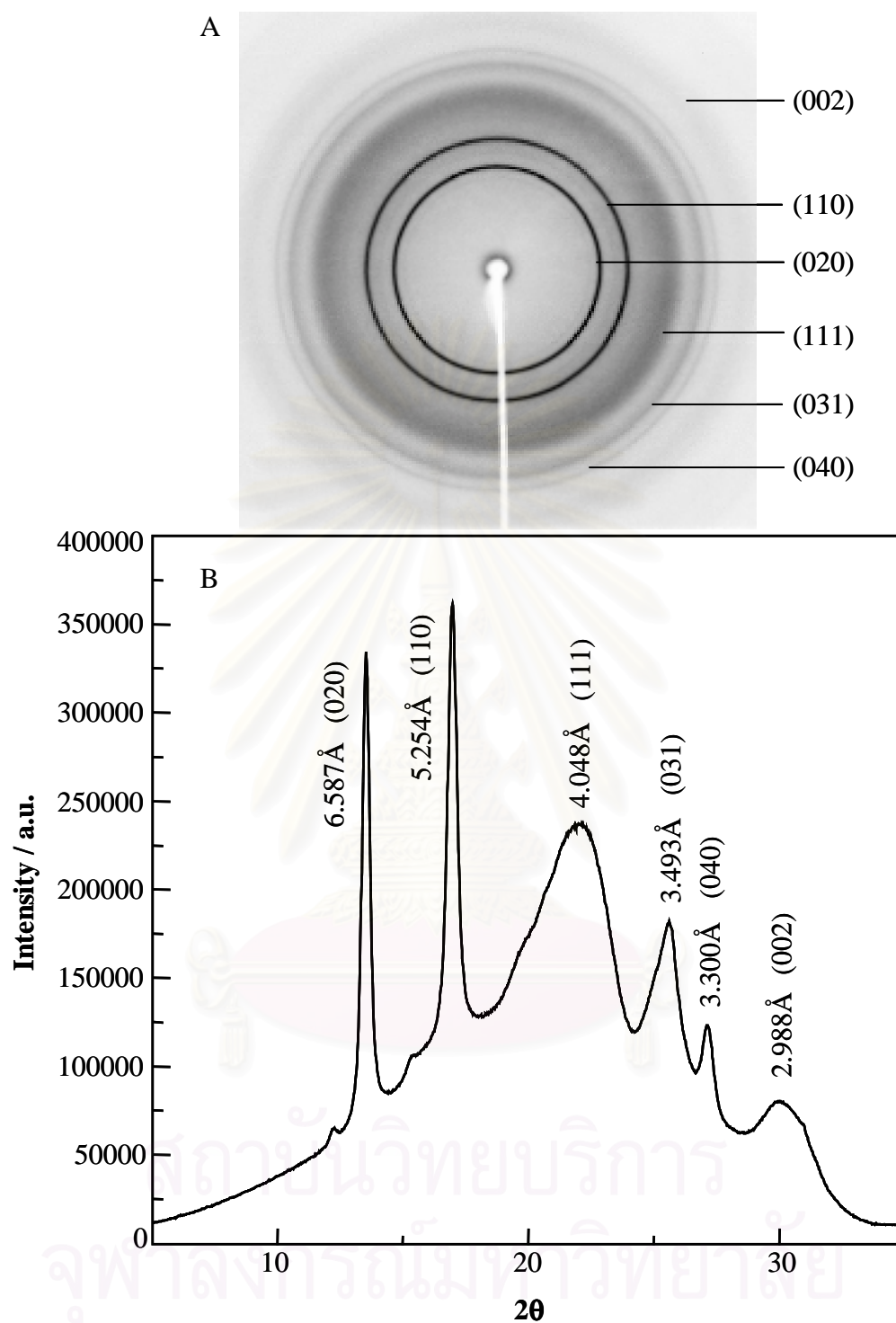


Figure 4.1 A WAXD pattern of the precipitated P(HB-co-HHx) sample measured at room temperature (A), and an XRD trace of P(HB-co-HHx) obtained by a radial microdensitometer scan of the diagram shown in (A).

Figure 4.2 shows the temperature-dependent WAXD patterns of the precipitated

P(HB-*co*-HHx) sample. It can be seen that the (110) d spacing expands as temperature increases. The (020), (040), and (031) d spacings, however, do not change with temperature. The peak due to the lattice constant a shifts to a large value as temperature increases. Referring to the crystalline structure of PHB and the proposed helical structure of P(HB-*co*-HHx) [9,10], one can assume that there are inter- and intramolecular interactions between the C=O and CH₃ groups in the P(HB-*co*-HHx) copolymer.

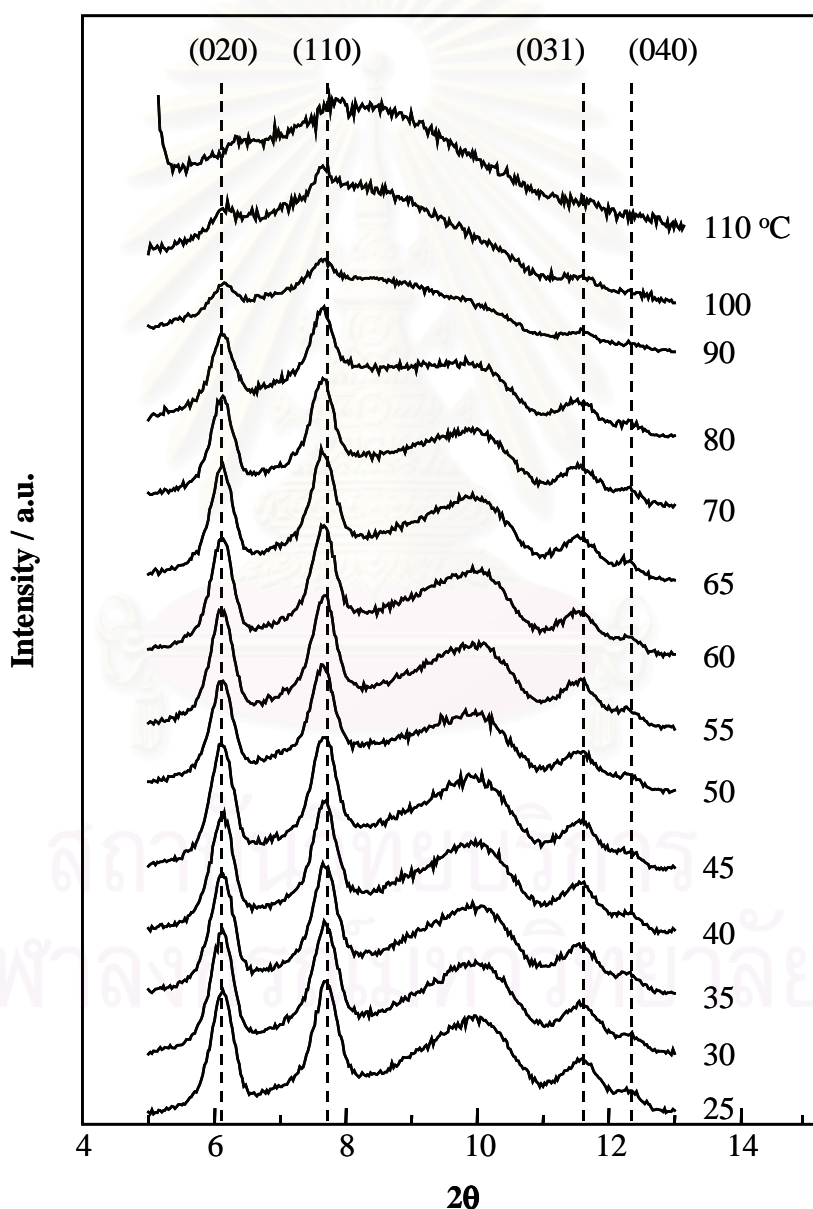


Figure 4.2 Temperature-dependent WAXD patterns of the precipitated P(HB-*co*-HHx) sample measured over a temperature range of 25-110 °C.

Figure 4.3 shows variations in the (110) peak area and the (110) d spacing versus temperature. The peak area and peak maximum indicate the crystallinity and thermal expansion of the sample, respectively. It is noted that the (110) d spacing expands gradually with temperature while the peak area slightly changes until 50 °C and shows a gradual decrease above 50 °C.

Figure 4.4 shows the temperature dependences of the (020) peak area and (020) d spacing. Note that the thermal behavior of the (020) peak area is similar to that of the (110) peak area. However, the (020) d spacing shows less thermal expansion compared to the (110) d spacing.

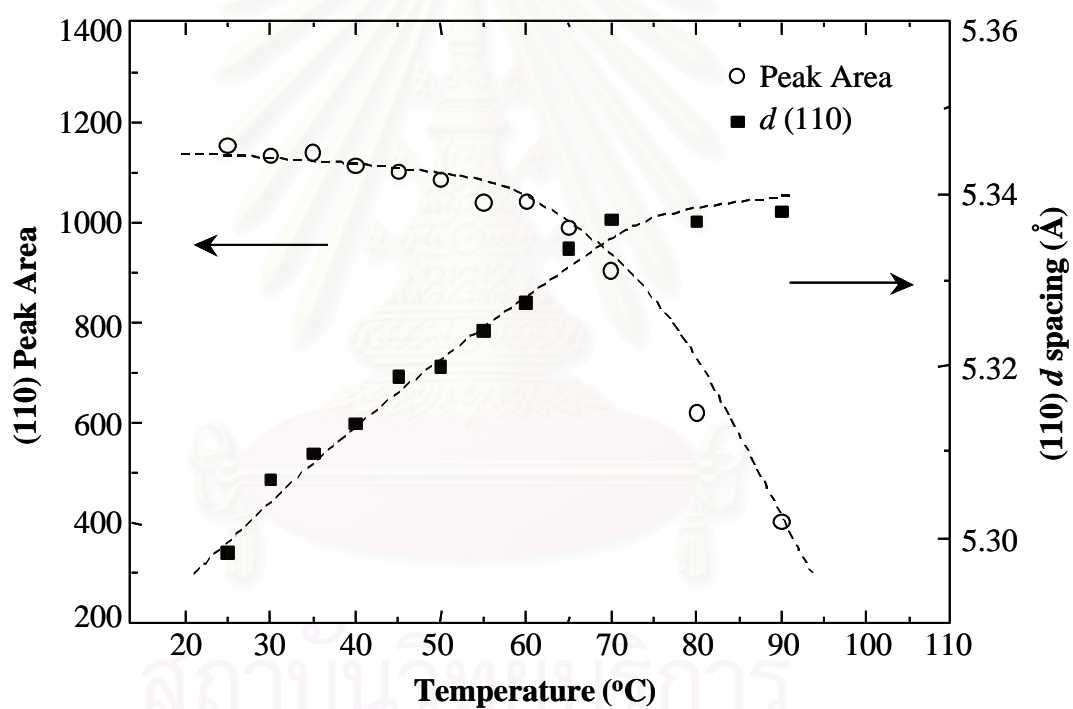


Figure 4.3 Temperature-dependent peak areas and d spacings of the (110) reflection of the precipitated P(HB-*co*-HHx) sample.

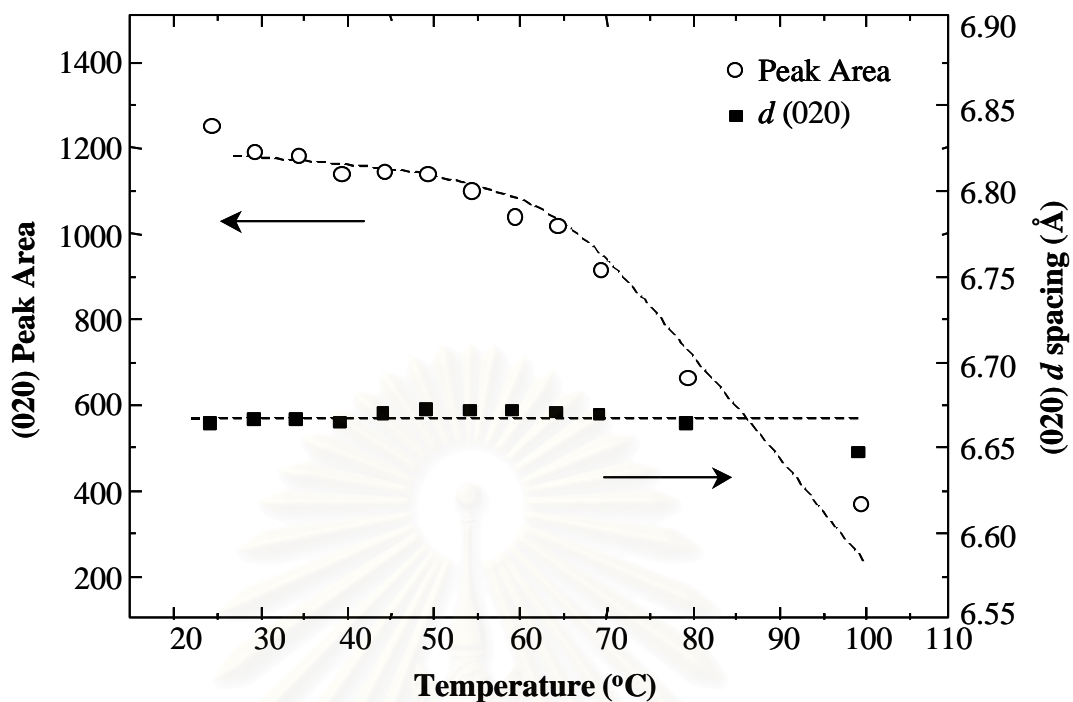


Figure 4.4 Temperature-dependent peak areas and d spacings of the (020) reflection of the precipitated P(HB-*co*-HHx) sample.

Figure 4.5 shows temperature-dependent variations in the lattice parameters, a and b , of the precipitated P(HB-*co*-HHx) sample. The a lattice parameter increases gradually with temperature while the b lattice parameter slightly changes. It is very likely that the increase in the a lattice parameter results from the decrease in the inter- and intramolecular interactions between the C=O and CH₃ groups along the a axis of the crystalline structure. The interaction is mainly concerned with the hydrogen bond between the C=O and CH₃ groups, but there is a possibility that some C=O groups interact with the propyl side chains.

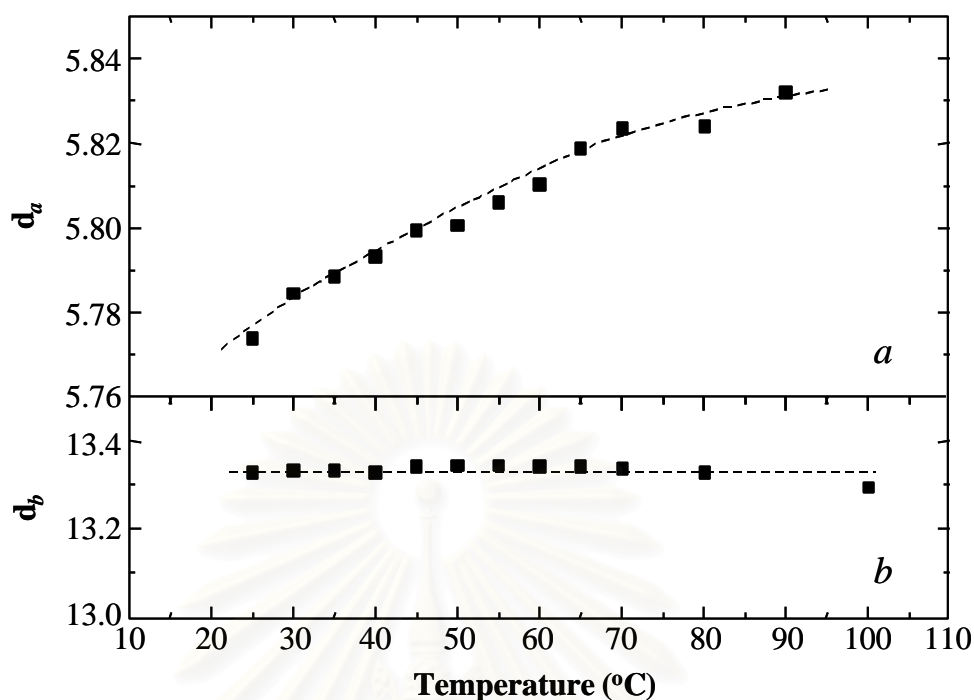


Figure 4.5 Changes in the lattice parameters, a and b , of the precipitated P(HB-*co*-HHx) sample versus temperature.

The temperature-dependent WAXD patterns of the chloroform solution-cast P(HB-*co*-HHx) sample are shown in Figure 4.6. The variations in the (110) peak area and (110) d spacing versus temperature are demonstrated in Figure 4.7. The temperature-dependent changes in the (110) peak area are quite different between the precipitated and solution-cast samples. The crystallinity of the precipitated sample slightly changes until around 50 °C while that of the solution-cast sample increases until around 54 °C. The maximum of the peak area around 54 °C suggests a recrystallization of the chloroform solution-cast sample.

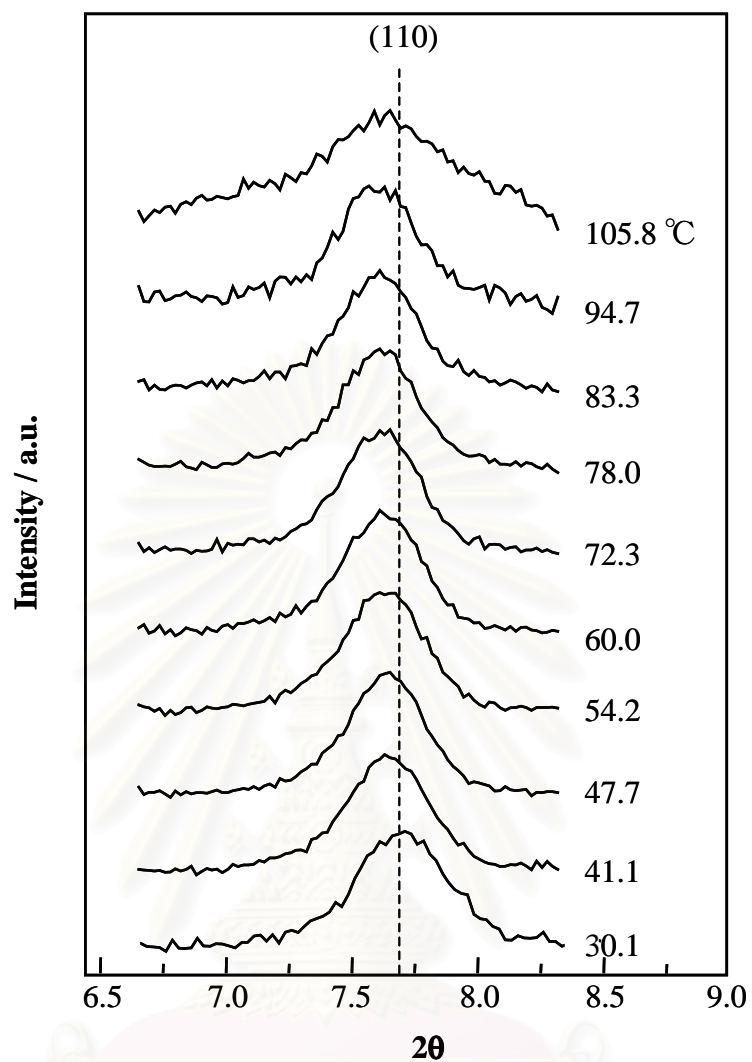


Figure 4.6 Temperature-dependent WAXD patterns of the chloroform solution-cast P(HB-co-HHx) sample measured over a temperature range of 30.1-105.8 °C.

สถาบันวิทยบริการ
จุฬาลงกรณ์มหาวิทยาลัย

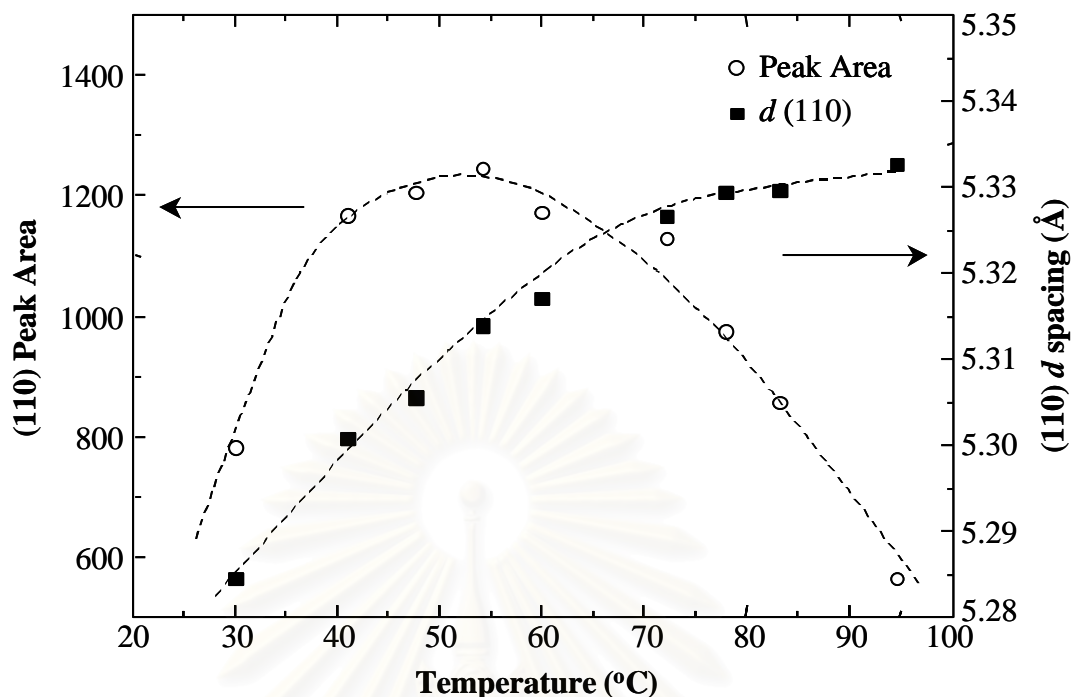


Figure 4.7 Temperature-dependent peak areas and d spacings of the (110) reflection of the chloroform solution-cast P(HB-*co*-HHx) sample.

Figure 4.8 depicts effects of temperature on the lattice parameter a of the solution-cast sample. Changes in the lattice parameters of polymers can be observed under various conditions. Information about the changes in the lattice parameters provides insight into the forces that bind atoms and molecules in the crystal structure and the factors that determine the crystal structure. There is a slight difference in the shift of the lattice parameter a between the precipitated and solution-cast samples. The change in the lattice parameter a of the solution-cast sample is somewhat larger than that of the precipitated sample. This difference arises from the difference in the crystallite size. The gradual peak shift of the WAXD patterns with temperature indicates the thermal expansion of the crystalline structure of the sample.

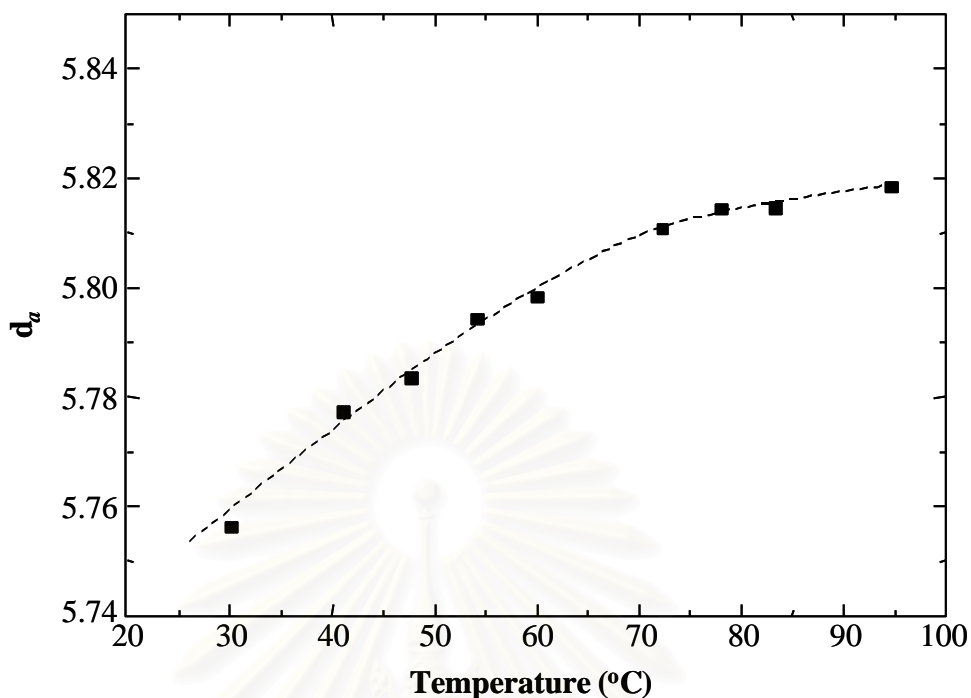


Figure 4.8 Changes in the lattice parameters, a , of the chloroform solution-cast P(HB-*co*-HHx) sample versus temperature.

The temperature-dependent WAXD patterns of the PHB sample are presented in Figure 4.9. The clear (020), (110), (111), (031), and (040) d spacings reveal that the crystallinity of PHB is higher than that of P(HB-*co*-HHx). Figure 4.10 A and B shows the temperature dependences of the (110) peak area and (110) d spacing and those of the (020) peak area and (020) d spacing of PHB, respectively. There is a drastic drop of the (110) and (020) peak areas around 160 °C. The (110) d spacing of PHB shows a gradual change with temperature as in the case of P(HB-*co*-HHx) while the (020) d spacing shows only a small shift, unlike that of P(HB-*co*-HHx). The (110) peak area of PHB remains nearly unchanged until 140 °C while that of P(HB-*co*-HHx) decreases gradually from fairly low temperature. The copolymerization of the HHx unit into the molecular chain of PHB significantly changes the thermal behavior of the resulting copolymer.

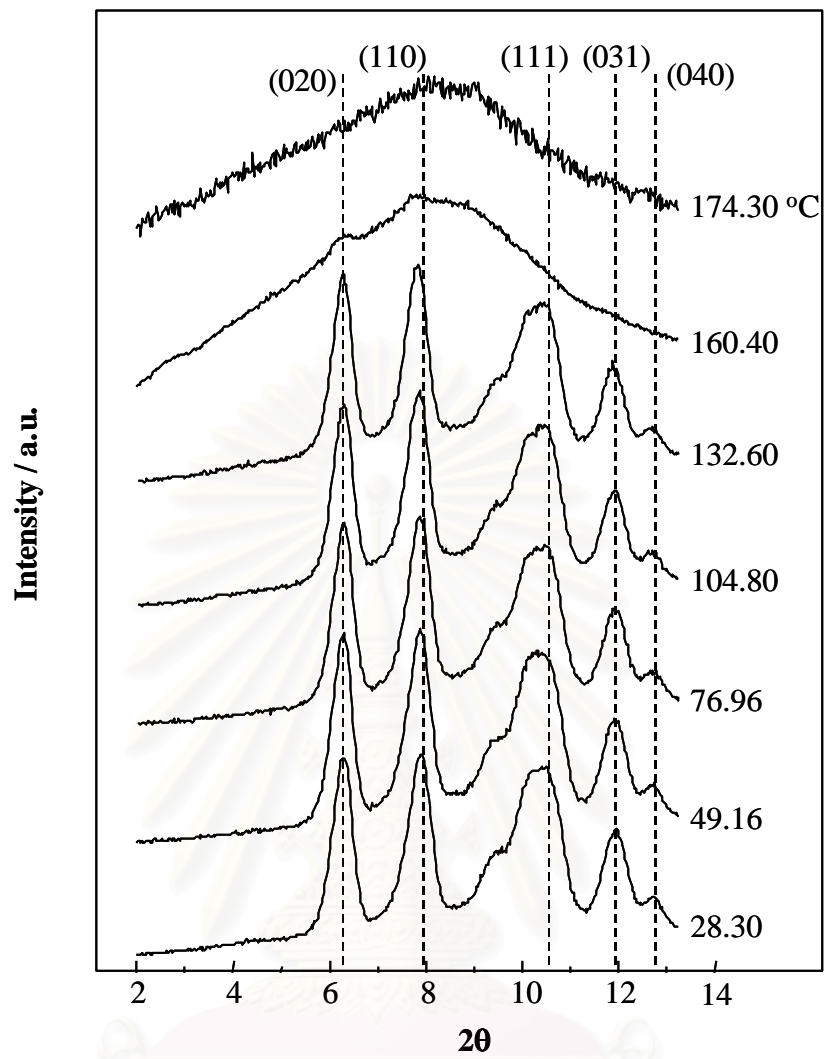


Figure 4.9 Temperature-dependent WAXD patterns of PHB measured over a temperature range of 28.30-174.30 °C.

สถาบันวิทยบริการ
จุฬาลงกรณ์มหาวิทยาลัย

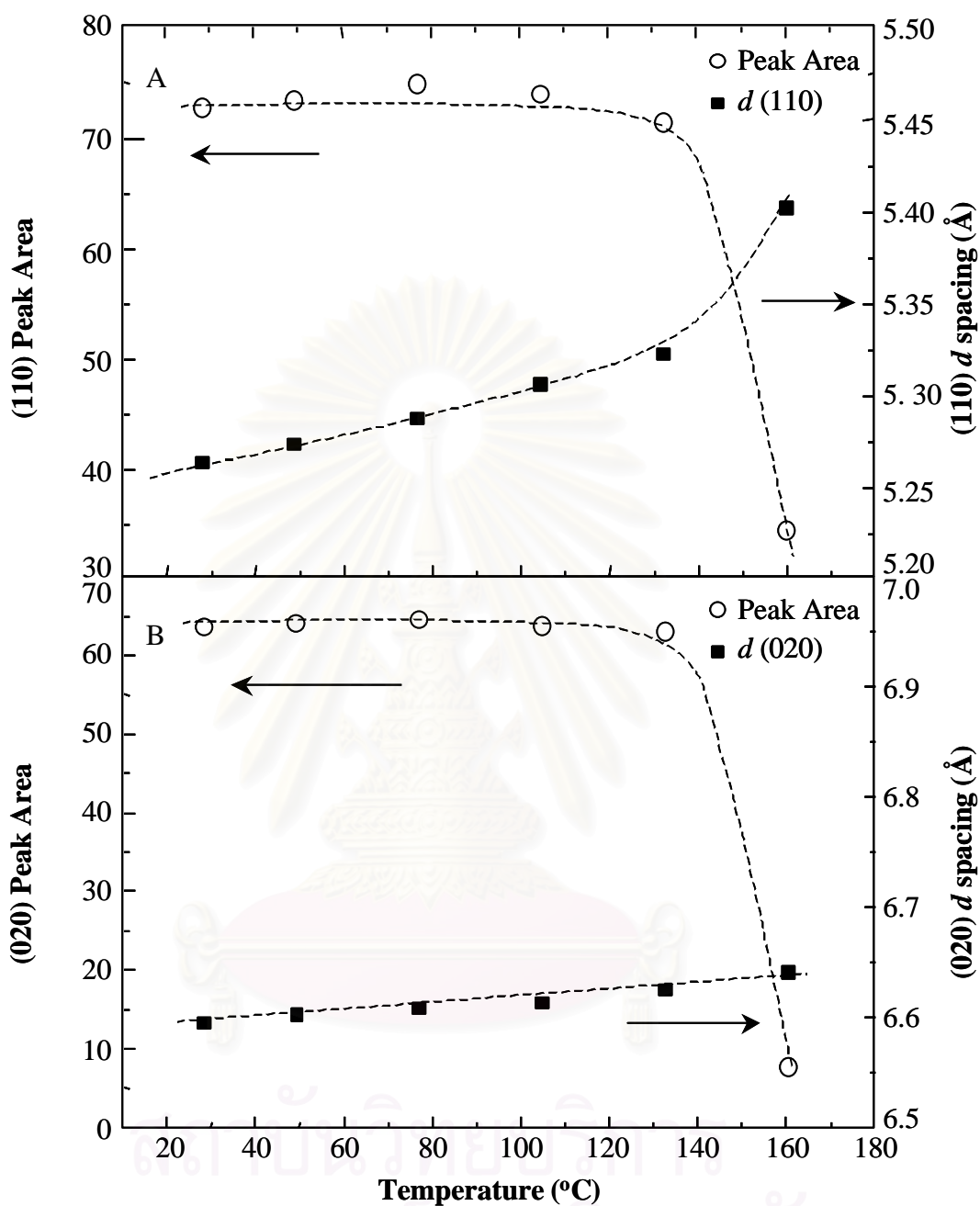


Figure 4.10 Temperature-dependent peak areas and d spacings of the (110) reflection (A) and (020) reflection (B) of PHB.

Effects of temperature on the lattice parameters of PHB are shown in Figure 4.11. The lattice parameters for both P(HB-co-HHx) and PHB show significant variations with temperature. This is an evidence showing that the inter- and intramolecular interactions are not strong along the a axis in P(HB-co-HHx) and

PHB crystallites. The variation in the lattice parameter a suggests that these interactions are due to the C=O and CH₃ groups [42-44].

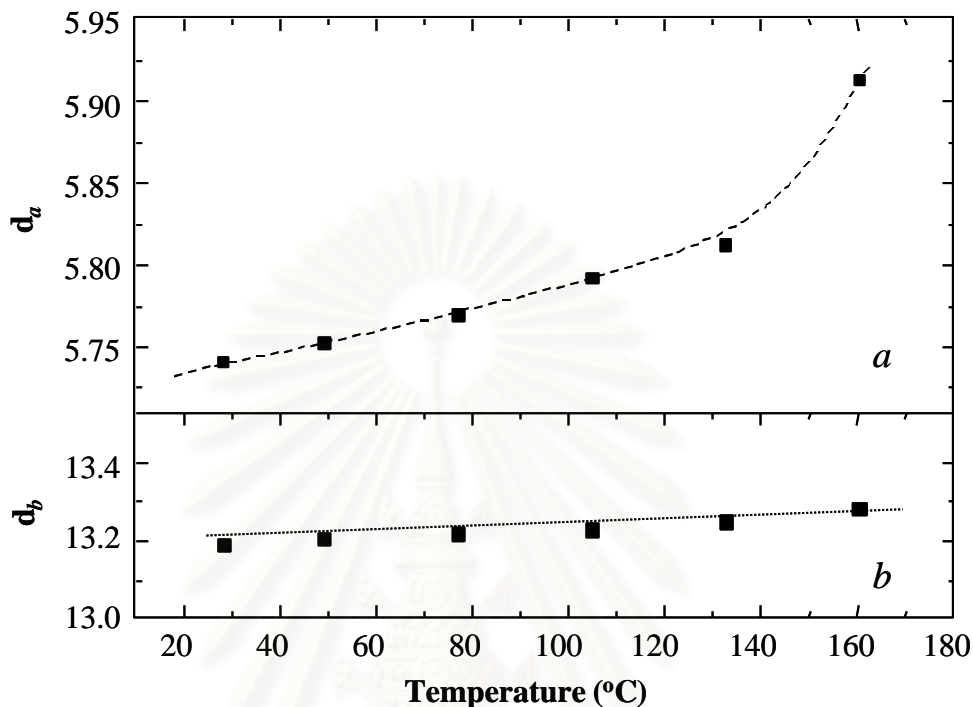


Figure 4.11 Changes in the lattice parameters, a and b , of PHB versus temperature.

4.1.2 Differential Scanning Calorimetry

Figure 4.12 A and B shows the DSC curves of the first cooling and second heating scans of the precipitated P(HB-co-HHx) sample while Figure 4.13 A and B shows those of the chloroform solution-cast sample. The WAXD patterns of the solution-cast sample show that the (110) peak area has a maximum value around 54 °C. The maximum of the (110) peak area may be ascribed to the recrystallization process of the solution-cast sample. Note that two peaks of T_m appear in the DSC curve of the solution-cast sample. There are two possibilities for the origin of the two peaks in the second heating scan of DSC; (1) the melt and recrystallization of the sample and (2) the presence of two types of crystalline lamellae in the sample.

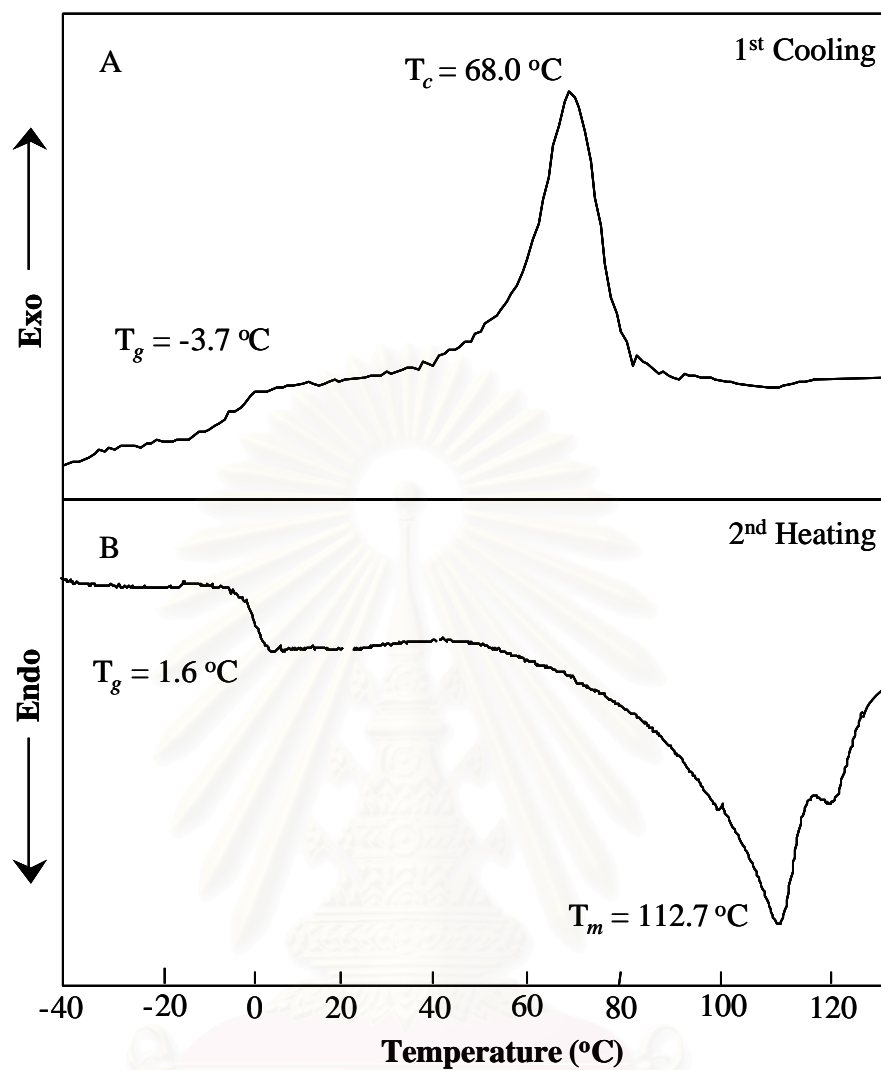


Figure 4.12 DSC curves of the first cooling scan (A) and second heating scan (B) of the precipitated P(HB-co-HHx) sample; heating and cooling rates were 10 °C min^{-1} .

สถาบันวิทยบริการ
จุฬาลงกรณ์มหาวิทยาลัย

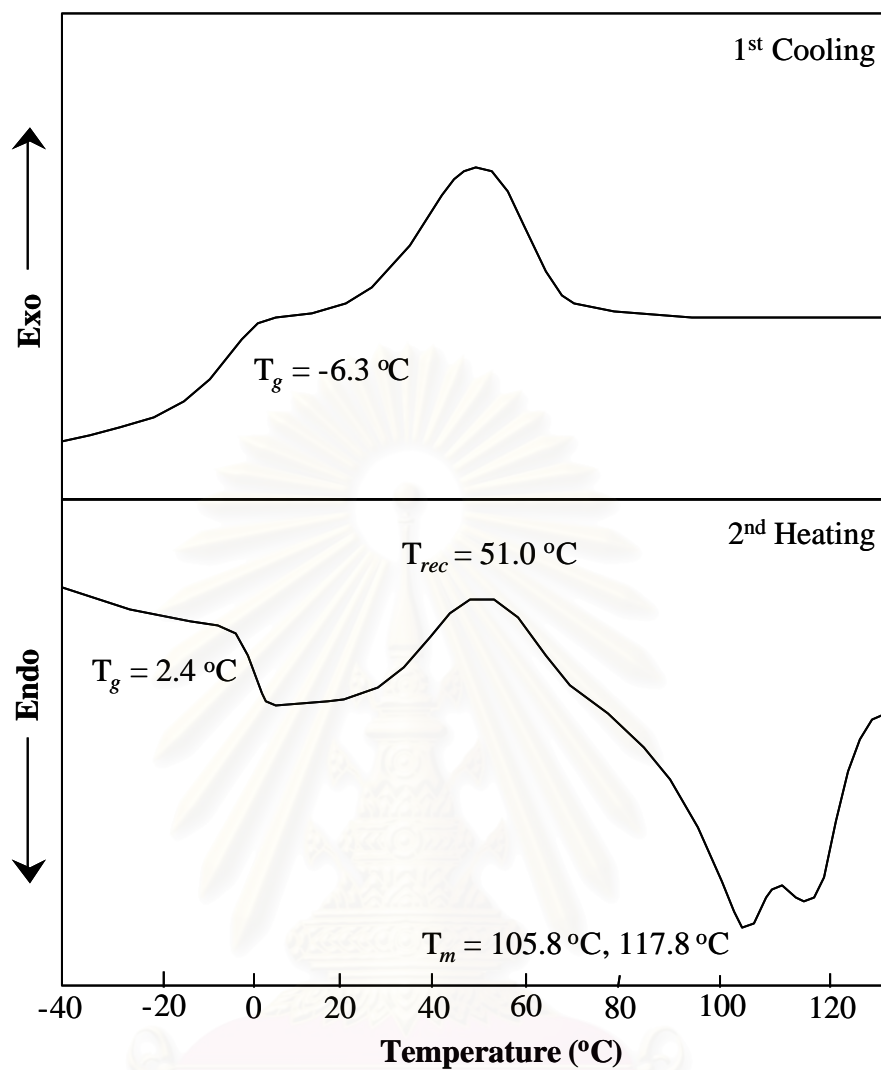


Figure 4.13 DSC curves of the first cooling scan (A) and second heating scan (B) of the chloroform solution-cast P(HB-co-HHx) sample; heating and cooling rates were 20 °C min^{-1} .

สถาบันวิทยบริการ
จุฬาลงกรณ์มหาวิทยาลัย

4.2 Thermally Induced Phase Transformation of PHB

4.2.1 Temperature-dependent Changes in the C=O Stretching Region

Figure 4.14 shows temperature-dependent IR spectra of PHB in the 1800-1680 cm^{-1} region where bands due to the C=O stretching modes appear. The band shape in this region changes largely from a sharp peak with a broad shoulder to a symmetrical broad band with increasing temperature.

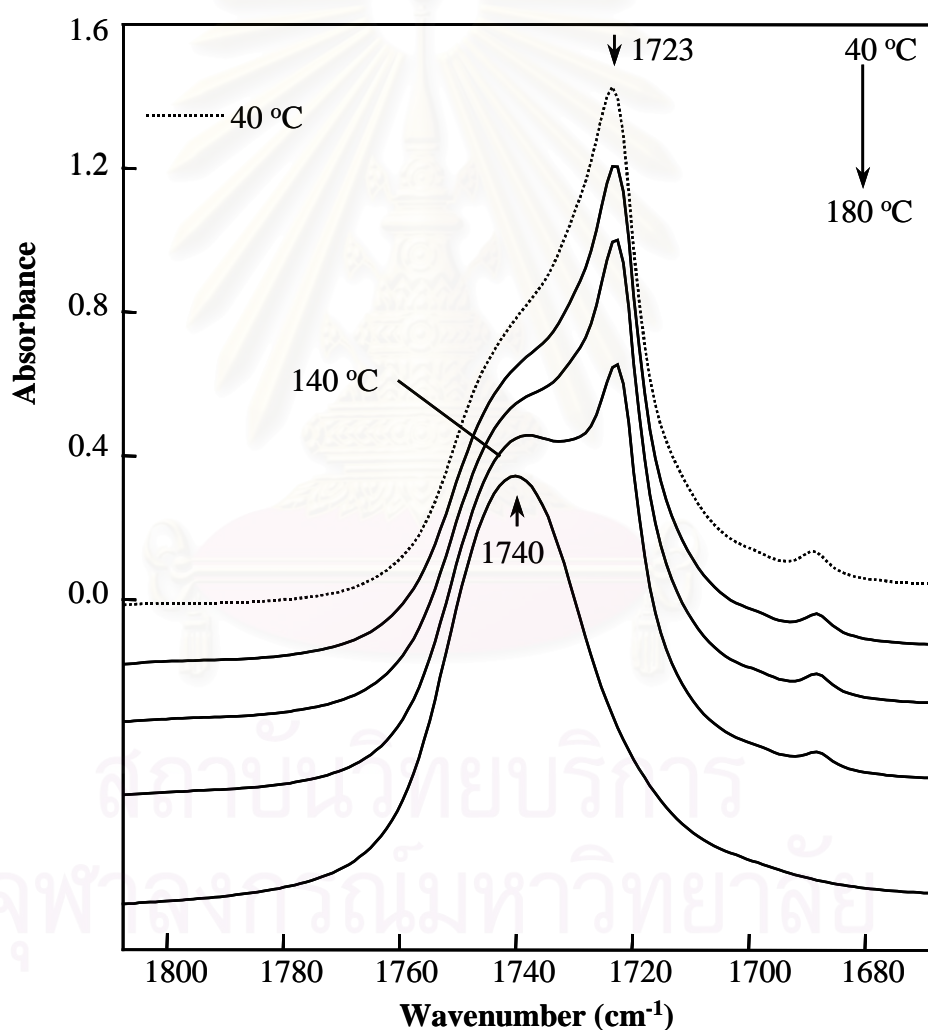


Figure 4.14 IR spectra of PHB in the C=O stretching region (1800-1680 cm^{-1}) collected over a temperature range of 40-180 °C.

A dramatic change in the IR spectra was observed in the vicinity of 140 °C. The

C=O stretching band region consists of at least two dominant bands. The sharp band at 1723 cm^{-1} arises from the crystalline C=O groups, and the broad band at 1740 cm^{-1} is attributed to the amorphous C=O groups [45]. The band at 1723 cm^{-1} decreases with increasing temperature and disappears above the T_m while the band at 1740 cm^{-1} gradually increases. The spectral changes observed in Figure 4.14 reflect the melting of PHB. The band at 1723 cm^{-1} is a unique indicator for monitoring the melting or crystallization process of PHA polymers.

There are two possible interpretations for the origin of the splitting of the C=O band observed below the T_m ; (1) an interaction between the C=O and CH_3 groups [42-44,46] and (2) a dipole-dipole coupling interaction between ester groups in an ordered structure [47-49].

The X-ray crystallographic studies of PHB showed that the distance between the C=O and CH_3 groups along the a axis is close enough for supposing the interactions between them. The temperature-dependent variations in WAXD patterns of PHB reveal that the lattice parameter a shows a significant change with the temperature increase. In other words, the thermal energy weakens the interactions along the a axis. The change in the interactions between the C=O and CH_3 groups may cause the change in the C=O stretching band. The sharp peak at 1723 cm^{-1} may arise from the C=O groups involved in the C=O and CH_3 interactions while the broad feature at 1740 cm^{-1} may be due to the free or non-interaction C=O groups.

Another possibility that causes the C=O band splitting is the transition dipole coupling of the ester groups in an ordered structure. For methyl acetate, which can be a model compound for the ester group incorporated in the main chain of PHB, the dipole practically lies along the C=O bond. Galbiati *et al.* [49] measured IR and Raman spectra of several aliphatic esters in gas, liquid, and solid phases. It was revealed that the observed frequencies of the C=O stretching vibrations ($\nu_{\text{C=O}}$) of the compounds can be grouped into three wavenumber regions for the three phases; (1) $\nu_{\text{C=O}} > 1760\text{ cm}^{-1}$ for the gas phase, (2) $1750\text{ cm}^{-1} > \nu_{\text{C=O}} > 1740\text{ cm}^{-1}$ for the liquid phase, and (3) $1730\text{ cm}^{-1} > \nu_{\text{C=O}} > 1720\text{ cm}^{-1}$ for the solid phase. They also performed MNDO (modified neglect of differential overlap) semiempirical quantum

chemical calculation for estimating the minimum-energy geometry and dipole moment and derived the following results: the dipole-dipole interaction causes a lower frequency shift of the C=O stretching band, and the maximum distance capable of producing a band splitting is not larger than *ca.* 4-5 Å. In polymer systems, a band splitting due to the dipole-dipole interaction is observed when the molecules form an ordered structure [48,50,51]. Torii and Tasumi [50,51] showed that the amide I bands of several proteins, which contain the ordered structures such as α -helix and β -sheet, are successfully reproduced by the model calculation based on the dipole-dipole coupling mechanism. Referring to the stereograph of the molecular structure for PHB in a crystalline state determined by XRD [9], the polymer chains form a helical structure, and the crystal lattice of the polymer contains two left-handed helical molecules in an antiparallel orientation. In the helical structure, the distance between the neighboring C=O groups along the chain is *ca.* 4-5 Å. Thus, the splitting of the C=O stretching band of PHB observed below the T_m possibly arises from the dipole-dipole interaction between the C=O groups in the crystalline structure.

To extract more detailed information about the spectral variations taking place during the phase transition process, 2D correlation spectroscopy was employed. Figure 4.15 A and B shows the synchronous and asynchronous 2D correlation spectra in the spectral region of 1780-1700 cm^{-1} generated from the temperature-dependent IR spectra measured over a temperature range of 40-150 °C, respectively. Two autopeaks developed at 1744 and 1724 cm^{-1} together with negative cross peaks at $\sim(1744, 1724) \text{ cm}^{-1}$ indicate the spectral variations of the amorphous and crystalline components of the PHB polymer. Three pairs of cross peaks are observed at $\sim(1744, 1731)$, $\sim(1744, 1722)$, and $\sim(1731, 1722) \text{ cm}^{-1}$ in the corresponding asynchronous spectrum. It should be noted that the existences of these bands are confirmed also by the second derivative of the spectrum of PHB at 40 °C shown in Figure 4.16. Although the band at 1731 cm^{-1} presents as a small peak in the second derivative spectrum, the asynchronous 2D spectrum clearly sorts out the existence of this band. The second derivative spectrum depicts two bands at 1748 and 1739 cm^{-1} in the amorphous region. These two bands, however, show no asynchronicity with each other in the 2D asynchronous spectrum. The positive synchronous spectral

intensity in the region containing the coordinate at $\sim(1731, 1722)$ cm^{-1} indicates the same direction of the intensity variations of these two bands while the negative synchronous spectral intensity containing the coordinates at $\sim(1744, 1731)$ and $\sim(1744, 1722)$ cm^{-1} suggests that the broad band located around 1744 cm^{-1} varies in the opposite direction from the two bands at 1731 and 1722 cm^{-1} .

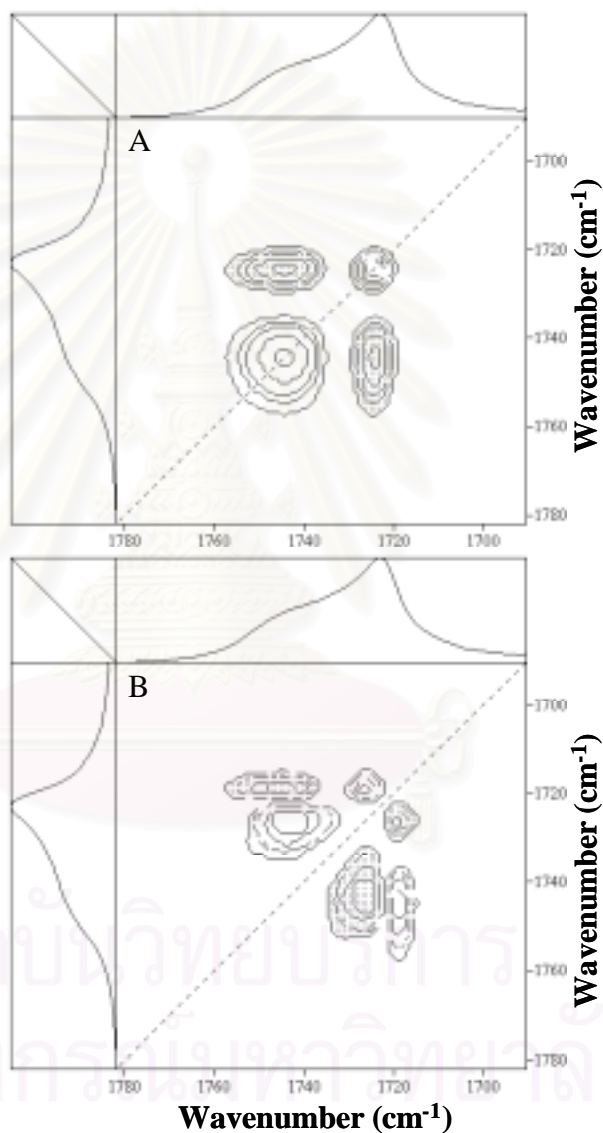


Figure 4.15 Synchronous (A) and asynchronous (B) correlation spectra of PHB in the C=O stretching region constructed from dynamic IR spectra in the melting process.

The highly overlapped bands located around 1744 and 1722 cm^{-1} are not resolved in the synchronous map because, unlike an asynchronous spectrum, which

is powerful in differentiating bands arising from different origins, a synchronous spectrum generally shows overall similarities of spectral variations. The frequencies of the bands in the C=O stretching region and their assignments are summarized in Table 4.1.

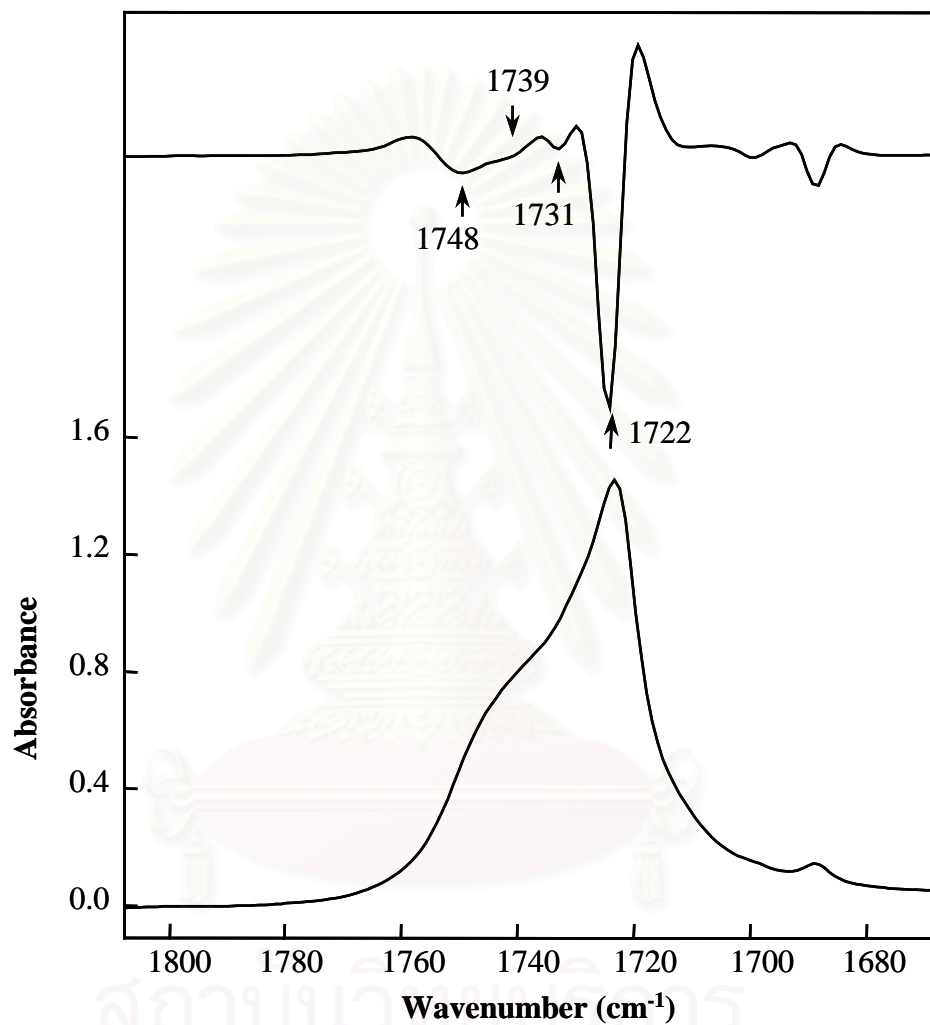


Figure 4.16 A second derivative spectrum calculated from the infrared spectrum of PHB in the C=O stretching region at 40 °C.

Of note in the asynchronous map is that there are asynchronous cross peaks between the crystalline and amorphous bands. This indicates that the decreases in the crystalline components and the increase in the amorphous component take place out of phase. It is very likely that the melting of PHB occurs through an intermediate state. However, no IR band due to the intermediate state is clearly detected.

Table 4.1 Assignments of IR bands in the C=O, C-O-C, and C-H stretching regions.

Functional groups	Wavenumber (cm ⁻¹)	Assignments
C=O	1748	amorphous
	1739	amorphous
	1731	crystalline
	1723	crystalline
C-O-C	1303	amorphous
	1294	crystalline
	1280	crystalline
	1263	crystalline
	1259	amorphous
	1230	crystalline
CH ₃	1183	amorphous
	3007	crystalline
	2995	crystalline
	2985	amorphous
	2975	crystalline
CH ₂	2967	crystalline
	2938	amorphous
	2934	crystalline
	2929	crystalline

The asynchronous 2D correlation spectrum resolves the two highly overlapped bands at 1731 and 1722 cm⁻¹ arising from the crystalline state. It can be seen from Figure 4.16 that the band at 1722 cm⁻¹ is much stronger than that at 1731 cm⁻¹. Based on its frequency and intensity, the band at 1722 cm⁻¹ may be assigned to the C=O stretching mode of the well-ordered crystalline state of PHB [45]. The minor band at 1731 cm⁻¹ may be due to the C=O stretching mode of the less ordered crystalline part of the polymer [45].

4.2.2 Temperature-dependent Changes in the C-O-C Stretching Region

Figure 4.17 shows the temperature-dependent changes in the IR spectra of PHB

in the $1320\text{-}1120\text{ cm}^{-1}$ region. A cluster of bands in this region is ascribed to the stretching vibrations of the C-O-C groups [45]. Although this region contains more bands than the C=O stretching region, the spectral changes caused by the melting process of the polymer are clear. The intensities of the bands at 1294 , 1280 , 1263 , and 1230 cm^{-1} decrease upon passing from the crystalline to the amorphous state of the polymer while those of the bands at 1303 , 1259 , and 1183 cm^{-1} increase in the course of temperature increase.

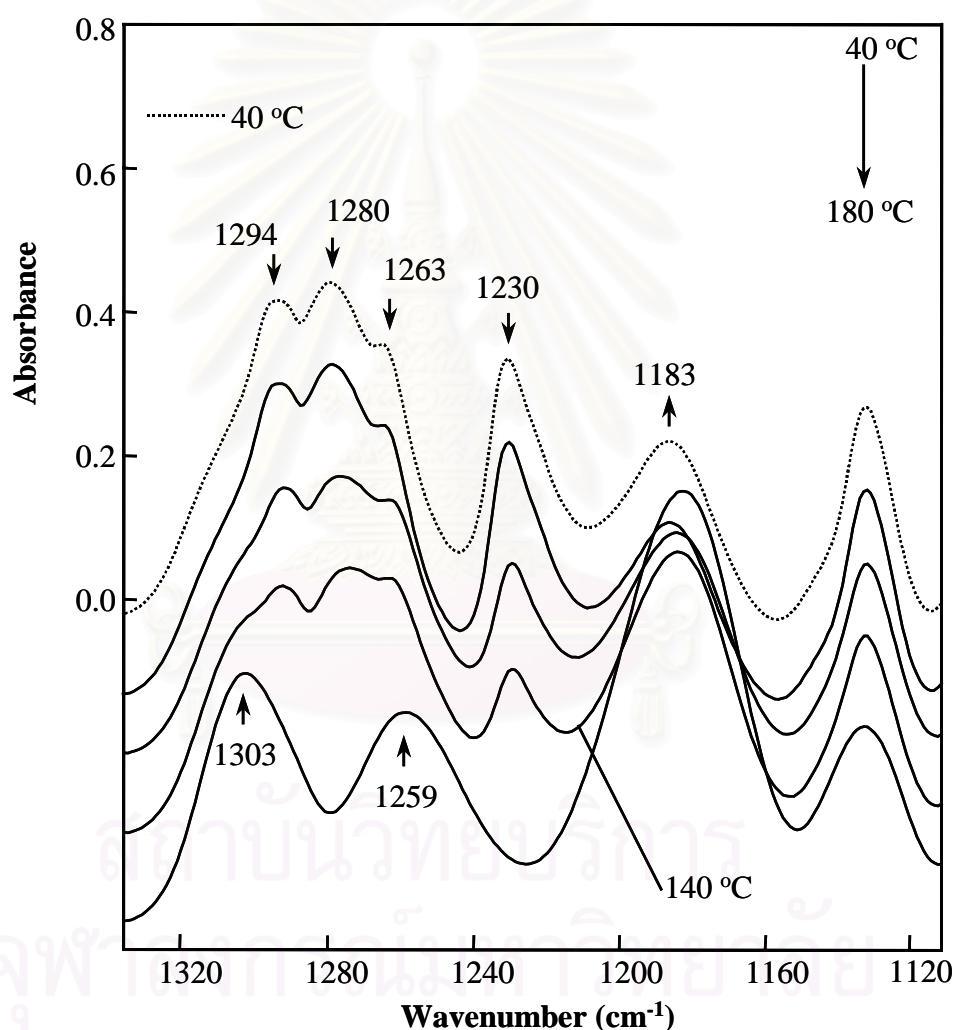


Figure 4.17 IR spectra of PHB in the C-O-C stretching region ($1320\text{-}1120\text{ cm}^{-1}$) collected over a temperature range of $40\text{-}180\text{ }^{\circ}\text{C}$.

The synchronous and asynchronous 2D correlation spectra in the $1330\text{-}1155\text{ cm}^{-1}$ region calculated from the temperature-dependent IR spectra of PHB are shown

in Figure 4.18 A and B, respectively. There are at least four autopeaks at 1294, 1254, 1230, and 1180 cm^{-1} . The autopeak at 1294 cm^{-1} extends to the vicinity of 1280 cm^{-1} , and that near 1180 cm^{-1} is very broad. Thus, it seems that both autopeaks consist of more than one peak.

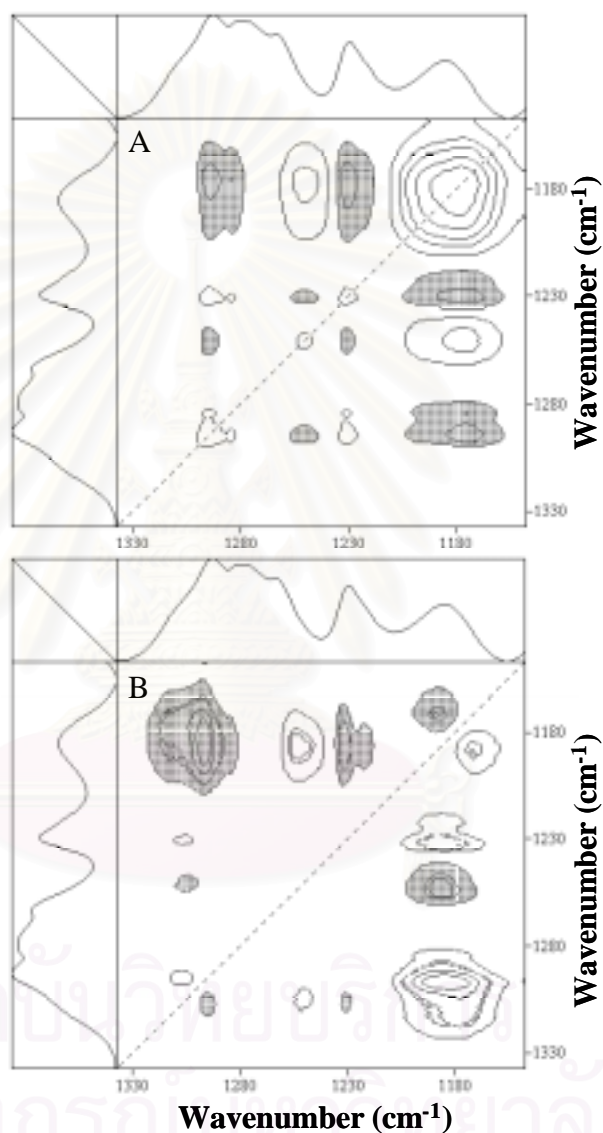


Figure 4.18 Synchronous (A) and asynchronous (B) correlation spectra of PHB in the C-O-C stretching region constructed from dynamic IR spectra in the melting process.

It is noted that the crystalline bands at 1294, 1280, 1263, and 1230 cm^{-1} do not share any asynchronous cross peak, and that there are several cross peaks between an

amorphous band (*e.g.*, 1180 cm^{-1}) and crystalline bands (*e.g.*, $\sim 1294\text{-}1280\text{ cm}^{-1}$ and 1230 cm^{-1}). These observations again indicate the existence of an intermediate state during the phase transition. The frequencies of the bands in the C-O-C stretching region and their assignments are summarized in Table 4.1.

4.2.3 Temperature-dependent Changes in the C-H Stretching Region

The temperature-dependent changes in the IR spectra of PHB in the $3100\text{-}2850\text{ cm}^{-1}$ region are shown in Figure 4.19. For the C-H stretching region, bands located around 2980 cm^{-1} are due to the CH_3 asymmetric stretching mode while those appear around 2930 cm^{-1} are attributed to the CH_2 antisymmetric stretching vibration. For PHB, the CH_3 group exists only on the side chain while the CH_2 group is located on the skeletal chain. As described in the INTRODUCTION, the chemical modification on the side chain of PHB is very important for improving its mechanical properties. Therefore, the investigation on the thermal behavior of the CH_3 group is very interesting.

As temperature increases, the CH_3 stretching band at 2975 cm^{-1} decreases while that at 2985 cm^{-1} increases. Similarly, the CH_2 stretching band at 2934 cm^{-1} decreases while that at 2938 cm^{-1} increases with increasing temperature. Note that at room temperature, there exist two peaks at 3007 and 2995 cm^{-1} , but they disappear at $180\text{ }^\circ\text{C}$. These two bands and the band at 2975 cm^{-1} may be ascribed to the crystalline CH_3 stretching bands resulting from the crystal field splitting of the band at 2985 cm^{-1} . Crystal field splittings of bands occur in some semi-crystalline polymers [23]. The crystal field splitting may be caused not only by the intramolecular interaction between analogous functional groups attached along a polymer chain but also by the intermolecular interaction between those groups located in the crystalline lattice. The crystalline band splittings of certain vibration modes have been reported for a number of polymers especially those having a helical chain structure [23]. The second derivatives of the IR spectra of PHB in this region for the amorphous (at $180\text{ }^\circ\text{C}$) and crystalline (at $40\text{ }^\circ\text{C}$) states are shown in Figure 4.20. Two additional bands at 2967 and 2929 cm^{-1} are detected in the second derivative spectrum for the crystalline state.

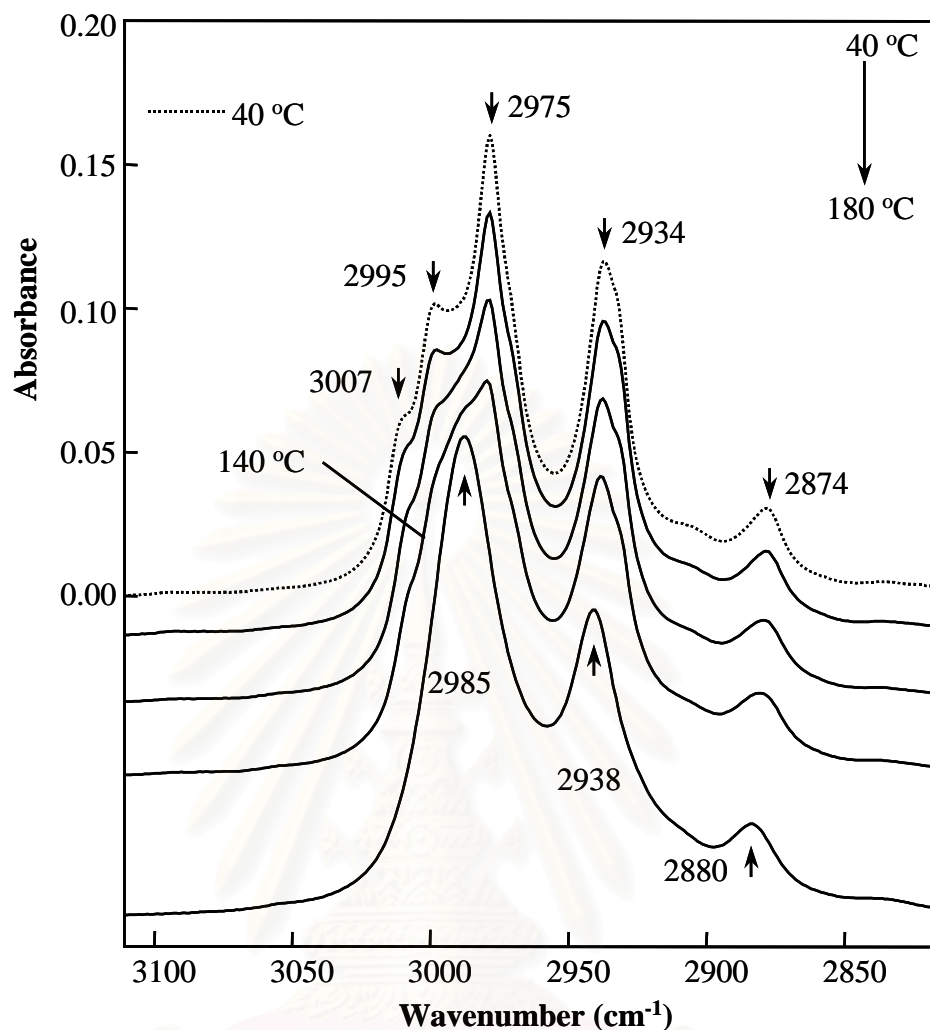


Figure 4.19 IR spectra of PHB in the C-H stretching region ($3100\text{-}2850\text{ cm}^{-1}$) collected over a temperature range of $40\text{-}180\text{ }^{\circ}\text{C}$.

Figure 4.21 A and B shows the synchronous and asynchronous 2D correlation spectra in the $3020\text{-}2915\text{ cm}^{-1}$ region constructed from the temperature-dependent IR spectra. Four autopeaks are clearly observed at 3009 , 2985 , 2975 , and 2930 cm^{-1} in the synchronous spectrum. The three peaks at 3009 , 2975 , and 2930 cm^{-1} share three positive cross peaks at $(3009, 2975)$, $(3009, 2930)$, and $(2975, 2930)\text{ cm}^{-1}$, and the peak at 2985 cm^{-1} shares negative cross peaks with those at 3009 , 2975 , and 2930 cm^{-1} . These observations confirm that the three bands at 3009 , 2975 , and 2930 cm^{-1} vary in the same direction, which is opposite to that of the band at 2985 cm^{-1} , with the change in temperature.

The asynchronous map and the second derivatives reveal that there are three bands at ~ 2940 , 2934 , and 2929 cm^{-1} assignable to the antisymmetric CH_2 stretching mode. The amorphous band at 2985 cm^{-1} shares asynchronous cross peaks with the crystalline bands at 3009 , 2975 , 2934 , and 2929 cm^{-1} . This observation also suggests that the amorphous phase does not appear simultaneously with the disappearance of the crystalline state. The synchronous and asynchronous 2D correlation spectra in the C-H stretching region reveal clearly that the intensity changes of all crystalline bands in this region occur simultaneously, *i.e.*, there is no asynchronicity between any crystalline band in the C-H stretching region. Therefore, it is very likely that the crystalline bands observed in this region are caused by the crystal field splittings.

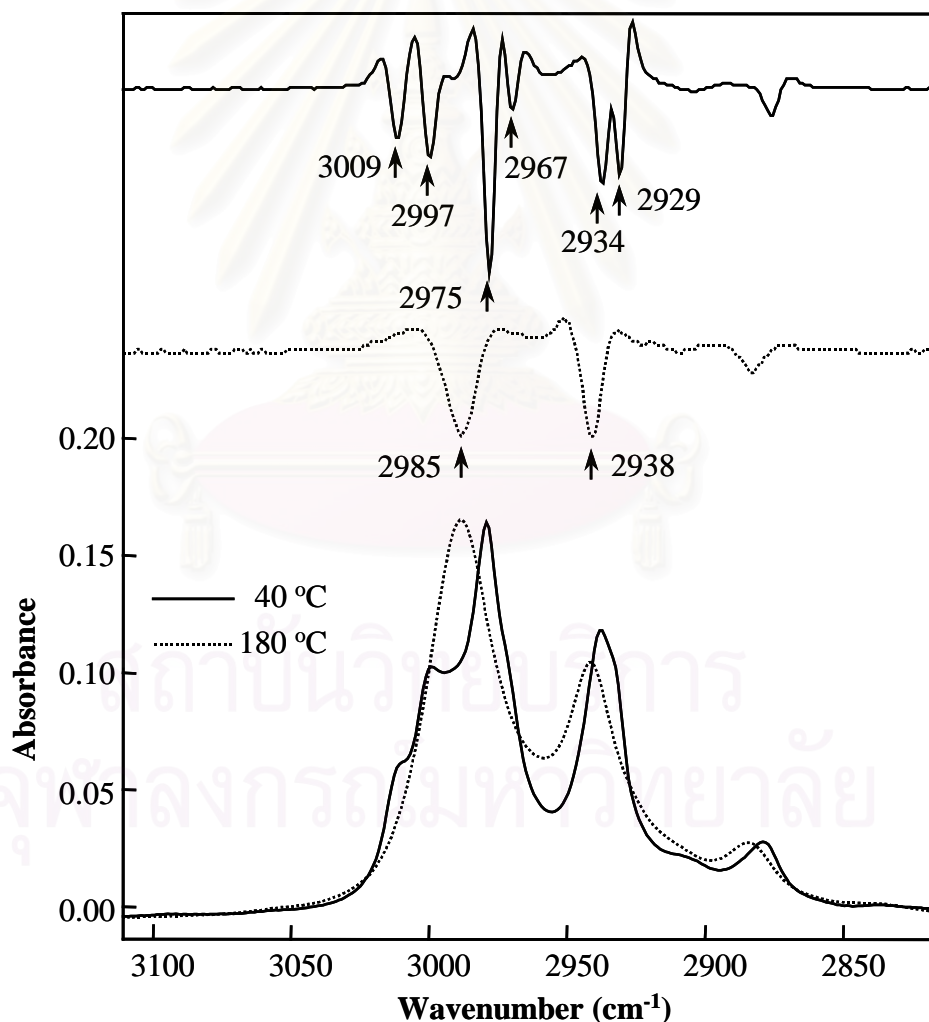


Figure 4.20 Second derivative spectra calculated from the infrared spectra of PHB in the C-H stretching region at 40 and 180 °C.

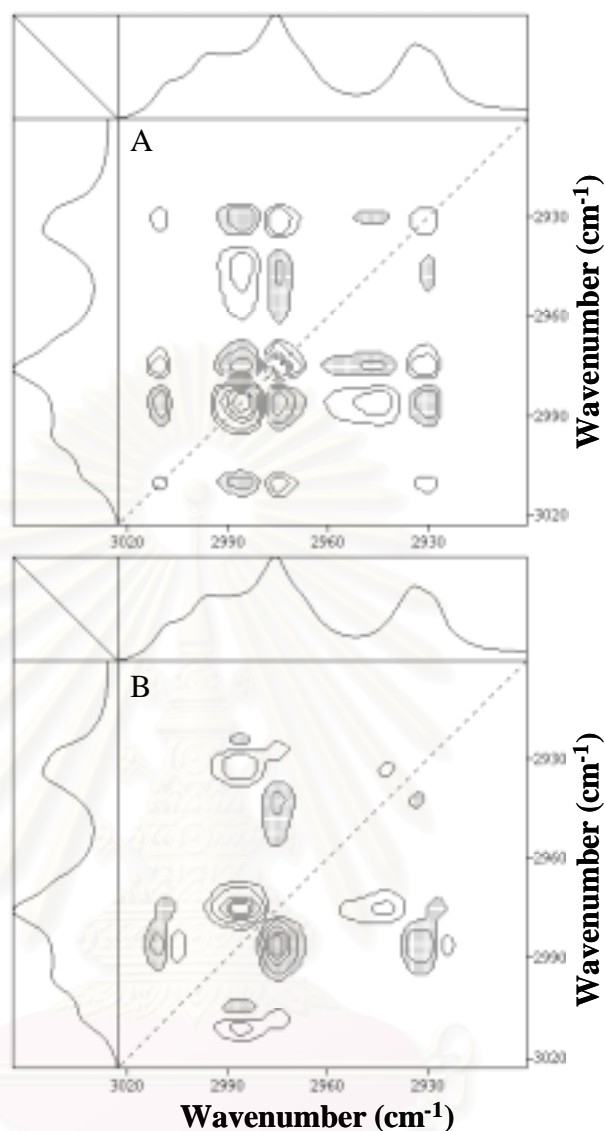


Figure 4.21 Synchronous (A) and asynchronous (B) correlation spectra of PHB in the C-H stretching region constructed from dynamic IR spectra in the melting process.

A synchronous 2D correlation spectrum between the C=O and C-H stretching regions was generated from the temperature-dependent IR spectra and is demonstrated in Figure 4.22. The synchronous cross peaks and their signs at the spectral coordinates of 1745 and 1725 cm^{-1} vs 3009, 2986, 2975, and 2930 cm^{-1} clarify that the bands located at 3007, 2975, 2934, and 2929 cm^{-1} arise from the crystalline part of the polymer while the band at 2985 cm^{-1} is ascribed to the amorphous part. The frequencies of the bands in the C-H stretching region and their

assignments are summarized in Table 4.1.

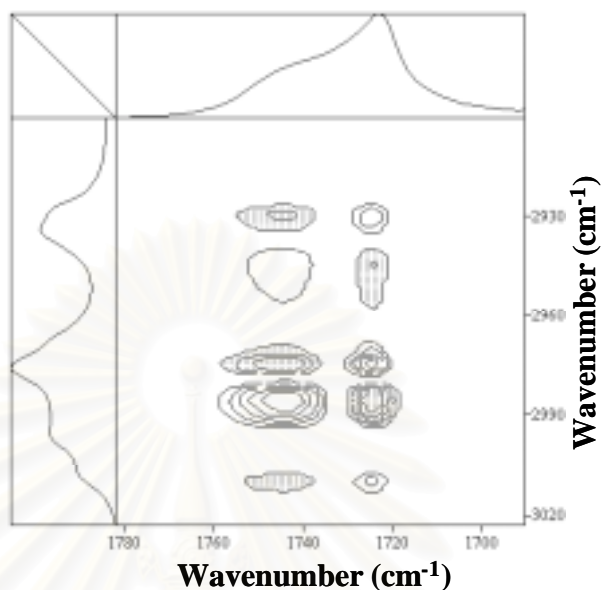


Figure 4.22 Hetero-correlation synchronous spectrum of PHB between the C=O and C-H stretching regions constructed from dynamic IR spectra in the melting process.

The temperature-dependent IR spectra of PHB during a cooling down process were also measured. 2D correlation maps for the C=O region show the similar patterns to those shown in Figure 4.15. That is, in the crystallization process of PHB, the decrease in the amorphous component and the increase in the crystalline component do not take place simultaneously.

4.3 Thermally Induced Phase Transformation of P(HB-*co*-HHx)

4.3.1 Temperature-dependent Changes in the C=O Stretching Region

Figure 4.23 shows temperature-dependent IR spectra of P(HB-*co*-HHx) in the 1780-1680 cm^{-1} region. A sharp band at 1723 cm^{-1} gradually decreases and eventually disappears with increasing temperature while a broad band at 1740 cm^{-1} increases in intensity. The band shape in the C=O stretching region changes markedly in the course of temperature increase. The sharp peak at 1723 cm^{-1} is

assigned to the crystalline C=O band while the broad band located at 1740 cm^{-1} is attributed to the amorphous C=O band [52]. The C=O group is very sensitive to its environment and particularly useful for monitoring the crystallization and melting processes of polymers in this class. The splitting of the C=O bands into the amorphous and crystalline bands observed at 1740 and 1723 cm^{-1} , respectively, in the IR spectra of P(HB-*co*-HHx) is also observed in those of PHB.

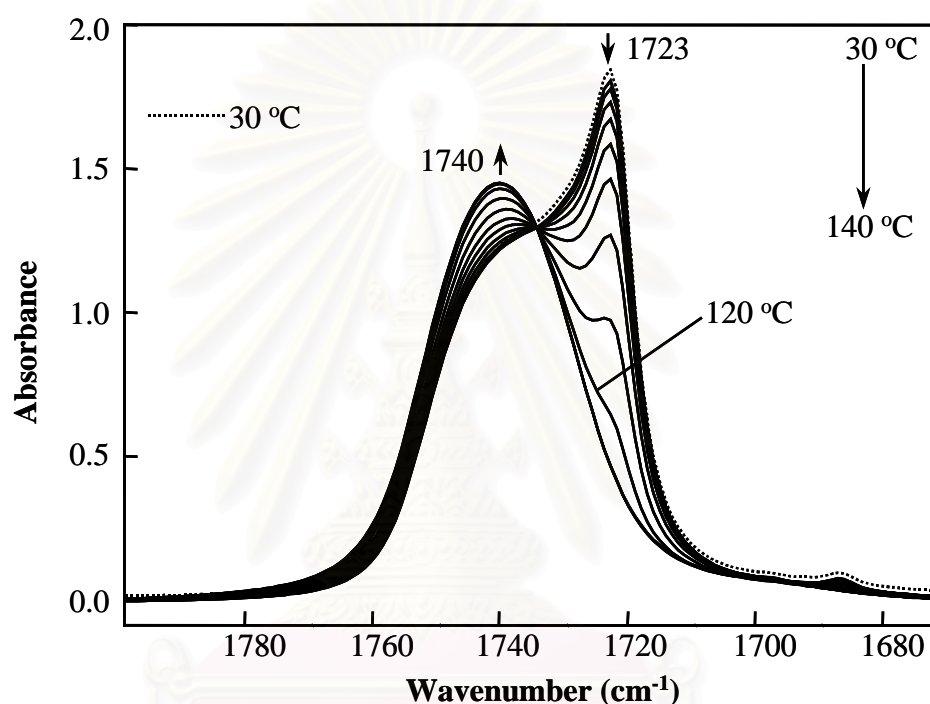


Figure 4.23 IR spectra of P(HB-*co*-HHx) in the C=O stretching region ($1780\text{-}1680\text{ cm}^{-1}$) measured over a temperature range of $30\text{-}140\text{ }^{\circ}\text{C}$.

To gain more detailed information about the spectral variations induced by the melting process, 2D correlation spectroscopy was employed. Figure 4.24 A and B shows the synchronous and asynchronous 2D correlation spectra in the spectral region of $1790\text{-}1670\text{ cm}^{-1}$ generated from the temperature-dependent IR spectra measured over the temperature range of $30\text{-}140\text{ }^{\circ}\text{C}$, respectively. Two autopeaks located at 1745 and 1723 cm^{-1} reflect the spectral variations due to the amorphous and crystalline components of the polymer, respectively.

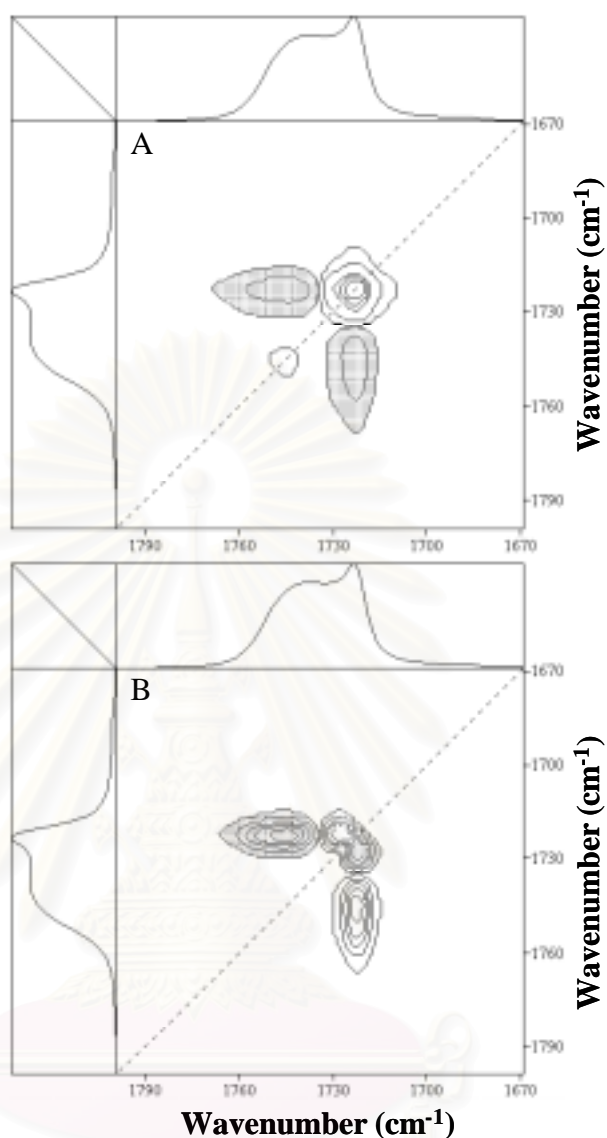


Figure 4.24 Synchronous (A) and asynchronous (B) correlation spectra of P(HB-*co*-HHx) in the C=O stretching region generated from the temperature-dependent IR spectra measured over a temperature range of 30-140 °C.

A pair of negative cross peaks developed at (1745, 1723) cm^{-1} in the synchronous spectrum indicates the opposite directions of the intensity variations in these two correlated bands. In the asynchronous spectrum, two pairs of cross peaks appear at (1745, 1722) and (1728, 1722) cm^{-1} . Note that in the original one-dimensional IR spectra, similar to PHB, only two absorption bands ascribed to the crystalline (*i.e.*, the band at 1723 cm^{-1}) and amorphous (*i.e.*, the band at 1740 cm^{-1}) parts of the copolymer are apparent, but another band is clearly sorted out at 1728

cm^{-1} in the 2D asynchronous spectrum. The existence of this band is confirmed also by the second derivative of the spectrum of P(HB-*co*-HHx) measured at 30 °C shown in Figure 4.25. The second derivative spectrum yields clear indication for the presence of the band around 1731 cm^{-1} , which is consistent with the cross peak developed in the 2D asynchronous spectrum.

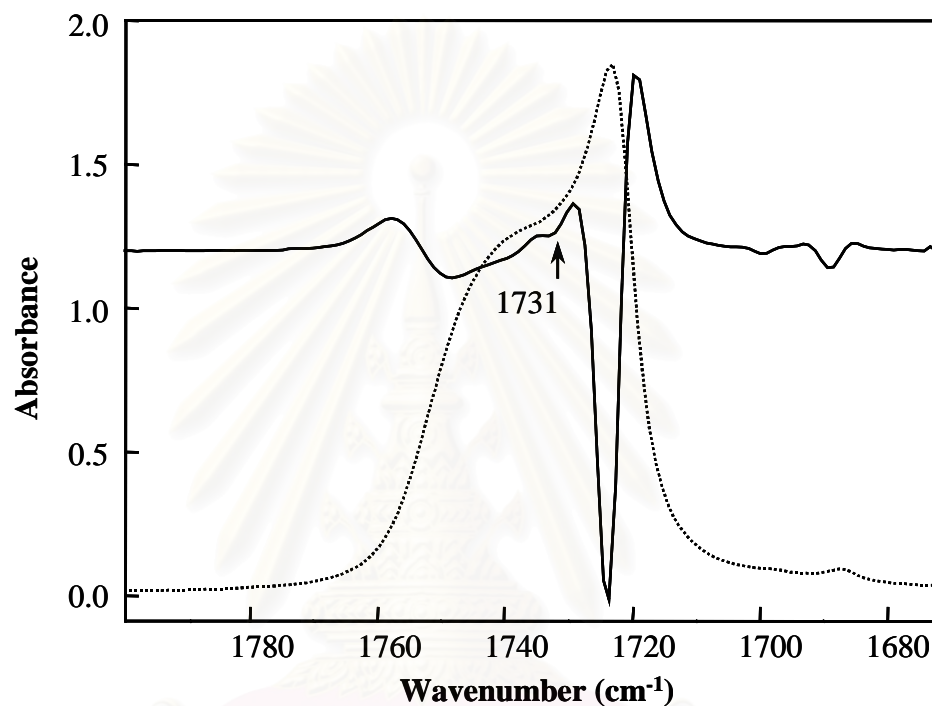


Figure 4.25 A second derivative spectrum calculated from the IR spectrum of P(HB-*co*-HHx) in the C=O stretching region at 30 °C.

The positive sign of the synchronous spectral intensity in the region containing the (1731, 1723) cm^{-1} coordinates indicates the same direction of the intensity variations in these two bands. The band at 1723 cm^{-1} is much more intense than that at 1731 cm^{-1} . Based on its frequency and band intensity, the band at 1723 cm^{-1} is assigned to the C=O stretching mode of the major crystalline component of P(HB-*co*-HHx). The weaker band at 1731 cm^{-1} may arise from the C=O stretching mode of the less ordered crystalline component of the copolymer [52]. These two highly overlapped crystalline bands are distinguished only in the 2D asynchronous spectrum because an asynchronous spectrum is very powerful in differentiating bands arising from different origins.

Of note in the 2D asynchronous spectrum shown in Figure 4.24 B is that there are asynchronous cross peaks between the crystalline and amorphous bands. This observation clearly indicates that the melting of the crystalline component does not proceed simultaneously with the formation of the completely amorphous component. It is very likely that the melting of P(HB-*co*-HHx) also takes place through an intermediate state. The existence of an intermediate state during the melting process was reported for some other polymers including PHB [12-14,45].

4.3.2 Temperature-dependent Changes in the C-O-C Stretching Region

Figure 4.26 shows temperature-dependent IR spectra of P(HB-*co*-HHx) in the 1320-1160 cm^{-1} region. Bands in this region are attributed to the stretching vibration modes of the C-O-C groups [52].

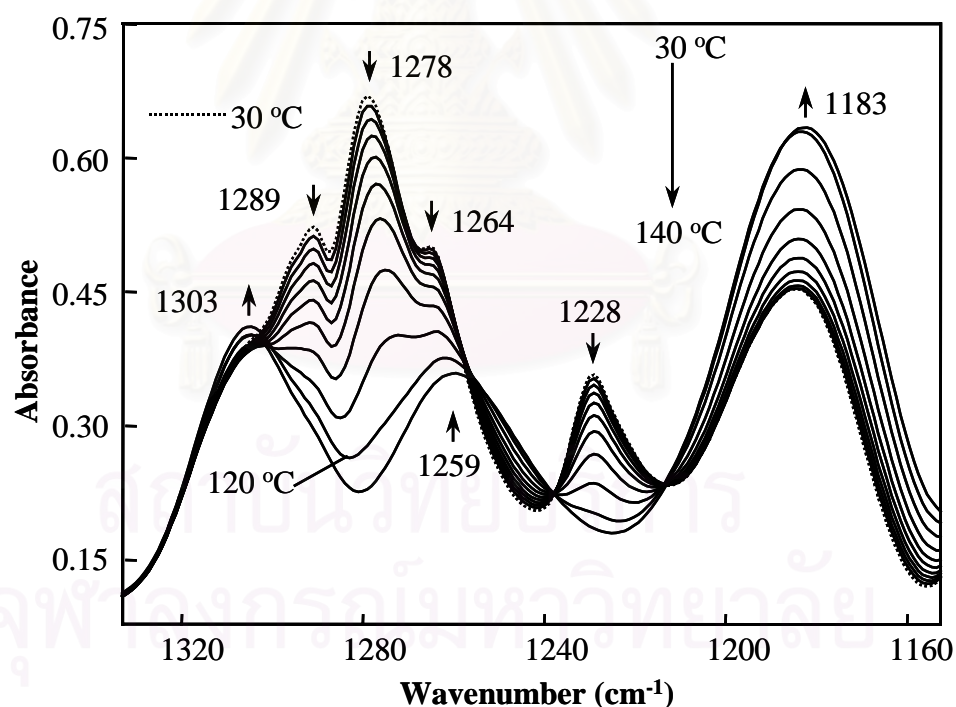


Figure 4.26 IR spectra of P(HB-*co*-HHx) in the C-O-C stretching region ($1320\text{-}1160\text{ cm}^{-1}$) measured over a temperature range of $30\text{-}140\text{ }^{\circ}\text{C}$.

It can be seen from Figure 4.26 that these bands change largely during the

melting process of P(HB-*co*-HHx). Bands at 1289, 1278, 1264, and 1228 cm^{-1} decrease with increasing temperature while three broad bands at 1303, 1259, and 1183 cm^{-1} are dominant above the T_m of the polymer. Therefore, the four bands at 1289, 1278, 1264, and 1228 cm^{-1} are ascribed to the crystalline component, and the three bands at 1303, 1259, and 1183 cm^{-1} are attributed to the amorphous part.

The synchronous and asynchronous 2D correlation spectra in the region of 1330-1150 cm^{-1} generated from the temperature-dependent IR spectra of P(HB-*co*-HHx) are shown in Figure 4.27 A and B, respectively. There are at least three autopeaks at 1280, 1230, and 1180 cm^{-1} . Negative and positive 2D synchronous cross peaks at (1280, 1180), (1180, 1230), and (1280, 1230) cm^{-1} reveal that the intensities of the bands located near 1280 and 1230 cm^{-1} (the crystalline bands) vary in the same direction, which is opposite to the intensity variations in the bands near 1180 cm^{-1} (the amorphous bands), in the course of melting. It is noted in Figure 4.27 B that there are several asynchronous cross peaks between amorphous bands (*e.g.*, bands near 1183 cm^{-1}) and crystalline bands (*e.g.*, bands near ~1289-1278 cm^{-1} and 1230 cm^{-1}). This observation again indicates the existence of an intermediate state during the phase transition of the polymer. It is very likely that the appearance of the asynchronous cross peaks at (1289, 1272) and (1280, 1272) cm^{-1} is caused by the band shift, and that at (1188, 1170) cm^{-1} is due to the band broadening and the baseline shift [53,54]. As can be seen from the original IR spectra (Figure 4.26) and the second derivatives (Figure 4.28) that there exist a large shift of the band at 1278 cm^{-1} and band broadening as well as a baseline shift of the band at 1183 cm^{-1} in the course of temperature increase.

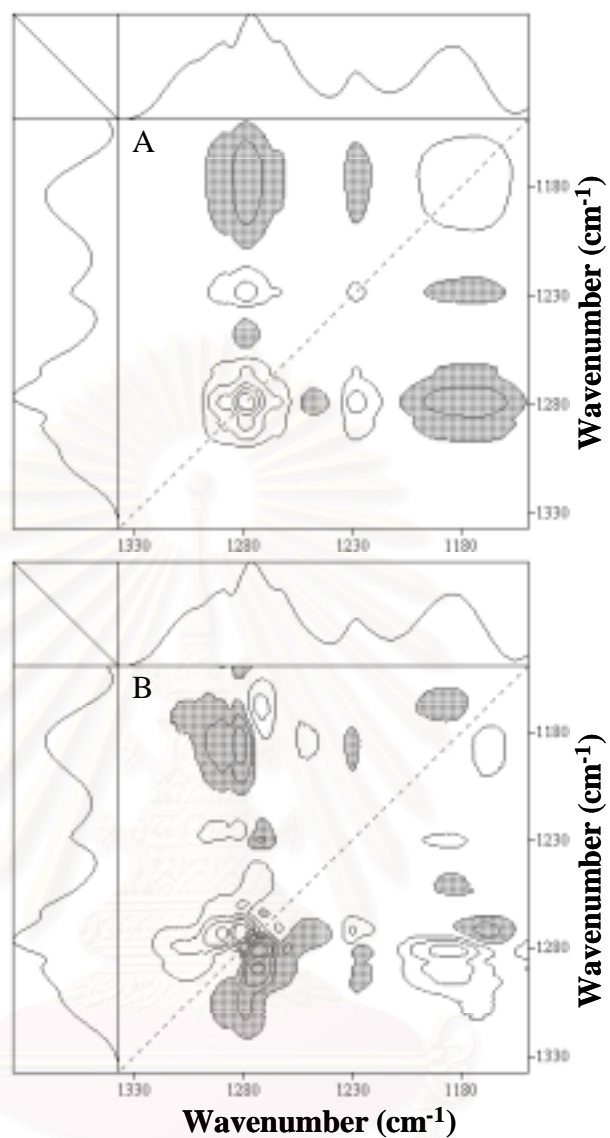


Figure 4.27 Synchronous (A) and asynchronous (B) correlation spectra of P(HB-*co*-HHx) in the C-O-C stretching region generated from the temperature-dependent IR spectra measured over a temperature range of 30-140 °C.

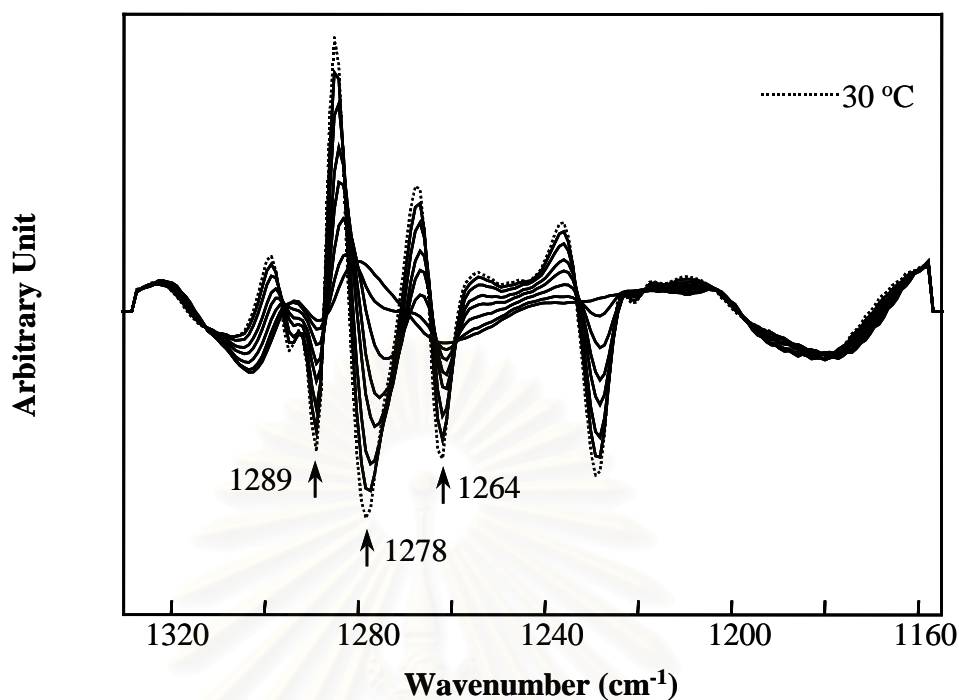


Figure 4.28 Second derivative spectra calculated from the IR spectra of P(HB-*co*-HHx) in the C-O-C stretching region over a temperature range of 30-140 °C.

4.3.3 Temperature-dependent Changes in the C-H Stretching Region

The structural difference between P(HB-*co*-HHx) and PHB lies in the length of the alkyl side chain attached to the polymer backbone. Accordingly, the temperature-dependent spectral variations in the CH₃ and CH₂ stretching band regions are important to reveal differences or similarities in the thermally induced microenvironmental changes of the side chains of these two polymers. Figure 4.29 shows temperature-dependent IR spectra of P(HB-*co*-HHx) in the region of 3050-2850 cm⁻¹. Bands around 2980 cm⁻¹ are attributed to the CH₃ asymmetric stretching modes while those due to the CH₂ antisymmetric stretching vibrations are identified around 2930 cm⁻¹. With the temperature increase, the CH₃ stretching band at 2975 cm⁻¹ decreases while that at 2984 cm⁻¹ increases in intensity. Similarly, the CH₂ stretching band at 2934 cm⁻¹ decreases and that at 2937 cm⁻¹ increases in intensity on passing from the crystalline to the amorphous phase. Bands in this region are highly overlapped. The second derivatives of the spectra of P(HB-*co*-HHx) at 30 and

140 °C were calculated and are shown in Figure 4.30. It can be seen from the second derivative spectrum of P(HB-*co*-HHx) at 30 °C that there are at least four major bands at 3008, 2997, 2975, and 2966 cm^{-1} in the CH_3 asymmetric stretching band region. For the CH_2 antisymmetric stretching band region, two bands at 2934 and 2927 cm^{-1} are shown up. These bands may be attributed to the crystalline bands arising from the crystal field splitting, which occurs in some semicrystalline polymers.

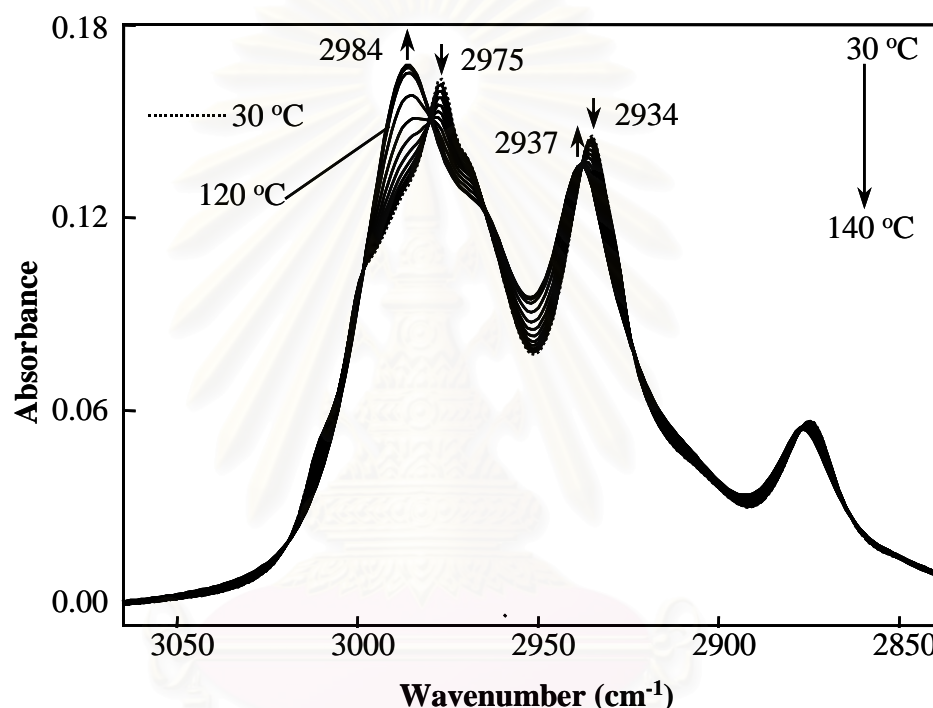


Figure 4.29 IR spectra of P(HB-*co*-HHx) in the C-H stretching region ($3050\text{-}2850\text{ cm}^{-1}$) measured over a temperature range of $30\text{-}140\text{ }^{\circ}\text{C}$.

Figure 4.31 A and B shows the synchronous and asynchronous 2D correlation spectra in the $3020\text{-}2900\text{ cm}^{-1}$ region generated from the temperature-dependent IR spectra. Four autopeaks are observed at 2985, 2975, 2944, and 2930 cm^{-1} in the synchronous spectrum. The band at 2985 cm^{-1} shares three negative synchronous cross peaks with the bands at 3008, 2975, and 2930 cm^{-1} . This indicates that the intensities of the bands at 3008, 2975, and those around 2930 cm^{-1} vary in the opposite direction to that of the band at 2985 cm^{-1} , with the change in temperature. In the corresponding asynchronous spectrum, the amorphous band at 2985 cm^{-1}

shares asynchronous cross peaks with the crystalline bands at 3007 and 2975 cm^{-1} . This observation also suggests that the completely amorphous component is not formed simultaneously with the melting of the crystalline component.

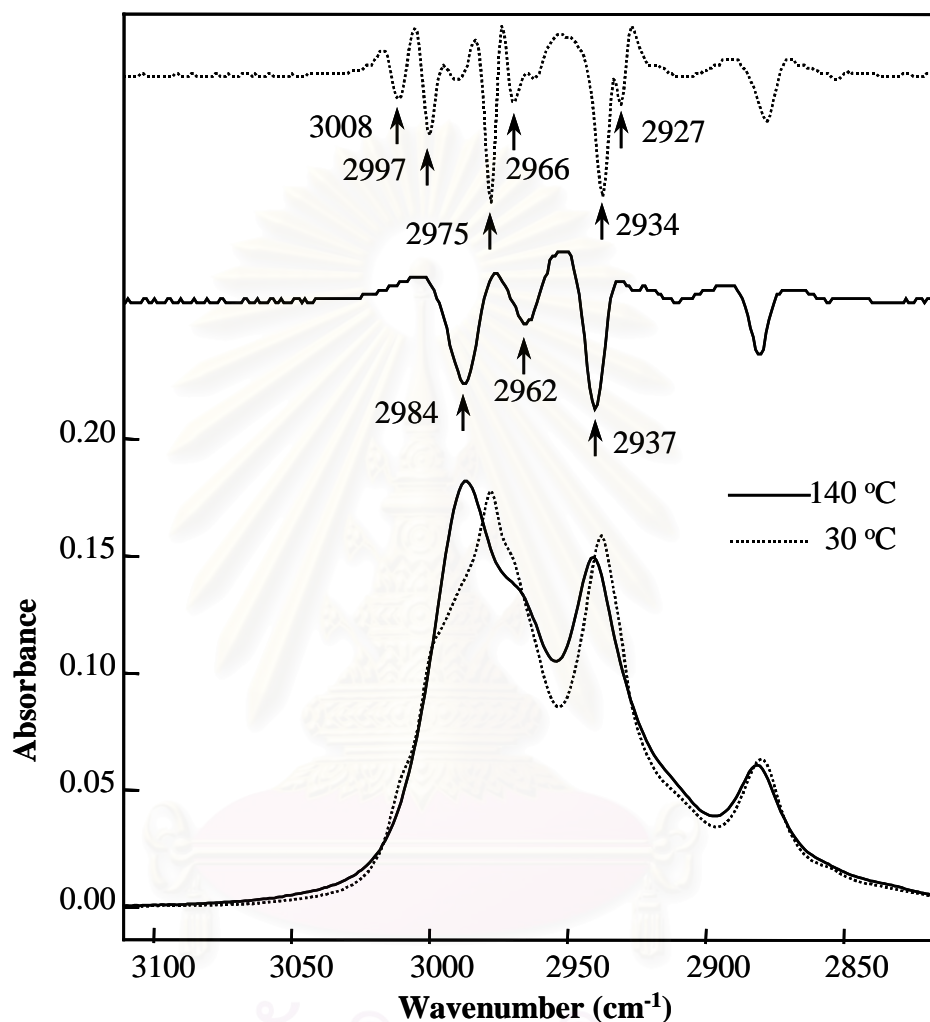


Figure 4.30 Second derivative spectra calculated from the IR spectra of P(HB-*co*-HHx) in the C-H stretching region at 30 and 140 °C.

Interestingly, a band at 2962 cm^{-1} observed in the C-H stretching region for P(HB-*co*-HHx) (Figure 4.30) is absent in that for PHB. Therefore, it is very likely that this band is attributed to the CH_3 asymmetric stretching mode of the side-chain group (propyl, $-\text{CH}_2\text{CH}_2\text{CH}_3$) incorporated in P(HB-*co*-HHx). It should be noted that no peak emerges at 2962 cm^{-1} in the 2D synchronous spectrum shown in Figure 4.31 A. This indicates that the temperature-induced intensity change in this band is

not prominent. In other words, the crystalline/amorphous phase transition of P(HB-*co*-HHx) does not strongly affect the behavior of the propyl side-chain groups. This is consistent with the fact that the propyl group is attached to the HHx comonomer, which functions as a less crystallizable unit in P(HB-*co*-HHx).

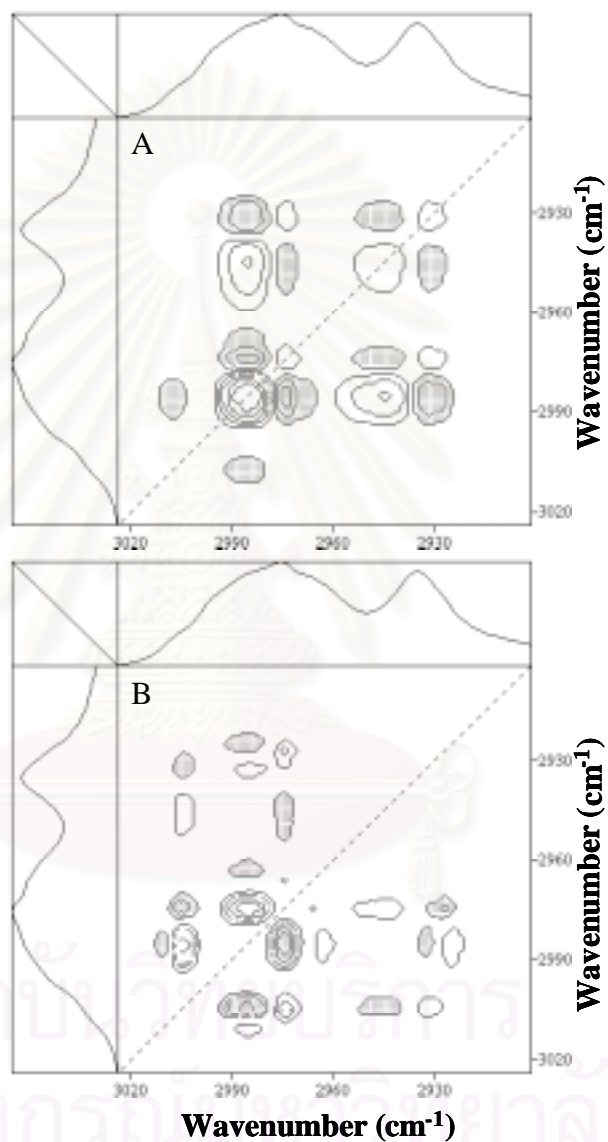


Figure 4.31 Synchronous (A) and asynchronous (B) correlation spectra of P(HB-*co*-HHx) in the C-H stretching region generated from the temperature-dependent IR spectra measured over a temperature range of 30-140 °C.

4.3.4 Spectral Changes during the Cooling Down Process

Temperature-perturbed IR spectral variations in the C=O stretching band region of P(HB-*co*-HHx) observed during the cooling down process were also investigated. IR spectra in the 1780-1680 cm^{-1} region collected as a function of decreasing temperature are shown in Figure 4.32.

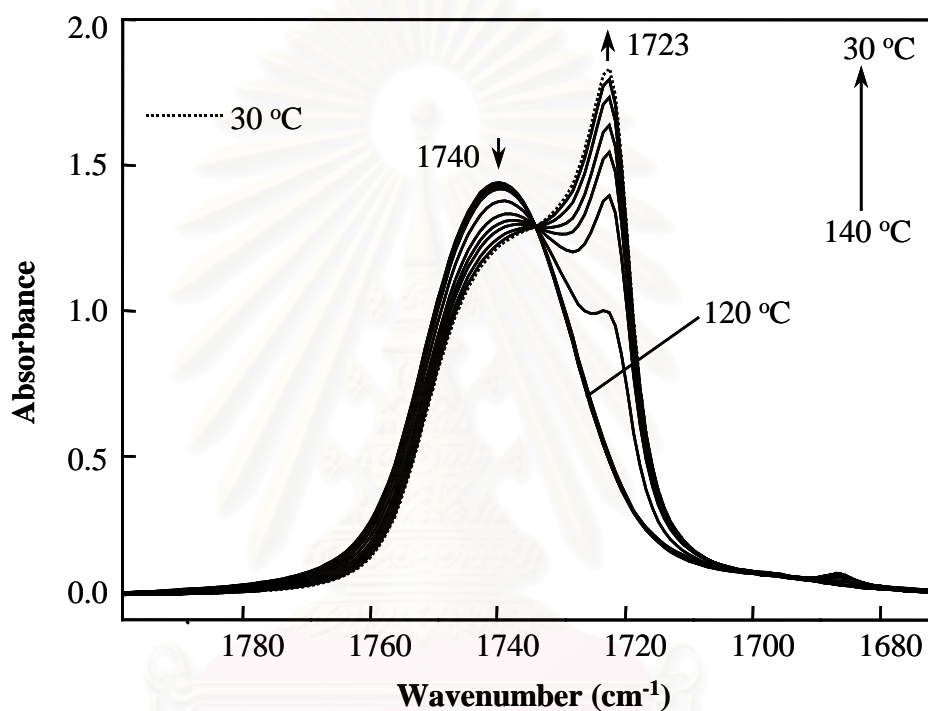


Figure 4.32 IR spectra of P(HB-*co*-HHx) in the C=O stretching region measured over a temperature range of 140-30 °C (cooling down process).

Figure 4.33 A and B shows synchronous and asynchronous 2D correlation spectra generated from the temperature-dependent IR spectra in the C=O stretching band region for the cooling down process, respectively. The pattern of the 2D asynchronous contour plot is almost the same as that for the melting process (Figure 4.24 B) except the signs of the cross peaks. It can be seen from Figure 4.32 that the amorphous C=O band at 1740 cm^{-1} decreases with the temperature decrease, and that the crystalline band at 1723 cm^{-1} appears at around 110 °C and develops down to room temperature. Two pairs of asynchronous cross peaks are developed at the same coordinates as those in the asynchronous spectrum generated for the melting process.

This observation also indicates the coexistence of two crystalline C=O bands, and suggests that, in the crystallization process, the formation of the crystalline component does not proceed simultaneously with the decrease in the amorphous component.

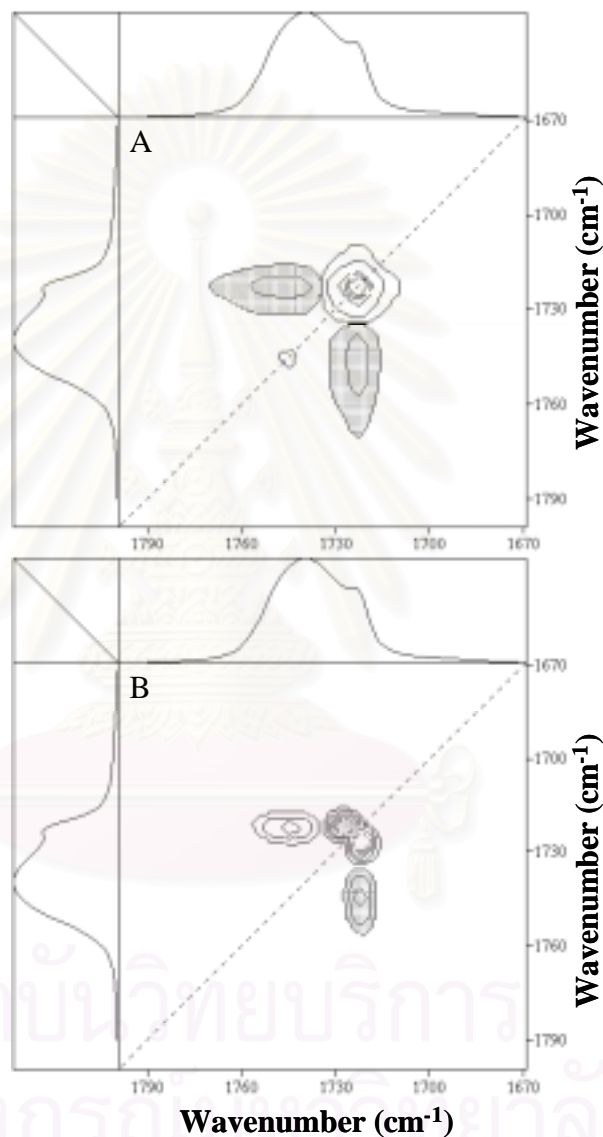


Figure 4.33 Synchronous (A) and asynchronous (B) correlation spectra of P(HB-*co*-HHx) in the C=O stretching region generated from the temperature-dependent IR spectra measured over a temperature range of 30-140 °C (cooling down process).

4.3.5 Crystalline/Amorphous Phase Transformation Behavior of P(HB-*co*-HHx)

The temperature-dependent IR spectra of P(HB-*co*-HHx) depict clearly that the crystalline C=O band observed at 1723 cm⁻¹ decreases during the heating up process and grows up during the cooling down process. The WAXD study shows that the crystalline part of P(HB-*co*-HHx) almost disappears above *ca.* 110 °C. A good agreement is obtained between the WAXD study and the temperature-dependent IR spectral variations observed in the melting process.

IR absorption bands are very sensitive to changes in microenvironments of molecules and the degree to which a vibrational mode is coupled to adjacent vibrations. The splitting of the C=O stretching band observed below the T_m of the polymer is possibly caused by some specific molecular interactions previously described. The analogous groups along the polymer chains are located very closely in the crystalline state of P(HB-*co*-HHx) because of the highly ordered and possible helical structure. As the temperature increases, the highly ordered structure collapses and, consequently, the inter- and intramolecular interactions between the repeating units along the polymer chains in a crystalline state are diminished. Therefore, the spectral changes of certain absorption bands concerning the crystalline/amorphous phase transition are clearly observed in the temperature-dependent IR spectra of P(HB-*co*-HHx).

4.3.6 Comparison between the Infrared Spectra of P(HB-*co*-HHx) and PHB

In the previous section, the temperature-dependent IR spectra of PHB were analyzed in detail. In this section, the one-dimensional IR spectra and also 2D correlation spectra of P(HB-*co*-HHx) and those of PHB are compared. In the C=O stretching region for PHB, three bands at 1740, 1731, and 1723 cm⁻¹ were observed. Note that the frequencies of the bands observed in the C=O stretching region for P(HB-*co*-HHx) are identical to those for PHB. This suggests that C=O groups of P(HB-*co*-HHx) and those of PHB experience very similar submolecular environments. However, the relative intensity ratio of the crystalline band at 1723

cm^{-1} to the amorphous band at 1740 cm^{-1} for P(HB-*co*-HHx) is much lower than that for PHB. The IR spectra reveal clearly that the percentage of crystallinity for P(HB-*co*-HHx) is lower than that for PHB.

In the CH_3 asymmetric stretching band region, the bands at 3008 and 2997 cm^{-1} for P(HB-*co*-HHx) were observed as shoulders of the band at 2975 cm^{-1} while those for PHB are very sharp and clear. The frequencies of the bands and the crystal field splitting pattern observed in the C-H stretching region for P(HB-*co*-HHx) are also very similar to those for PHB. These spectral features again imply a higher crystallinity of PHB and similar microenvironments in which the C-H groups of these two polymers are located. The shapes of the bands in the C-O-C stretching region below the T_m for P(HB-*co*-HHx) are also different from those for PHB, *e.g.*, the relative intensity of the bands in the region of $1295\text{-}1260 \text{ cm}^{-1}$ are different between the two polymer samples.

The temperature-induced IR spectral changes in the C=O, C-O-C, and C-H stretching regions for P(HB-*co*-HHx) and those for PHB are similar. However, the temperatures at which the significant intensity changes in the three spectral regions occur are different between the two polymer systems. Marked intensity changes in the three spectral regions for P(HB-*co*-HHx) were observed at much lower temperature than those for PHB. It is also noted that the intensity changes in the IR spectra of P(HB-*co*-HHx) occur gradually with increasing temperature, indicating a gradual deformation of its highly ordered and helical structure. On the other hand, the intensities of the IR spectra of PHB change abruptly in the vicinity of the T_m of PHB, suggesting that the highly ordered and helical structure of PHB collapses rapidly at the temperature right around the T_m .

The observations described above agree very well with the WAXD and DSC studies, which indicate that P(HB-*co*-HHx) assumes an orthorhombic crystal system, which is identical to that of PHB, and that the percentage of crystallinity of these two polymers are remarkably different. The crystallinity of PHB is higher than that of P(HB-*co*-HHx). We observed several remarkable differences between the temperature-dependent IR spectra of P(HB-*co*-HHx) and those of PHB, however, the

phase transition behaviors revealed by 2D correlation spectroscopy for these two polymer systems are basically similar. The results indicate clearly that the HHx comonomer does not alter the crystalline structure of PHB. Its major role is to break down the crystalline structure from place to place, and hence increasing the amorphous entity of the copolymer.

4.4 Surface Melting and Crystallization Behavior of PHB and P(HB-*co*-HHx)

4.4.1 Temperature-dependent Attenuated Total Reflection Spectra in the C=O Stretching Region of P(HB-*co*-HHx) during the Melting Process

Figure 4.34 shows temperature-dependent ATR spectra of P(HB-*co*-HHx) in the 1780-1680 cm^{-1} region. A sharp band at 1720 cm^{-1} gradually decreases with increasing temperature while a broad band at 1731 cm^{-1} increases. These spectral variations reflect the melting process of the copolymer.

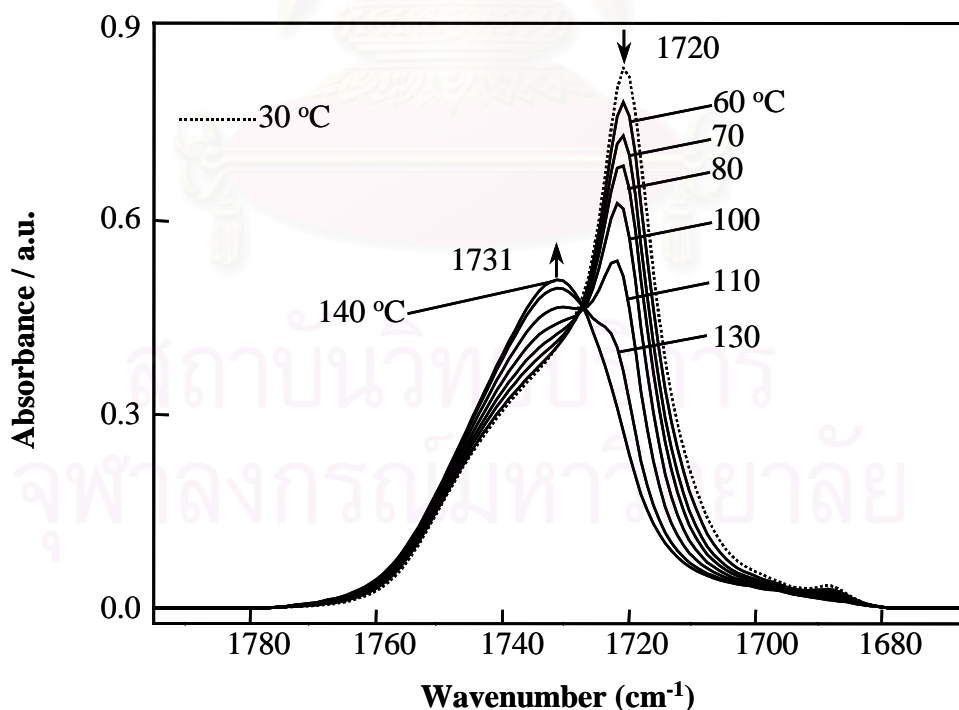


Figure 4.34 Representative ATR spectra of P(HB-*co*-HHx) in the C=O stretching region (1780-1680 cm^{-1}) measured over a temperature range of 30-140 °C.

Although the relative intensity of bands in the C=O stretching vibration region is different, the temperature-dependent changes observed for the ATR measurement are similar to those previously observed for the transmission measurement.

Figure 4.35 shows ATR (solid line) and transmission (dotted line) spectra of the annealed P(HB-co-HHx) film sample in the C=O stretching region measured at 30 °C. It can be seen that the major difference between the ATR and transmission spectra lies in the relative intensity of the highly ordered crystalline C=O band at 1720 cm⁻¹ and the amorphous C=O band at 1740 cm⁻¹; the band at 1720 cm⁻¹ in the ATR spectrum is more sharp and intense than that in the transmission spectrum.

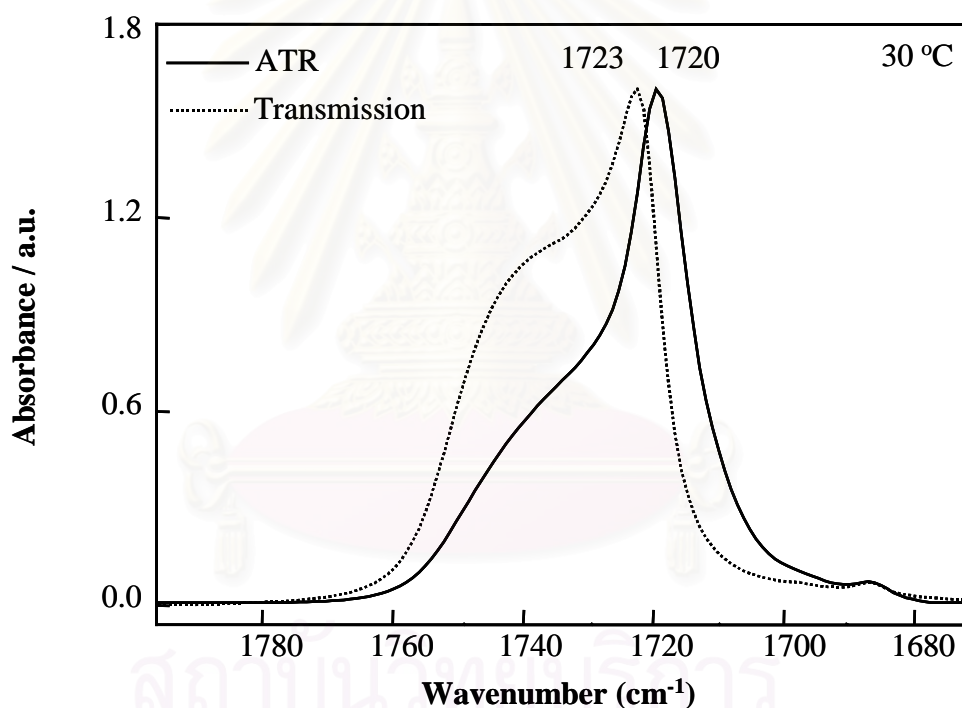


Figure 4.35 ATR (solid line) and transmission (dotted line) spectra of P(HB-co-HHx) in the C=O stretching region measured at 30 °C.

In general, the refractive index of organic compounds is 1.5 ± 0.2 [33], and that of ZnSe is 2.4. Accordingly, for the present study, the penetration depth (d_p) calculated for the C=O stretching vibration region, $d_p(1720 \text{ cm}^{-1})$ is $1.17 \mu\text{m}$. Due to the shallow sampling depth of the ATR technique, the ATR spectra shown in Figures 4.34 and 4.35 (solid line), therefore, contain only the spectral information associated

with the chemical species situated just a few micrometers beyond the sample surface. Thus, it is very likely that the differences between the ATR and transmission spectra are due primarily to the different behavior of molecules located at the surface and in the bulk of the sample. The intensity ratio of the highly ordered crystalline C=O band to the amorphous one for the ATR spectrum is much higher than that for the transmission spectrum (Figure 4.35), suggesting that the crystallinity of the polymer is much higher at the film surface than in the bulk. The broad feature at 1740 cm^{-1} in the ATR spectrum exists only as a slope with weak intensity.

Figure 4.36 A and B shows the synchronous and asynchronous 2D correlation spectra in the spectral region of $1790\text{--}1670\text{ cm}^{-1}$ generated from the temperature-dependent ATR spectra measured during the temperature increase in the range of $30\text{--}100\text{ }^{\circ}\text{C}$, respectively. A pair of negative cross peaks developed at $(1736, 1718)\text{ cm}^{-1}$ in the synchronous spectrum indicates the opposite directions of the intensity variations in these two correlated bands.

In the asynchronous spectrum, a pair of cross peaks appears at $(1732, 1718)\text{ cm}^{-1}$. The presence of asynchronous cross peaks indicates the out-of-phase changes in the intensity of the band at 1732 cm^{-1} and that of the band at 1718 cm^{-1} . This observation clearly suggests that the disappearance of the highly ordered crystalline component of the copolymer does not simultaneously result in the formation of the amorphous structure. That is, the surface melting of P(HB-*co*-HHx) also takes place through an intermediate state [55].

The 2D correlation spectra generated from the temperature-dependent ATR spectra also reveal that the spectral changes occurring at the surface region particularly involve the highly ordered crystalline component and the amorphous structure [55]. On the other hand, 2D correlation spectra generated from the temperature-dependent transmission spectra of P(HB-*co*-HHx) in the C=O stretching region clearly reveal that the bulk melting of P(HB-*co*-HHx) involves two crystalline components and the amorphous phase [52]. These observations suggest that the polymer crystals tend to grow at the surface in a manner different from the bulk. It is very likely that the molecules situated at the surface region of the P(HB-*co*-HHx)

film sample prefer the highly ordered molecular chain structure [55].

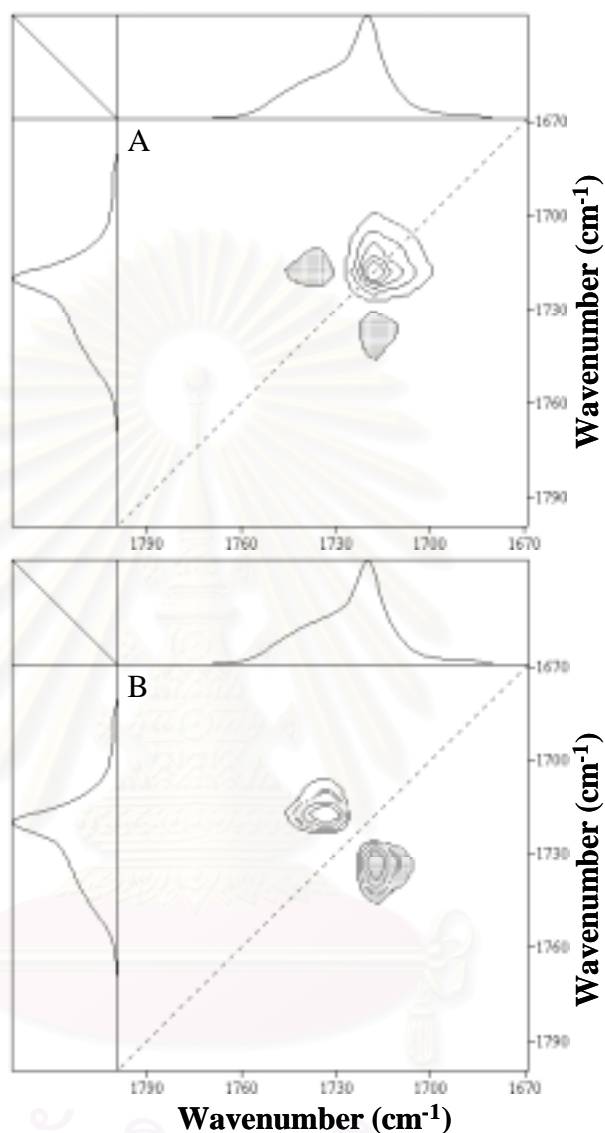


Figure 4.36 Synchronous (A) and asynchronous (B) correlation spectra of P(HB-*co*-HHx) in the C=O stretching region generated from the temperature-dependent ATR spectra measured over a temperature range of 30-100 °C.

4.4.2 Time-dependent Infrared Spectra in the C=O Stretching Region of P(HB-*co*-HHx)

Figure 4.37 A and B shows time-dependent ATR and transmission spectra of P(HB-*co*-HHx) in the C=O stretching region, respectively. The IR spectral changes

induced by the time-dependent crystallization are clearly observed both from the ATR (A) and transmission (B) measurements. This is because the crystallization rate of P(HB-*co*-HHx) is slow, one can supercool the system away from the thermal equilibrium. Consequently, an amorphous sample can be obtained well below its apparent T_m , and the time-dependent crystal growth can be monitored.

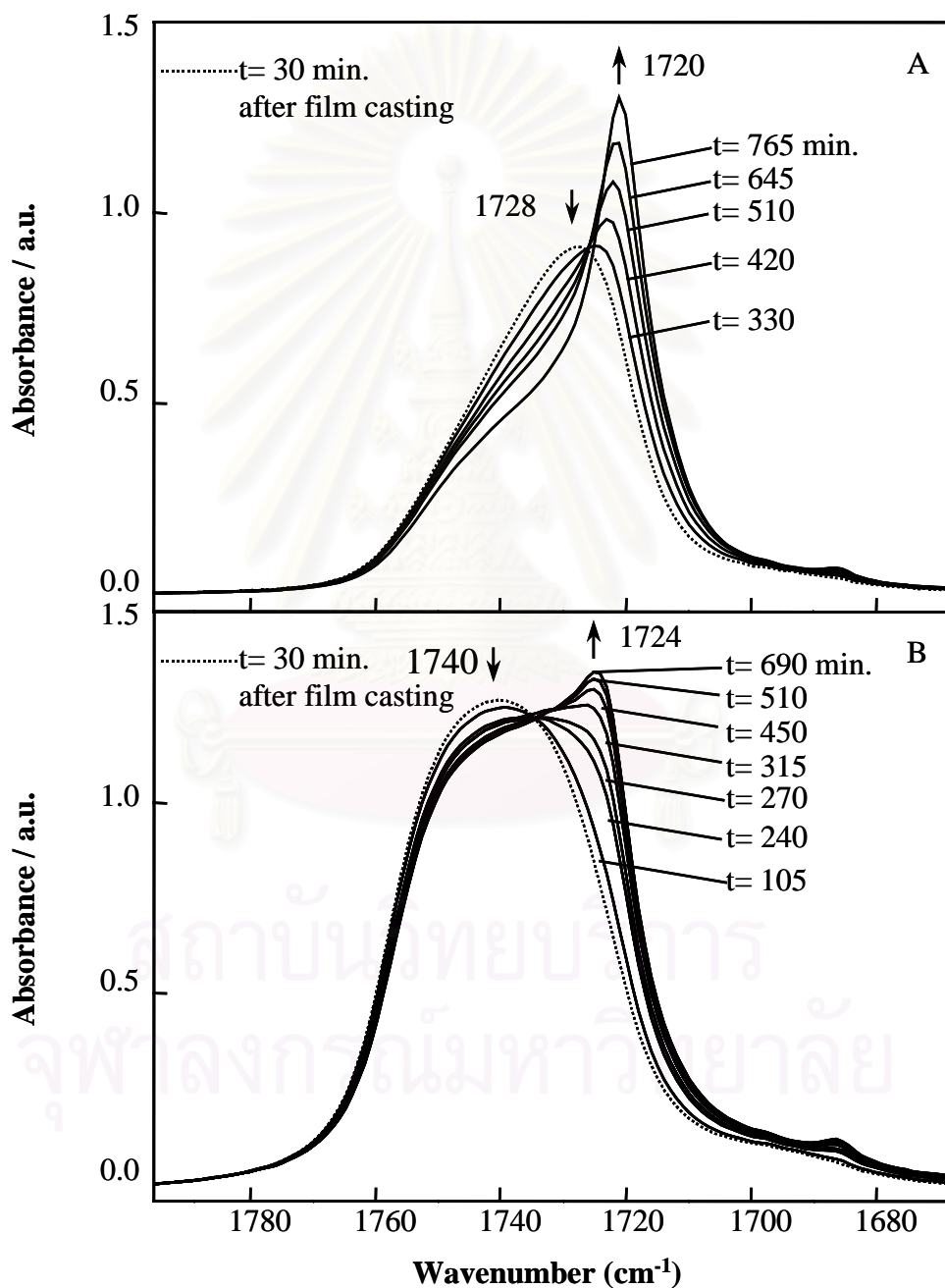


Figure 4.37 Representative time-dependent ATR (A) and transmission (B) spectra of P(HB-*co*-HHx) in the C=O stretching region measured at room temperature.

The transition from the amorphous to the crystalline state causes the downward shift in the C=O stretching region. However, the spectral features of the ATR spectra and those of the transmission spectra are substantially different from each other. The highly ordered crystalline C=O band observed in the transmission spectra is not so sharp and intense as that observed in the ATR spectra. In other words, the ATR spectra show higher crystalline characteristic while the transmission spectra manifest more of the amorphous feature.

A direct comparison between the ATR and transmission spectra measured under the same experimental conditions shows clear spectral differences. Figure 4.38 depicts the ATR and transmission spectra measured at 30 minutes after the film casting (A) and those measured when the crystal growth was completed (B). The spectra shown in Figure 4.38 clearly indicate that the surface and bulk chemical species exhibit different crystallization behavior. To minimize the effect of a localized anomalous refractive index dispersion results from absorption peaks, the Ge IRE was employed. Figure 4.39 shows ATR spectra of P(HB-*co*-HHx) measured with the Ge IRE under the same experimental conditions as those shown in Figure 4.38. The ATR spectra taken with the Ge IRE also show markedly different characteristics from those of the transmission spectra. For the ATR spectra measured when the crystal growth was completed (Figure 4.39 (solid line)), the highly ordered crystalline C=O band at 1721 cm^{-1} is very sharp and intense while the amorphous band at 1740 cm^{-1} is very weak. The spectral features and peak positions are similar to those of the ATR spectra taken with the ZnSe IRE. This observation confirms the difference in the surface and bulk crystallinity of the P(HB-*co*-HHx) copolymer.

By comparing Figures 4.35 and 4.38 B, the effect of the crystallization temperature on the crystal growth at the film surface and that in the bulk can be discussed. The highly ordered crystalline C=O band in the transmission spectrum of the annealed P(HB-*co*-HHx) sample (Figure 4.35 (dotted line)) is more intense than that of the non-annealed P(HB-*co*-HHx) sample (Figure 4.38 B (dotted line)). This observation suggests that the crystallization in the bulk proceeds far better when the sample is annealed at an elevated temperature. On the other hand, the crystallization at the film surface is not strongly affected by the temperature at which the

crystallization takes place. As seen in Figures 4.35 (solid line) and 4.38 B (solid line), the overall ATR spectral features of the C=O stretching bands for both cases are very similar.

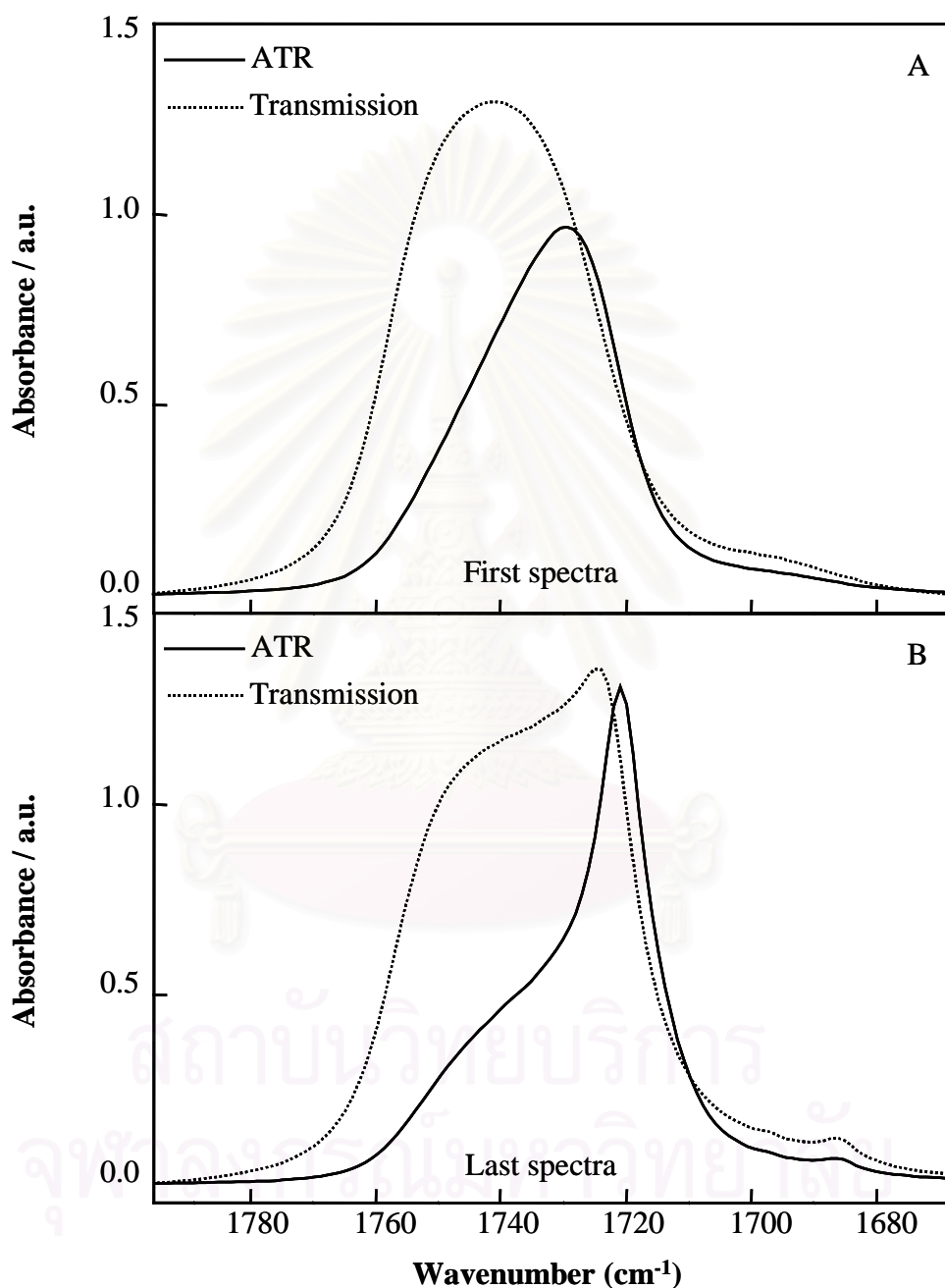


Figure 4.38 ATR (solid line) and transmission (dotted line) spectra of P(HB-*co*-HHx) in the C=O stretching region: first (A) and last (B) spectra measured during the time-dependent IR measurements.

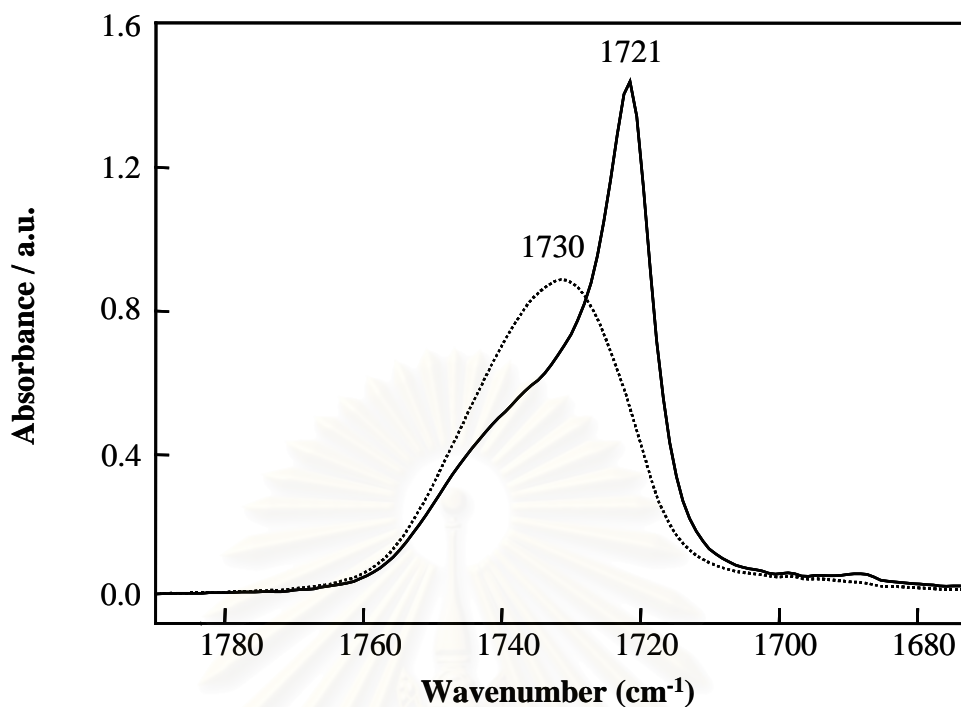


Figure 4.39 ATR spectra of P(HB-*co*-HHx) in the C=O stretching region measured at 30 minutes after the solvent casting (dotted line) and when the crystal growth was completed (solid line) by using the Ge IRE.

Figure 4.40 A and B shows the synchronous and asynchronous 2D correlation spectra in the spectral region of 1790-1670 cm^{-1} generated from the time-dependent ATR spectra, respectively. A pair of cross peaks developed at (1732, 1720) cm^{-1} in the asynchronous spectrum (Figure 4.40 B) reveals that the time-dependent surface crystallization process of P(HB-*co*-HHx) also occurs through an intermediate state. The reorganization of the amorphous structure does not simultaneously result in the fully formed highly ordered crystalline component. Similar to the surface melting, the time-dependent surface crystallization of P(HB-*co*-HHx) mainly involves the highly ordered crystalline component and the amorphous structure. This observation also suggests that at the film surface, polymer molecules favor the highly ordered molecular chain structure.

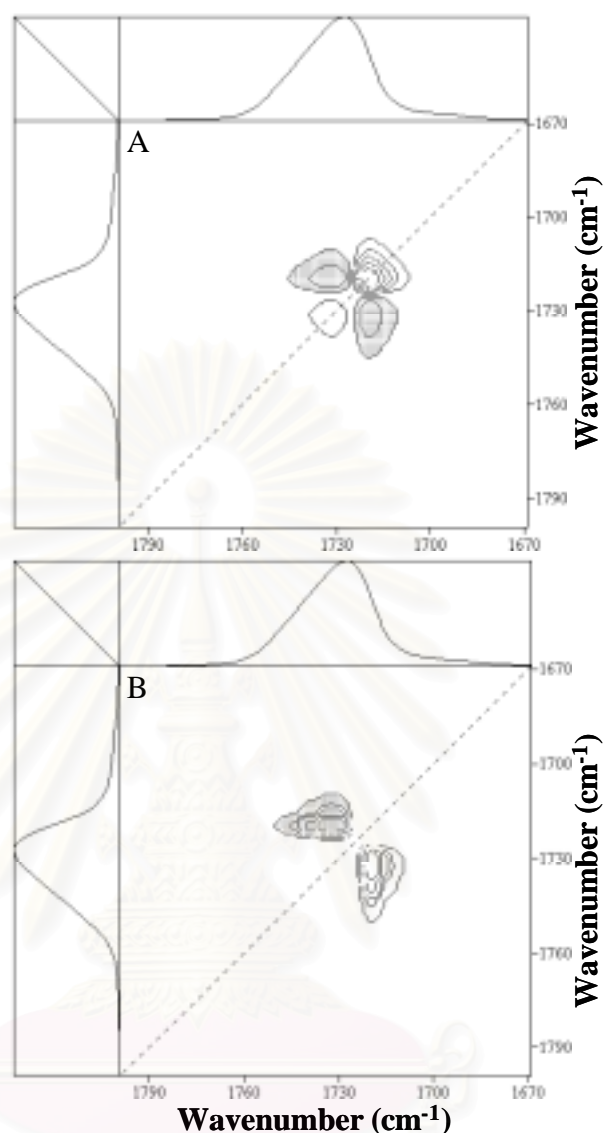


Figure 4.40 Synchronous (A) and asynchronous (B) correlation spectra of P(HB-*co*-HHx) in the C=O stretching region generated from the time-dependent ATR spectra shown in Figure 4.37 A.

Figure 4.41 A and B shows the synchronous and asynchronous 2D correlation spectra in the spectral region of 1790-1670 cm^{-1} generated from the time-dependent transmission spectra, respectively. Two pairs of cross peaks develop at (1742, 1722) and (1728, 1722) cm^{-1} in the asynchronous spectrum. The presence of asynchronous cross peaks indicates that the time-dependent bulk crystallization process of P(HB-*co*-HHx) occurs through an intermediate state. Note that, similar to the bulk melting process of P(HB-*co*-HHx), two crystalline C=O bands (*i.e.*, bands at *ca.* 1728 and

1722 cm^{-1}) appear in the 2D correlation spectra generated from the time-dependent transmission spectra. This observation suggests that the time-dependent crystallization occurring in the bulk of the film sample also involves two crystalline components and the amorphous phase [55].

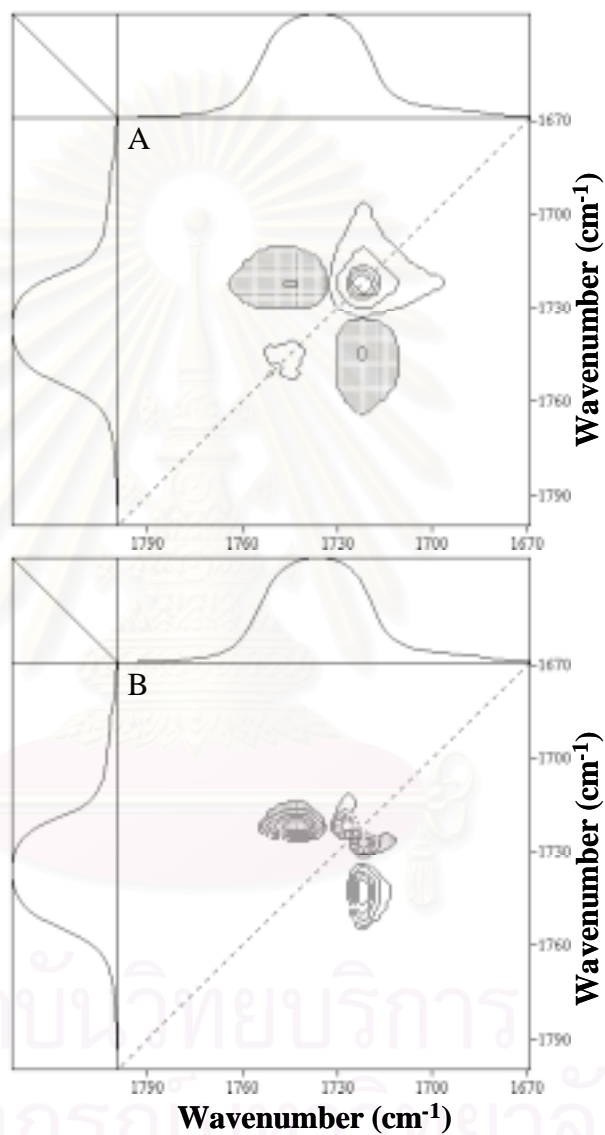


Figure 4.41 Synchronous (A) and asynchronous (B) correlation spectra of P(HB-*co*-HHx) in the C=O stretching region generated from the time-dependent transmission spectra shown in Figure 4.37 B.

4.4.3 Comparison between the Time-dependent Crystal Growth of P(HB-*co*-HHx) and PHB

The introduction of the HHx unit into the molecular chain of PHB results in dramatically improved mechanical properties of the resulting P(HB-*co*-HHx) copolymer. The HHx units act as a less crystallizable part and thereby depress the degree of crystallinity of the PHB homopolymer significantly [6]. From this aspect, effects of the HHx units on the crystallization process of the PHB homopolymer are very interesting.

Figure 4.42 A and B shows time-dependent ATR and transmission spectra of PHB in the C=O stretching region, respectively. The observed IR spectra again indicate the different crystallization behavior at the surface and in the bulk of the PHB film sample. As expected, the ATR spectra of PHB strongly represent the crystalline characteristic, and the amorphous feature at 1740 cm^{-1} is very weak. Similar to P(HB-*co*-HHx), transmission spectra of PHB show higher amorphous characteristic as compared to the ATR spectra. However, time-dependent IR spectral variations for PHB shown in Figure 4.42 A and B are different from those for P(HB-*co*-HHx) shown in Figure 4.37 A and B.

In chloroform solution, both IR spectra of P(HB-*co*-HHx) and PHB show fully random-coil feature (see Figure 4.43). After chloroform evaporated, P(HB-*co*-HHx) and PHB started to crystallize. However, we could not observe the IR spectra of the fully random-coil PHB for the solvent-free state. PHB assumes a crystalline state right after the solvent evaporation. This observation indicates that PHB crystallizes rapidly, much faster than P(HB-*co*-HHx). Although the highly ordered crystalline C=O band at 1720 cm^{-1} continues to develop as time passes, the overall spectral changes occurred during the time-dependent crystal growth are not pronounced. That is to say, PHB crystallizes at a much higher rate than P(HB-*co*-HHx). In other words, the HHx comonomer incorporated in P(HB-*co*-HHx) significantly reduces the crystallization rate of the PHB homopolymer. This is because the HHx unit is less crystallizable, and the presence of the HHx units in the PHB molecular chains may encumber the crystallization of the polymer from place to place.

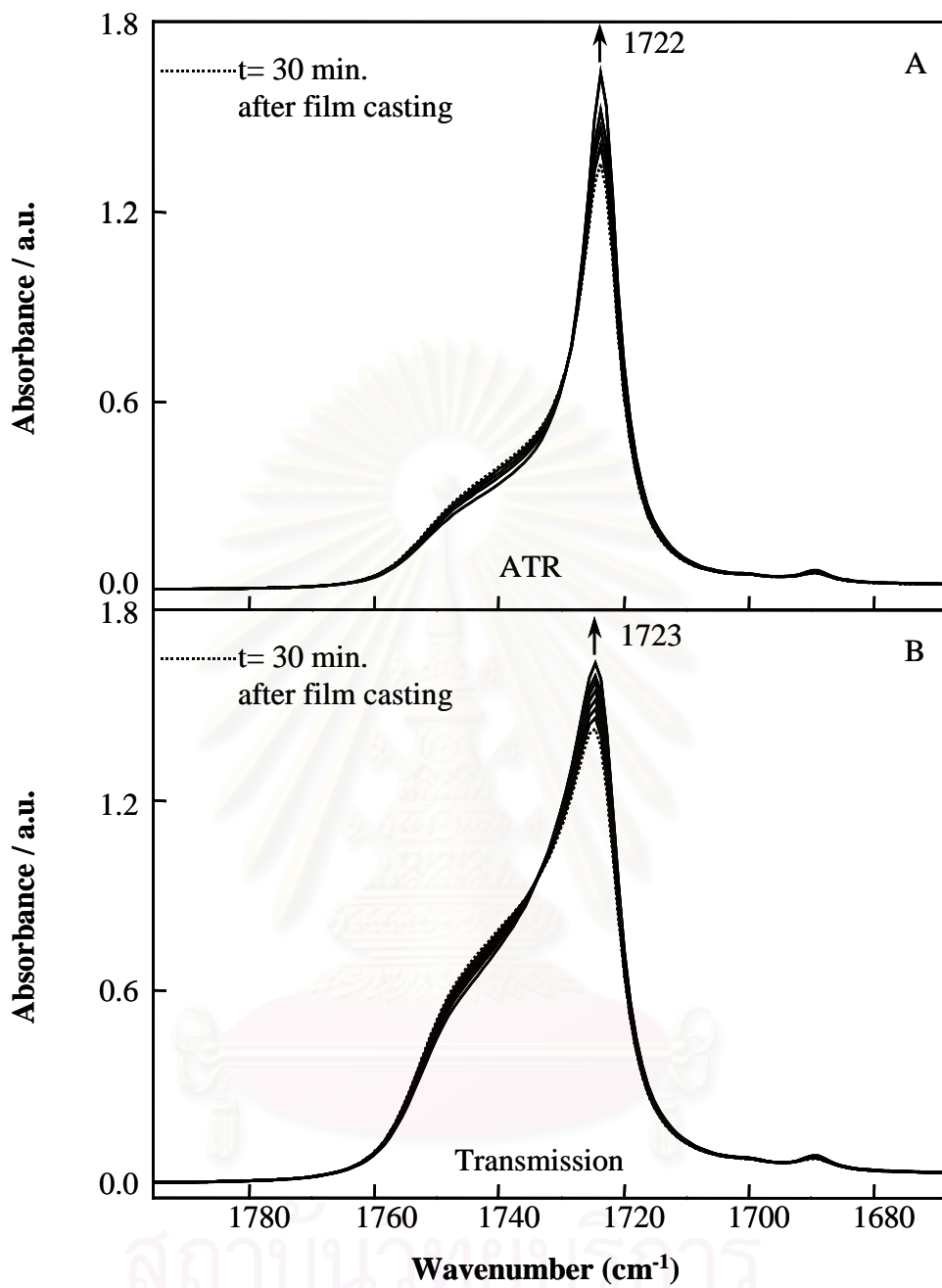


Figure 4.42 Representative time-dependent ATR (A) and transmission (B) spectra of PHB in the C=O stretching region measured at room temperature.

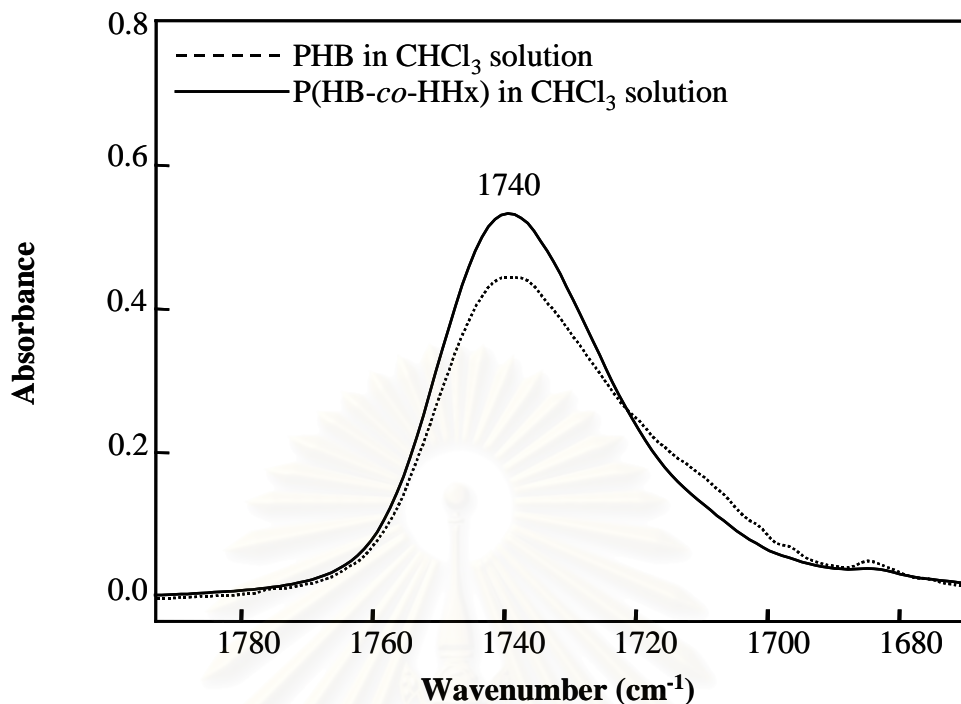


Figure 4.43 Transmission spectra of P(HB-*co*-HHx) (solid line) and PHB (dotted line) in CHCl₃ solution.

4.5 Crystallization Behavior of P(HB-*co*-HHx) under Different Crystallization Conditions

4.5.1 Gradual Cooling Crystallization

Figure 4.44 shows temperature-dependent IR spectra of P(HB-*co*-HHx) in the 1780-1680 cm⁻¹ region. A broad band at 1740 cm⁻¹ decreases while a sharp band at 1723 cm⁻¹ gradually increases in intensity during the course of temperature decrease. The sharp band at 1723 cm⁻¹ arises from the crystalline part of P(HB-*co*-HHx), and the broad band at 1740 cm⁻¹ is attributed to the amorphous component. These spectral variations reflect the crystallization process of P(HB-*co*-HHx).

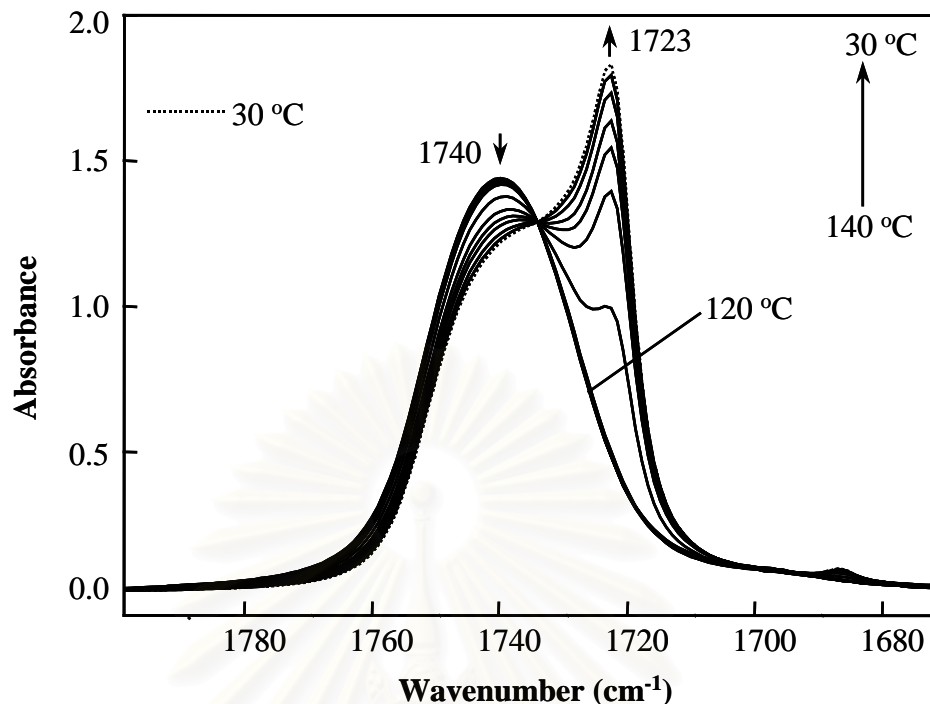


Figure 4.44 IR spectra of P(HB-*co*-HHx) in the C=O stretching region measured during the gradual cooling crystallization of the melt over a temperature range of 140-30 °C.

Figure 4.45 A and B shows the synchronous and asynchronous 2D correlation spectra in the spectral region of 1790-1670 cm^{-1} generated from the temperature-dependent IR spectra. A pair of negative cross peaks developed at (1745, 1723) cm^{-1} in the synchronous spectrum indicates the opposite directions of the intensity variations in these two correlated bands. In the asynchronous spectrum, two pairs of cross peaks appear at (1745, 1723) and (1728, 1723) cm^{-1} . The band at around 1728 cm^{-1} revealed by the asynchronous 2D correlation spectrum arises from the less ordered crystalline component of P(HB-*co*-HHx). The presence of asynchronous cross peaks indicates the out-of-phase changes in the intensity of the correlated bands. Figure 4.45 B suggests that, during the crystallization process, the decrease in intensity of the amorphous C=O band at 1745 cm^{-1} and the increase in intensity of the crystalline C=O band at 1723 cm^{-1} do not occur simultaneously.

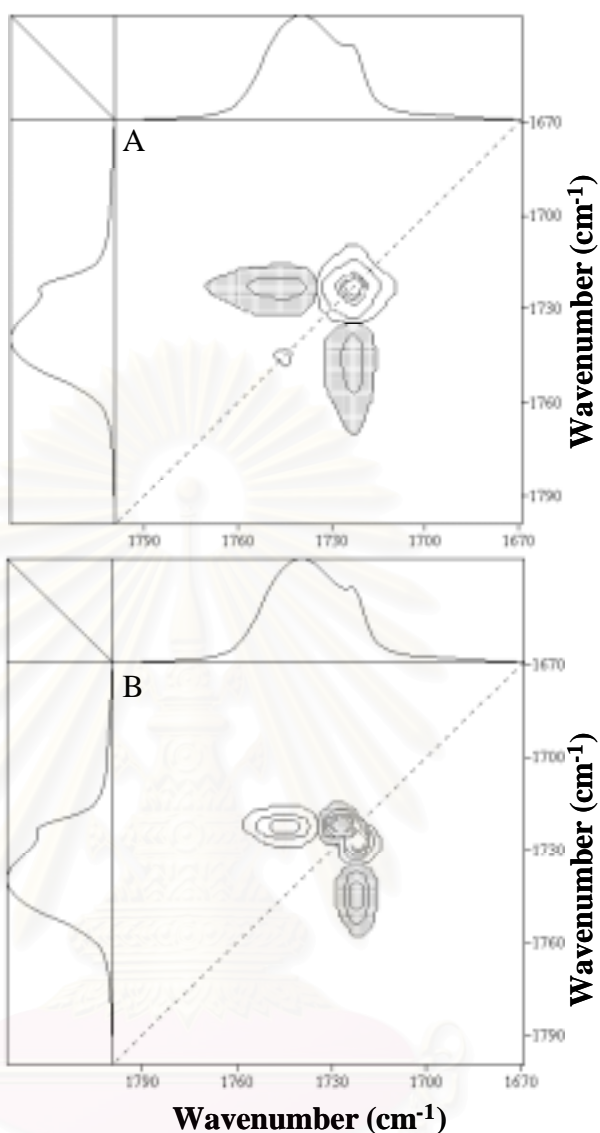


Figure 4.45 Synchronous (A) and asynchronous (B) correlation spectra of P(HB-*co*-HHx) in the C=O stretching region generated from the temperature-dependent IR spectra shown in Figure 4.44.

Of note in Figure 4.45 B is that the two crystalline C=O bands at 1728 and 1723 cm⁻¹ share asynchronous cross peaks. This observation indicates that the development of the highly ordered crystalline component and that of the less ordered crystalline component take place out of phase. The negative sign of the asynchronous cross peak at (1728, 1723) cm⁻¹ and the positive sign of the corresponding synchronous spectral intensity reveal that the formation of the highly ordered crystalline component proceeds prior to that of the less ordered crystalline

structure during the course of the gradual cooling crystallization [56].

4.5.2 Supercooled Melt Crystallization

Figure 4.46 shows time-dependent IR spectra of P(HB-*co*-HHx) in the C=O stretching band region measured during the isothermal crystallization of the supercooled melt. The representative spectra shown in Figure 4.46 were collected at 0 (start), 540, 900, 1020, 1140, 1380, 1560, 1740, 1920, 2100, and 2220 minutes after the initiation of the isothermal crystallization.

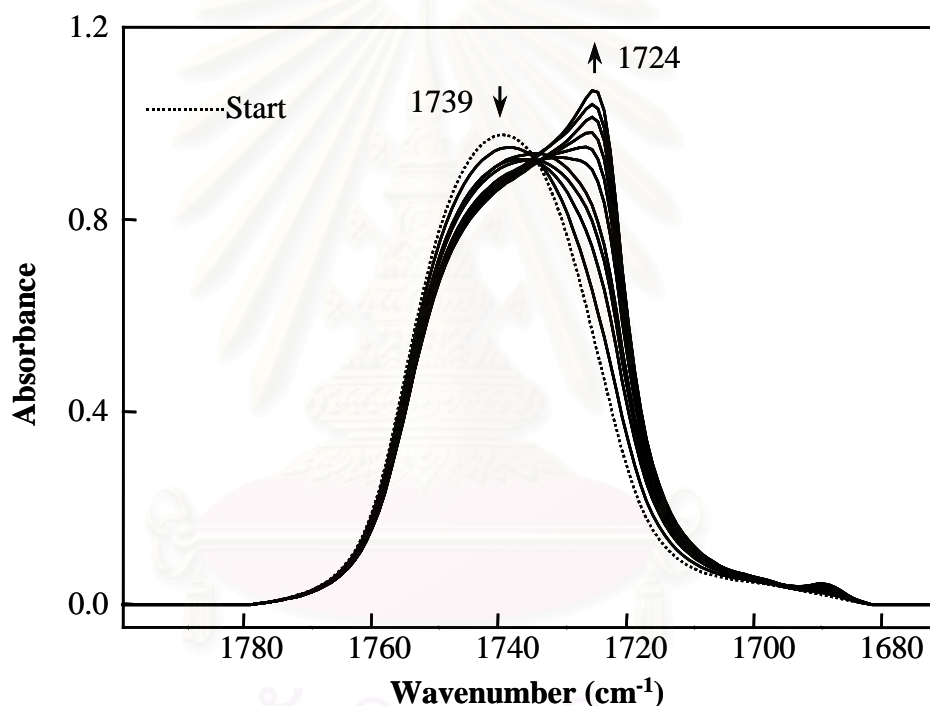


Figure 4.46 IR spectra of P(HB-*co*-HHx) in the C=O stretching region measured during the isothermal crystallization of the supercooled liquid at room temperature.

Because the crystallization rate of P(HB-*co*-HHx) is slow, one can supercool the system away from the thermal equilibrium, and an amorphous sample can be obtained well below its T_m . The time-dependent crystal growth of the supercooled melt was clearly revealed by the changes in intensity of the amorphous C=O band at 1739 cm^{-1} and the crystalline C=O band at 1724 cm^{-1} . The trend of the spectral variations induced by the crystallization of the supercooled melt is similar to that

induced by the gradual cooling crystallization shown in Figure 4.44. The amorphous C=O band at 1739 cm^{-1} decreases while the crystalline C=O band at 1724 cm^{-1} gradually increases in intensity during the crystallization process. However, the details of spectral features for the supercooled melt crystallization are substantially different from those for the gradual cooling process. The crystalline band observed during the gradual cooling crystallization is more sharp and intense than that observed during the supercooled melt crystallization. This observation implies that the crystallinity of the gradually cooled sample is much higher than that of the sample crystallized from the supercooled melt at room temperature. In addition, the crystalline band observed during the gradual cooling process appeared very clearly as a well-separated band at 1723 cm^{-1} below the T_m of the sample and developed down to room temperature. On the other hand, the crystalline band observed during the isothermal crystallization of the supercooled melt developed very slowly.

Figure 4.47 A and B shows the synchronous and asynchronous 2D correlation spectra in the spectral region of $1790\text{-}1670\text{ cm}^{-1}$ generated from the time-dependent IR spectra shown in Figure 4.46. Two autopeaks developed at 1745 and 1724 cm^{-1} reflect the spectral variations of the amorphous and crystalline C=O bands, respectively. A pair of negative cross peaks appeared at $(1745, 1724)\text{ cm}^{-1}$ indicates the opposite directions of the intensity variations in these two bands. The asynchronous spectrum shows two pairs of asynchronous cross peaks at $(1745, 1723)$ and $(1728, 1723)\text{ cm}^{-1}$ similar to that for the gradual cooling crystallization case. This result indicates that the disappearance of the amorphous component does not proceed simultaneously with the appearance of the crystalline component during the supercooled melt crystallization. The two crystalline C=O bands at 1728 and 1723 cm^{-1} for the supercooled melt crystallization also share asynchronous cross peaks, indicating the time lag between the increase in intensity of these two crystalline C=O bands. However, the signs of the asynchronous cross peaks shown in Figure 4.47 B are opposite to those shown in Figure 4.45 B. The positive sign of the asynchronous cross peak at $(1728, 1723)\text{ cm}^{-1}$ and the corresponding positive synchronous spectral intensity suggest that the increase in intensity of the band at 1728 cm^{-1} occurs before that of the band at 1723 cm^{-1} . That is, during the supercooled melt crystallization, the formation of the less ordered crystalline component proceeds

before that of the highly ordered crystalline component. In other words, the order of crystal growth steps is different from that for the gradual cooling crystallization process [56].

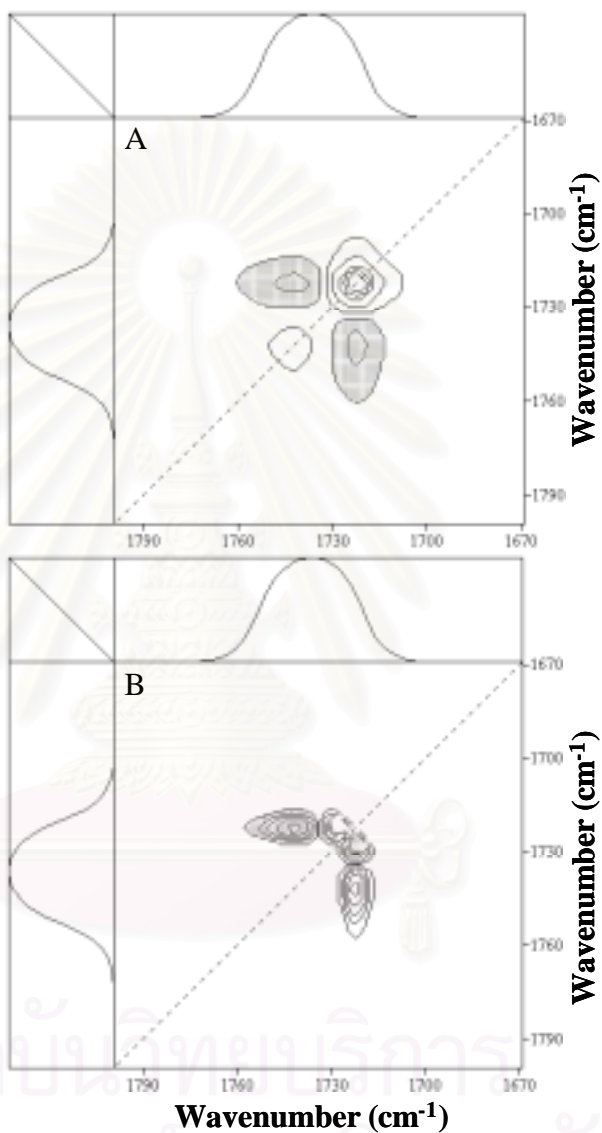


Figure 4.47 Synchronous (A) and asynchronous (B) correlation spectra of P(HB-*co*-HHx) in the C=O stretching region generated from the time-dependent IR spectra shown in Figure 4.46.

4.5.3 Solvent-cast Film Crystallization

Figure 4.48 shows time-dependent IR spectra of P(HB-*co*-HHx) in the C=O

stretching region measured during the isothermal crystallization of the solution-cast film. The representative spectra shown in Figure 4.48 were collected at 0 (start), 75, 210, 240, 285, 315, 375, 420, 480, 660, and 1080 minutes after the initiation of the isothermal crystallization.

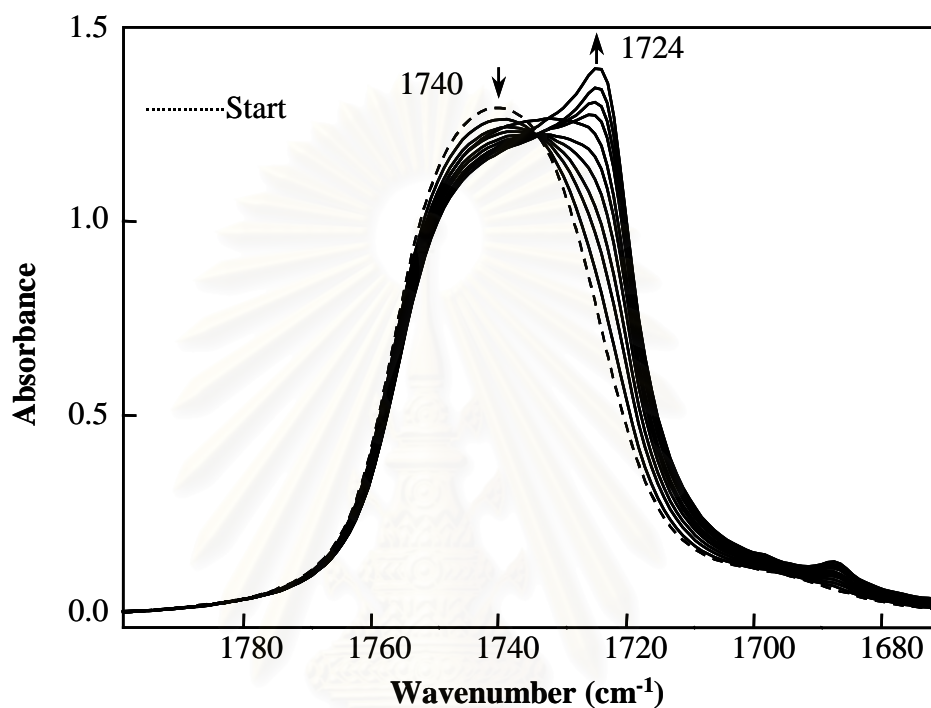


Figure 4.48 IR spectra of P(HB-*co*-HHx) in the C=O stretching region measured during the isothermal crystallization of the solvent-cast film at room temperature.

The time-dependent crystal growth of the sample was also observed for the solution-cast film as indicated by the changes in intensity of the amorphous C=O band at 1740 cm^{-1} and the crystalline C=O band at 1724 cm^{-1} . The spectral variations shown in Figure 4.48 are very similar to those for the supercooled melt crystallization shown in Figure 4.46. The development of the crystalline C=O band proceeded slowly, and the band shape is not sharp and intense.

Figure 4.49 A and B shows the synchronous and asynchronous 2D correlation spectra in the spectral region of $1790\text{-}1670\text{ cm}^{-1}$ generated from the time-dependent IR spectra shown in Figure 4.48. The 2D correlation spectra shown in Figure 4.49 A and B are very similar to those generated for the supercooled melt crystallization

shown in Figure 4.47 A and B. Two pairs of asynchronous cross peaks appear at (1745, 1723) and (1728, 1723) cm^{-1} . The signs of the asynchronous cross peaks and the corresponding synchronous intensity reveal that the formation of the less ordered crystalline component proceeds before that of the highly ordered crystalline component during the crystallization of the solution-cast film. This order of crystal growth steps is the same as that for the supercooled melt crystallization [56].

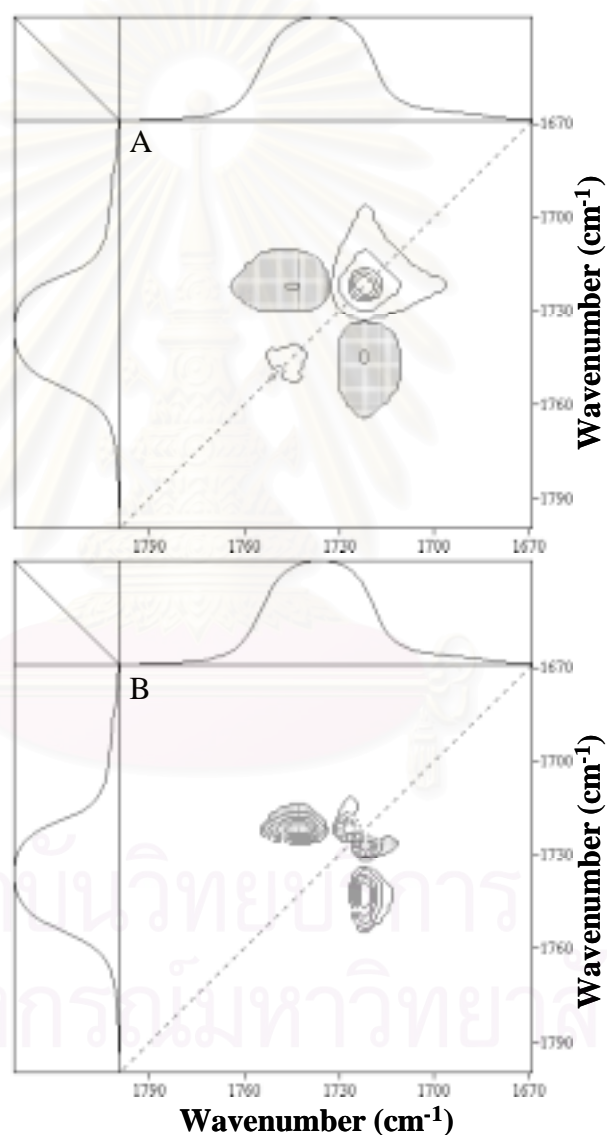


Figure 4.49 Synchronous (A) and asynchronous (B) correlation spectra of P(HB-co-HHx) in the C=O stretching region generated from the time-dependent IR spectra shown in Figure 4.48.

4.5.4 Comparison among the Three Types of Crystallization Processes

2D IR correlation spectroscopy suggests that the order of crystal growth steps for the gradual cooling crystallization is different from that of the supercooled melt and solution-cast film crystallization. For the gradual cooling process, the development of the highly ordered crystals occurs prior to the formation of the less ordered crystals. On the other hand, for the supercooled melt and solution-cast film crystallization, the formation of the less ordered crystals takes place first, and the highly ordered crystals develop later.

Being kinetically controlled, structures formed during the crystallization of partially crystalline polymers are strongly affected by the thermal history and preceding processes. In the gradual cooling condition, the sample is slowly cooled from the melt to a temperature below the T_m . At each temperature, the sample is allowed to reach the equilibrium state. Consequently, the crystallization occurs by nucleation and growth of spherulites [15]. The highly ordered crystals develop first and fill the specimen volume with a skeletal structure of crystalline lamellae. The inter crystalline regions, which remained amorphous, still have the potential to crystallize upon further cooling. The secondary crystallization follows at lower temperatures. The formation of the less ordered crystals proceeds via insertion into the original stack of the crystalline lamellae. The reduction of the order of these secondary crystals arises from the spatial constraint. Clearly, the additional crystalline lamellae formed at lower temperatures are generally thinner, less uniform, and include more internal disorder.

For the supercooled melt crystallization, the sample is quenched rapidly from 140 to 25 °C. In this state, the crystallization is substantially retarded due to the reduced segmental mobility of the polymer when approaching the T_g . Under such a condition, the transition from the disordered phase to the higher ordered structure proceeds through a continuous sequence of states rather than building up a two-phase structure from the very beginning. The increase in the crystallinity of the supercooled melt sample is very slow. The crystal growth occurs as the formation of numerous less ordered crystallites. The apparent reduction of the order in these

crystallites arises from the interfacial effect of the very small size of crystals. The radius of curvature is too small to have a well-developed crystal. The interfacial effect is different from the effect of the over crowding by the volume filling crystal lamellae already existing as in the case of the gradual cooling crystallization. Once these tiny crystallites are formed, the additional growth of the highly ordered crystals, which is characterized by the band at 1723 cm^{-1} , will occur. This process, however, is very slow. The system is hardly at the crystal volume filled stage during the crystallization period. The solution-cast P(HB-co-HHx) film exhibits similar crystallization behavior to that of the supercooled melt P(HB-co-HHx). The crystallization was carried out starting from the state in which the mobility of the entanglements is suppressed. The crystallization takes long time to proceed. The very slow on-going increase in the crystallinity with long times indicates the difficulty in approaching the perfect fully crystalline state of the sample. This lack of crystal growth results in the very weak intensity of the crystalline band observed for the supercooled melt and solution-cast film crystallization.

For all three types of crystallization, there is no asynchronous cross peak between the bands at 1745 and 1728 cm^{-1} in the 2D correlation spectra. This observation suggests that the transition from the amorphous state to the small crystallites with a less ordered structure is a one step transformation.

CHAPTER V

CONCLUSIONS

5.1 Wide-angle X-ray Diffraction Study and Thermal Analysis of P(HB-*co*-HHx) and PHB

The WAXD pattern of the P(HB-*co*-HHx) copolymer at room temperature indicates that P(HB-*co*-HHx) assumes an orthorhombic crystal system ($\alpha = \beta = \gamma = 90^\circ$) with $a = 5.76 \text{ \AA}$, $b = 13.20 \text{ \AA}$, $c = 5.96 \text{ \AA}$, which is identical to that of PHB. Only the a lattice parameter that shows the thermal expansion. This observation suggests that there are inter- and intramolecular interactions between the C=O and CH₃ groups along the a axis of P(HB-*co*-HHx) crystallites. The temperature-dependent variations in the (110) peak area for P(HB-*co*-HHx) and PHB reveal that PHB keeps its crystalline structure until around 140 °C while that of P(HB-*co*-HHx) starts breaking down from around 50 °C. The second heating DSC scan of the chloroform solution-cast P(HB-*co*-HHx) sample shows a recrystallization peak around 51 °C. This result is in a good agreement with the WAXD result that shows the maximum of the (110) peak area around 54 °C.

5.2 Thermally Induced Phase Transformation of PHB

The melting behavior of PHB was investigated by using generalized 2D IR correlation spectroscopy. The asynchronous 2D correlation spectrum generated from the temperature-induced dynamic IR spectra of PHB in the C=O stretching region resolves two highly overlapped crystalline bands located at 1731 and 1722 cm⁻¹. The intense band at 1722 cm⁻¹ is attributed to the major crystalline part of the polymer, and the much weaker feature at 1731 cm⁻¹ is assignable to the minor crystalline component with a less ordered structure. The asynchronous cross peaks between the crystalline and amorphous bands suggest the existence of an intermediate state in the melting process of PHB.

Bands in the C-O-C and C-H stretching regions were classified into those arising from the crystalline and amorphous parts of the polymer. The CH₃ asymmetric stretching bands and CH₂ antisymmetric stretching bands of the crystalline phase split into four bands at 3007, 2995, 2975, and 2967 cm⁻¹, and two bands at 2934 and 2929 cm⁻¹, respectively. These bands share positive synchronous cross peaks, and there is no asynchronicity among them, suggesting that these bands arise from the crystal field splitting.

5.3 Thermally Induced Phase Transformation of P(HB-*co*-HHx)

The melting behavior of P(HB-*co*-HHx) was investigated by using generalized 2D IR correlation spectroscopy. The significant intensity changes in the C=O, C-O-C, and C-H stretching regions start taking place at much lower temperature in the spectra of P(HB-*co*-HHx) than in the spectra of PHB. This observation indicates that the crystallinity decreases gradually even at low temperature for P(HB-*co*-HHx).

The asynchronous 2D correlation spectrum generated from the temperature-induced dynamic IR spectra of P(HB-*co*-HHx) in the C=O stretching region also differentiates two highly overlapped crystalline bands located at 1731 and 1723 cm⁻¹. Similar to the melting of PHB, the 2D asynchronous cross peaks between the crystalline and amorphous bands of P(HB-*co*-HHx) indicate the existence of an intermediate state during the melting process of P(HB-*co*-HHx).

The CH₃ asymmetric stretching bands and CH₂ antisymmetric stretching bands exhibit a crystal field splitting, which is often observed for polymers with a helical structure. The similarity in the frequencies of the C=O, C-O-C, and C-H stretching bands of the crystalline components between PHB and P(HB-*co*-HHx) reveals that the helical structure of P(HB-*co*-HHx) is very close to that of PHB. The HHx unit locally disrupts the highly ordered and helical structure of the copolymer from place to place, increasing the amorphous entity, which gives the better physical and mechanical properties to the copolymer.

5.4 Surface Melting and Crystallization Behavior of PHB and P(HB-*co*-HHx)

The melting behavior at the surface of P(HB-*co*-HHx) was studied by using ATR IR spectroscopy and the generalized 2D correlation analysis. Similar to the bulk melting of P(HB-*co*-HHx), the surface melting of P(HB-*co*-HHx) takes place through an intermediate state. However, the surface melting of P(HB-*co*-HHx) involves particularly the highly ordered crystalline component and the amorphous phase while the bulk melting involves two crystalline components and the amorphous phase.

The time-dependent crystallization at the surface and bulk of P(HB-*co*-HHx) and PHB film samples was monitored by using ATR and transmission IR spectroscopy, respectively. It was revealed by the 2D correlation spectra generated from the time-dependent IR spectra of P(HB-*co*-HHx) in the C=O stretching region that the surface and bulk crystal growth of P(HB-*co*-HHx) film also occurs through an intermediate state. Time-dependent ATR and transmission spectra of PHB indicate that PHB crystallizes at a much higher rate than P(HB-*co*-HHx). This observation suggests that the HHx units incorporated in the P(HB-*co*-HHx) copolymer significantly reduce not only the degree of crystallinity but also the crystallization rate of the PHB homopolymer. For both P(HB-*co*-HHx) and PHB film samples, it is very likely that the population of polymer crystals at the surface is higher than that in the bulk.

5.5 Crystallization Behavior of P(HB-*co*-HHx) under Different Crystallization Conditions

2D IR correlation spectroscopy was employed to study the crystallization behavior of P(HB-*co*-HHx). The order of crystal growth steps for the three different types of crystallization, i.e., the gradual cooling, supercooled melt, and solution-cast film crystallization, was investigated. The 2D IR correlation spectra generated for the C=O stretching band region suggested that, for the gradual cooling crystallization, the development of the highly ordered crystalline component proceeds prior to that of the less ordered crystalline component. On the other hand, for the supercooled melt and solution-cast film crystallization, the formation of the

less-ordered crystalline component occurs before that of the highly ordered crystalline component. The transition from the amorphous state to the less-ordered crystalline structure is a one step transformation for all three types of crystallization.



สถาบันวิทยบริการ
จุฬาลงกรณ์มหาวิทยาลัย

REFERENCES

1. Williams, S. F. and Martin, D. P. (2002). Applications of PHAs in Medicine and Pharmacy. In Steinbüchel, A. and Doi, Y. (Eds.), Biopolymers, pp. 91-121. Wienheim: Wiley-VCH.
2. Lara, L. M. and Gjalt, W. H. (1991). Metabolic Engineering of Poly(3-hydroxyalkanoates): From DNA to Plastic. Microbiol. Mol. Biol. Rev. 63: 21-53.
3. Anderson, A. J. and Dawes, E. A. (1990). Occurrence, Metabolism, Metabolic Role, and Industrial Uses of Bacterial Polyhydroxyalkanoates. Microbiol. Rev. 54: 450-472.
4. Jendrossek, D. (2001). Extracellular Polyhydroxyalkanoate Depolymerases: The Key Enzymes of PHA Degradation. In Steinbüchel, A. and Doi, Y. (Eds.), Biopolymers, pp. 41-83. Wienheim: Wiley-VCH.
5. Lee, S. Y. (1996). Bacterial Polyhydroxyalkanoates. Biotechnol. Bioeng. 49: 1-14.
6. Satkowski, M. M., Melik, D. H., Autran, J.-P., Green, P. R., Noda, I., and Schechtman, L. A. (2001). Physical and Processing Properties of Polyhydroxyalkanoate Copolymers. In Steinbüchel, A. and Doi, Y. (Eds.), Biopolymers, pp. 231-263. Wienheim: Wiley-VCH.
7. Caballero, K. P., Karel, S. F., and Register, R. A. (1995). Biosynthesis and Characterization of Hydroxybutyrate-hydroxycaproate Copolymers. Int. J. Bio. Macromol. 17: 86-92.
8. The Procter and Gamble Company. (2001). Nodax™[Online]. Available from: <http://www.nodax.com/>[2001, April 6].
9. Yokouchi, M., Chatani, Y., Tadokoro, H., Teranishi, K., and Tani, H. (1973). Structural Studies of Polyesters: 5. Molecular and Crystal Structures of Optically Active and Racemic Poly (β -hydroxybutyrate). Polymer 14: 267-272.
10. Cornibert, J. and Marchessault, R. H. (1975). Conformational Isomorphism. A General 2_1 Helical Conformation for Poly(β -alkanoates). Macromolecules

- 8: 296-305.
11. Mitomo, H. and Doi, Y. (1999). Lamellar Thickening and Cocrystallization of Poly(hydroxyalkanoate)s on Annealing. Int. J. Biol. Macromol. 25: 201-205.
 12. Wu, Q., Tian, G., Sun, S., Noda, I., and Chen, G.-Q. (2001). Study of Microbial Poly(hydroxybutyrate-*co*-hydroxyhexanoate) Using Two-Dimensional Fourier-Transform Infrared Correlation Spectroscopy. J. Appl. Polym. Sci. 82: 934-940.
 13. Tian, G., Wu, Q., Sun, S., Noda, I., and Chen, G.-Q. (2002). Two-Dimensional Fourier-Transform Infrared Spectroscopy Study of Biosynthesized Poly(hydroxybutyrate-*co*-hydroxyhexanoate) and Poly(hydroxybutyrate-*co*-hydroxyvalerate). J. Polym. Sci. B 40: 649-656.
 14. Tian, G., Wu, Q., Sun, S., Noda, I., and Chen, G.-Q. (2001). Study of Thermal Melting Behavior of Microbial Polyhydroxyalkanoates Using Two-Dimensional Fourier-Transform Infrared FT-IR Correlation Spectroscopy. Appl. Spectrosc. 55: 888-894.
 15. Strobl, G. R. (1996). The Physics of Polymers: Concepts for Understanding Their Structures and Behavior. 2nd Edition. Berlin: Springer-Verlag.
 16. Kai, Z., Ying, D., and Guo-Qiang, C. (2003). Effects of Surface Morphology on the Biocompatibility of Polyhydroxyalkanoates. Biochem. Eng. J. 16: 115-123.
 17. Saad, B., Neuenschwander, P., Uhlschmid, G. K., and Suter, U. W. (1999). New Versatile, Elastomeric, Degradable Polymeric Materials for Medicine. Int. J. Biol. Macromol. 25: 293-301.
 18. Labarre, D. (2001). Improving Blood-compatibility of Polymeric Surfaces. Trends Biomater. Artif. Organs 15: 1-3.
 19. Sasaki, S., Tashiro, K., Kobayashi, M., Izumi, Y., and Kobayashi, K. (1999). Microscopically Viewed Structural Change of PE during the Isothermal Crystallization from the Melt: II. Conformational Ordering and Lamellar Formation Mechanism Derived from the Coupled Interpretation of Time-resolved SAXS and FTIR Data. Polymer 40: 7125-7135.
 20. Tashiro, K., and Sasaki, S. (2002). Structural Changes in the Ordering Process of Polymers as Studied by an Organized Combination of the Various

- Measurement Techniques. Prog. Polym. Sci. 28: 451-519.
21. Jiang, Y., Gu, Q., Li, L., Shen, D.-Y., Jin, X.-G., and Chan, C.-M. (2003). Conformational Changes in the Induction Period of Crystallization as Measured by FT-IR. Polymer 44: 3509-3513.
 22. Tashiro, K., Sasaki, S., Gose, N., and Kobayashi, M. (1998). Microscopically-viewed Structural Change of Polyethylene during Isothermal Crystallization from the Melt I. Time-resolved FT-IR Spectral Measurements. Polym. J. 30: 485-491.
 23. Mallapragada, S. K. and Narasimhan, B. (2000). Infrared Spectroscopy in Analysis of Polymer Crystallinity. In Meyers, R. A. (Ed.), Encyclopedia of Analytical Chemistry, pp. 7644-7658. Chichester: John Wiley & Sons.
 24. Zhang, J., Duan, Y., Shen, D., Yan, S., Noda, I., and Ozaki, Y. (2004). Structure Changes during the Induction Period of Cold Crystallization of Isotactic Polystyrene Investigated by Infrared and Two-dimensional Infrared Correlation Spectroscopy. Macromolecules 37: 3292-3298.
 25. Noda, I. (1989). Two dimensional Infrared Spectroscopy. J. Am. Chem. Soc. 111: 8116-8118.
 26. Noda, I. (1990). Two-dimensional Infrared (2D IR) Spectroscopy: Theory and Applications. Appl. Spectrosc. 44: 550-561.
 27. Noda, I. (1993). Generalized Two-Dimensional Correlation Method Applicable to Infrared, Raman, and Other Types of Spectroscopy. Appl. Spectrosc. 47: 1329-1336.
 28. Noda, I., Dowrey, A. E., Marcott, C., Story, G. M., and Ozaki, Y. (2000). Generalized Two-dimensional Correlation Spectroscopy. Appl. Spectrosc. 54: 236A-248A.
 29. Noda, I., Story, G. M., and Marcott, C. (1999). Pressure-induced Transitions of Polyethylene Studied by Two-Dimensional Infrared Correlation Spectroscopy. Vib. Spectrosc. 19: 461-465.
 30. Neagle, W. and Randell, D. R. (1990). Surface Analysis Techniques and Applications. Cambridge: Royal Society of Chemistry.
 31. Berquier, J.-M. and Arribart, H. (1998). Attenuated Total Reflection Fourier Transform Infrared Spectroscopy Study of Poly(methyl methacrylate)

- Adsorption on a Silica Thin Film: Polymer/Surface Interactions. Langmuir 14: 3716-3719.
32. Chen, J. and Gardella, Jr. J. A. (1998). Quantitative ATR-FTIR Analysis of Surface Segregation of Polymer Blends of Polystyrene/Poly(dimethylsiloxane)-co-polystyrene. Appl. Spectrosc. 52: 361-366.
 33. Iwamoto, R. and Ohta, K. (1984). Quantitative Surface Analysis by Fourier Transform Attenuated Total Reflection Infrared Spectroscopy. Appl. Spectrosc. 38: 359-365.
 34. Harrick, N. J. (1967). Internal Reflection Spectroscopy. New York: Harrick Scientific Corporation.
 35. Urban, M. W. (1996). Attenuated Total Reflectance Spectroscopy of Polymers: Theory and Practice. Washington, DC: American Chemical Society.
 36. Mirabella, F. M. Jr. (1993). Internal Reflection Spectroscopy: Theory and Application. New York: Marcel Dekker.
 37. Yoshie, N., Oike, Y., Kasuya, K., Doi, Y., and Inoue, Y. (2002). Change of Surface Structure of Poly(3-hydroxybutyrate) Film upon Enzymatic Hydrolysis by PHB Depolymerase. Biomacromolecules 3: 1320-1326.
 38. Abe, H., Doi, Y., Aoki, H., and Akehata, T. (1998). Solid-State Structures and Enzymatic Degradabilities for Melt-crystallized Films of Copolymers of (*R*)-3-Hydroxybutyric Acid with Different Hydroxyalkanoic Acids. Macromolecules 31: 1791-1797.
 39. Doi, Y., Kitamura, S., and Abe, H. (1995). Microbial Synthesis and Characterization of Poly(3-hydroxybutyrate-co-3-hydroxyhexanoate). Macromolecules 28: 4822-4828.
 40. Marchessault, R. H., Morikawa, H., Revol, F. J., and Bluhm, T. L. (1984). Physical Properties of a Naturally Occurring Polyester: Poly(β -hydroxyvalerate)/Poly(β -hydroxybutyrate). Macromolecules 17: 1882-1884.
 41. Kunioka, M., Tamaki, A., and Doi, Y. (1989). Crystalline and Thermal Properties of Bacterial Copolyesters: Poly(3-hydroxybutyrate-co-3-hydroxyvalerate) and Poly(3-hydroxybutyrate-co-4-hydroxybutyrate). Macromolecules 22: 694-697.
 42. Sato, H., Padermshoke, A., Nakamura, M., Murakami, R., Hirose, F., Senda, K.,

- Terauchi, H., Ekgasit, S., Noda, I., and Ozaki, Y. Infrared Spectroscopy and X-ray Diffraction Studies on the Structure and Thermal Behavior of Biodegradable Polyhydroxyalkanoates. Macromol. Symp. in press.
43. Sato, H., Nakamura, M., Padermshoke, A., Yamaguchi, H., Terauchi, H., Ekgasit, S., Noda, I., and Ozaki, Y. (2004). Thermal Behavior and Molecular Interaction of Poly(3-hydroxybutyrate-co-3-hydroxyhexanoate) Studied by Wide-Angle X-ray Diffraction. Macromolecules 37: 3763-3769.
44. Sato, H., Murakami, R., Padermshoke, A., Hirose, F., Senda, K., Noda, I., and Ozaki, Y. (2004). Infrared Spectroscopy Studies of CH---O Hydrogen Bondings and Thermal Behavior of Biodegradable Polyhydroxyalkanoate. Macromolecules, in press.
45. Padermshoke, A., Katsumoto, Y., Sato, H., Ekgasit, S., Noda, I., and Ozaki, Y. (2005). Melting Behavior of Poly(3-hydroxybutyrate) Investigated by Two-Dimensional Infrared Correlation Spectroscopy. Spectrochim. Acta A 61: 541-550.
46. Chang, H.-C., Lee, K. M., Jiang, J.-C., Lin, M.-S., Chen, J.-S., Lin, I. J. B., and Lin, S. H. (2002). Charge-enhanced C-H---O Interactions of a Self-assembled Triple Helical Spine Probed by High-pressure. J. Chem. Phys. 117: 1723-1728.
47. Dybal, J., and Schneider, B. (1985). Raman Spectroscopic Study of the Intermolecular Coupling of C=O Stretching Vibrations in Liquid Methyl Acetate and Acetone. Spectrochim. Acta A 41: 691-695.
48. Dybal, J., Spevacek, J., and Schneider, B. (1986). Ordered Structures of Syndiotactic Poly(methyl methacrylates) Studied by a Combination of Infrared, Raman, and NMR Spectroscopy. J. Polym. Sci., B, Polym. Phys. 24: 657-674.
49. Galbiati, E., Zoppo, M. D., Tieghi, G., and Zerbi, G. (1993). Dipole-dipole Interactions in Simple Esters and in Liquid-crystal Polyesters. Polymer 34: 1806-1810.
50. Torii, H. and Tasumi, M. (1998). *Ab Initio* Molecular Orbital Study of the Amide I Vibrational Interactions Between the Peptide Groups in Di- and

Tripeptides and Considerations on the Conformation of the Extended Helix. J. Raman Spectrosc. 29: 81-86.

51. Torii, H. and Tasumi, M. (1992). Model Calculations on the Amide-I Infrared Bands of Globular Proteins. J. Chem. Phys. 96: 3379-3387.
52. Padermshoke, A., Sato, H., Katsumoto, Y., Ekgasit, S., Noda, I., and Ozaki, Y. (2004). Thermally Induced Phase Transition of Poly(3-hydroxybutyrate-co-3-hydroxyhexanoate) Investigated by Two-Dimensional Infrared Correlation Spectroscopy. Vib. Spectrosc. in press.
53. Gericke, A., Gadaleta, S. I., Brauner, J. W., and Mendelshon, R. (1996). Characterization of Biological Samples by Two-dimensional Infrared Spectroscopy. Simulations of Frequency, Bandwidth and Intensity changes. Biospectroscopy 2: 341-351.
54. Nabet, A., Auger, M., and Pézolet, M. (2000). Investigation of the Temperature Behavior of the Methylene Stretching Bands of Phospholipid Acyl Chains by Two-dimensional Infrared Correlation Spectroscopy. Appl. Spectrosc. 54: 948-955.
55. Padermshoke, A., Katsumoto, Y., Sato, H., Ekgasit, S., Noda, I., and Ozaki, Y. Surface Melting and Crystallization Behavior of Polyhydroxyalkanoates Studied by Attenuated Total Reflection Infrared Spectroscopy. Polymer, in press.
56. Padermshoke, A., Katsumoto, Y., Sato, H., Ekgasit, S., Noda, I., and Ozaki, Y. Crystallization Behavior of Poly(3-hydroxybutyrate-co-3-hydroxyhexanoate) Studied by 2D IR Correlation Spectroscopy. Polymer, in press.



APPENDICES

สถาบันวิทยบริการ
จุฬาลงกรณ์มหาวิทยาลัย



Melting behavior of poly(3-hydroxybutyrate) investigated by two-dimensional infrared correlation spectroscopy

Adchara Padermshoke^{a,b}, Yukiteru Katsumoto^c, Harumi Sato^a, Sanong Ekgasit^b,
Isao Noda^d, Yukihiko Ozaki^{a,*}

^a Department of Chemistry, School of Science and Technology, Kwansai-Gakuin University, 2-1, Gakuen, Sanda, Hyogo 669-1337, Japan

^b Sensor Research Unit, Department of Chemistry, Faculty of Science, Chulalongkorn University, Patumwan, Bangkok 10330, Thailand

^c Department of Chemistry, Graduate School of Science, Hiroshima University, Higashi-Hiroshima, Hiroshima 739-8526, Japan

^d The Procter and Gamble Company, 8611 Beckett Road, West Chester, OH 45069, USA

Received 31 March 2004; accepted 5 May 2004

Abstract

The melting behavior of a bacterially synthesized biodegradable polymer, poly(3-hydroxybutyrate) (PHB), was investigated by using generalized two-dimensional infrared (2D IR) correlation spectroscopy. Temperature-dependent spectral variations in the regions of the C–H stretching ($3100\text{--}2850\text{ cm}^{-1}$), C=O stretching ($1800\text{--}1680\text{ cm}^{-1}$), and C–O–C stretching ($1320\text{--}1120\text{ cm}^{-1}$) bands were monitored during the melting process. The asynchronous 2D correlation spectrum for the C=O stretching band region resolved two crystalline bands at 1731 and 1723 cm^{-1} . The intense band at 1723 cm^{-1} may be due to the highly ordered crystalline part of PHB, and the weak band at 1731 cm^{-1} possibly arises from the crystalline part with a less ordered structure. These crystalline bands at 1731 and 1723 cm^{-1} share asynchronous cross peaks with a band at around 1740 cm^{-1} assignable to the C=O band due to the amorphous component. This observation indicates that the decreases in the crystalline components do not proceed simultaneously with the increase in the amorphous component. In the $3020\text{--}2915\text{ cm}^{-1}$ region where bands due to the asymmetric CH_3 stretching and antisymmetric CH_2 stretching modes are expected to appear, eight bands are identified at 3007 , 2995 , 2985 , 2975 , 2967 , 2938 , 2934 , and 2929 cm^{-1} . The bands at 2985 and 2938 cm^{-1} are ascribed to the amorphous part while the rest come from crystal field splitting, which is a characteristic of polymers with a helical structure.

© 2004 Elsevier B.V. All rights reserved.

Keywords: Polyhydroxybutyrate; Melting behavior; 2D IR correlation spectroscopy

1. Introduction

Bacterially synthesized poly(3-hydroxyalkanoate)s (PHAs) are a class of naturally occurring biodegradable polyesters accumulated as energy-storing inclusion body granules in the cells of certain microorganisms [1–4]. Since PHAs can be biologically derived from renewable resources and are biodegradable, they have attracted a great attention as a new family of environmentally friendly polymeric materials [2,5–7]. Among various bacterially synthesized PHA polymers, poly(3-hydroxybutyrate) (PHB), the oldest known bacterial polyester, is the most abundant polyester found in bacteria [3,7]. The chemical structure of PHB, and

its proposed helical structure [8,9] are shown in Fig. 1(A) and (B), respectively.

PHB bears similar glass transition temperature (T_g), melting temperature (T_m), and comparable ultimate tensile strength to those of polypropylene (PP) [4,7]. PHB is perfectly biocompatible, and therefore its medical use is one of the important potential applications being considered. However, due to the high stereoregularity of biologically produced macromolecules, PHB is a highly crystalline polymer that is stiff and brittle. It is also thermally unstable during processing [7]. The molecular weight of PHB degrades significantly at temperature just above the T_m . This unfortunate aspect of properties poses a limitation of, for example, the application to a flexible film, which is one of the largest uses of biodegradable polymers. As a consequence, many attempts to copolymerize a comonomer with PHB monomer for improving its

* Corresponding author. Tel.: +81 79 565 8349; fax: +81 79 565 9077.
E-mail address: ozaki@ksc.kwansei.ac.jp (Y. Ozaki).

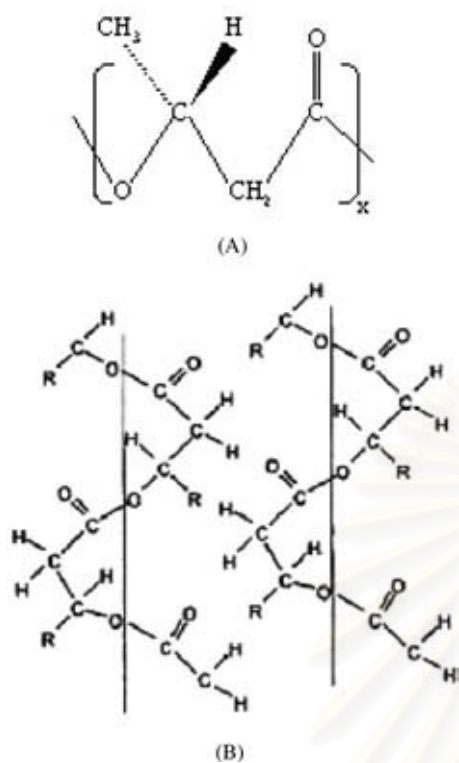


Fig. 1. Chemical structure of PHB (A), and the proposed helical structure model^{8,9} for polyhydroxyalkanoates (B).

mechanical properties have been made. One idea is to include a more bulky comonomer to reduce the crystallinity and presumably increase the flexibility of the resulting copolymers. The copolymerization with 3-hydroxyvalerate (3-HV) was the first attempt performed by ICI (Billingham, UK) in the early 1980s [7]. However, the crystallinity of poly(3-hydroxybutyrate-*co*-3-hydroxyvalerate) (P(HB-*co*-HV)) never falls below 50% due to the isodimorphism of the P(HB-*co*-HV) copolymer [7]. It has been reported that poly(3-hydroxybutyrate-*co*-3-hydroxyhexanoate) (P(HB-*co*-HHx)) shows a greater T_m drop, at a given mol% comonomer, in comparison to P(HB-*co*-HV) [7]. Interestingly, hexanoate and larger comonomers depress T_m in the same manner regardless of their molecular sizes [7]. This feature indicates the break down of the isodimorphism occurring in the P(HB-*co*-HV) copolymer by the incorporation of comonomer units with three or more carbon unit side groups [7].

The main factor to determine mechanical properties of the polymer is the degree of crystallinity. A fundamental understanding of the crystallization and melting process of this class of polymers is essential for improving their mechanical properties of biopolyesters. We have been undertaking a series of studies on the structure and thermal behavior of PHB and P(HB-*co*-HHx) by using temperature-dependent wide-angle X-ray diffraction (WAXD), differential scanning calorimetry (DSC), and two-dimensional infrared (2D IR) correlation spectroscopy [10–12]. The WAXD study

suggested that there are inter- and intramolecular interactions between the C=O and CH₃ groups in PHB and P(HB-*co*-HHx), and the interactions decrease along the *a* axis of the crystal lattice of PHB and P(HB-*co*-HHx) with temperature [10,11]. IR spectroscopy has been successfully applied to the studies of crystalline/amorphous phase transition process of a number of polymers [12–15,17,18]. This is because IR absorption bands are very sensitive to changes in inter- and intramolecular interactions and conformational changes of polymers [17]. IR spectra of polymers are often complicated. In such a case, 2D correlation analysis proposed by Noda [18,19] enables a more detailed analysis of IR spectral variations of polymers [12–15,18–21]. The asynchronous 2D correlation spectrum generated for the C=O stretching band region of P(HB-*co*-HHx) revealed the coexistence of two crystalline bands at 1731 and 1723 cm⁻¹ [12]. The band at 1723 cm⁻¹ contributes to the highly ordered crystalline component, and that at 1731 cm⁻¹ arises from the less ordered crystalline structure [12].

The present study aims at exploring the melting behavior of PHB by using 2D IR correlation spectroscopy. IR spectra of PHB, which is a basic polymer for all other PHA polymers, have never been analyzed in detail. Therefore, outcome of the present study is important not only for the study of PHB itself but also for the future study of other PHAs. In order to extract as much information related with the phase transition behavior of PHB polymer as possible, we analyzed not only the C=O stretching band region but also the C–O–C stretching band and C–H stretching band regions by employing 2D IR correlation spectroscopy. 2D IR correlation spectroscopy was successfully employed for studying the phase transitions of a number of PHA copolymers [12–15].

2. Experimental

2.1. Materials

The purified PHB sample was provided by the Procter and Gamble Company (Cincinnati, USA) and used as received. Chloroform (CHCl₃) was purchased from Wako Pure Chemical Industries Ltd. (Osaka, Japan) and used as a solvent without further purification.

2.2. IR spectroscopic measurements

A film of PHB sample was prepared by casting its chloroform solution on a CaF₂ window. The film was kept in a vacuum-dried oven at 60 °C for 12 h and cooled down to room temperature. IR spectra of the PHB film were collected at a 2 cm⁻¹ spectral resolution by using a Nicolet Magna-IRTM 550 spectrometer equipped with a mercury cadmium telluride (MCT) detector. To ensure a high signal-to-noise ratio, 512 scans were co-added. The temperature of the sample cell that holds the CaF₂ window with

the PHB film was controlled by using a temperature controller unit (CHINO, model SU). The spectral acquisitions were performed over a temperature range of 40–180 °C with an increment of 10 °C.

2.3. 2D correlation analysis

All IR spectra were baseline-corrected prior to the 2D correlation analysis. The calculations of 2D correlation spectra were performed by using the 2D-Pocha software composed by Daisuke Adachi (Kwansei-Gakuin University, Japan). Temperature-averaged IR spectra were used as the reference spectra for the 2D correlation calculations.

3. Results and discussion

3.1. Temperature-dependent changes in the C=O stretching vibration region

Fig. 2 shows temperature-dependent IR spectra of PHB in the 1800–1680 cm^{-1} region where bands due to the C=O stretching modes are expected to appear. The band shape in the C=O stretching vibration region changes largely from a sharp peak with a broad shoulder to a symmetrical broad band with increasing temperature. A dramatic change in the IR spectra was observed in the vicinity of 140 °C. PHB is known as a semi-crystalline polymer, and the T_m of PHB was reported to be 170 °C [11]. The spectral changes observed in Fig. 2 reflect the melting of PHB. The C=O stretching band region consists of at least two dominant bands. The sharp band at 1723 cm^{-1} arises from the crystalline C=O groups, and the broad band at 1740 cm^{-1} is attributed to the amorphous C=O groups [12–16]. The band at 1723 cm^{-1} decreases with increasing temperature and disappears above the T_m while the band at 1740 cm^{-1} gradually increases. Accordingly, the band at 1723 cm^{-1} is a unique indicator for monitoring the melting or crystallization process of PHA polymers.

There are two possible interpretations for the origin of the splitting of the C=O band observed below the T_m : (1) an interaction between the C=O and CH_3 groups [10,11,22] and (2) a dipole-dipole coupling interaction between ester groups in an ordered structure [23–25].

It was reported that PHB assumes an orthorhombic crystal system, $P2_12_12_1(D_2^4)$, ($\alpha = \beta = \gamma = 90^\circ$) with $a = 5.76 \text{ \AA}$, $b = 13.20 \text{ \AA}$, $c = 5.96 \text{ \AA}$ (fiber axis) [9,26]. The x-ray crystallographic studies of PHB showed that the distance between the C=O and CH_3 groups along the a axis is close enough for supposing the interactions between them. We studied the thermal properties of PHB by using WAXD and DSC [10,11]. The temperature-dependent variations in WAXD of PHB revealed that the lattice parameter a shows a significant variation with the temperature increase. In other words, the thermal energy weakens the interaction along

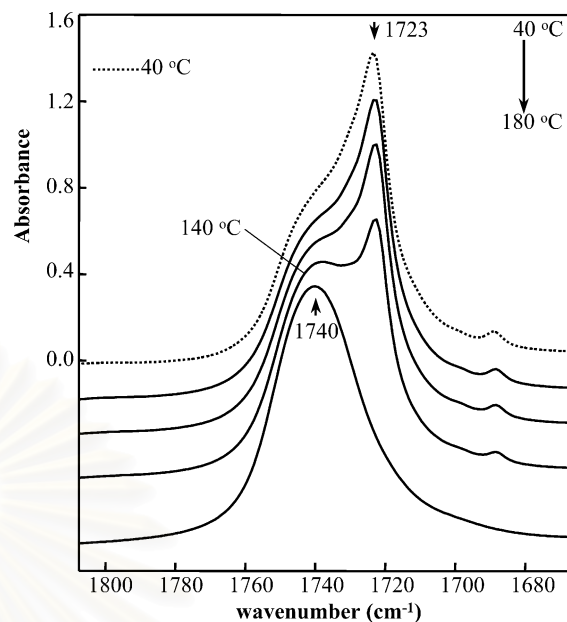


Fig. 2. IR spectra of PHB in the C=O stretching vibration region (1800–1680 cm^{-1}) collected over a temperature range of 40–180 °C.

the a axis. The change in the interaction between the C=O and CH_3 groups may cause the change in the C=O stretching band. The sharp peak at 1723 cm^{-1} may arise from the C=O groups involved in the C=O and CH_3 interactions while the broad feature at 1740 cm^{-1} may be due to the free or non-interaction C=O groups.

Another possibility that causes the C=O band splitting is the transition dipole coupling of the ester groups in an ordered structure [23–25]. For methyl acetate, which can be a model compound for the ester group incorporated in the main chain of PHB, the dipole practically lies along the C=O bond. Galbiati et al. [25] measured IR and Raman spectra of several aliphatic esters in gas, liquid, and solid phases. It was revealed that the observed frequencies of the C=O stretching vibrations ($\nu_{\text{C=O}}$) of the compounds can be grouped into three wavenumber regions for the three phases: (1) $\nu_{\text{C=O}} > 1760 \text{ cm}^{-1}$ for the gas phase, (2) $1750 \text{ cm}^{-1} > \nu_{\text{C=O}} > 1740 \text{ cm}^{-1}$ for the liquid phase, and (3) $1730 \text{ cm}^{-1} > \nu_{\text{C=O}} > 1720 \text{ cm}^{-1}$ for the solid phase. They also performed MNDO (modified neglect of differential overlap) semiempirical quantum chemical calculation for estimating the minimum-energy geometry and dipole moment and derived the following results: the dipole-dipole interaction causes a lower frequency shift of the C=O stretching band, and the maximum distance capable of producing a band splitting is not larger than ca. 4–5 Å [25]. In polymer systems, a band splitting due to the dipole-dipole interaction (often called dipole-dipole coupling) is observed when the molecules form an ordered structure [24,27,28]. Torii and Tasumi showed that the amide I bands of several proteins, which contain the ordered structures such as α -helix and β -sheet, are successfully reproduced by the model calculation based on the dipole-dipole coupling mechanism [27,28].

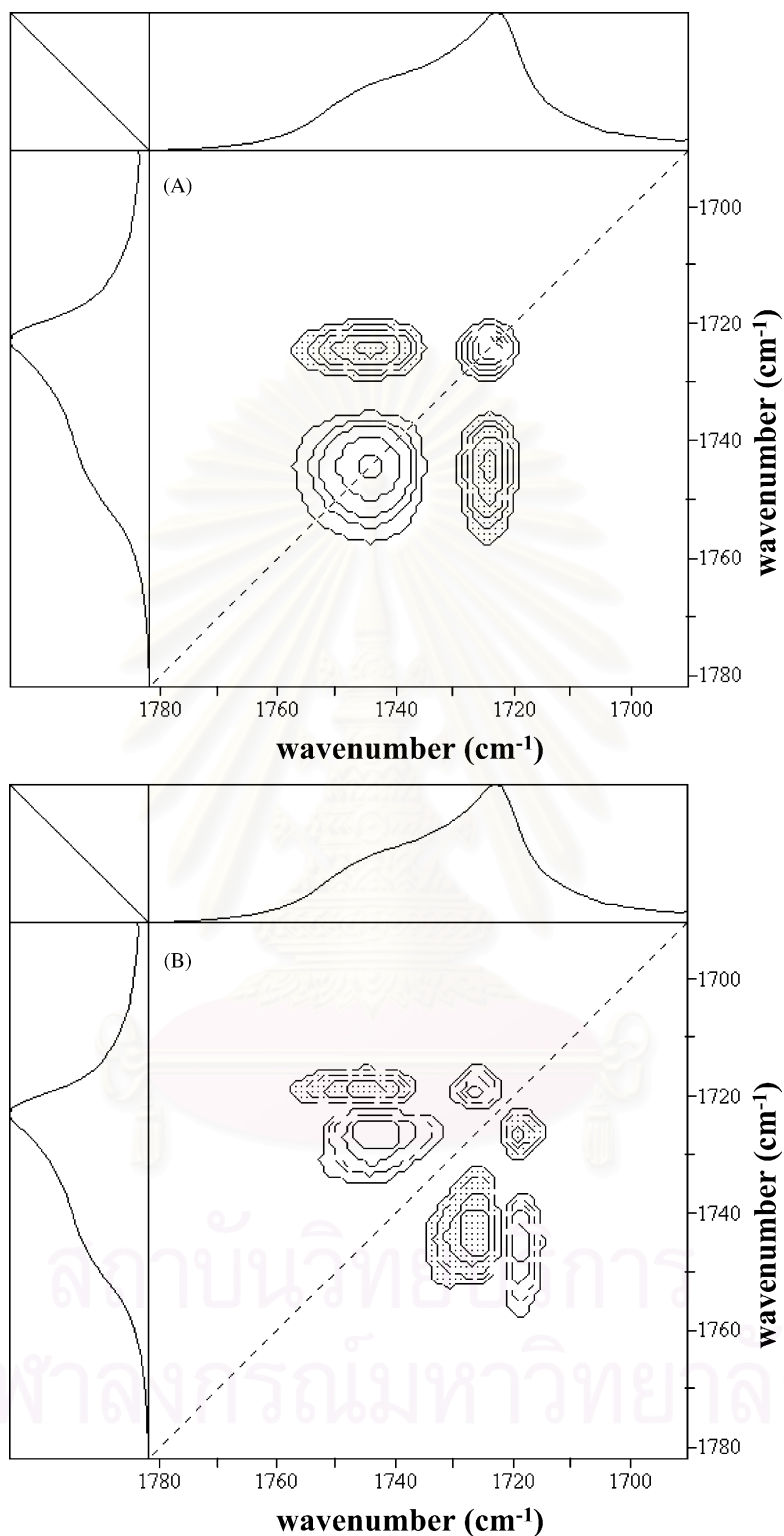


Fig. 3. Synchronous (A) and asynchronous (B) correlation spectra of PHB in the C=O stretching vibration region constructed from dynamic IR spectra in the melting process.

Referring to the stereograph of the molecular structure for PHB in a crystalline state determined by X-ray diffraction [9], the polymer chains form a helical structure, and the crystal lattice of the polymer contains two left-handed helical molecules in an antiparallel orientation. In the helical

structure, the distance between the neighboring C=O groups along the chain is ca. 4–5 Å. Thus, the splitting of the C=O stretching band of PHB observed below the T_m possibly arises from the dipole-dipole interaction between the C=O groups in the crystalline structure.

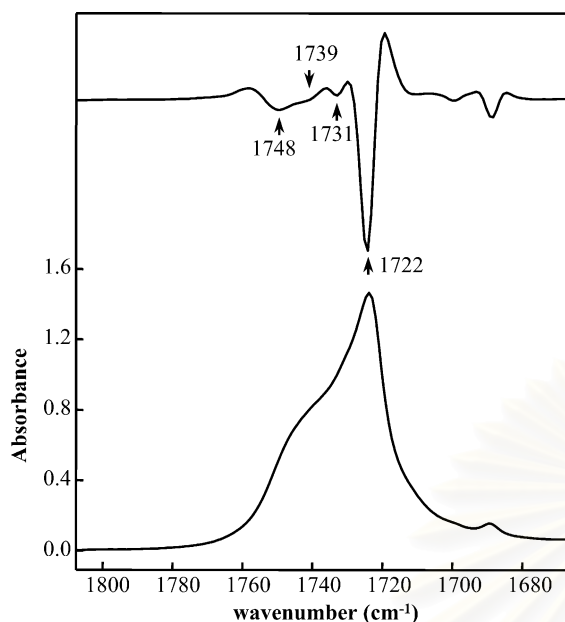


Fig. 4. A second derivative spectrum calculated from the infrared spectrum of PHB in the C=O stretching vibration region at 40 °C.

To extract more detailed information about the spectral variations taking place during the phase transition process, 2D correlation spectroscopy was employed. Fig. 3(A) and (B) shows the synchronous and asynchronous 2D correlation spectra, respectively, in the spectral region of 1780–1700 cm^{-1} generated from the temperature-dependent IR spectra measured over a temperature range of 40–150 °C. Two autopeaks developed at around 1744 and 1724 cm^{-1} together with negative cross peaks at $\sim(1744, 1724) \text{cm}^{-1}$ indicate the spectral variations of the amorphous and crystalline components of the PHB polymer. Three pairs of cross

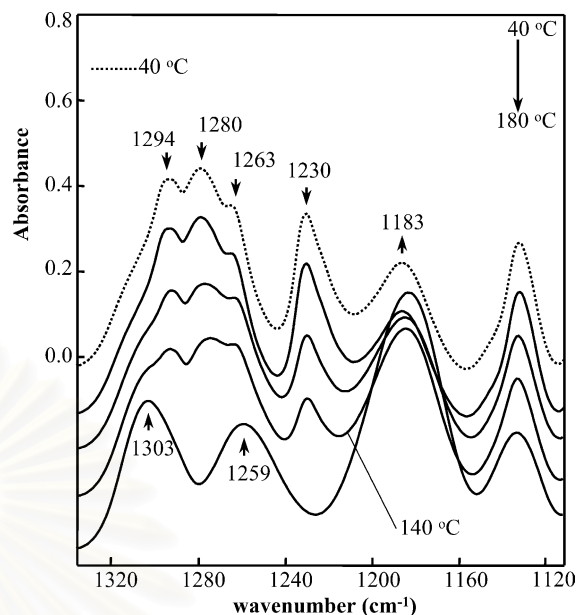


Fig. 5. IR spectra of PHB in the C–O–C stretching vibration region (1320–1120 cm^{-1}) collected over a temperature range of 40–180 °C.

peaks are observed at $\sim(1744, 1731)$, $\sim(1744, 1722)$, and $\sim(1731, 1722) \text{cm}^{-1}$ in the corresponding asynchronous spectrum. It should be noted that the existences of these bands are confirmed also by the second derivative of the spectrum of PHB at 40 °C shown in Fig. 4. Although the band at 1731 cm^{-1} presents as a small peak in the second derivative spectrum, the asynchronous 2D spectrum clearly sorts out the existence of this band. The second derivative spectrum depicts two bands at 1748 and 1739 cm^{-1} in the amorphous region. These two bands, however, show no asynchronicity with each other in the 2D asynchronous map. The positive synchronous spectral intensity in the region containing the coordinate at $\sim(1731, 1722) \text{cm}^{-1}$ indicates the same direction of the intensity variations of these two bands while the negative synchronous spectral intensity containing the coordinates at $\sim(1744, 1731)$ and $\sim(1744, 1722) \text{cm}^{-1}$ suggests that the broad band located around 1744 cm^{-1} varies in the opposite direction from the two bands at 1731 and 1722 cm^{-1} . The highly overlapped bands located around 1744 and 1722 cm^{-1} are not resolved in the synchronous map because, unlike an asynchronous spectrum, which is powerful in differentiating bands arising from different origins, a synchronous spectrum generally shows overall similarities of spectral variations. The frequencies of the bands in the C=O stretching vibration region and their assignments are summarized in Table 1.

The asynchronous 2D correlation spectrum resolves the two highly overlapped bands at around 1731 and 1722 cm^{-1} arising from the crystalline state. It can be seen from Fig. 4 that the band at 1722 cm^{-1} is much stronger than that at 1731 cm^{-1} . Based on its frequency and intensity, the band at 1722 cm^{-1} may be assigned to the C=O stretching mode of the well-ordered crystalline state of PHB [12]. The minor

Table 1

Assignments of IR bands in the C=O, C–O–C, and C–H stretching vibration regions

Functional groups	Wavenumber (cm^{-1})	Assignments
C=O	1748	amorphous
	1739	amorphous
	1731	crystalline
	1723	crystalline
C–O–C	1303	amorphous
	1294	crystalline
	1280	crystalline
	1263	crystalline
	1259	amorphous
	1230	crystalline
CH ₃	1183	amorphous
	3007	crystalline
	2995	crystalline
	2985	amorphous
	2975	crystalline
CH ₂	2967	crystalline
	2938	amorphous
	2934	crystalline
	2929	crystalline

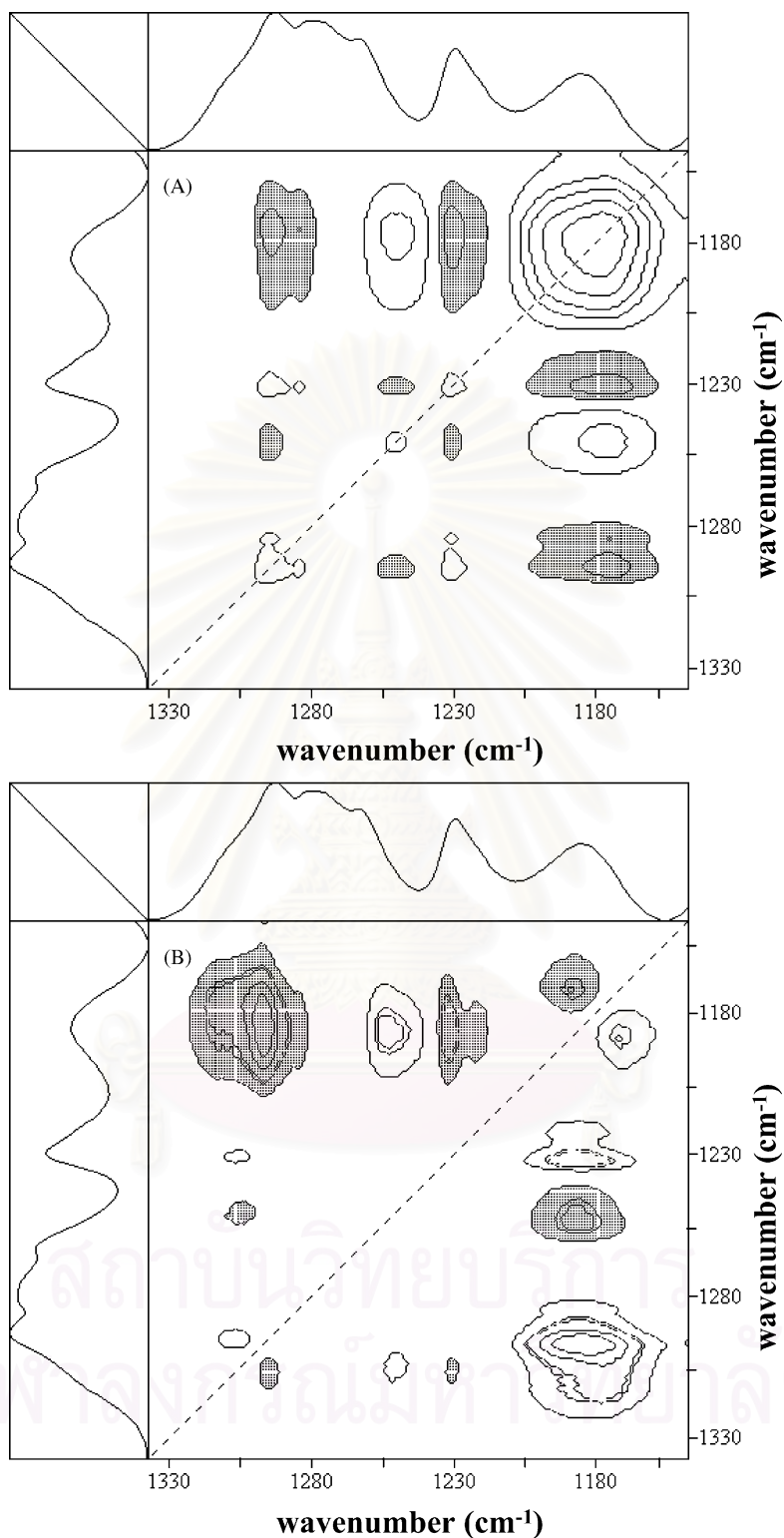


Fig. 6. Synchronous (A) and asynchronous (B) correlation spectra of PHB in the C–O–C stretching vibration region constructed from dynamic IR spectra in the melting process.

band at 1731 cm^{-1} may be due to the C=O stretching mode of the less ordered crystalline part of the polymer [12].

Of note in the asynchronous map is that there are asynchronous cross peaks between the crystalline and amorphous

bands. This indicates that the decreases in the crystalline components and the increase in the amorphous component take place out of phase. It is very likely that the melting of PHB occurs through an intermediate state. However, no

IR band due to the intermediate state is clearly detected. In our previous study [12], it was revealed that the melting of P(HB-co-HHx) (12 mol% HHx) proceeds through an intermediate state. Wu et al. [13] and Tian et al. [14] investigated the melting behavior of P(HB-co-HHx) (10 mol% HHx) and P(HB-co-HV) (20.4 mol% HV), respectively, by using 2D IR correlation spectroscopy and suggested from the asynchronous spectra for the C=O stretching region that an intermediate state appears in the course of the melting process. Thus, the present study indicates that an intermediate state exists commonly in the melting process of this class of polymers.

3.2. Temperature-dependent changes in the C–O–C stretching vibration region

Fig. 5 shows the temperature-dependent changes in the IR spectra of PHB in the 1320–1120 cm^{-1} region. The cluster of bands in this region is ascribed to the stretching vibrations of the C–O–C groups [12–15]. Although this region contains more bands than the C=O stretching vibration region, the spectral changes caused by the melting process of the polymer are clear. The intensities of the bands at 1294, 1280, 1263, and 1230 cm^{-1} decrease upon passing from the crystalline to the amorphous state of the polymer, whereas those of the bands at 1303, 1259, and 1183 cm^{-1} increase in the course of temperature increase.

The synchronous and asynchronous 2D correlation spectra in the 1330–1155 cm^{-1} region calculated from the temperature-dependent IR spectra of PHB are shown in Fig. 6(A) and (B), respectively. There are at least four autopeaks at 1294, 1254, 1230, and 1180 cm^{-1} . The autopeak at 1294 cm^{-1} extends to the vicinity of 1280 cm^{-1} , and that near 1180 cm^{-1} is very broad. Thus, it seems that both autopeaks consist of more than one peak. A pair of asynchronous peaks at (1188, 1170 cm^{-1}) may be due to a band shift, but the autopeak near 1180 cm^{-1} is so broad and thus, there may be two bands near 1180 cm^{-1} . It is noted that the crystalline bands at 1294, 1280, 1263, and 1230 cm^{-1} do not share any asynchronous peak, and that there are several cross peaks between an amorphous band (e.g., 1180 cm^{-1}) and crystalline bands (e.g., 1294–1280 and 1230 cm^{-1}). These observations again indicate the existence of an intermediate state during the phase transition. The frequencies of the bands in the C–O–C stretching vibration region and their assignments are summarized in Table 1.

3.3. Temperature-dependent changes in the C–H stretching vibration region

The temperature-dependent changes in the IR spectra of PHB in the 3100–2850 cm^{-1} region are shown in Fig. 7. For the C–H stretching vibration region, bands located around 2980 cm^{-1} are due to the CH₃ asymmetric stretching mode while those appeared around 2930 cm^{-1} are attributed to the CH₂ antisymmetric stretching vibration. For PHB, the CH₃

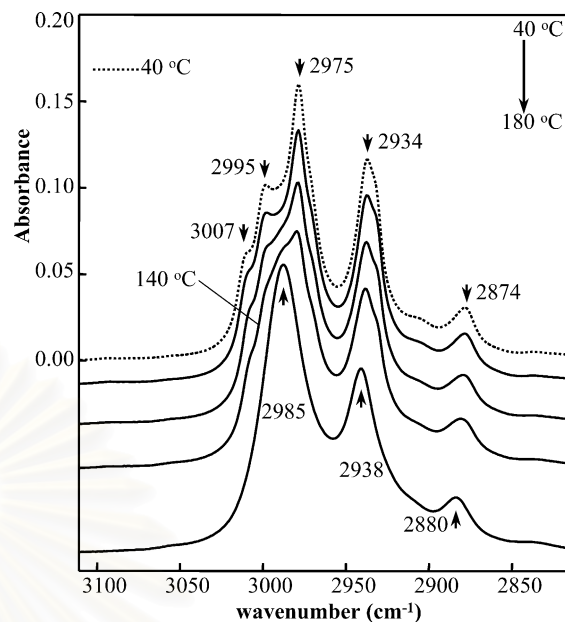


Fig. 7. IR spectra of PHB in the C–H stretching vibration region (3100–2850 cm^{-1}) collected over a temperature range of 40–180 °C.

group exists only on the side chain while the CH₂ group is located on the skeletal chain. As described in the introduction, the chemical modification on the side chain of PHB is very important for improving its mechanical properties, therefore the investigation on the thermal behavior of the CH₃ group is very interesting.

As temperature increases, the CH₃ stretching band at 2975 cm^{-1} decreases while that at 2985 cm^{-1} increases. Similarly, the CH₂ stretching band at 2934 cm^{-1} decreases while that at 2938 cm^{-1} increases with increasing

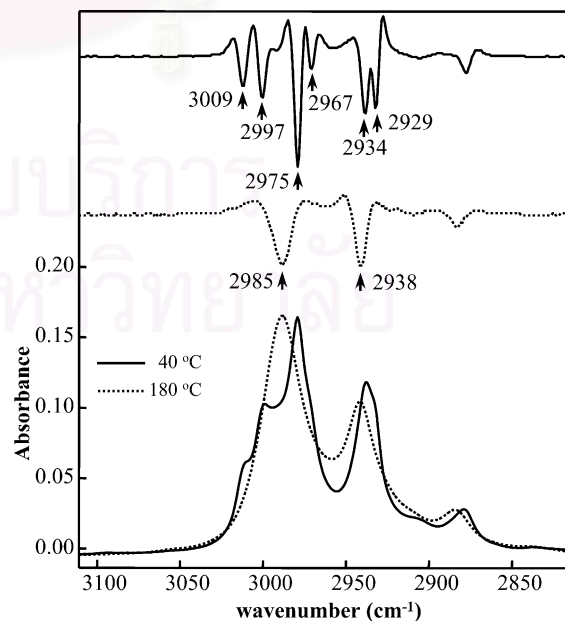


Fig. 8. Second derivative spectra calculated from the infrared spectra of PHB in the C–H stretching vibration region at 40 and 180 °C.

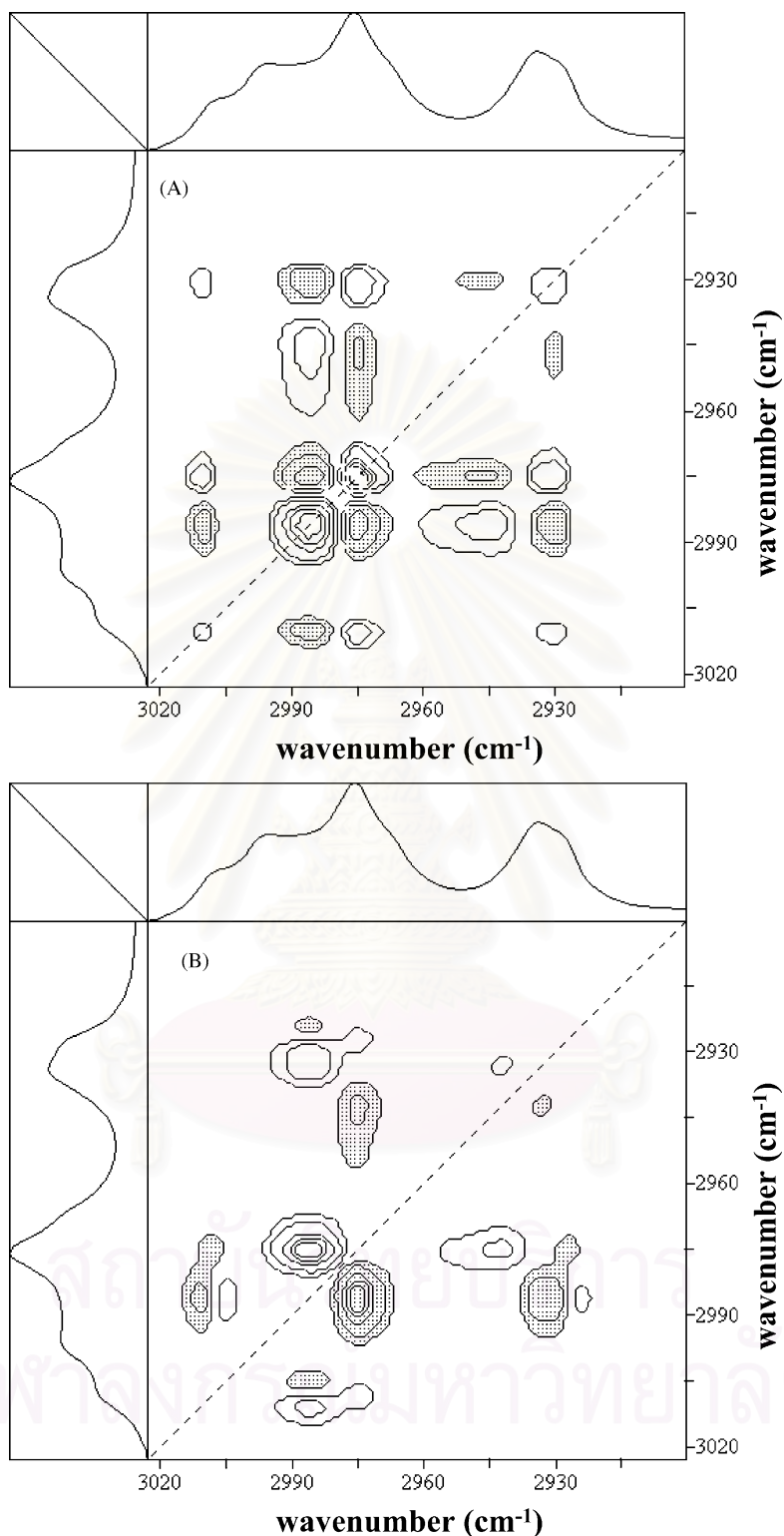


Fig. 9. Synchronous (A) and asynchronous (B) correlation spectra of PHB in the C–H stretching vibration region constructed from dynamic IR spectra in the melting process.

temperature. Note that at room temperature, there exist two peaks at 3007 and 2995 cm⁻¹, but they disappear at 180 °C. These two bands and the band at 2975 cm⁻¹ may be ascribed to the crystalline CH₃ stretching vibration bands resulting from the crystal field splitting of the band at

2985 cm⁻¹. Crystal field splittings of bands occur in some semi-crystalline polymers [17]. The crystal field splitting may be caused not only by the intramolecular interaction between analogous functional groups attached along a polymer chain but also by the intermolecular interaction be-

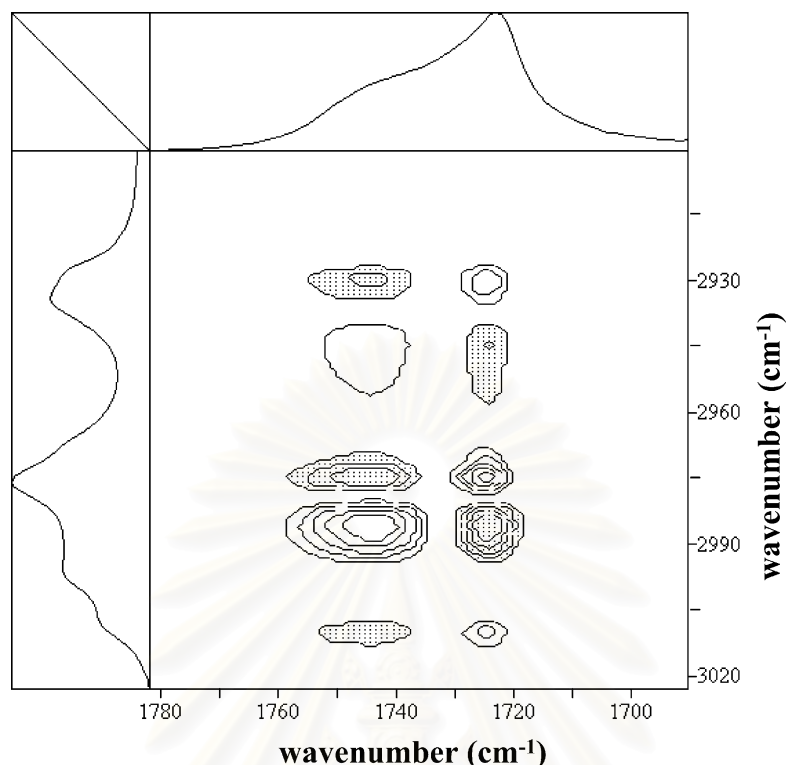


Fig. 10. Hetero-correlation synchronous spectrum of PHB between the C=O and C–H stretching vibration regions constructed from dynamic IR spectra in the melting process.

tween those groups located in the crystalline lattice. The crystalline band splittings of certain vibration modes have been reported for a number of polymers especially those having a helical chain structure [17]. The second derivatives of the IR spectra of PHB in this region for the amorphous (at 180 °C) and crystalline (at 40 °C) states are shown in Fig. 8. Two additional bands at 2967 and 2929 cm^{-1} are detected in the second derivative spectrum for the crystalline state.

Fig. 9(A) and (B) illustrates the synchronous and asynchronous 2D correlation spectra in the 3020–2915 cm^{-1} region constructed from the temperature-dependent IR spectra. Four autopeaks are clearly observed at 3009, 2985, 2975, and 2930 cm^{-1} in the synchronous map. The three peaks at 3009, 2975, and 2930 cm^{-1} share three positive cross peaks at (3009, 2975), (3009, 2930), and (2975, 2930) cm^{-1} , and the peak at 2985 cm^{-1} shares negative cross peaks with those at 3009, 2975, and 2930 cm^{-1} . These observations confirm that the three bands at 3009, 2975, and 2930 cm^{-1} vary in the same direction, which is opposite to that of the band at 2985 cm^{-1} , with the change in temperature.

The asynchronous map and the second derivatives (Fig. 8) reveal that there are three bands at \sim 2940, 2934, and 2929 cm^{-1} assignable to the antisymmetric CH_2 stretching mode. The amorphous band at 2985 cm^{-1} shares asynchronous cross peaks with the crystalline bands at 3009, 2975, 2934, and 2929 cm^{-1} . This also suggests that the

amorphous phase does not appear simultaneously with the disappearance of the crystalline state. The synchronous and asynchronous 2D correlation spectra in the C–H stretching vibration region reveal clearly that the intensity changes of all crystalline bands in this region occur simultaneously, i.e., there is no asynchronicity between any crystalline band in the C–H stretching vibration region. Therefore, it is very likely that the crystalline bands observed in this region are caused by the crystal field splittings.

A synchronous 2D correlation spectrum between the C=O and C–H stretching regions was generated from the temperature-dependent IR spectra and is demonstrated in Fig. 10. The synchronous cross peaks and their signs at the spectral coordinates of 1745 and 1725 cm^{-1} versus 3009, 2986, 2975, and 2930 cm^{-1} clarify that the bands located at 3007, 2975, 2934, and 2929 cm^{-1} arise from the crystalline part of the polymer while the band at 2985 cm^{-1} is ascribed to the amorphous part. The frequencies of the bands in the C–H stretching vibration region and their assignments are summarized in Table 1.

We also measured the temperature-dependent IR spectra of PHB during a cooling down process. 2D correlation maps for the C=O region show the similar patterns to those shown in Fig. 3. That is to say, in the crystallization process of PHB, the decrease in the amorphous component and the increase in the crystalline component do not take place simultaneously.

4. Conclusion

The melting behavior of PHB was investigated by using generalized 2D IR correlation spectroscopy. The spectral intensities in the C=O, C–O–C, and C–H stretching vibration regions are markedly changed with the temperature change. The crystalline bands decrease while the amorphous bands increase during the melting process. This is because the highly ordered and helical structure of the PHB polymer is diminished at high temperature.

The asynchronous 2D correlation spectrum generated from the temperature-induced dynamic IR spectra in the C=O stretching vibration region resolves two highly overlapped crystalline bands located at around 1731 and 1722 cm^{-1} . The coexistence of these two bands is confirmed also by the second derivative of the spectrum of PHB in the C=O stretching band region at 40 °C. The intense band at 1722 cm^{-1} may be attributed to the major crystalline part of the polymer, and the much weaker feature at around 1731 cm^{-1} is possibly assignable to the minor crystalline component with a less ordered structure. The appearances of the asynchronous cross peaks at $\sim(1744, 1731)$ and $\sim(1744, 1722)$ cm^{-1} indicate the out-of-phase variations of the crystalline and amorphous parts, suggesting the existence of an intermediate state in the melting process.

Bands in the C–O–C and C–H stretching regions have also been classified into those arising from the crystalline and amorphous parts. The CH_3 asymmetric stretching bands and CH_2 antisymmetric stretching bands of the crystalline phase split into four bands at 3007, 2995, 2975, and 2967 cm^{-1} , and two bands at 2934 and 2929 cm^{-1} , respectively. This splitting is very likely due to crystal field splitting, which is often observed for polymers with a helical structure. These bands share positive synchronous cross peaks, and there is no asynchronicity among them, confirming that these bands arise from the crystal field splitting.

Acknowledgements

A.P. gratefully thanks the Thailand Research Fund (TRF) for the financial support via the Royal Golden Jubilee (RGJ) Ph.D. program (Grant contract number: PHD/0066/2544).

References

- [1] L.M. Lara, W.H. Gjalt, *Microbiol. Mol. Biol. Rev.* 63 (1991) 21.
- [2] A.J. Anderson, E.A. Dawes, *Microbiol. Rev.* 54 (1990) 450.
- [3] D. Jendrosseck, in: A. Steinbüchel, Y. Doi (Eds.), *Biopolymers*, Wiley-VCH, Weinheim, 2001, p. 41.
- [4] S.F. Williams, D.P. Martin, in: A. Steinbüchel, Y. Doi (Eds.), *Biopolymers*, Wiley-VCH, Weinheim, 2002, p. 91.
- [5] S.Y. Lee, *Biotechnol. Bioeng.* 49 (1996) 1.
- [6] <http://www.nodax.com>.
- [7] M.M. Satkowski, D.H. Melik, J.-P. Aufran, P.R. Green, I. Noda, L.A. Schechtman, in: A. Steinbüchel, Y. Doi (Eds.), *Biopolymers*, Wiley-VCH, Weinheim, 2001, p. 231.
- [8] J. Cornibert, R.H. Marchessault, *Macromolecules* 8 (1975) 296.
- [9] M. Yokouchi, Y. Chatani, H. Tadokoro, K. Teranishi, H. Tani, *Polymer* 14 (1973) 267.
- [10] H. Sato, M. Nakamura, A. Padermshoke, H. Yamaguchi, H. Terauchi, S. Ekgasit, I. Noda, Y. Ozaki, *Macromolecules* 37 (2004) 3763.
- [11] H. Sato, A. Padermshoke, M. Nakamura, R. Murakami, F. Hirose, K. Senda, H. Terauchi, S. Ekgasit, I. Noda, Y. Ozaki, *Macromol. Symp.* (2004) in press.
- [12] A. Padermshoke, H. Sato, Y. Katsumoto, S. Ekgasit, I. Noda, Y. Ozaki, *Vib. Spectrosc.*, in press.
- [13] Q. Wu, G. Tian, S. Sun, I. Noda, G.-Q. Chen, *J. Appl. Polym. Sci.* 82 (2001) 934.
- [14] G. Tian, Q. Wu, S. Sun, I. Noda, G.-Q. Chen, *J. Polym. Sci. Part B: Polym. Phys.* 40 (2002) 649.
- [15] G. Tian, Q. Wu, S. Sun, I. Noda, G.-Q. Chen, *Appl. Spectrosc.* 55 (2001) 888.
- [16] P. Iruondo, J.J. Iruin, M.J. Fernandez-Berridi, *Polymer* 36 (1995) 3235.
- [17] S.K. Mallapragada, B. Narasimhan, in: R.A. Meyers (Ed.), *Encyclopedia of Analytical Chemistry*, John Wiley and Sons, Chichester, 2000, p. 7644.
- [18] I. Noda, *Bull. Am. Phys. Soc.* 31 (1986) 520.
- [19] I. Noda, *Appl. Spectrosc.* 47 (1993) 1329.
- [20] I. Noda, G.M. Story, C. Marcott, *Vib. Spectrosc.* 19 (1999) 461.
- [21] I. Noda, A.E. Dowrey, C. Marcott, G.M. Story, Y. Ozaki, *Appl. Spectrosc.* 54 (2000) 236A.
- [22] H.-C. Chang, K.M. Lee, J.-C. Jiang, M.-S. Lin, J.-S. Chen, I.J.B. Lin, S.H. Lin, *J. Chem. Phys.* 117 (2002) 1723.
- [23] J. Dybal, B. Schneider, *Spectrochim. Acta A* 41 (1985) 691.
- [24] J. Dybal, J. Spevacek, B. Schneider, *J. Polym. Sci. Part B: Polym. Phys.* 24 (1986) 657.
- [25] E. Galbiati, M.D. Zoppo, G. Tieghi, G. Zerbi, *Polymer* 34 (1993) 1806.
- [26] J. Cornibert, R.H. Marchessault, *J. Mol. Biol.* 71 (1972) 735.
- [27] H. Torii, M. Tasumi, *J. Raman Spectrosc.* 29 (1998) 81.
- [28] H. Torii, M. Tasumi, *J. Chem. Phys.* 96 (1992) 3379.



Thermally induced phase transition of poly(3-hydroxybutyrate-co-3-hydroxyhexanoate) investigated by two-dimensional infrared correlation spectroscopy

Adchara Padermshoke^{a,b}, Harumi Sato^a, Yukiteru Katsumoto^c,
Sanong Ekgasit^b, Isao Noda^d, Yukihiro Ozaki^{a,*}

^aDepartment of Chemistry, School of Science and Technology, Kwansai-Gakuin University, Sanda, Hyogo 669-1337, Japan

^bDepartment of Chemistry, Faculty of Science, Chulalongkorn University, Patumwan, Bangkok 10330, Thailand

^cDepartment of Chemistry, Graduate School of Science, Hiroshima University, Higashi-Hiroshima, Hiroshima 739-8526, Japan

^dThe Procter and Gamble Company, 8611 Beckett Road, West Chester, OH 45069, USA

Received 3 October 2003; received in revised form 13 November 2003; accepted 13 November 2003

Abstract

The thermally induced crystalline/amorphous phase transition process of a newly developed biodegradable polymer, poly(3-hydroxybutyrate-co-3-hydroxyhexanoate) (P(HB-co-HHx)) (HHx = 12 mol%), was investigated by using generalized two-dimensional infrared (2D IR) correlation spectroscopy. Three spectral regions, the C–H stretching (3100–2800 cm⁻¹), C=O stretching (1780–1680 cm⁻¹), and C–O–C stretching (1330–1200 cm⁻¹) band regions were analyzed in order to explore the phase transition behavior of the copolymer. The asynchronous 2D spectrum generated from the temperature-induced variations in IR spectra in the C=O stretching band region clearly revealed the coexistence of two crystalline bands at 1731 and 1723 cm⁻¹. The dominant band at 1723 cm⁻¹ may arise from the highly ordered crystalline component of the copolymer, and the weaker band at 1731 cm⁻¹ is possibly due to the minor crystalline component with a less ordered structure. The major crystalline band at 1723 cm⁻¹ shares asynchronous cross peaks with the amorphous band at 1740 cm⁻¹. This observation suggests that the melting of the crystalline structure does not simultaneously result in the formation of the completely amorphous structure. The phase transition process of P(HB-co-HHx) (12 mol% HHx) takes place through an intermediate state. It is noted that the vibrational frequencies of the C=O, C–O–C, and C–H stretching bands due to the crystalline components of P(HB-co-HHx) (12 mol% HHx) are almost identical to those of PHB. These observations indicate that the helical structure of P(HB-co-HHx) (12 mol% HHx) is very similar to that of PHB. The inclusion of the HHx comonomer locally disrupts the highly ordered and helical structure of PHB from place to place, thereby reducing the crystallinity of the copolymer. It was also found that the helical structure of P(HB-co-HHx) (12 mol% HHx) is deformed gradually from much lower temperature than that of PHB.

© 2004 Elsevier B.V. All rights reserved.

Keywords: Polyhydroxyalkanoates (PHAs); Phase transition; 2D IR spectroscopy

1. Introduction

Bacterially synthesized poly(3-hydroxyalkanoate)s (PHAs) are a class of naturally occurring biodegradable polyesters accumulated as energy-storing inclusion body granules in the cells of certain microorganisms [1–4]. Since PHAs can be biologically synthesized from renewable resources and degraded by bacteria in the soil, they have received a great attention as a new family of environmental friendly polymeric materials [2,5,6]. Despite their completely natural origin, PHAs bear a fairly close resemblance to

some petroleum-based synthetic polymers in chemical structures and physical characteristics and possess an attractive combined set of end use properties. One of the simplest and largely produced PHA polymers is poly(3-hydroxybutyrate) (PHB) [3,4]. Its ultimate tensile strength is comparable to that of isotactic polypropylene (PP) [4]. Since PHB is biocompatible, its utilization for medical purposes is also being contemplated. However, PHB is stiff and brittle due to the high degree of crystallinity, and it is also thermally unstable during processing [7]. Consequently, various efforts have been made to copolymerize PHB with other comonomers to improve its mechanical properties [7]. Recently, the Procter and Gamble Company (Cincinnati, USA) has introduced a new family of commercial PHA

* Corresponding author. Tel.: +81-79-565-8349; fax: +81-79-565-9077.
E-mail address: ozaki@ksc.kwansei.ac.jp (Y. Ozaki).

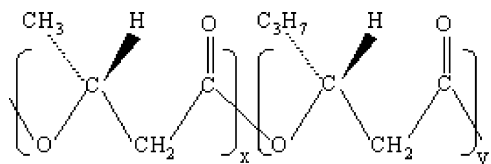


Fig. 1. Molecular structure of P(HB-*co*-HHx).

copolymers under the trade name NodaxTM [6]. Nodax copolymer is comprised of 3-hydroxybutyrate and other longer side-chain 3-hydroxyalkanoates [6]. Poly(3-hydroxybutyrate-*co*-3-hydroxyhexanoate) (P(HB-*co*-HHx)) with the melting temperature (T_m) of about 110–160 °C and approximately 35–45% crystallinity are typical available commercial grades of Nodax copolymers. The molecular structure of P(HB-*co*-HHx) is shown in Fig. 1 [8,9].

The copolymer being investigated in the present study is P(HB-*co*-HHx) with 12 mol% HHx comonomer. The introduction of less crystallizable units, i.e., 3HHx, into the molecular chain of PHB dramatically improves the physical and mechanical properties of the resulting copolymer [6]. As a consequence, P(HB-*co*-HHx) possesses many attractive features, which are not only the notable physical and mechanical properties, but also the additional beneficial characteristics of polyesters. P(HB-*co*-HHx) has excellent surface properties (e.g., printability, dyeability, dispersibility, adhesion, etc.), and it is compatible with various additives and other polymers [6]. Examples of the potential applications of P(HB-*co*-HHx) include flushable products, films and flexible packaging, coated papers, synthetic papers, and bioresorbable medical devices [6].

Since the crystallinity is one of the most important key parameters for material applications of polymers and their further chemical or mechanical processing, the crystalline/amorphous phase transition behavior of PHAs has gained keen interest [5,10–13]. We have been performing a series of studies on the structure and thermal behavior of PHB and P(HB-*co*-HHx) by using temperature-dependent wide-angle x-ray diffraction (WAXD) [14,15], differential scanning calorimetry (DSC) [14,15], and infrared (IR) spectroscopy [15,16]. The WAXD study [14,15] suggested that there are inter- and intramolecular interactions between the C=O and CH₃ groups in PHB and P(HB-*co*-HHx), and that the interactions decrease along the *a* axis of the crystal lattice of PHB and P(HB-*co*-HHx) with temperature. Two-dimensional (2D) IR correlation analysis [16] indicated that the phase transition of PHB involves one major and one minor crystalline components. Asynchronous 2D correlation maps generated from the temperature-dependent IR spectra of PHB revealed clearly the existence of an intermediate state during the phase transition of PHB. Since the copolymerization of the HHx comonomer with PHB results in dramatically improved physical and mechanical properties of the resulting material, it is of great interest to reveal how the HHx units affect the crystallinity of P(HB-*co*-HHx) copolymer. In this paper, the thermal-melting behavior of P(HB-*co*-HHx)

(12 mol% HHx) was explored by using 2D IR correlation spectroscopy in comparison to that of PHB homopolymer, which is the basic unit of this class of biopolyesters.

IR spectroscopy is very suitable for the studies of crystalline/amorphous phase transitions of polymers because it allows one to gain insight into the phase transition behavior at the molecular functional group level [17]. The combination of IR spectroscopy with 2D correlation analysis proposed by Noda [18–20] enables a more detailed analysis on the spectral variations of polymers under various types of external perturbations [10–12,16,18–22]. 2D IR correlation spectroscopy possesses several distinctive advantages for analyzing severely overlapped bands and determining the sequential order of the intensity changes of bands caused by an external perturbation. Accordingly, the studies on the crystalline/amorphous phase transition by using 2D IR correlation spectroscopy have been carried out for some PHA polymers [10–12,16]. Wu et al. [10] and Tian et al. [12] showed, based on the 2D asynchronous spectra generated from the temperature-dependent IR spectra in the C=O stretching vibration region, the existence of an intermediate state during the phase transition of P(HB-*co*-HHx) (10 mol% HHx) and that of P(HB-*co*-HV), respectively. Recently, we investigated the changes in the crystalline structure of PHB during thermal melting process by using 2D IR correlation spectroscopy [16]. The 2D correlation maps generated from the temperature-dependent IR spectra in the C=O, C–O–C, and C–H stretching vibration regions showed a clear spectroscopic evidence for the coexistence of one major and one minor crystalline components and the presence of an intermediate state during the melting of the polymer.

The purpose of the present study is to investigate the crystalline/amorphous phase transition behavior of P(HB-*co*-HHx) (12 mol% HHx) ($T_m \cong 110^\circ\text{C}$) by using 2D IR correlation spectroscopy. This study allows us to gain a microscopic view of the transition behavior of the copolymer at the functional group level. The present investigation is complementary to our previous studies on PHB and P(HB-*co*-HHx) (12 mol% HHx) by DSC and WAXD [14,15]. The comparison between the phase transition behavior of P(HB-*co*-HHx) and that of PHB homopolymer is also discussed here in order to reveal effects of the copolymerized HHx units on the structure of P(HB-*co*-HHx).

2. Experimental

2.1. Materials

Bacterially synthesized P(HB-*co*-HHx) (12 mol% HHx) (the Procter and Gamble Company, USA) was purified by dissolving in hot chloroform (CHCl₃), re-precipitating in methanol (CH₃OH), and vacuum-drying at 60 °C for 24 h. The purified P(HB-*co*-HHx) (12 mol% HHx) sample thus obtained was used in all IR experiments. Chloroform and

methanol were purchased from Wako Pure Chemical Industries, Ltd. (Osaka, Japan) and used as received. A film of P(HB-*co*-HHx) (12 mol% HHx) for IR measurements was prepared by casting its chloroform solution on a CaF₂ window. The film was kept at 60 °C in a vacuum-dried oven for 12 h and cooled down to room temperature before the measurements.

2.2. IR spectroscopic measurements

IR spectra of the film sample were measured at a 2 cm⁻¹ spectral resolution by using a Nicolet Magna-IRTM 550 spectrometer equipped with a mercury cadmium telluride (MCT) detector. To ensure a high signal-to-noise ratio, 512 scans were co-added. The temperature of the sample cell that holds the CaF₂ window with the P(HB-*co*-HHx) (12 mol% HHx) film was controlled by using a temperature controller unit (CHINO, model SU) with an accuracy of ±2 °C. The temperature-perturbed dynamic IR spectra were collected throughout a temperature range of 30–140 °C with an increment of 10 °C.

2.3. 2D correlation analysis

The calculations of 2D correlation spectra were performed by using the 2D-Pocha software composed by Daisuke Adachi (Kwansei-Gakuin University, Japan). All IR spectra were baseline-corrected prior to the 2D correlation calculation.

3. Results and discussion

3.1. Changes in the C=O stretching band region during the melting process

Fig. 2 shows temperature-dependent IR spectra of P(HB-*co*-HHx) (12 mol% HHx) in the 1780–1680 cm⁻¹ region

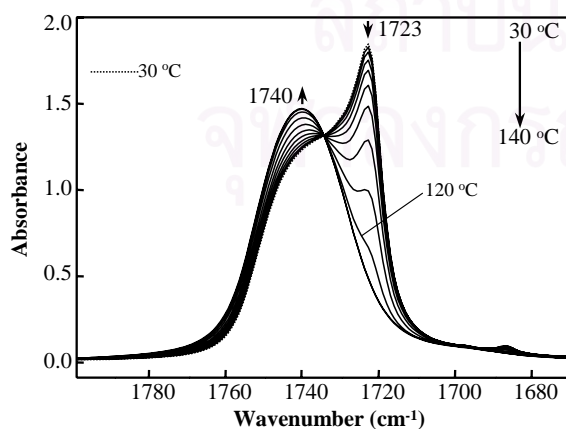


Fig. 2. IR spectra of P(HB-*co*-HHx) (12 mol% HHx) in the C=O stretching vibration region (1780–1680 cm⁻¹) measured over a temperature range of 30–140 °C.

where bands due to the C=O stretching mode are expected to appear. A sharp band at 1723 cm⁻¹ gradually decreases and eventually disappears with increasing temperature, while a broad band at 1740 cm⁻¹ increases in intensity. The band shape in the C=O stretching vibration region changes greatly from a sharp peak with a broad shoulder to a symmetrical broad band in the course of temperature increase. The sharp peak near 1723 cm⁻¹ is assigned to a crystalline band associated with the ordered C=O groups in PHA polymers, while the broad band located around 1740 cm⁻¹ is ascribable to an amorphous C=O band [10–12,16]. The C=O group is very sensitive to its environment [23]. Therefore, bands in the C=O stretching vibration region are particularly useful for monitoring the crystallization and melting processes of polymers in this class [10–12,16].

The splitting of the C=O stretching bands into the amorphous and crystalline bands observed at 1740 and 1723 cm⁻¹, respectively, in the IR spectra of P(HB-*co*-HHx) (12 mol% HHx) is also observed in those of PHB [16].

To gain more detailed information about the spectral variations induced by the thermal-melting process, 2D correlation spectroscopy was employed. Fig. 3(A) and (B) shows the synchronous and asynchronous 2D correlation spectra in the spectral region of 1790–1670 cm⁻¹ generated from the temperature-dependent IR spectra measured over the temperature range of 30–140 °C, respectively. Two autopeaks located at 1745 and 1723 cm⁻¹ reflect the spectral variations due to the amorphous and crystalline components of the polymer, respectively. A pair of negative cross peaks developed at (1745, 1723) cm⁻¹ in the synchronous spectrum indicates the opposite directions of the intensity variations in these two correlated bands. In the asynchronous spectrum (Fig. 3(B)), two pairs of cross peaks appear at (1745, 1722) and (1728, 1722) cm⁻¹. Note that in the original one-dimensional IR spectra, only two absorption bands ascribed to the crystalline (i.e., the band at 1723 cm⁻¹) and amorphous (i.e., the band at 1740 cm⁻¹) parts of the copolymer are apparent, while another band is now clearly sorted out at 1728 cm⁻¹ in the 2D asynchronous spectrum. We also found the additional band in the C=O stretching vibration region for PHB at around 1731 cm⁻¹ by the use of 2D correlation analysis [16]. The existence of this band is confirmed also by the second derivative of the spectrum of P(HB-*co*-HHx) measured at 30 °C shown in Fig. 4. The second derivative spectrum yields clear indication for the presence of a band around 1731 cm⁻¹, which is consistent with the cross peak developed in the 2D asynchronous spectrum.

The positive sign of the synchronous spectral intensity in the region containing the (1731, 1723) cm⁻¹ coordinates indicates the same direction of the intensity variations in these two bands. The band at 1723 cm⁻¹ is much more intense than that at 1731 cm⁻¹. Based on its frequency and band intensity, the band at 1723 cm⁻¹ may be assigned to the C=O stretching mode of the major crystalline component of

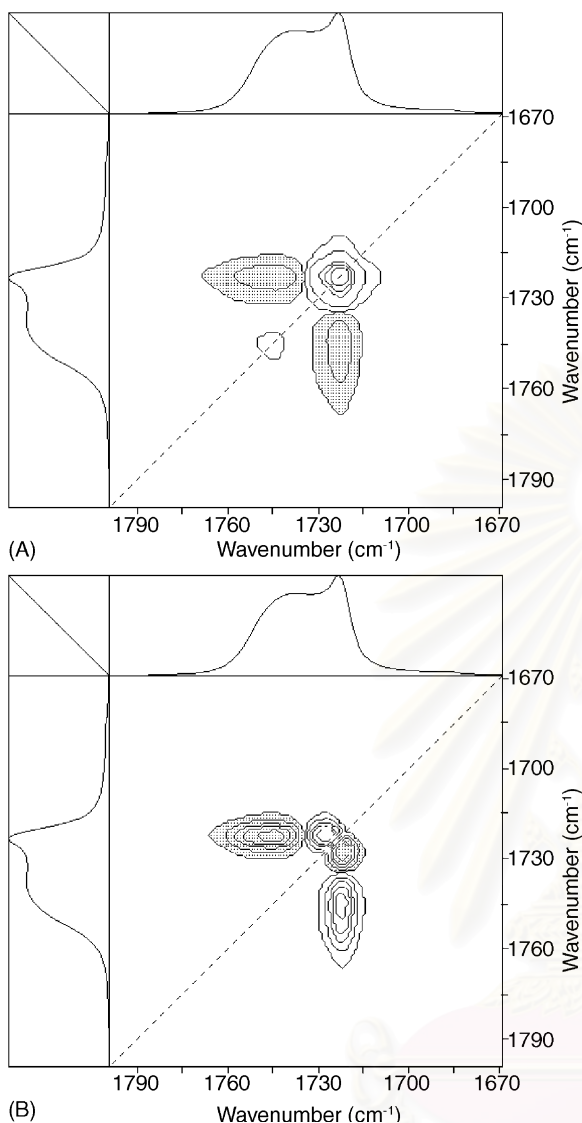


Fig. 3. Synchronous (A) and asynchronous (B) correlation spectra of P(HB-*co*-HHx) (12 mol% HHx) in the C=O stretching vibration region generated from the temperature-dependent IR spectra measured over a temperature range of 30–140 °C.

P(HB-*co*-HHx). The weaker band at 1731 cm⁻¹ may arise from the C=O stretching mode of the less ordered crystalline component of the copolymer [16]. These two highly overlapped crystalline bands are distinguished only in the 2D asynchronous spectrum because an asynchronous spectrum is very powerful in differentiating bands arising from different origins, while a synchronous spectrum generally shows overall similarities of spectral variations.

Of note in the 2D asynchronous spectrum shown in Fig. 3(B) is that there are asynchronous cross peaks between the crystalline and amorphous bands. This observation clearly indicates that the melting of the crystalline component does not proceed simultaneously with the formation of the completely amorphous component. It is very likely that the melting of P(HB-*co*-HHx) takes place through an intermediate state. The existence of an intermediate state during

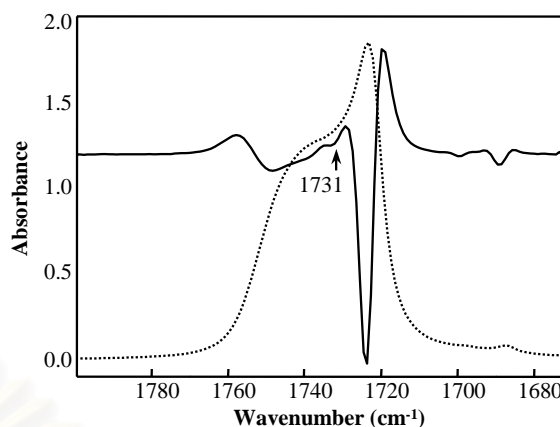


Fig. 4. A second derivative spectrum calculated from the IR spectrum of P(HB-*co*-HHx) (12 mol% HHx) in the C=O stretching vibration region at 30 °C.

the melting process was also reported for some other polymers including PHB [10,12,16]. Thus, the present study indicates that P(HB-*co*-HHx) (12 mol% HHx) undergoes the melting process through an intermediate state as other PHA polymers.

3.2. Changes in the C–O–C stretching band region during the melting process

Fig. 5 shows temperature-dependent IR spectra of P(HB-*co*-HHx) (12 mol% HHx) in the 1320–1160 cm⁻¹ region. Bands in this region are attributed to the stretching vibration modes of the C–O–C groups [10–12,16]. It can be seen from Fig. 5 that these bands change largely during the melting process of the copolymer. Bands at 1289, 1278, 1264, and 1228 cm⁻¹ decrease with increasing temperature, while three broad bands at 1303, 1259, and 1183 cm⁻¹ are dominant above the *T_m* of the copolymer. Therefore, the four bands at 1289, 1278, 1264, and 1228 cm⁻¹ are ascribed to

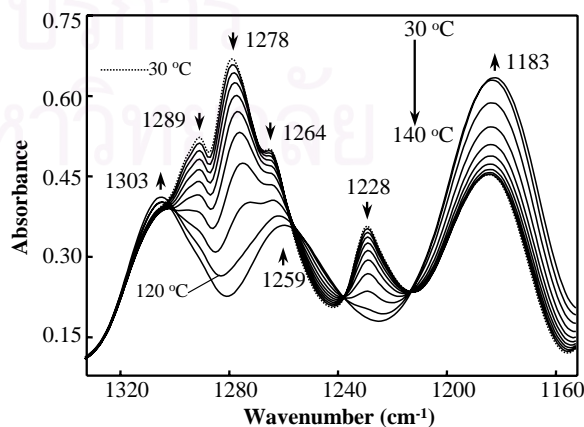


Fig. 5. IR spectra of P(HB-*co*-HHx) (12 mol% HHx) in the C–O–C stretching vibration region (1320–1160 cm⁻¹) measured over a temperature range of 30–140 °C.

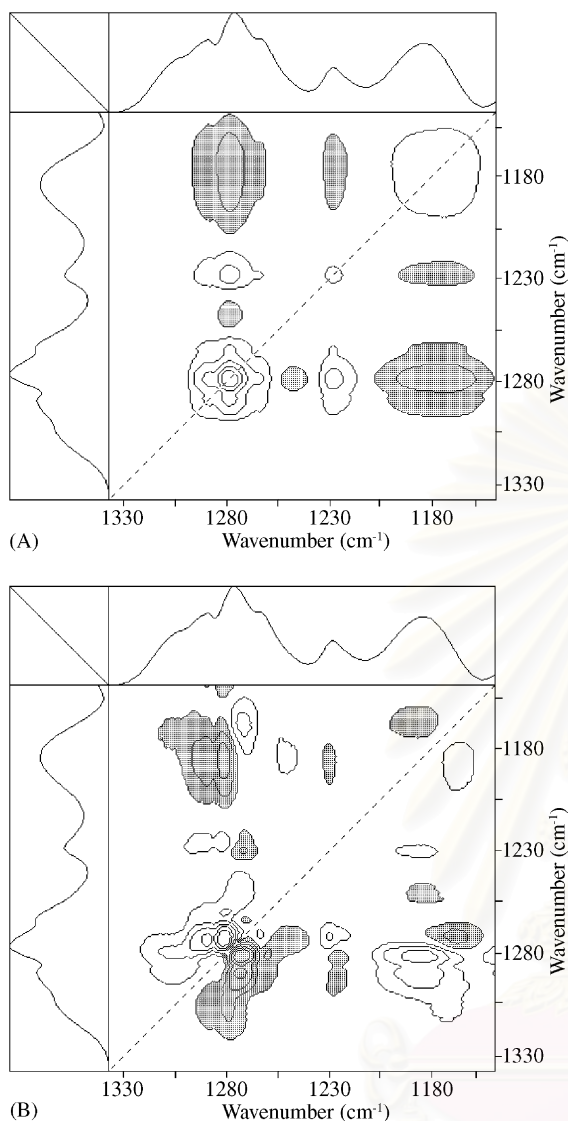


Fig. 6. Synchronous (A) and asynchronous (B) correlation spectra of P(HB-*co*-HHx) (12 mol% HHx) in the C–O–C stretching vibration region generated from the temperature-dependent IR spectra measured over a temperature range of 30–140 °C.

the crystalline component, and the three features at 1303, 1259, and 1183 cm^{-1} are attributed to the amorphous part.

The synchronous and asynchronous 2D correlation spectra in the region of 1330–1150 cm^{-1} generated from the temperature-dependent IR spectra of P(HB-*co*-HHx) are shown in Fig. 6(A) and (B), respectively. There are at least three autopeaks at 1280, 1230, and 1180 cm^{-1} . The autopeak at 1280 cm^{-1} extends to the vicinity of 1289 and 1264 cm^{-1} , and that at 1180 cm^{-1} is very broad. Thus, both autopeaks may consist of more than one peak. Negative and positive 2D synchronous cross peaks at (1280, 1180), (1180, 1230), and (1280, 1230) cm^{-1} reveal that the intensities of the bands located near 1280 and 1230 cm^{-1} (the crystalline bands) vary in the same direction, which is opposite to the intensity variations in the bands near 1180 cm^{-1} (the amorphous bands), in the course of melting. It is noted in Fig. 6(B)

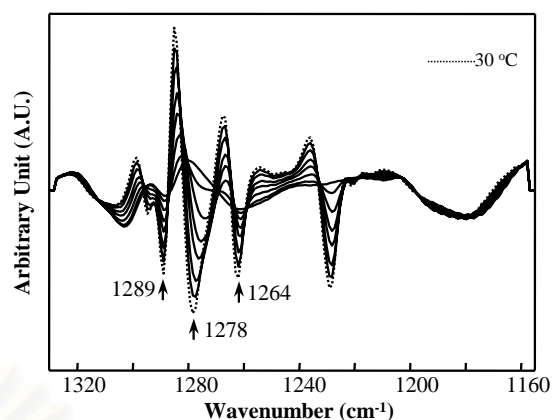


Fig. 7. Second derivative spectra calculated from the IR spectra of P(HB-*co*-HHx) (12 mol% HHx) in the C–O–C stretching vibration region over a temperature range of 30–140 °C.

that there are several asynchronous cross peaks between amorphous bands (e.g., bands near 1183 cm^{-1}) and crystalline bands (e.g., bands near \sim 1289–1278 and 1230 cm^{-1}). This observation again indicates the existence of an intermediate state during the phase transition of the copolymer. It is very likely that the appearance of the asynchronous cross peaks at (1289, 1272) and (1280, 1272) cm^{-1} is caused by the band shift, and that at (1188, 1170) cm^{-1} is due to the band broadening and the baseline shift [24,25]. As can be seen from the original IR spectra (Fig. 5) and the second derivatives (Fig. 7) that there exist a large shift of the band at 1278 cm^{-1} and band broadening as well as a baseline shift of the band at 1183 cm^{-1} in the course of temperature increase.

3.3. Changes in the C–H stretching band region during the melting process

The structural difference between P(HB-*co*-HHx) and PHB lies in the length of the alkyl side chain attached to the polymer backbone. Accordingly, the temperature-dependent spectral variations in the CH₃ and CH₂ stretching band regions are important to reveal differences or similarities in the thermally induced microenvironmental changes of the side chains of these two polymers. Fig. 8 shows temperature-dependent IR spectra of P(HB-*co*-HHx) (12 mol% HHx) in the region of 3050–2850 cm^{-1} . Bands around 2980 cm^{-1} are attributed to the CH₃ asymmetric stretching modes, while those due to the CH₂ antisymmetric stretching vibrations are identified around 2930 cm^{-1} . With the temperature increase, the CH₃ stretching band at 2975 cm^{-1} decreases, while that at 2984 cm^{-1} increases in intensity. Similarly, the CH₂ stretching band at 2934 cm^{-1} decreases and that at 2937 cm^{-1} increases in intensity on passing from the crystalline to the amorphous phase. Bands in this region are highly overlapped. The second derivatives of the spectra of P(HB-*co*-HHx) at 30 and 140 °C were calculated and are shown in Fig. 9. It can be seen from the second derivative spectrum of P(HB-*co*-HHx) at 30 °C that there are at least

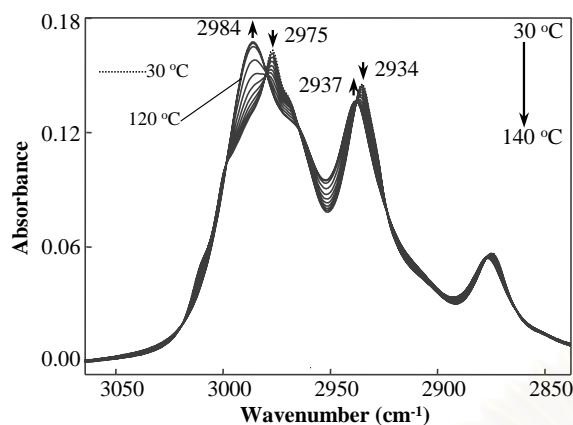


Fig. 8. IR spectra of P(HB-co-HHx) (12 mol% HHx) in the C–H stretching vibration region (3050–2850 cm^{-1}) measured over a temperature range of 30–140 $^{\circ}\text{C}$.

four major bands at 3008, 2997, 2975, and 2966 cm^{-1} in the CH_3 asymmetric stretching band region. For the CH_2 anti-symmetric stretching band region, two bands at 2934 and 2927 cm^{-1} are shown up. These bands may be attributed to the crystalline bands arising from the crystal field splitting, which occurs in some semicrystalline polymers [16,17]. The crystal field splitting may be caused not only by the intramolecular interaction between analogous functional groups attached along a polymer chain, but also by the intermolecular interaction between those groups located closely in the crystalline lattice. The crystalline band splittings of certain vibration modes have been reported for a number of polymers especially those having a helical chain structure [16,17].

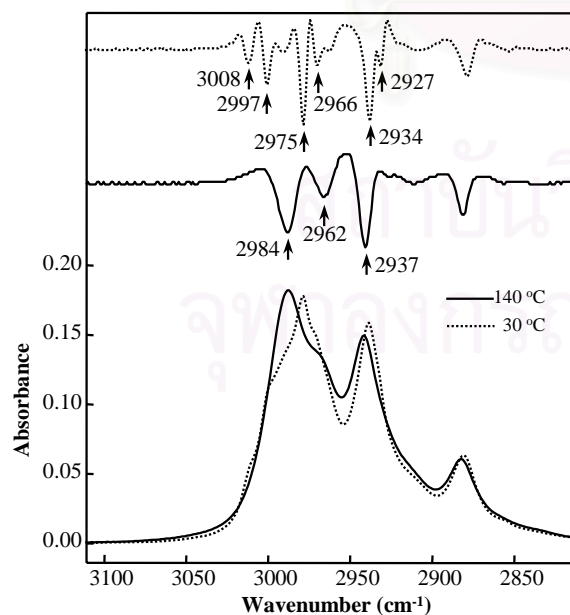


Fig. 9. Second derivative spectra calculated from the IR spectra of P(HB-co-HHx) (12 mol% HHx) in the C–H stretching vibration region at 30 and 140 $^{\circ}\text{C}$.

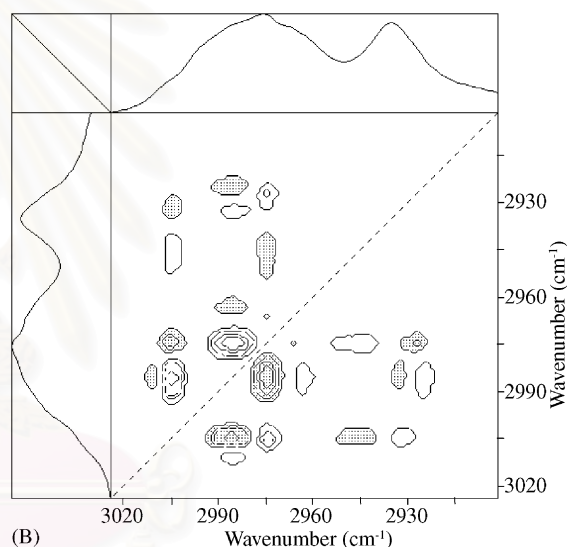
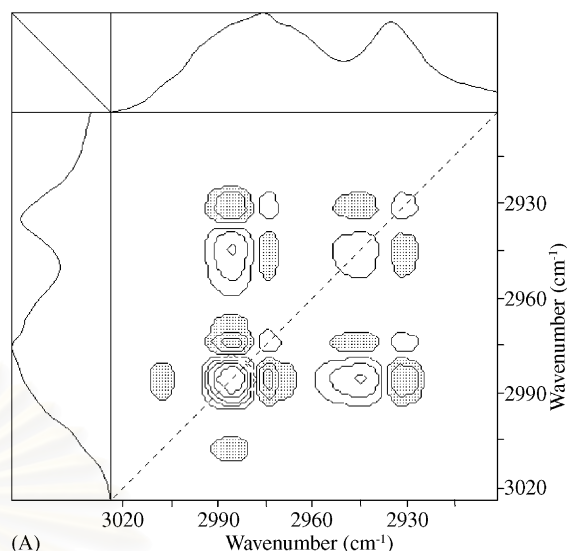


Fig. 10. Synchronous (A) and asynchronous (B) correlation spectra of P(HB-co-HHx) (12 mol% HHx) in the C–H stretching vibration region generated from the temperature-dependent IR spectra measured over a temperature range of 30–140 $^{\circ}\text{C}$.

Fig. 10(A) and (B) shows the synchronous and asynchronous 2D correlation spectra in the 3020–2900 cm^{-1} region generated from the temperature-dependent IR spectra. Four autopeaks are observed at 2985, 2975, 2944, and 2930 cm^{-1} in the synchronous spectrum. The band at 2985 cm^{-1} shares three negative synchronous cross peaks with the bands at 3008, 2975, and 2930 cm^{-1} . This indicates that the intensities of the bands at 3008, 2975, and those around 2930 cm^{-1} vary in the opposite direction to that of the band at 2985 cm^{-1} , with the change in temperature. In the corresponding asynchronous spectrum, the amorphous band at 2985 cm^{-1} shares asynchronous cross peaks with the crystalline bands at 3007 and 2975 cm^{-1} . This observation also suggests that the completely amorphous component is not formed simultaneously with the melting of the crystalline component.

Interestingly, a band at 2962 cm^{-1} observed in the C–H stretching region for P(HB-*co*-HHx) (12 mol% HHx) (Fig. 9) is absent in that for PHB. Therefore, it is very likely that this band is attributed to the CH_3 asymmetric stretching mode of the side-chain group (propyl, $-\text{CH}_2\text{CH}_2\text{CH}_3$) incorporated in P(HB-*co*-HHx) (12 mol% HHx). It should be noted that no peak emerges at 2962 cm^{-1} in the 2D synchronous spectrum shown in Fig. 10(A). This indicates that the temperature-induced intensity change in this band is not prominent. In other words, the crystalline/amorphous phase transition of P(HB-*co*-HHx) does not strongly affect the behavior of the propyl side-chain groups. This is consistent with the fact that the propyl group is attached to the HHx comonomer, which functions as a less crystallizable unit in P(HB-*co*-HHx).

3.4. Spectral changes during the cooling down process

Temperature-perturbed IR spectral variations in the C=O stretching band region of P(HB-*co*-HHx) observed during the cooling down process were also investigated. IR spectra in the $1780\text{--}1680\text{ cm}^{-1}$ region collected as a function of decreasing temperature are shown in Fig. 11. Fig. 12(A) and (B) shows synchronous and asynchronous 2D correlation spectra generated from the temperature-dependent IR spectra in the C=O stretching band region for the cooling down process, respectively. The pattern of the 2D asynchronous contour plot is almost the same as that for the melting process (Fig. 3(B)) except the signs of the cross peaks. It can be seen from Fig. 11 that the amorphous C=O band at 1740 cm^{-1} decreases with the temperature decrease, and that the crystalline band at 1723 cm^{-1} appears at around $110\text{ }^\circ\text{C}$ and develops down to room temperature. Two pairs of asynchronous cross peaks are developed at the same coordinates as those in the asynchronous spectrum generated for the melting process. This observation also indicates the

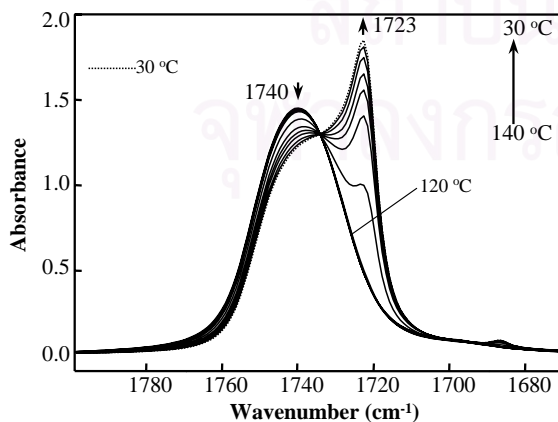


Fig. 11. IR spectra of P(HB-*co*-HHx) (12 mol% HHx) in the C=O stretching vibration region measured over a temperature range of $140\text{--}30\text{ }^\circ\text{C}$ (cooling down process).

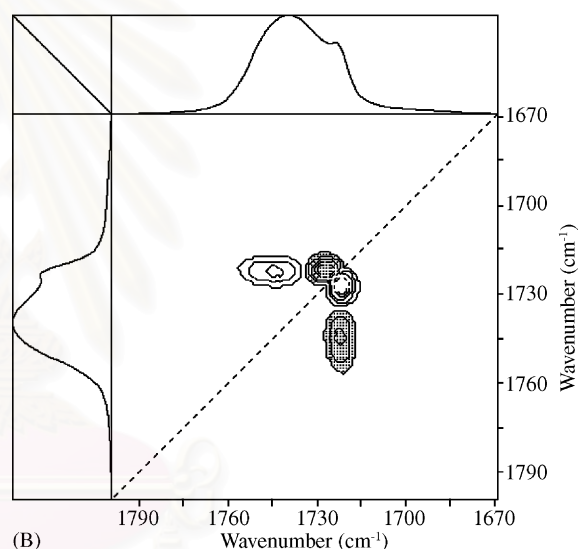
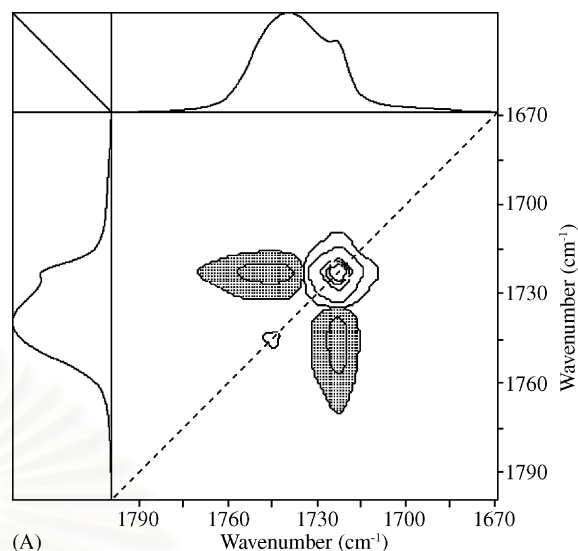


Fig. 12. Synchronous (A) and asynchronous (B) correlation spectra of P(HB-*co*-HHx) (12 mol% HHx) in the C=O stretching vibration region generated from the temperature-dependent IR spectra measured over a temperature range of $30\text{--}140\text{ }^\circ\text{C}$ (cooling down process).

coexistence of two crystalline C=O bands, and suggests that, in the crystallization process, the formation of the crystalline component does not proceed simultaneously with the decrease in the amorphous component.

3.5. Crystalline/amorphous phase transition behavior of P(HB-*co*-HHx)

The temperature-dependent IR spectra of P(HB-*co*-HHx) (12 mol% HHx) depict clearly that the crystalline C=O band observed at 1723 cm^{-1} decreases during the heating up process and grows up during the cooling down process. Recent WAXD study showed that the crystalline part of P(HB-*co*-HHx) almost disappears above ca. $110\text{ }^\circ\text{C}$ [14,15]. A good agreement is obtained between the WAXD study and

the temperature-dependent IR spectral variations observed in the melting process.

IR absorption bands are very sensitive to changes in microenvironments of molecules and the degree to which a vibrational mode is coupled to adjacent vibrations. The splitting of the C=O stretching band observed below the T_m of the copolymer is possibly caused by some specific molecular interactions [14–16]. The analogous groups along the polymer chains are located very closely in the crystalline state of P(HB-co-HHx) because of the highly ordered and possible helical structure. As the temperature increases, the highly ordered structure collapses and, consequently, the inter- and intramolecular interactions between the repeating units along the polymer chains in a crystalline state are diminished. Therefore, the spectral changes of certain absorption bands concerning the crystalline/amorphous phase transition are clearly observed in the temperature-dependent IR spectra of P(HB-co-HHx) (12 mol% HHx).

3.6. Comparison between the IR spectra of P(HB-co-HHx) and those of PHB

In our previous study on PHB [16], we analyzed the temperature-dependent IR spectra of PHB in detail. In the present study, we compare the one-dimensional IR spectra and also 2D correlation spectra of P(HB-co-HHx) (12 mol% HHx) with those of PHB. In the C=O stretching band region for PHB, three bands at 1740, 1731, and 1723 cm^{-1} were observed. Note that the frequencies of the bands observed in the C=O stretching region for P(HB-co-HHx) are identical to those for PHB. This suggests that C=O groups of P(HB-co-HHx) and those of PHB experience very similar submolecular environments. However, the relative intensity ratio of the crystalline band at 1723 cm^{-1} to the amorphous band at 1740 cm^{-1} for P(HB-co-HHx) (12 mol% HHx) is much lower than that for PHB. The IR spectra reveal clearly that the percentage of crystallinity for P(HB-co-HHx) is lower than that for PHB.

In the CH_3 asymmetric stretching band region, the bands at 3008 and 2997 cm^{-1} for P(HB-co-HHx) were observed as shoulders of the band at 2975 cm^{-1} , while those for PHB are very sharp and clear. The frequencies of the bands and the crystal field splitting pattern observed in the C–H stretching region for P(HB-co-HHx) are also very similar to those for PHB. These spectral features again imply a higher crystallinity of PHB and similar microenvironments in which the C–H groups of these two polymers are located. The shapes of the bands in the C–O–C stretching region below the T_m for P(HB-co-HHx) are also different from those for PHB, e.g., the relative intensity of the bands in the region of 1295–1260 cm^{-1} are different between the two polymer samples.

The temperature-induced IR spectral changes in the C=O, C–O–C, and C–H stretching regions for P(HB-co-HHx) (12 mol% HHx) and those for PHB are similar. However, the temperatures at which the significant intensity changes in the three spectral regions occur are different between the two

polymer systems. Marked intensity changes in the three spectral regions for P(HB-co-HHx) were observed at much lower temperature than those for PHB. It is also noted that the intensity changes in the IR spectra of P(HB-co-HHx) (Figs. 2, 5 and 8) occur gradually with increasing temperature, indicating a gradual deformation of its highly ordered and helical structure. On the other hand, the intensities of the IR spectra of PHB change abruptly in the vicinity of the T_m of PHB [16], suggesting that the highly ordered and helical structure of PHB collapses rapidly at the temperature right around the T_m .

The observations described above agree very well with the WAXD and DSC studies [14,15], which indicated that P(HB-co-HHx) (12 mol% HHx) assumes an orthorhombic crystal system, which is identical to that of PHB, and that the percentage of crystallinity of these two polymers are remarkably different. The crystallinity of PHB is higher than that of P(HB-co-HHx). We observed several remarkable differences between the temperature-dependent IR spectra of P(HB-co-HHx) and those of PHB, however, the phase transition behaviors revealed by 2D correlation spectroscopy for these two polymer systems are fundamentally similar. The present study indicates clearly that the HHx comonomer does not alter the crystalline structure of PHB. Its major role is to break down the crystalline structure from place to place, and hence increasing the amorphous entity of the copolymer.

4. Conclusion

The thermal melting behavior of P(HB-co-HHx) (12 mol% HHx) was investigated by using generalized 2D IR correlation spectroscopy. The C=O, C–H, and C–O–C stretching vibration regions depict marked temperature-dependent IR spectral variations. The crystalline bands decrease while the amorphous bands increase during the melting process. This is because the highly ordered and helical structure of P(HB-co-HHx) is diminished at high temperature.

The significant intensity changes in the C=O, C–O–C, and C–H stretching regions start taking place at much lower temperature in the spectra of P(HB-co-HHx) (12 mol% HHx) than in the spectra of PHB. This observation indicates that the crystallinity decreases gradually even at low temperature for P(HB-co-HHx).

The asynchronous 2D correlation spectrum generated from the temperature-induced dynamic IR spectra in the C=O stretching vibration region clearly resolves two highly overlapped crystalline bands located at 1731 and 1723 cm^{-1} . The intense band at 1723 cm^{-1} may be attributed to the major crystalline component of the copolymer, and the weaker band at 1731 cm^{-1} is possibly assignable to the minor crystalline component with a less ordered structure. The appearance of the 2D asynchronous cross peaks between the crystalline and amorphous bands suggests the

existence of an intermediate state during the phase transition process.

The CH₃ asymmetric stretching bands and CH₂ antisymmetric stretching bands exhibit a crystal field splitting, which is often observed for polymers with a helical structure. In comparison to PHB, this study suggests that the HHx comonomer does not alter the crystalline structure of PHB. The close similarity in the frequencies of the C=O, C–O–C, and C–H stretching bands of the crystalline components between PHB and P(HB-co-HHx) (12 mol% HHx) reveals that the helical structure of P(HB-co-HHx) is very close to that of PHB. The HHx unit locally disrupts the highly ordered and helical structure of the copolymer from place to place, increasing the amorphous entity, which gives the better physical and mechanical properties to the copolymer.

Acknowledgements

A.P. gratefully thanks the Thailand Research Fund (TRF) for the financial support via the Royal Golden Jubilee (RGJ) PhD program (Grant contract number: PHD/0066/2544).

References

- [1] S.F. Williams, D.P. Martin, in: A. Steinbüchel, Y. Doi (Eds.), *Biopolymers*, Wiley-VCH, Weinheim, 2002.
- [2] L.M. Lara, W.H. Gjalt, *Microbiol. Mol. Biol. Rev.* 63 (1991) 21.
- [3] A.J. Anderson, E.A. Dawes, *Microbiol. Rev.* 54 (1990) 450.
- [4] D. Jendrossek, in: A. Steinbüchel, Y. Doi (Eds.), *Biopolymers*, Wiley-VCH, Weinheim, 2001.
- [5] S.Y. Lee, *Biotechnol. Bioeng.* 49 (1996) 1.
- [6] Web site; <http://www.nodax.com>.
- [7] M.M. Satkowski, D.H. Melik, J.-P. Autran, P.R. Green, I. Noda, L.A. Schechtman, in: A. Steinbüchel, Y. Doi (Eds.), *Biopolymers*, Wiley-VCH, Weinheim, 2001.
- [8] M. Yokouchi, Y. Chatani, H. Tadokoro, K. Teranishi, H. Tani, *Polymer* 14 (1973) 267.
- [9] J. Cornibert, R.H. Marchessault, *Macromolecules* 8 (1975) 296.
- [10] Q. Wu, G. Tian, S. Sun, I. Noda, G.-Q. Chen, *J. Appl. Polym. Sci.* 82 (2001) 934.
- [11] G. Tian, Q. Wu, S. Sun, I. Noda, G.-Q. Chen, *J. Polym. Sci. B* 40 (2002) 649.
- [12] G. Tian, Q. Wu, S. Sun, I. Noda, G.-Q. Chen, *Appl. Spectrosc.* 55 (2001) 888.
- [13] K.P. Caballero, S.F. Karel, R.A. Register, *Int. J. Bio. Macromol.* 17 (1995) 86.
- [14] H. Sato, M. Nakamura, A. Padermshoke, H. Yamaguchi, H. Terauchi, S. Ekgasit, I. Noda, Y. Ozaki, *Macromolecules*, submitted.
- [15] H. Sato, A. Padermshoke, M. Nakamura, R. Murakami, F. Hirose, K. Senda, H. Terauchi, S. Ekgasit, I. Noda, Y. Ozaki, *Macromol. Symp.*, in press.
- [16] A. Padermshoke, Y. Katsumoto, H. Sato, S. Ekgasit, I. Noda, Y. Ozaki, *Appl. Spectrosc.*, submitted.
- [17] S.K. Mallapragada, B. Narasimhan, in: R.A. Meyers (Ed.), *Encyclopedia of Analytical Chemistry*, Wiley, Chichester, 2000.
- [18] I. Noda, *Bull. Am. Phys. Soc.* 31 (1986) 520.
- [19] I. Noda, *Appl. Spectrosc.* 44 (1990) 550.
- [20] I. Noda, *Appl. Spectrosc.* 47 (1993) 1329.
- [21] I. Noda, A.E. Dowrey, C. Marcott, G.M. Story, Y. Ozaki, *Appl. Spectrosc.* 54 (2000) 236A.
- [22] I. Noda, G.M. Story, C. Marcott, *Vib. Spectrosc.* 19 (1999) 461.
- [23] E. Galbiati, M.D. Zoppo, G. Tieghi, G. Zerbi, *Polymer* 34 (1993) 1806.
- [24] A. Gericke, S.I. Gadaleta, J.W. Brauner, R. Mendelshon, *Biospectroscopy* 2 (1996) 341.
- [25] A. Nabet, M. Auger, M. Pézolet, *Appl. Spectrosc.* 54 (2000) 948.



Surface melting and crystallization behavior of polyhydroxyalkanoates studied by attenuated total reflection infrared spectroscopy

Adchara Padermshoke^{a,b}, Yukiteru Katsumoto^c, Harumi Sato^a, Sanong Ekgasit^b,
Isao Noda^d, Yukihiko Ozaki^{a,*}

^aDepartment of Chemistry, School of Science and Technology, Kwansai-Gakuin University, Sanda, Hyogo 669-1337, Japan

^bSensor Research Unit, Department of Chemistry, Faculty of Science, Chulalongkorn University, Patumwan, Bangkok 10330, Thailand

^cDepartment of Chemistry, Graduate School of Science, Hiroshima University, Higashi-Hiroshima, Hiroshima 739-8526, Japan

^dThe Procter and Gamble Company, 8611 Beckett Road, West Chester, Ohio 45069, USA

Received 10 March 2004; received in revised form 29 June 2004; accepted 16 July 2004

Abstract

The surface melting and crystallization behavior of two biodegradable polyesters, poly(3-hydroxybutyrate-co-3-hydroxyhexanoate) (P(HB-co-HHx)) (HHx = 12 mol%) and poly(3-hydroxybutyrate) (PHB), were investigated by using attenuated total reflection (ATR) and transmission infrared (IR) spectroscopy coupled with the generalized two-dimensional (2D) correlation analysis. IR bands in the C=O stretching vibration region were analyzed to explore the changes in crystallinity at the surface and those in the bulk of the polymer film samples during the melting and crystallization processes. Due to the intrinsic sub-micrometer sampling depth of the ATR technique, spectral information attributed to the chemical moieties situated at the surface region of the film samples can be observed. The present study revealed that the surface melting of P(HB-co-HHx) takes place through an intermediate state. The distribution of crystalline phase detected by the ATR technique and that detected by the transmission technique suggested that the polymer crystals tend to grow at the surface in a manner different from that in the bulk. It is very likely that the population of polymer crystals at the surface is higher than that in the bulk for both P(HB-co-HHx) and PHB. The time-dependent IR spectral variations for P(HB-co-HHx) and those for PHB indicated that P(HB-co-HHx) crystallizes much slower than PHB. This observation suggested that the HHx units incorporated in P(HB-co-HHx) markedly reduce not only the degree of crystallinity but also the crystallization rate of PHB homopolymer.

© 2004 Published by Elsevier Ltd.

Keywords: Polyhydroxyalkanoates; Surface melting; 2D IR spectroscopy

1. Introduction

The surface layer of a polymer often exhibits different properties, e.g. morphology, composition, and structure, from the bulk material [1], and it sometimes determines the overall characteristic of the polymer. In applications of polymers to thin films and coatings, it is often the interfacial behavior that governs the material performance rather than the bulk. For biocompatible objects such as a polymeric scaffold, the tissue/polymer interface where a cellular adhesion occurs is also very important [2–4]. The

biocompatibility depends strongly on the surface morphology of the polymer [2]. Consequently, the surface properties and surface phenomena of polymers are of great interest from both fundamental and technological points of views.

Crystallization behavior of macromolecules at the surface and interface regions plays an important role in numerous properties, e.g. mechanical strength, chemical compatibility, and biocompatibility, of polymeric materials [1,2]. Therefore, an insight into the surface crystallization behavior of polymers not only allows us to understand fundamental surface phenomena but also assists us to develop polymer products of high potential. In order to precisely extract the surface information, a non-destructive characterization technique capable of selectively probing surface molecules is required. There are various techniques

* Corresponding author. Tel.: +81-79-565-8349; fax: +81-79-565-9077.

E-mail address: ozaki@ksc.kwansei.ac.jp (Y. Ozaki).

applicable to polymer surface analysis, for examples, scanning electron microscopy (SEM) [2], X-ray photoelectron spectroscopy (XPS) [5], and atomic force microscopy (AFM) [5]. Attenuated total reflection (ATR) infrared (IR) spectroscopy is known as one of powerful surface characterization techniques that can provide information, e.g. chemical reactions, functional groups, and molecular orientation, at the surface and interface regions of polymers [6–11]. Quantitative information of a sample can also be obtained from a system with an optical contact between the sample and an internal reflection element (IRE) [8–11]. ATR IR spectroscopy possesses several advantages such as non-destructive nature, easy and fast operation, and little or no sample preparation [9–11].

In the present study, we have investigated the surface melting and crystallization behavior of two polyhydroxyalkanoate (PHA) polymers; poly(3-hydroxybutyrate-*co*-3-hydroxyhexanoate) (P(HB-*co*-HHx)) (HHx = 12 mol%) and poly(3-hydroxybutyrate) (PHB). PHA polymers can be biologically derived from renewable carbon source like glucose or fatty acids and are subjected to degradation by bacteria in the soil [12–16]. Their chemical structures and physical characteristics are fairly similar to those of certain petroleum-based synthetic polymers [12–17]. Therefore, PHA polymers have received a great attention as an environmentally friendly polymeric material. PHB is the simplest and most abundant PHA polymer found in bacteria [12,15]. Since it is stiff and brittle due to the high degree of crystallinity [12–15], many attempts have been made to improve the mechanical properties of PHB [17]. It has been reported that P(HB-*co*-HHx) copolymers possess much better mechanical properties than PHB homopolymer [17, 18]. The applications of P(HB-*co*-HHx) copolymers, therefore, have been expanded to a greater extent including biodegradable films and coatings. From this aspect, the studies on the surface properties of this class of polymers are crucial not only for improving the performances of existing film products but also for developing new generation of biodegradable films.

We have conducted a series of studies on the structures and thermal behavior of PHB and P(HB-*co*-HHx) (12 mol% HHx) by using temperature-dependent wide-angle X-ray diffraction (WAXD) [19,20], differential scanning calorimetry (DSC) [19,20], and IR spectroscopy [20–22]. It was revealed by the previous studies that the phase transition process of P(HB-*co*-HHx) (12 mol% HHx) takes place through an intermediate state [22], and that the inclusion of the HHx comonomer locally disrupts the highly ordered and helical structure of PHB, thereby reducing the crystallinity of the PHB homopolymer without altering the crystalline structure [20,22]. The existence of an intermediate state during the phase transition of P(HB-*co*-HHx) (10 mol% HHx) and that of P(HB-*co*-HV) was also reported by Wu et al. [23] and Tian et al. [24], respectively. Recently, Kai et al. [2] investigated the effects of surface morphology on the biocompatibility of P(HB-*co*-HHx)/PHB blends by using

SEM. It was found that the presence of P(HB-*co*-HHx) in the blends strongly improves the biocompatibility of PHB by providing the blending films with a fairly regular and smooth surface that allows cell attachment and growth. This study demonstrated an example of the influence of surface characteristics on the medical applications of P(HB-*co*-HHx) and PHB. However, the melting and crystallization behavior of P(HB-*co*-HHx) and PHB viewed at the film surface and interface regions have never been reported. The present study aims at investigating the melting and crystallization behavior of P(HB-*co*-HHx) copolymer and PHB homopolymer at the film/ATR crystal interface by using ATR and transmission IR spectroscopy coupled with the generalized two-dimensional (2D) correlation analysis. The time-dependent ATR and transmission spectra of P(HB-*co*-HHx) and those of PHB were monitored in order to follow the time-dependent crystal growth at the surface and in the bulk of the two polymers. The temperature-dependent IR spectral variations observed for the surface of a P(HB-*co*-HHx) film sample during the melting process were also compared to those observed for the bulk sample [22].

2. Experimental section

2.1. Materials

Bacterially synthesized P(HB-*co*-HHx) (12 mol% HHx) ($T_m \cong 110^\circ\text{C}$ and $\sim 35\%$ crystallinity [18]) and PHB ($T_m \cong 170^\circ\text{C}$ and $\sim 55\%$ crystallinity [17]) were provided by the Procter and Gamble Company, Cincinnati, USA. Purification of the P(HB-*co*-HHx) sample was performed by dissolving P(HB-*co*-HHx) in hot chloroform (CHCl_3), reprecipitating in methanol (CH_3OH), and vacuum-drying at 60°C for 24 h. The CHCl_3 : CH_3OH volume ratio for the reprecipitation was approximately 1:10. The PHB sample is a purified sample and, thus, was used as received. Chloroform and methanol were purchased from Wako Pure Chemical Industries, Ltd, Osaka, Japan. Chloroform was used as a solvent for P(HB-*co*-HHx) and PHB film castings.

2.2. IR spectroscopic measurements

2.2.1. Temperature-dependent ATR measurements

A multiple reflection ATR accessory (Spectra Tech, USA) with a 45° ZnSe IRE ($10 \times 75.5 \times 3$ mm) was employed for the temperature-dependent ATR measurements. The temperature of the attachment that holds the ZnSe IRE with the P(HB-*co*-HHx) film sample was controlled by using a temperature controller unit (model LT230, CHINO). To assure the optical contact between the film sample and the IRE, the P(HB-*co*-HHx) film sample was prepared by casting its chloroform solution directly on the ZnSe IRE. The film was annealed at 60°C in a vacuum-dried oven for 12 h and cooled down to room temperature (25°C). Temperature-dependent ATR spectra of the film

sample were collected at a 2 cm^{-1} spectral resolution by using a Nicolet Magna-IR™ 550 spectrometer equipped with a mercury cadmium telluride (MCT) detector. A number-of-scan of 512 was accumulated to ensure a high signal-to-noise ratio. The measurements were carried out over a temperature range of 30–140 °C with an increment of 10 °C.

2.2.2. Time-dependent IR measurements

The same ATR experimental set up as above without the temperature controller unit was employed for the time-dependent ATR measurements of P(HB-co-HHx) and PHB film samples. Time-dependent transmission measurements were also performed for P(HB-co-HHx) and PHB. The film samples were prepared by casting their chloroform solutions on ZnSe transmission windows in a same manner as that for the ATR measurements.

All time-dependent measurements were conducted at room temperature. After the solvent castings, the film samples were air-dried for 30 min before the measurements. The time-dependent IR spectra were collected every 15 min until the crystal growth was by and large completed (i.e. no significant spectral change was observed).

In order to directly compare the surface information obtained from the ATR technique with the bulk information obtained from the transmission technique, all ATR spectra were penetration depth-corrected to eliminate the artifact arising from the wavenumber-dependent sampling depth of the ATR technique [25]. It should be noted that the inherent wavenumber-dependent ATR spectral intensity is eliminated by this operation. However, the corrected ATR spectra still carry the surface information of the polymer film samples since the actual sampling depth of the entire spectra is up to a few micrometers from the sample surface while the transmission spectra carry the bulk information of the whole film samples.

2.3. 2D Correlation analysis

All IR spectra were baseline-corrected prior to the 2D correlation analysis. The calculations of 2D correlation spectra were performed by using the 2D-Pocha software composed by Daisuke Adachi (Kwansei-Gakuin University, Japan). Temperature-averaged and time-averaged spectra were used as the reference spectra for the 2D correlation calculations of the temperature- and time-dependent IR spectra, respectively.

3. Results and discussion

3.1. Temperature-dependent ATR spectral variations in the C=O stretching vibration region of P(HB-co-HHx) (12 mol% HHx) during the melting process

Fig. 1 shows temperature-dependent ATR spectra of

P(HB-co-HHx) in the $1780\text{--}1680\text{ cm}^{-1}$ region where bands due to the C=O stretching modes are expected to appear. A sharp band at 1720 cm^{-1} gradually decreases with increasing temperature while a broad band at 1731 cm^{-1} increases. These spectral variations reflect the melting process of the copolymer. Although the relative intensity of bands in the C=O stretching vibration region is different, the temperature-dependent changes observed for the ATR measurement are similar to those previously observed for the transmission measurement [22]. In our previous paper [22], the C=O stretching band observed at ca. 1720 cm^{-1} in the IR spectra of P(HB-co-HHx) was assigned to that of the highly ordered crystalline structure while that observed at ca. 1740 cm^{-1} was attributed to the amorphous phase.

Fig. 2 shows ATR (solid line) and transmission (dotted line) spectra of the annealed P(HB-co-HHx) film sample in the C=O stretching vibration region measured at 30 °C. It can be seen that the major difference between the ATR and transmission spectra lies in the relative intensity of the highly ordered crystalline C=O band at ca. 1720 cm^{-1} and the amorphous C=O band at ca. 1740 cm^{-1} ; the band at ca. 1720 cm^{-1} in the ATR spectrum is more sharp and intense than that in the transmission spectrum. In general, the refractive index (RI) of organic compounds is 1.5 ± 0.2 [8], and that of ZnSe is 2.4 [8]. Accordingly, for the present study, the penetration depth (d_p) calculated for the C=O stretching vibration region, $d_p(1720\text{ cm}^{-1})$ is $1.17\text{ }\mu\text{m}$. Due to the shallow sampling depth of the ATR technique, the ATR spectra shown in Figs. 1 and 2 (solid line), therefore, contain only the spectral information associated with the chemical species situated just a few micrometers beyond the sample surface. Thus, it is very likely that the differences between the ATR and transmission spectra are due primarily to the different behavior of molecules located at the surface and in the bulk of the film sample. The intensity ratio of the highly ordered crystalline C=O band to the amorphous one for the ATR spectrum is much higher than that for the transmission spectrum (Fig. 2), suggesting that the

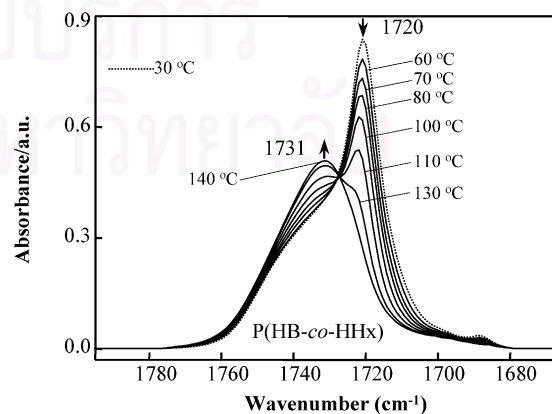


Fig. 1. Representative ATR spectra of P(HB-co-HHx) (12 mol% HHx) in the C=O stretching vibration region ($1780\text{--}1680\text{ cm}^{-1}$) measured over a temperature range of 30–140 °C. Arrows indicate the direction of absorbance changes as temperature increases.

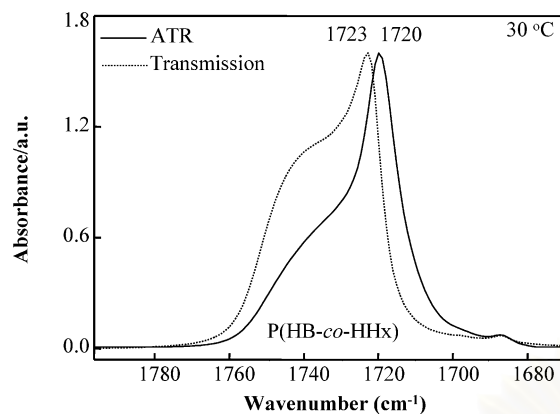


Fig. 2. ATR (solid line) and transmission (dotted line) spectra of P(HB-co-HHx) (12 mol% HHx) in the C=O stretching vibration region measured at 30 °C.

crystallinity of the polymer is much higher at the film surface than in the bulk. The broad feature at ca. 1740 cm^{-1} in the ATR spectrum exists only as a slope with weak intensity.

To extract more detailed information about the spectral variations induced by the temperature change, 2D correlation analysis was employed. Fig. 3(A) and (B) shows the synchronous and asynchronous 2D correlation spectra in the spectral region of $1790\text{--}1670\text{ cm}^{-1}$ generated from the temperature-dependent ATR spectra measured during the temperature increase in the range of $30\text{--}100\text{ °C}$, respectively. The spectra measured above 100 °C were excluded in the calculation of the 2D spectra. A pair of negative cross peaks developed at $1736, 1718\text{ cm}^{-1}$ in the synchronous spectrum (Fig. 3(A)) indicates the opposite directions of the intensity variations in these two correlated bands. In the asynchronous spectrum (Fig. 3(B)), a pair of cross peaks appears at $1732, 1718\text{ cm}^{-1}$. The presence of asynchronous cross peaks indicates the out-of-phase changes in the intensity of the band at ca. 1732 cm^{-1} and that of the band at ca. 1718 cm^{-1} . This observation clearly suggests that the disappearance of the highly ordered crystalline component of the copolymer does not simultaneously result in the formation of the amorphous structure. That is, the surface melting of P(HB-co-HHx) takes place through an intermediate state. The existence of an intermediate state was also reported for the bulk melting process of P(HB-co-HHx) (12 mol% HHx) [22] and that of some other copolymers [23,24].

The 2D correlation spectra generated from the temperature-dependent ATR spectra also reveal that the spectral changes occurring at the surface region particularly involve the highly ordered crystalline component and the amorphous structure. On the other hand, 2D correlation spectra generated from the temperature-dependent transmission spectra of P(HB-co-HHx) in the C=O stretching vibration region clearly reveal that the bulk melting of P(HB-co-HHx) involves two crystalline components (i.e. the highly ordered crystalline component and the minor crystalline component

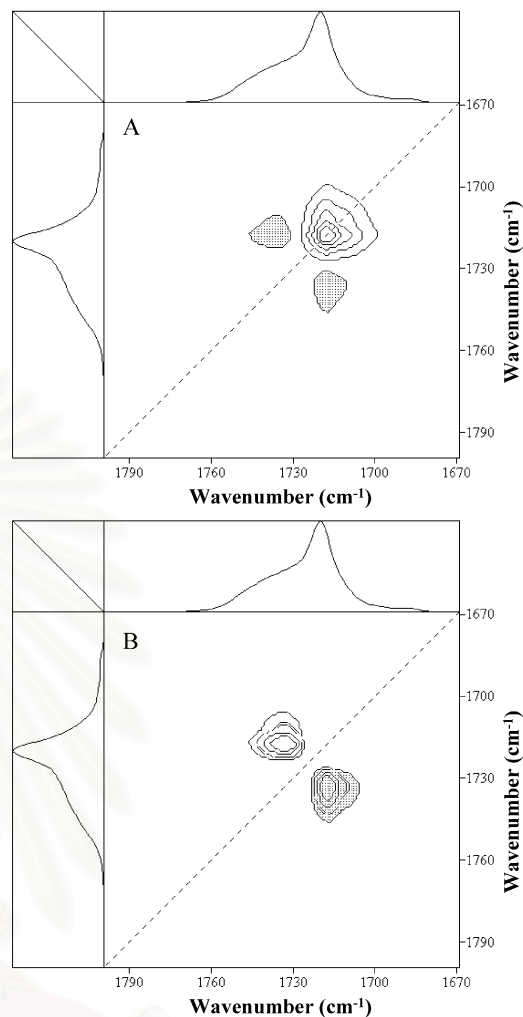


Fig. 3. Synchronous (A) and asynchronous (B) IR correlation spectra of P(HB-co-HHx) (12 mol% HHx) in the C=O stretching vibration region generated from the temperature-dependent ATR spectra measured over a temperature range of $30\text{--}100\text{ °C}$.

with a less-ordered structure) and the amorphous phase [22]. These observations suggest that the polymer crystals tend to grow at the surface in a manner different from the bulk. It is very likely that the molecules situated at the surface region of the P(HB-co-HHx) film sample prefer the highly ordered molecular chain structure.

3.2. Time-dependent IR spectral variations in the C=O stretching vibration region of P(HB-co-HHx) (12 mol% HHx)

Fig. 4(A) and (B) shows time-dependent ATR and transmission spectra of P(HB-co-HHx) in the C=O stretching vibration region, respectively. The IR spectral changes induced by the time-dependent crystallization are clearly observed both from the ATR (A) and transmission (B) measurements. This is because the crystallization rate of P(HB-co-HHx) is slow, one can supercool the system away from the thermal equilibrium. Consequently, an amorphous

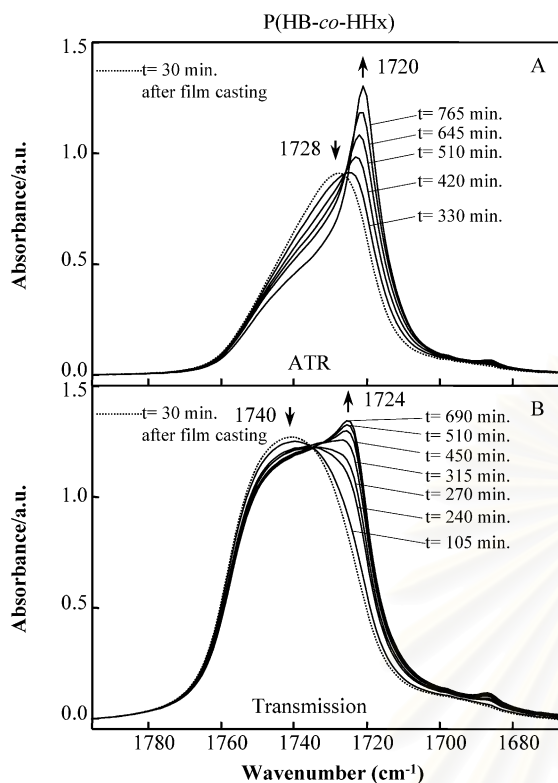


Fig. 4. Representative time-dependent ATR (A) and transmission (B) spectra of P(HB-co-HHx) (12 mol% HHx) in the C=O stretching vibration region measured at room temperature (25 °C). Arrows indicate the direction of absorbance changes as time increases.

sample can be obtained well below its apparent T_m , and the time-dependent crystal growth can be monitored. The transition from the amorphous to the crystalline state causes the downward shift in the C=O stretching vibration region. However, the spectral features of the ATR spectra and those of the transmission spectra are substantially different from each other. The highly ordered crystalline C=O band observed in the transmission spectra is not so sharp and intense as that observed in the ATR spectra. In other words, the ATR spectra show higher crystalline characteristic while the transmission spectra manifest more of the amorphous feature.

A direct comparison between the ATR and transmission spectra measured under the same experimental conditions shows clear spectral differences. Fig. 5 depicts the ATR and transmission spectra measured at 30 min after the film casting (A) and those measured when the crystal growth was completed (B). The spectra shown in Fig. 5 clearly indicate that the surface and bulk chemical species exhibit different crystallization behavior. To minimize the effect of a localized anomalous refractive index dispersion results from absorption peaks, a Ge IRE with higher refractive index ($RI_{Ge}=4.0$) was employed. Fig. 6 shows ATR spectra of P(HB-co-HHx) measured with the Ge IRE under the same experimental conditions as those shown in Fig. 5. The ATR spectra taken with the Ge IRE also show markedly

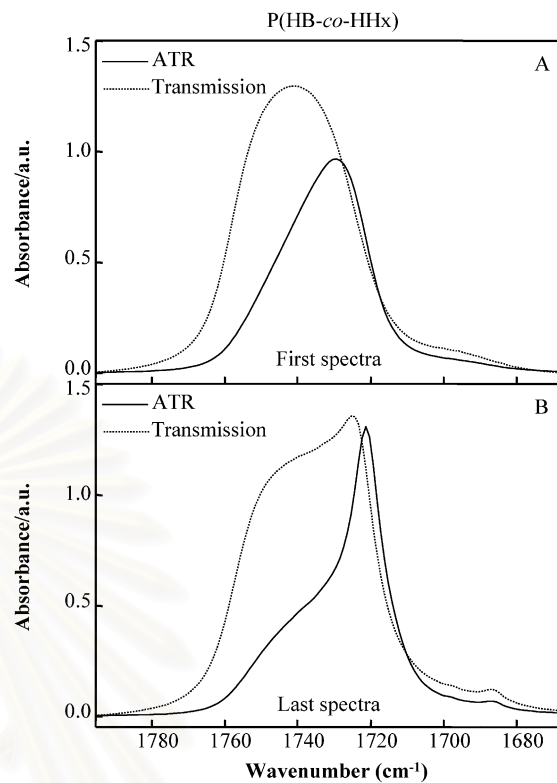


Fig. 5. ATR (solid line) and transmission (dotted line) spectra of P(HB-co-HHx) (12 mol% HHx) in the C=O stretching vibration region: first (A) and last (B) spectra measured during the time-dependent IR measurements.

different characteristics from those of the transmission spectra. For the ATR spectra measured when the crystal growth was completed (Fig. 6 (solid line)), the highly ordered crystalline C=O band at 1721 cm^{-1} is very sharp and intense while the amorphous band at ca. 1740 cm^{-1} is very weak. The spectral features and peak positions are similar to those of the ATR spectra taken with the ZnSe IRE. This observation confirms the difference in the surface and bulk crystallinity of the P(HB-co-HHx) copolymer.

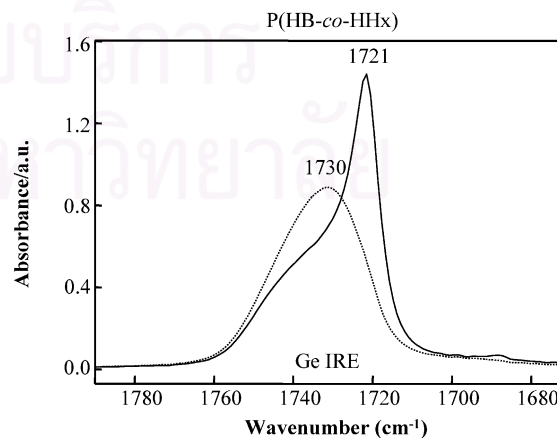


Fig. 6. ATR spectra of P(HB-co-HHx) (12 mol% HHx) in the C=O stretching vibration region measured at 30 min after the solvent casting (dotted line) and when the crystal growth was completed (solid line) by using the Ge IRE.

By comparing Figs. 2 and 5(B), the effect of the crystallization temperature on the crystal growth at the film surface and that in the bulk can be discussed. The highly ordered crystalline C=O band in the transmission spectrum of the annealed P(HB-co-HHx) sample (Fig. 2 (dotted line)) is more intense than that of the non-annealed P(HB-co-HHx) sample (Fig. 5(B) (dotted line)). This observation suggests that the crystallization in the bulk proceeds far better when the sample is annealed at an elevated temperature (60 °C). On the other hand, the crystallization at the film surface is not strongly affected by the temperature at which the crystallization takes place. As seen in Figs. 2 (solid line) and 5(B) (solid line), the overall ATR spectral features of the C=O stretching bands for both cases are very similar.

Fig. 7(A) and (B) shows the synchronous and asynchronous 2D correlation spectra in the spectral region of 1790–1670 cm^{-1} generated from the time-dependent ATR spectra, respectively. A pair of cross peaks developed at 1732, 1720 cm^{-1} in the asynchronous spectrum (Fig. 7(B)) reveals that the time-dependent surface crystallization process of P(HB-co-HHx) also occurs through an intermediate state. The reorganization of the amorphous structure does not simultaneously result in the fully formed highly ordered crystalline component. Similar to the surface melting, the time-dependent surface crystallization of P(HB-co-HHx) mainly involves the highly ordered crystalline component and the amorphous structure. This observation also suggests that at the film surface, polymer molecules favor the highly ordered molecular chain structure.

Fig. 8(A) and (B) shows the synchronous and asynchronous 2D correlation spectra in the spectral region of 1790–1670 cm^{-1} generated from the time-dependent transmission spectra, respectively. Two pairs of cross peaks develop at (1742, 1722) and (1728, 1722) cm^{-1} in the asynchronous spectrum (Fig. 8(B)). The presence of asynchronous cross peaks indicates that the time-dependent bulk crystallization process of P(HB-co-HHx) occurs through an intermediate state. Note that, similar to the bulk melting process of P(HB-co-HHx) [22], two crystalline C=O bands (i.e. bands at ca. 1728 and 1722 cm^{-1}) appear in the 2D correlation spectra generated from the time-dependent transmission spectra. This observation suggests that the time-dependent crystallization occurring in the bulk of the film sample also involves two crystalline components and the amorphous phase.

3.3. Comparisons between the time-dependent crystal growth of P(HB-co-HHx) (12 mol% HHx) and PHB

It is known that the introduction of HHx units into the molecular chain of PHB results in dramatically improved mechanical properties of the resulting P(HB-co-HHx) copolymer [17]. The HHx units act as a less crystallizable part and thereby depress the degree of crystallinity of the

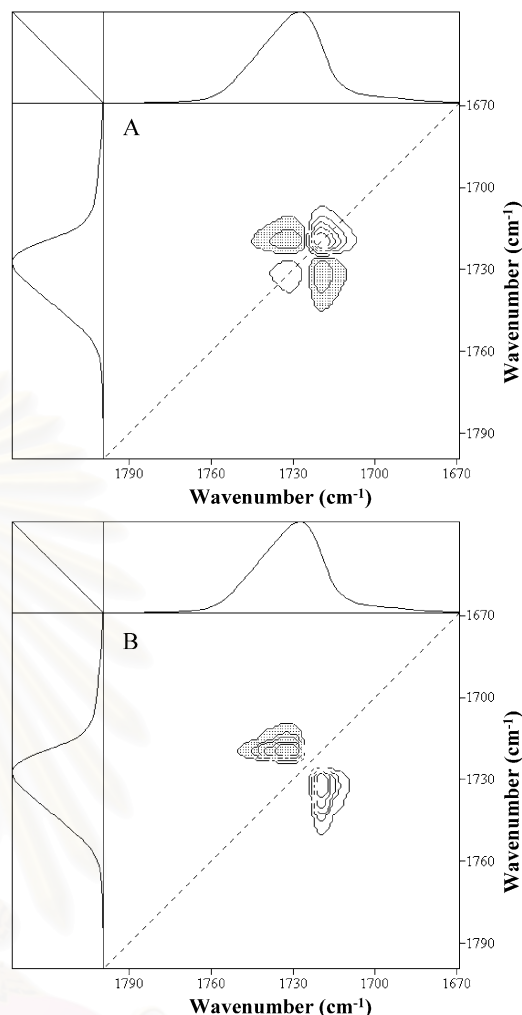


Fig. 7. Synchronous (A) and asynchronous (B) correlation spectra of P(HB-co-HHx) (12 mol% HHx) in the C=O stretching vibration region generated from the time-dependent ATR spectra shown in Fig. 4(A).

PHB homopolymer significantly [17]. From this aspect, effects of the HHx units on the crystallization process of the PHB homopolymer are very interesting.

Fig. 9(A) and (B) shows time-dependent ATR and transmission spectra of PHB in the C=O stretching vibration region, respectively. The observed IR spectra again indicate the different crystallization behavior at the surface and in the bulk of the PHB film sample. As expected, the ATR spectra of PHB (Fig. 9(A)) strongly represent the crystalline characteristic, and the amorphous feature at ca. 1740 cm^{-1} is very weak. Similar to P(HB-co-HHx), transmission spectra of PHB show higher amorphous characteristic as compared to the ATR spectra. However, time-dependent IR spectral variations for PHB shown in Fig. 9(A) and (B) are different from those for P(HB-co-HHx) shown in Fig. 4(A) and (B). In chloroform solution, both IR spectra of P(HB-co-HHx) and PHB show fully random-coil feature (see Fig. 10). After chloroform evaporated, P(HB-co-HHx) and PHB started to crystallize. However, we could not observe the IR spectra of the fully

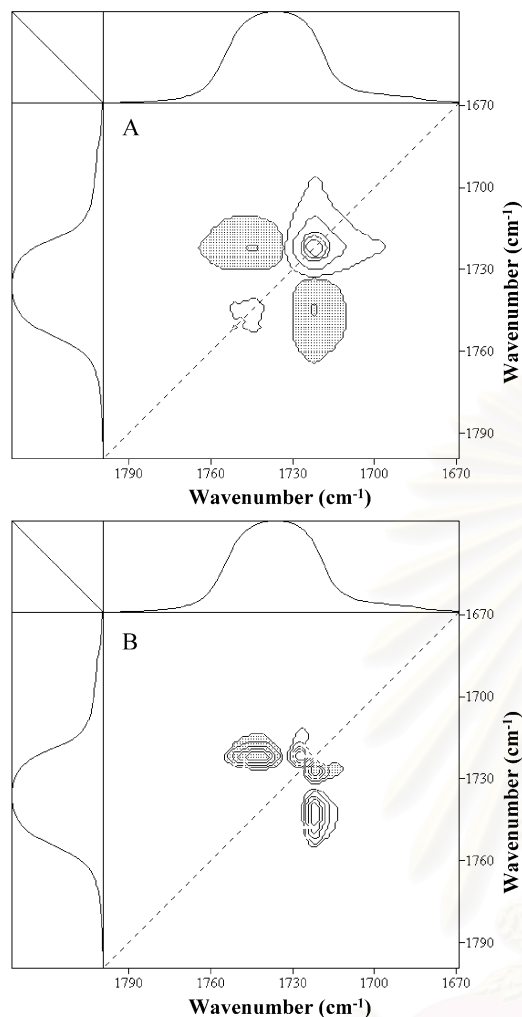


Fig. 8. Synchronous (A) and asynchronous (B) correlation spectra of P(HB-co-HHx) (12 mol% HHx) in the C=O stretching vibration region generated from the time-dependent transmission spectra shown in Fig. 4(B).

random-coil PHB for the solvent-free state. PHB assumes a crystalline state right after the solvent evaporation. This observation indicates that PHB crystallizes rapidly, much faster than P(HB-co-HHx). Although the highly ordered crystalline C=O band at ca. 1720 cm^{-1} continues to develop as time passes, the overall spectral changes occurred during the time-dependent crystal growth are not pronounced. That is to say, PHB crystallizes at a much higher rate than P(HB-co-HHx). In other words, the HHx comonomer incorporated in P(HB-co-HHx) significantly reduces the crystallization rate of the PHB homopolymer. This is because the HHx unit is less crystallizable, and the presence of the HHx units in the PHB molecular chains may encumber the crystallization of the polymer from place to place.

4. Conclusion

The melting behavior at the surface of P(HB-co-HHx) (12 mol% HHx) film sample was investigated by using ATR

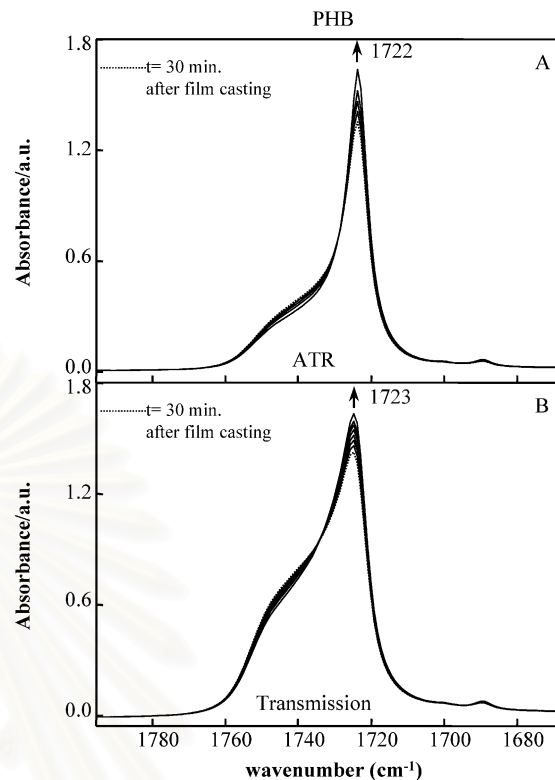


Fig. 9. Representative time-dependent ATR (A) and transmission (B) spectra of PHB in the C=O stretching vibration region measured at room temperature. Arrows indicate the direction of absorbance changes as time increases.

IR spectroscopy and the generalized 2D correlation analysis. The ATR technique is capable of probing the chemical moieties situated just a few micrometers beyond the sample surface. The 2D correlation spectra generated from the temperature-dependent ATR spectra in the C=O stretching vibration region suggest that the disappearance of the highly ordered crystalline component at the film surface does not simultaneously result in the formation of the amorphous structure. Similar to the bulk melting of P(HB-co-HHx), the surface melting of P(HB-co-HHx) takes place

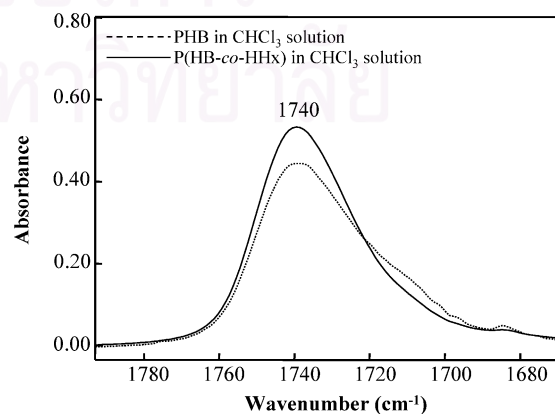


Fig. 10. Transmission spectra of P(HB-co-HHx) (12 mol% HHx) (solid line) and PHB (dotted line) in CHCl_3 solution.

through an intermediate state. However, the surface melting of P(HB-*co*-HHx) involves particularly the highly ordered crystalline component and the amorphous phase while the bulk melting involves two crystalline components (i.e. the highly ordered crystalline component and the minor crystalline component with a less-ordered structure) and the amorphous phase.

The time-dependent crystallization at the surface and bulk of P(HB-*co*-HHx) and PHB film samples was monitored by using ATR and transmission IR spectroscopy, respectively. It was revealed by the 2D correlation spectra generated from the time-dependent IR spectra of P(HB-*co*-HHx) in the C=O stretching vibration region that the surface and bulk crystal growth of P(HB-*co*-HHx) film also occurs through an intermediate state. Time-dependent ATR and transmission spectra of PHB indicate that PHB crystallizes at a much higher rate than P(HB-*co*-HHx). This observation suggests that the HHx units incorporated in the P(HB-*co*-HHx) copolymer significantly reduce not only the degree of crystallinity but also the crystallization rate of the PHB homopolymer. For both P(HB-*co*-HHx) and PHB film samples, it is very likely that the population of polymer crystals at the surface is higher than that in the bulk.

Acknowledgements

A.P. gratefully thanks the Thailand Research Fund (TRF) for the financial support via the Royal Golden Jubilee (RGJ) PhD program (Grant contract number: PHD/0066/2544).

References

- [1] Strobl GR. The physics of polymers: concepts for understanding their structures and behavior. Berlin: Springer; 1996.
- [2] Kai Z, Ying D, Guo-Qiang C. Biochem Eng J 2003;16:115.
- [3] Saad B, Neuenschwander P, Uhlschmid GK, Suter UW. Int J Biol Macromol 1999;25:293.
- [4] Labarre D. Trends Biomater Artif Organs 2001;15:1.
- [5] Neagle W, Randell DR. In: Surface analysis techniques and applications. Cambridge: Royal Society of Chemistry; 1990.
- [6] Berquier J-M, Arribart H. Langmuir 1998;14:3716.
- [7] Chen J, Gardella Jr. JA. Appl Spectrosc 1998;52:361.
- [8] Iwamoto R, Ohta K. Appl Spectrosc 1984;38:359.
- [9] Mallapragada SK, Narasimhan B. In: Meyers RA, editor. Encyclopedia of analytical chemistry. Chichester: Wiley; 2000. p. 7644.
- [10] Harrick NJ. Internal reflection spectroscopy. New York: Harrick Scientific Corporation; 1967.
- [11] Urban MW. Attenuated total reflectance spectroscopy of polymers: theory and practice. Washington, DC: American Chemical Society; 1996.
- [12] Williams SF, Martin DP. In: Steinbüchel A, Doi Y, editors. Biopolymers. Wienheim: Wiley-VCH; 2002. p. 91.
- [13] Lara LM, Gjalt WH. Microbiol Mol Biol Rev 1991;63:21.
- [14] Anderson AJ, Dawes EA. Microbiol Rev 1990;54:450.
- [15] Jendrossek D. In: Steinbüchel A, Doi Y, editors. Biopolymers. Wienheim: Wiley-VCH; 2001. p. 41.
- [16] Lee SY. Biotechnol Bioeng 1996;49:1.
- [17] Satkowski MM, Melik DH, Autran J-P, Green PR, Noda I, Schechtman LA. In: Steinbüchel A, Doi Y, editors. Biopolymers. Wienheim: Wiley-VCH; 2001. p. 231.
- [18] See website: www.nodax.com.
- [19] Sato H, Nakamura M, Padermshoke A, Yamaguchi H, Terauchi H, Ekgasit S, Noda I, Ozaki Y. Macromolecules 2004;37:3763.
- [20] Sato H, Padermshoke A, Nakamura M, Murakami R, Hirose F, Senda K, Terauchi H, Ekgasit S, Noda I, Ozaki Y. Macromol Symp 2004 in press.
- [21] Padermshoke A, Katsumoto Y, Sato H, Ekgasit S, Noda I, Ozaki Y. Spectrochim Acta A 2005;61:541.
- [22] Padermshoke A, Sato H, Katsumoto Y, Ekgasit S, Noda I, Ozaki Y. Vib Spectrosc 2004 in press.
- [23] Wu Q, Tian G, Sun S, Noda I, Chen G-Q. J Appl Polym Sci 2001;82: 934.
- [24] Tian G, Wu Q, Sun S, Noda I, Chen G-Q. Appl Spectrosc 2001;55: 888.
- [25] Mirabella Jr. FM. Internal reflection spectroscopy: theory and application. New York: Marcel Dekker; 1993.



Crystallization behavior of poly(3-hydroxybutyrate-co-3-hydroxyhexanoate) studied by 2D IR correlation spectroscopy

Adchara Padermshoke^{a,b}, Harumi Sato^a, Yukiteru Katsumoto^c, Sanong Ekgasit^b,
Isao Noda^d, Yukihiro Ozaki^{a,*}

^aDepartment of Chemistry, School of Science and Technology, Kwansai-Gakuin University, 2-1 Gakuen, Sanda, Hyogo 669-1337, Japan

^bSensor Research Unit, Department of Chemistry, Faculty of Science, Chulalongkorn University, Patumwan, Bangkok 10330, Thailand

^cDepartment of Chemistry, Graduate School of Science, Hiroshima University, Higashi-Hiroshima, Hiroshima 739-8526, Japan

^dThe Procter and Gamble Company, 8611 Beckett Road, West Chester, OH 45069, USA

Received 30 April 2004; received in revised form 4 August 2004; accepted 23 August 2004

Abstract

Crystallization behavior of poly(3-hydroxybutyrate-co-3-hydroxyhexanoate) (P(HB-co-HHx)) (HHx = 12 mol%) was studied by means of two-dimensional infrared (2D IR) correlation spectroscopy. Three types of crystallization; the gradual cooling from the melt, the isothermal crystallization of the supercooled melt, and the isothermal crystallization of the solution-cast film were investigated. The order of crystal growth steps taking place during the three different types of crystallization processes was analyzed in detail. It was revealed by the asynchronous 2D correlation spectra generated from the dynamic IR spectra in the C=O stretching band region that the development of the highly ordered crystals occurs prior to that of the less ordered crystals for the gradual cooling crystallization. On the other hand, for the supercooled melt and solution-cast film crystallization, the formation of the less ordered crystals takes place before that of the highly ordered crystals. The transition from the amorphous phase to the less ordered crystals is a simultaneous process for all three types of crystallization. © 2004 Published by Elsevier Ltd.

Keywords: Crystallization behavior; Two-dimensional (2D-IR) correlation spectroscopy; Infrared spectroscopy

1. Introduction

Industrial materials derived from petroleum-based synthetic polymers are indispensable for modern human life. These materials, however, cause tremendous environmental problems especially at the waste disposal process. As a consequence, many researchers and manufacturers are driven to move towards materials that can be produced from renewable resources and would not persist in the environment.

Bacterially synthesized poly(3-hydroxyalkanoate)s (PHAs) have received a keen attention as environmentally friendly polymeric materials [1–6]. PHAs are biodegradable

polyesters accumulated as energy-storing inclusion body granules in the cells of certain microorganisms [1–6]. Their chemical structures and physical characteristics are fairly similar to those of certain petroleum-based synthetic polymers [1,4,6]. Due to the high stereoregularity of biologically produced macromolecules, some PHA polymers are highly crystalline and, hence, too rigid, stiff, and brittle [1,6]. Accordingly, many attempts have been made to reduce the crystallinity of PHAs in order to improve their physical and mechanical properties [6]. It has been reported that the copolymerization of a longer side-chain 3-hydroxyhexanoate (3-HHx) comonomer with the highly crystalline 3-hydroxybutyrate (3-HB) units significantly reduces the crystallinity and increases the flexibility of PHB [6]. The resulting P(HB-co-HHx) copolymers possess dramatically improved physical and mechanical properties compared with those of PHB homopolymer [6,7]. The crystallinity and

* Corresponding author. Tel.: +81-79-565-8349; fax: +81-79-565-9077.

E-mail address: ozaki@ksc.kwansei.ac.jp (Y. Ozaki).

113 crystallization behavior of PHA polymers are crucial for
114 determining their overall performances and characteristics.
115 The thermal behavior, biodegradation mechanism, and
116 mechanical properties of P(HB-*co*-HHx) were revealed by
117 several research groups [6,8–10].

118 Infrared (IR) spectroscopy has been successfully
119 employed to investigate the conformational changes and
120 local molecular environments of polymers during their
121 crystallization [11–19]. This is because the technique
122 provides not only sensitivity to changes in molecular
123 interactions and polymer crystallinity but also substantial
124 advantages that allow the dynamic studies at the micro-
125 scopic molecular level. Two-dimensional (2D) correlation
126 analysis proposed by Noda [20,21] enables a more detailed
127 analysis of the IR spectral variations of polymers. It
128 emphasizes spectral information not readily observable in
129 conventional one-dimensional (1D) spectra. Asynchronous
130 2D spectra are very powerful in differentiating highly
131 overlapped bands that vary out of phase under the external
132 perturbation [22]. The signs of synchronous and asynchro-
133 nous cross peaks indicate the successive order of the events
134 taking place in the system of interest under the applied
135 perturbation [19,23]. These features make the technique
136 ideally suitable for the study of polymer crystallization.

137 We have studied the melting behavior of P(HB-*co*-HHx)
138 (12 mol% HHx) by using the generalized 2D IR correlation
139 spectroscopy [24]. In our previous study, the asynchronous
140 2D correlation spectrum generated for the C=O stretching
141 band region of P(HB-*co*-HHx) (HHx = 12 mol%) revealed
142 the coexistence of two crystalline bands at 1731 and
143 1723 cm^{-1} [24]. The band at 1723 cm^{-1} is possibly
144 ascribed to the highly ordered crystalline component, and
145 that at 1731 cm^{-1} may arise from the less ordered
146 crystalline part [24]. The presence of the asynchronous
147 cross peaks between these two crystalline bands suggested
148 that the intensities of the two crystalline bands change
149 successively during the melting process of the copolymer
150 [24]. The vibrational frequencies of bands in the C=O
151 stretching region of P(HB-*co*-HHx) are identical to those of
152 PHB [25]. The asynchronous 2D correlation spectrum
153 generated for the C=O stretching band region of the PHB
154 homopolymer also showed the coexistence of two crystal-
155 line bands at around 1731 and 1723 cm^{-1} [25]. The
156 presences of the C=O bands at around 1728 and
157 1722 cm^{-1} in IR spectra of PHB are also reported by
158 Yoshie et al. [26], and they assigned these two C=O bands
159 to the interfacial and crystalline phases, respectively [26].

160 In general, the formation of an ordered structure during
161 the crystallization of semi-crystalline polymers depends
162 strongly on the crystallization conditions [27]. The present
163 study reveals the mechanism of the crystallization of P(HB-
164 *co*-HHx) (12 mol% HHx) under different crystallization
165 conditions by using 2D IR correlation analysis. Three types
166 of crystallization; the gradual cooling from the melt, the
167 isothermal crystallization of the supercooled melt, and the
168 isothermal crystallization of the solution-cast film were

performed to verify the differences and similarities of the
crystallization behavior among these three processes.

2. Experimental

2.1. Materials

Bacterially synthesized P(HB-*co*-HHx) (12 mol% HHx)
was provided by the Procter and Gamble Company,
Cincinnati, USA. The glass transition temperature (T_g),
crystallization temperature (T_c), melting temperature (T_m),
and percentage of crystallinity of the sample are approxi-
mately 2.4, 51, 110 °C, and 35%, respectively. Purification
of the P(HB-*co*-HHx) sample was performed by dissolving
P(HB-*co*-HHx) in hot chloroform (CHCl_3), re-precipitating
in methanol (CH_3OH), and vacuum-drying at 60 °C for 24 h.
Chloroform and methanol were purchased from Wako Pure
Chemical Industries, Ltd, Osaka, Japan. Chloroform was
used as a solvent for preparing the sample solution. The
concentration of the chloroform solution of P(HB-*co*-HHx)
was approximately 0.004 g/ml.

2.2. IR spectroscopic measurements

2.2.1. Gradual cooling crystallization

A film of P(HB-*co*-HHx) (12 mol% HHx) for IR
measurements was prepared by casting its chloroform
solution on a CaF_2 window. After chloroform had
evaporated, the film was heated to 140 °C and kept for
30 min. IR spectra of the film sample were measured at a
2 cm^{-1} spectral resolution by using a Thermo Nicolet
Magna-IR™ 550 spectrometer equipped with a mercury
cadmium telluride (MCT) detector. To ensure a high signal-
to-noise ratio, 512 scans were co-added. The temperature of
the sample cell that holds the CaF_2 window with the P(HB-
co-HHx) film was controlled by using a temperature
controller unit (CHINO, model SU) with an accuracy of
 ± 1 °C. The temperature-dependent dynamic IR spectra
were collected throughout a temperature range of 140–30 °C
with a decrement interval of 10 °C. The cooling rate was
2 °C/min. The sample film was kept at each temperature for
15 min before the measurement.

2.2.2. Supercooled melt crystallization

The sample film was prepared by casting its chloroform
solution on a CaF_2 window in the same manner as that for
the gradual cooling crystallization. After chloroform had
evaporated, the film was heated to 140 °C and kept for
30 min before rapidly quenched to room temperature
(25 °C). The time-dependent IR spectra were collected at
room temperature with a time interval of 30 min until the
crystal growth was completed (i.e. no significant spectral
change was observed). The instrumental parameters were
the same as those described in Section 2.2.1.

2.2.3. Solvent-cast film crystallization

The sample film was prepared by casting its chloroform solution on a CaF₂ window. After the solvent casting, the sample film was air-dried for 30 min before the measurements. The IR spectrum of the sample film measured after the solvent had evaporated showed no spectroscopic evidence for the presence of chloroform. The time-dependent IR spectra were collected at room temperature with a time interval of 15 min until the crystal growth was completed (i.e. no significant spectral change was observed). The instrumental parameters were the same as those described in Section 2.2.1.

2.3. 2D correlation analysis

The IR spectra were preprocessed to minimize the effect of baseline instability prior to the 2D correlation analysis. The spectral region of interest (1800–1660 cm⁻¹) was subjected to a linear baseline correction, followed by offsetting to the zero absorbance value. The calculations of 2D correlation spectra were performed by using the 2D-Pocha software composed by Daisuke Adachi (Kwansei-Gakuin University, Japan). Temperature-averaged and time-averaged IR spectra in the selected wavenumber region were used as the reference spectra for the 2D correlation calculations of the temperature and time-dependent IR spectra, respectively.

3. Results and discussion

3.1. Gradual cooling crystallization

Fig. 1 shows temperature-dependent IR spectra of P(HB-co-HHx) (12 mol% HHx) in the 1780–1680 cm⁻¹ region, where bands due to the C=O stretching modes appear. A broad band at 1740 cm⁻¹ decreases while a sharp band at 1723 cm⁻¹ gradually increases in intensity during the

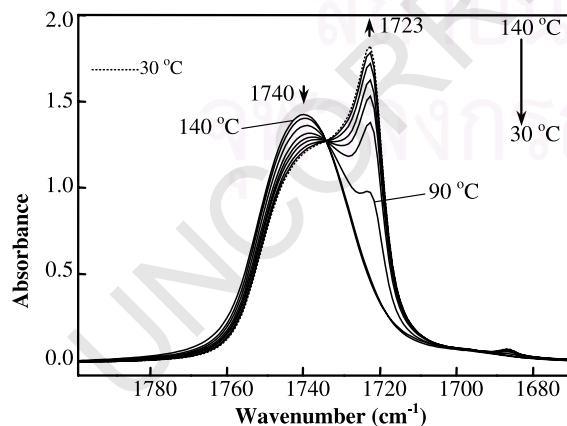


Fig. 1. IR spectra of P(HB-co-HHx) (12 mol% HHx) in the C=O stretching vibration region measured during the crystallization from the melt over a temperature range of 140–30 °C.

course of temperature decrease. The sharp band at 1723 cm⁻¹ arises from the crystalline part of P(HB-co-HHx), and the broad band at 1740 cm⁻¹ is attributed to the amorphous component [24]. These spectral variations reflect the crystallization process of P(HB-co-HHx).

To extract more detailed information about the spectral variations induced by the gradual cooling crystallization process, 2D correlation analysis was employed. Fig. 2(A) and (B) shows the synchronous and asynchronous 2D correlation spectra in the spectral region of 1790–1670 cm⁻¹ generated from the temperature-dependent IR spectra. A pair of negative cross peaks developed at (1745, 1723) cm⁻¹ in the synchronous spectrum (Fig. 2(A)) indicates the opposite directions of the intensity variations in these two

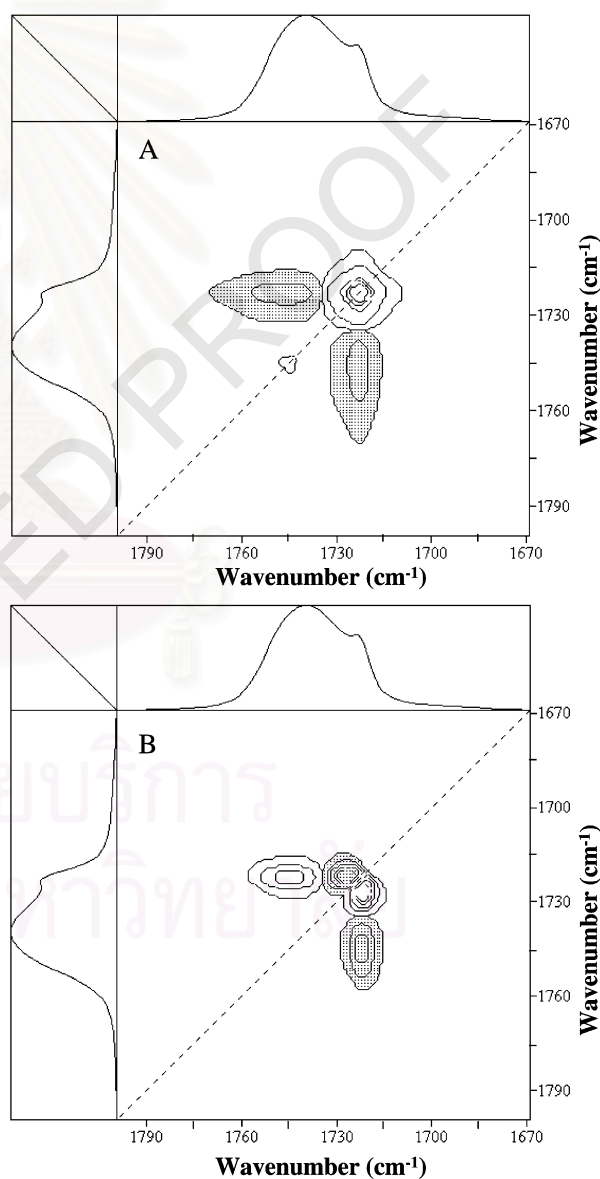


Fig. 2. Synchronous (A) and asynchronous (B) 2D IR correlation spectra of P(HB-co-HHx) (12 mol% HHx) in the C=O stretching vibration region generated from the temperature-dependent IR spectra measured over a temperature range of 140–30 °C.

correlated bands. In the asynchronous spectrum (Fig. 2(B)), two pairs of cross peaks appear at (1745, 1723) and (1728, 1723) cm^{-1} . The band at around 1728 cm^{-1} revealed by the asynchronous 2D correlation spectrum may arise from the less ordered crystalline component of P(HB-co-HHx) [24]. The presence of asynchronous cross peaks indicates the out-of-phase changes in the intensity of the correlated bands. Fig. 2(B) suggests that, during the crystallization process, the decrease in intensity of the amorphous C=O band at 1745 cm^{-1} and the increase in intensity of the crystalline C=O band at 1723 cm^{-1} do not occur simultaneously. Of note in Fig. 2(B) is that the two crystalline C=O bands at 1728 and 1723 cm^{-1} share asynchronous cross peaks. This observation indicates that the development of the highly ordered crystalline component and that of the less ordered crystalline component take place out of phase. The negative sign of the asynchronous cross peak at (1728, 1723) cm^{-1} and the positive sign of the corresponding synchronous spectral intensity reveal that the formation of the highly ordered crystalline component proceeds prior to that of the less ordered crystalline structure during the course of the gradual cooling crystallization.

3.2. Supercooled melt crystallization

Fig. 3 shows time-dependent IR spectra of P(HB-co-HHx) (12 mol% HHx) in the C=O stretching band region measured during the isothermal crystallization of the supercooled melt. The representative spectra shown in Fig. 3 were collected at 0 (start), 540, 900, 1020, 1140, 1380, 1560, 1740, 1920, 2100, and 2220 min after the initiation of the isothermal crystallization. Because the crystallization rate of P(HB-co-HHx) is slow, one can supercool the system away from the thermal equilibrium, and an amorphous sample can be obtained well below its T_m . The time-dependent crystal growth of the supercooled melt was clearly revealed by the changes in intensity of the amorphous C=O band at 1739 cm^{-1} and the crystalline C=O band at 1724 cm^{-1} . The trend of the spectral variations induced by the crystallization of the supercooled

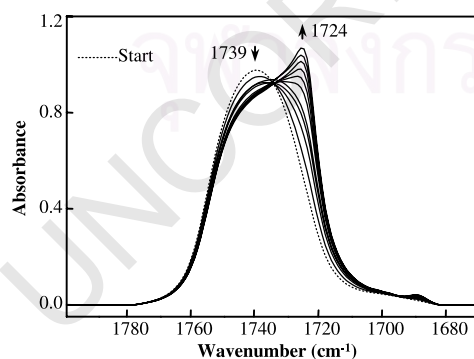


Fig. 3. IR spectra of P(HB-co-HHx) (12 mol% HHx) in the C=O stretching vibration region measured during the crystallization of the supercooled melt at room temperature.

melt is similar to that induced by the gradual cooling crystallization shown in Fig. 1. The amorphous C=O band at 1739 cm^{-1} decreases while the crystalline C=O band at 1724 cm^{-1} gradually increases in intensity during the crystallization process. However, the details of spectral features for the supercooled melt crystallization are substantially different from those of the gradual cooling process. The crystalline band observed during the gradual cooling crystallization is more sharp and intense than that observed during the supercooled melt crystallization. This observation implies that the crystallinity of the gradually cooled sample is much higher than that of the sample crystallized from the supercooled melt at room temperature. In addition, the crystalline band observed during the gradual cooling process (Fig. 1) appeared very clearly as a well-separated band at 1723 cm^{-1} below the T_m of the sample and developed down to room temperature. On the other hand, the crystalline band observed during the isothermal crystallization of the supercooled melt developed very slowly.

Fig. 4(A) and (B) shows the synchronous and asynchronous 2D correlation spectra in the spectral region of 1790–1670 cm^{-1} generated from the time-dependent IR spectra shown in Fig. 3. Two autopeaks developed at 1745 and 1724 cm^{-1} reflect the spectral variations of the amorphous and crystalline C=O bands, respectively. A pair of negative cross peaks appeared at (1745, 1724) cm^{-1} indicates the opposite directions of the intensity variations in these two bands. The asynchronous spectrum (Fig. 4(B)) shows two pairs of asynchronous cross peaks at (1745, 1723) and (1728, 1723) cm^{-1} similar to that for the gradual cooling crystallization case. This result indicates that the disappearance of the amorphous component does not proceed simultaneously with the appearance of the crystalline component during the supercooled melt crystallization. The two crystalline C=O bands at 1728 and 1723 cm^{-1} for the supercooled melt crystallization also share asynchronous cross peaks, indicating the time lag between the increase in intensity of these two crystalline C=O bands. However, the signs of the asynchronous cross peaks shown in Fig. 4(B) are opposite to those shown in Fig. 2(B). The positive sign of the asynchronous cross peak at (1728, 1723) cm^{-1} and the corresponding positive synchronous spectral intensity suggest that the increase in intensity of the band at 1728 cm^{-1} occurs before that of the band at 1723 cm^{-1} , i.e. during the supercooled melt crystallization, the formation of the less ordered crystalline component proceeds before that of the highly ordered crystalline component. In other words, the order of crystal growth steps is different from that for the gradual cooling crystallization process.

3.3. Solvent-cast film crystallization

Fig. 5 shows time-dependent IR spectra of P(HB-co-HHx) (12 mol% HHx) in the C=O stretching band region measured during the isothermal crystallization of the

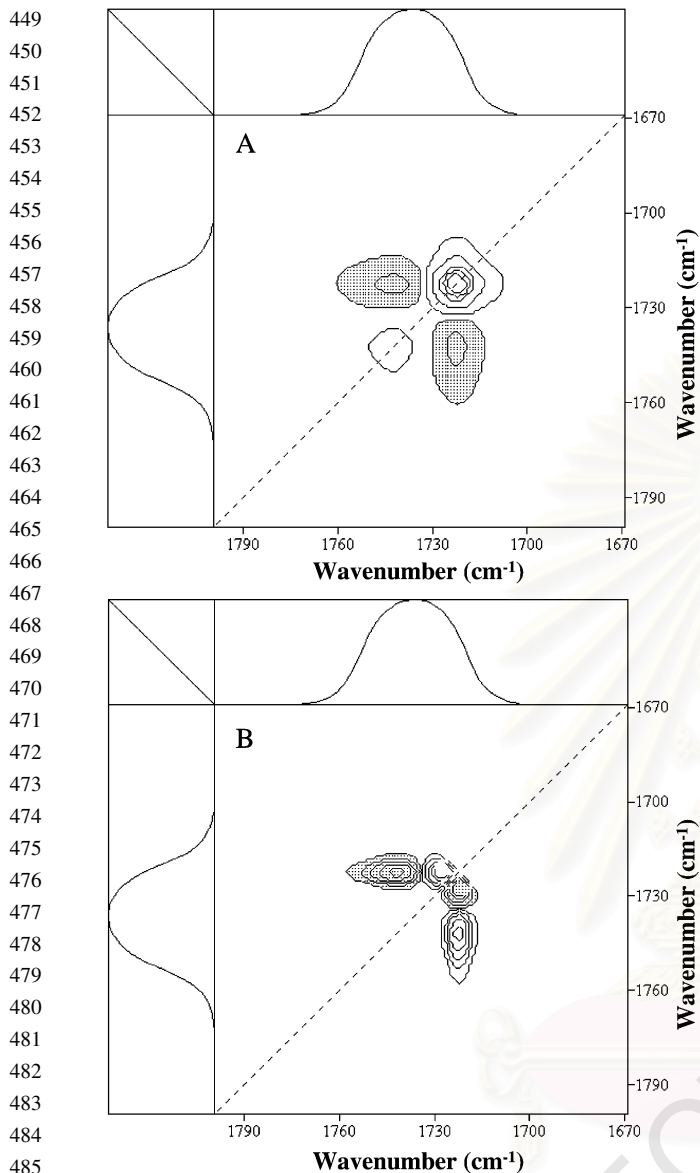


Fig. 4. Synchronous (A) and asynchronous (B) 2D IR correlation spectra of P(HB-co-HHx) (12 mol% HHx) in the C=O stretching vibration region generated from the time-dependent IR spectra measured during the crystallization of the supercooled melt at room temperature.

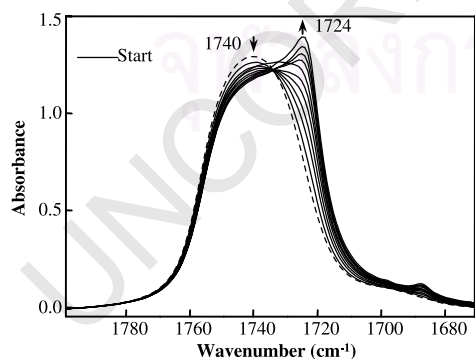


Fig. 5. IR spectra of P(HB-co-HHx) (12 mol% HHx) in the C=O stretching vibration region measured during the crystallization of the solvent-cast film at room temperature.

solution-cast film. The representative spectra shown in Fig. 5 were collected at 0 (start), 75, 210, 240, 285, 315, 375, 420, 480, 660, and 1080 min after the initiation of the isothermal crystallization. The time-dependent crystal growth of the sample was also observed for the solution-cast film as indicated by the changes in intensity of the amorphous C=O band at 1740 cm^{-1} and the crystalline C=O band at 1724 cm^{-1} . The spectral variations shown in Fig. 5 are very similar to those for the supercooled melt crystallization shown in Fig. 3. The development of the crystalline C=O band proceeded slowly, and the band shape is not sharp and intense.

Fig. 6(A) and (B) shows the synchronous and asynchronous 2D correlation spectra in the spectral region

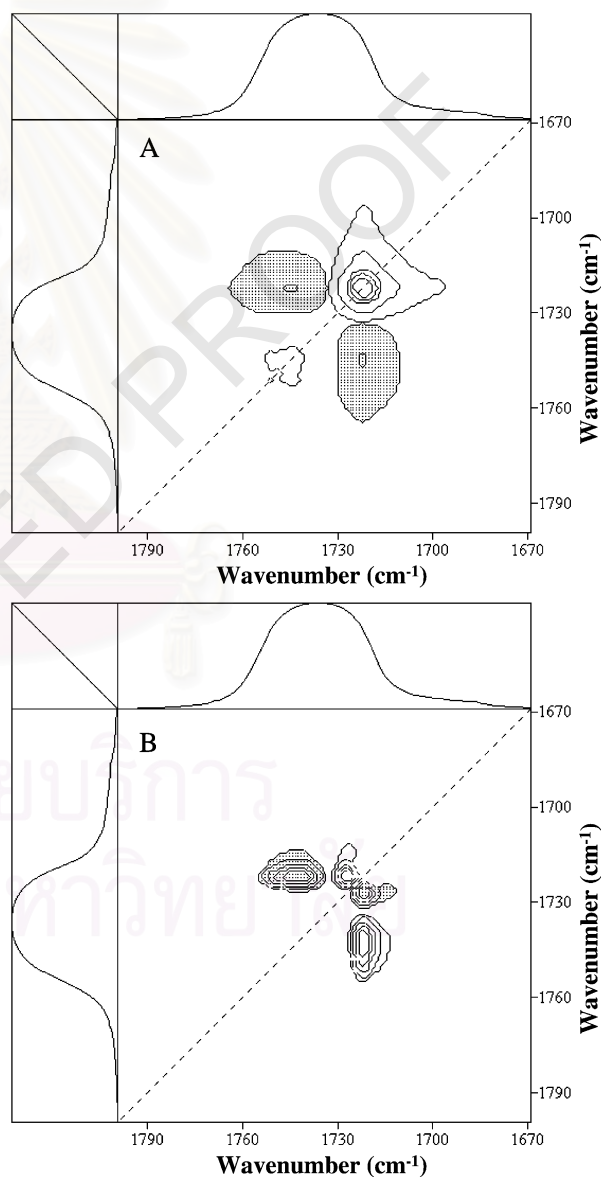


Fig. 6. Synchronous (A) and asynchronous (B) 2D IR correlation spectra of P(HB-co-HHx) (12 mol% HHx) in the C=O stretching vibration region generated from the time-dependent IR spectra measured during the crystallization of the solvent-cast film at room temperature.

of 1790–1670 cm^{-1} generated from the time-dependent IR spectra shown in Fig. 5. The 2D correlation spectra shown in Fig. 6(A) and (B) are very similar to those generated for the supercooled melt crystallization shown in Fig. 4(A) and (B). Two pairs of asynchronous cross peaks appear at (1745, 1723) and (1728, 1723) cm^{-1} . The signs of the asynchronous cross peaks and the corresponding synchronous intensity reveal that the formation of the less ordered crystalline component proceeds before that of the highly ordered crystalline component during the crystallization of the solution-cast film. This order of crystal growth steps is the same as that for the supercooled melt crystallization.

3.4. Comparison among the three types of crystallization processes

2D IR correlation spectroscopy suggests that the order of crystal growth steps for the gradual cooling crystallization is different from that of the supercooled melt and solution-cast film crystallization. For the gradual cooling process, the development of the highly ordered crystals occurs prior to the formation of the less ordered crystals. On the other hand, for the supercooled melt and solution-cast film crystallization, the formation of the less ordered crystals takes place first, and the highly ordered crystals develop later.

In general, being kinetically controlled, structures formed during the crystallization of partially crystalline polymers are strongly affected by the thermal history and preceding processes. In the gradual cooling condition, the sample is slowly cooled from the melt to a temperature below the T_m . At each temperature, the sample is allowed to reach the equilibrium state. Consequently, the crystallization occurs by nucleation and growth of spherulites [27]. The highly ordered crystals develop first and fill the specimen volume with a skeletal structure of crystalline lamellae. The inter crystalline regions, which remained amorphous, still have the potential to crystallize upon further cooling. The secondary crystallization follows at lower temperatures. The formation of the less ordered crystals proceeds via insertion into the original stack of the crystalline lamellae. The reduction of the order of these secondary crystals arises from the spatial constraint. The crystalline lamellae generated in the secondary crystallization are geometrically strained because they are sandwiched in the narrow space between the already existing lamellae. Clearly, the additional lamellae formed at lower temperatures are generally thinner, less uniform, and include more internal disorder [27].

For the supercooled melt crystallization, the sample is quenched rapidly from 140 to 25 °C. In this state, the crystallization is substantially retarded due to the reduced segmental mobility of the polymer when approaching the T_g . Under such a condition, the transition from the disordered phase to the higher ordered structure proceeds through a continuous sequence of states rather than building up a two-phase structure from the very beginning. The

increase in the crystallinity of the supercooled melt sample is very slow. The crystal growth occurs as the formation of numerous less ordered crystallites. The apparent reduction of the order in these crystallites arises from the interfacial effect of the very small size of crystals. The radius of curvature is too small to have a well-developed crystal. The interfacial effect is different from the effect of the over crowding by the volume filling crystal lamellae already existing as in the case of the gradual cooling crystallization. Once these tiny crystallites are formed, the additional growth of the highly ordered crystals, which is characterized by the band at 1723 cm^{-1} , will occur. In other words, for the isothermal crystallization of the amorphous solid at room temperature, the geometrically strained nuclei change to more ordered crystallites. This process, however, is very slow. The system is hardly at the crystal volume filled stage during the crystallization period. The solution-cast P(HB-co-HHx) film exhibits similar crystallization behavior to that of the supercooled melt P(HB-co-HHx). The crystallization was carried out starting from the state in which the mobility of the entanglements is suppressed. The crystallization takes a long time to proceed. The very slow ongoing increase in the crystallinity with long times indicates the difficulty in approaching the perfect fully crystalline state of the sample. This lack of crystal growth results in the very weak intensity of the crystalline band observed for the supercooled melt and solution-cast film crystallization.

For all three types of crystallization, there is no asynchronous cross peak between the bands at 1745 and 1728 cm^{-1} in the 2D correlation spectra. This observation suggests that the transition from the amorphous state to the small crystallites with a less ordered structure is a one step transformation.

4. Conclusion

2D IR correlation spectroscopy was employed to study the crystallization behavior of P(HB-co-HHx) (12 mol% HHx). The order of crystal growth steps for the three different types of crystallization, i.e. the gradual cooling, supercooled melt, and solution-cast film crystallization, was investigated. The C=O stretching band region showed the coexistence of two crystalline bands, which might be assignable to the differently ordered crystalline parts of the polymer. The 2D IR correlation spectra generated for the C=O stretching band region suggested that, for the gradual cooling crystallization, the development of the highly ordered crystalline component proceeds prior to that of the less ordered crystalline component. On the other hand, for the supercooled melt and solution-cast film crystallization, the formation of the less ordered crystalline component occurs before that of the highly ordered crystalline component. The transition from the amorphous state to the less ordered crystalline component is a one step transformation for all three types of crystallization.

Acknowledgements

A.P. gratefully thanks the Thailand Research Fund (TRF) for the financial support via the Royal Golden Jubilee (RGJ) PhD program (Grant contract number: PHD/0066/2544).

References

- [1] Williams SF, Martin DP. In: Steinbüchel A, Doi Y, editors. *Biopolymers*. Wienheim: Wiley-VCH; 2002. p. 91.
- [2] Lara LM, Gjalt WH. *Microbiol Mol Biol Rev* 1991;63:21.
- [3] Anderson AJ, Dawes EA. *Microbiol Rev* 1990;54:450.
- [4] Jendrossek D. In: Steinbüchel A, Doi Y, editors. *Biopolymers*. Wienheim: Wiley-VCH; 2001. p. 41.
- [5] Lee SY. *Biotechnol Bioeng* 1996;49:1.
- [6] Satkowski MM, Melik DH, Autran J-P, Green PR, Noda I, Schechtman LA. In: Steinbüchel A, Doi Y, editors. *Biopolymers*. Wienheim: Wiley-VCH; 2001. p. 231.
- [7] <http://www.nodax.com>.
- [8] Sato H, Nakamura M, Padermshoke A, Yamaguchi H, Terauchi H, Ekgasit S, Noda I, Ozaki Y. *Macromolecules* 2004;37:3763.
- [9] Abe H, Doi Y, Aoki H, Akehata T. *Macromolecules* 1998;31:1791.
- [10] Doi Y, Kitamura S, Abe H. *Macromolecules* 1995;28:4822.
- [11] Sasaki S, Tashiro K, Kobayashi M, Izumi Y, Kobayashi K. *Polymer* 1999;40:7125.
- [12] Tashiro K, Sasaki S. *Prog Polym Sci* 2003;28:451.
- [13] Jiang Y, Gu Q, Li L, Shen D-Y, Jin X-G, Chan C-M. *Polymer* 2003; 44:3509.
- [14] Tashiro K, Sasaki S, Gose N, Kobayashi M. *Polym J* 1998;30:485.
- [15] Hauser G, Schmidtke J, Strobl G. *Macromolecules* 1998;31:6250.
- [16] Heintz AM, McKiernan RL, Gido SP, Penelle J, Hsu SL, Sasaki S, Takahara A, Kajiyama T. *Macromolecules* 2002;35:3117.
- [17] Radhakrishnan J, Kaito A. *Polymer* 2001;42:3859.
- [18] Mallapragada SK, Narasimhan B. In: Meyers RA, editor. *Encyclopedia of analytical chemistry*. Chichester: Wiley; 2000. p. 7644.
- [19] Zhang J, Duan Y, Shen D, Yan S, Noda I, Ozaki Y. *Macromolecules* 2004 in press.
- [20] Noda I. *Bull Am Phys Soc* 1986;31:520.
- [21] Noda I. *Appl Spectrosc* 1993;47:1329.
- [22] Noda I. *J Am Chem* 1989;111:8116.
- [23] Noda I, Dowrey AE, Marcott C, Story GM, Ozaki Y. *Appl Spectrosc* 2001;54:236A.
- [24] Padermshoke A, Sato H, Katsumoto Y, Ekgasit S, Noda I, Ozaki Y. *Vib Spectrosc* 2004 in press.
- [25] Padermshoke A, Katsumoto Y, Sato H, Ekgasit S, Noda I, Ozaki Y. *Spectrochim Acta A* 2005;61:541.
- [26] Yoshie N, Oike Y, Kasuya K, Doi Y, Inoue Y. *Biomacromolecules* 2002;3:1320.
- [27] Strobl G. *The physics of polymers: concepts for understanding their structures and behavior*. Berlin: Springer; 1996.

Thermal Behavior and Molecular Interaction of Poly(3-hydroxybutyrate-*co*-3-hydroxyhexanoate) Studied by Wide-Angle X-ray Diffraction

Harumi Sato,[†] Masayuki Nakamura,[‡] Adchara Padermshoke,^{†,§}
Hiroshi Yamaguchi,[†] Hikaru Terauchi,[‡] Sanong Ekgasit,[§] Isao Noda,[⊥] and
Yukihiro Ozaki^{*,†}

Department of Chemistry, School of Science and Technology, Kwansai-Gakuin University, Sanda, Hyogo 669-1337, Japan; Department of Physics, School of Science and Technology, Kwansai-Gakuin University, Sanda, Hyogo 669-1337, Japan; Sensor Research Unit, Department of Chemistry, Faculty of Science, Chulalongkorn University, Patumwan, Bangkok 10330, Thailand; and The Procter and Gamble Company, 8611 Beckett Road, West Chester, Ohio 45069

Received January 19, 2004; Revised Manuscript Received March 5, 2004

ABSTRACT: The thermal behavior and molecular interaction of a new type of bacterial copolyester, poly(3-hydroxybutyrate-*co*-3-hydroxyhexanoate), P(HB-*co*-HHx) (HHx = 12 mol %), was investigated by using wide-angle X-ray diffraction (WAXD) and differential scanning calorimetry (DSC). The WAXD measurements were carried out over a temperature range from 25 to 110 °C in the scattering angle range of $2\theta = 5\text{--}13^\circ$. The WAXD pattern at room temperature shows that the P(HB-*co*-HHx) copolymer has an orthorhombic system ($\alpha = \beta = \gamma = 90^\circ$) with $a = 5.76 \text{ \AA}$, $b = 13.20 \text{ \AA}$, and $c = 5.96 \text{ \AA}$ (fiber repeat), which is identical to the crystal system of poly(3-hydroxybutyrate) (PHB) homopolymer. However, temperature-dependent variations in the lattice parameters, a and b , of P(HB-*co*-HHx) are quite different from those of PHB. Only the a lattice parameter increases with temperature, while the b lattice parameter changes very little in the case of crystalline P(HB-*co*-HHx). It seems that the intermolecular and intramolecular interactions between the C=O group and the CH₃ group decrease along the a axis of crystalline P(HB-*co*-HHx) with temperature. The (110) peak area of P(HB-*co*-HHx) starts decreasing from around 50 °C while that of PHB changes little at least until 140 °C, indicating that the crystallinity of PHB remains almost unchanged until 140 °C, but that of P(HB-*co*-HHx) decreases gradually from fairly low temperature (~50 °C). The DSC measurement of the chloroform solution cast P(HB-*co*-HHx) shows a recrystallization peak around 51 °C. The (110) peak area of WAXD pattern of the chloroform solution cast P(HB-*co*-HHx) shows a maximum value at around 54 °C. The maximum of the (110) peak area demonstrates the recrystallization process of P(HB-*co*-HHx). The result is in a good agreement with the result of the DSC measurement.

Introduction

Poly(3-hydroxybutyrate) (PHB) and its copolymers, poly(hydroxyalkanoate)s (PHAs), are biologically synthesized polyesters produced by a number of microorganisms and are consequently subjected to degradation by bacteria in the soil.^{1–5} PHAs are completely biodegradable under aerobic and anaerobic conditions and can be produced from renewable resources. Among all natural polymers, only PHA polymers possess thermoplasticity and mechanical properties similar to those of synthetic polymers.^{6–8} Since these polymers are biodegradable, they have been receiving much attention as new environmentally friendly materials, and numerous industrial applications, including new medical applications, are explored.⁹

PHB is one of the most well-studied bacterial polyesters in the PHA polymer. The thermal properties of PHB have been investigated by several research groups.^{8,10–12} It has been claimed that PHB has similar thermal and mechanical properties to isotactic polypropylene (iPP).¹³ The crystal structure of PHB was inves-

tigated by X-ray diffraction, and it was found that PHB has an orthorhombic system, $P2_12_12_1(D_2^4)$ with a fiber repeat of 5.96 Å.^{14,15} PHB shows high crystallinity because of the perfect stereoregularity produced by bacteria. The high crystallinity of PHB makes it rigid and stiff, not necessarily well-suited for certain applications as a commodity plastic. To reduce the excess crystallinity and modify the overall physical properties of PHB,¹³ other monomers are sometimes copolymerized with PHB. The PHB-based copolymers show a wide range of physical properties depending on the chemical structure of the comonomer units as well as the comonomer composition.¹⁶ The copolymerization of 3-hydroxyvalerate (3HV) units in the molecular chain of PHB was introduced to regulate the physical properties of PHB, especially the excess crystallinity and T_m .¹⁷ Unfortunately, the desired effect of 3HV incorporation was surprisingly limited due to the crystalline isodimorphism of 3HB and 3HV units.¹⁸

Recently, the Procter and Gamble Co. (Cincinnati, OH) has introduced a new kind of PHA copolymer with a small amount of medium length side groups, which has been commercialized under the trade name Nodax.¹⁹ This class of copolymers demonstrate some attractive properties, for example, anaerobic and aerobic degradability, alkaline digestability, hydrolytic stability, good odor and oxygen barrier, ideal surface properties for printability, and so on. It further shows substantially

[†] Department of Chemistry, Kwansai-Gakuin University.

[‡] Department of Physics, Kwansai-Gakuin University.

[§] Chulalongkorn University.

[⊥] The Procter and Gamble Company.

* To whom correspondence should be addressed: FAX +81-79-565-9077, e-mail ozaki@ksc.kwansai.ac.jp.

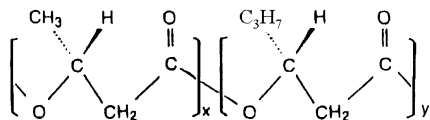


Figure 1. Molecular structure of poly(3-hydroxybutyrate-*co*-3-hydroxyhexanoate), P(HB-*co*-HHx) (HHx = 12 mol %).

reduced crystallinity and increased flexibility compared to the PHB homopolymer. Furthermore, Nodax has excellent compatibility with other biodegradable polymers and synthetic polymers.¹⁹ Nodax may be used in a variety of polymer applications because they can control their mechanical properties by changing the comonomer composition and can be processed into fibers and films as well as molded plastic products. These new products are expected to be used not only for biodegradable polymers but also for medical materials in terms of their biocompatibility.

One of the representative members of the Nodax copolymer family is the poly(3-hydroxybutyrate-*co*-3-hydroxyhexanoate) or P(HB-*co*-HHx), which is a random copolymer of [*R*]-3-hydroxybutyrate and [*R*]-3-hydroxyhexanoate units. Figure 1 shows a molecular structure of P(HB-*co*-HHx) (HHx = 12 mol %). The biodegradation mechanism, chemical synthesis, and mechanical properties of P(HB-*co*-HHx) were reported by several research groups.^{20–22} The thermal behavior of P(HB-*co*-HHx) was also investigated by differential scanning calorimetry (DSC).^{20,22} However, so far there is no literature describing X-ray diffraction studies and infrared (IR) studies of the thermal behavior of P(HB-*co*-HHx). The WAXD measurements of PHA polymers were carried out only at room temperature to characterize their crystallinity and crystal structure.²³

Investigations of temperature-dependent variations in the X-ray diffraction pattern and IR spectrum are very important to explore the crystal-to-amorphous transition and variations in the inter- and intramolecular interactions. The unit cell dimensions change with temperature as a result of thermal expansion, and the thermal expansion of the polymer is often highly anisotropic. We have investigated the thermal properties of one of the new types of bacterial copolyesters, P(HB-*co*-HHx) (HHx = 12 mol %), by using wide-angle X-ray diffraction (WAXD), DSC, and IR spectroscopy. The present study reveals unique constraint factors of the atoms and molecules observed in the crystal structure of P(HB-*co*-HHx). The IR study will be reported separately.²⁴

Experimental Section

Samples. Bacterially synthesized P(HB-*co*-HHx) and PHB were obtained from the Procter and Gamble Co. The P(HB-*co*-HHx) sample was dissolved in hot chloroform, reprecipitated in methanol as fine powder, and vacuum-dried at 60 °C. The purified P(HB-*co*-HHx) and PHB samples thus obtained were used for all the experiments. Some of the purified powder sample was redissolved in chloroform and then cast as a film by evaporating the solvent.

Wide-Angle X-ray Diffraction (WAXD). A WAXD pattern and an X-ray diffraction trace of the precipitated powder of P(HB-*co*-HHx) were measured at room temperature in the scattering angle range of $2\theta = 5–35^\circ$ by using a Rigaku R-Axis IV imaging plate diffractometer. Cu K α radiation (wavelength 1.5418 Å) from a Rigaku Ultra-X18 rotating anode X-ray generator was used as an incident X-ray source (40 kV, 100 mA) (Figure 2a,b). The temperature-dependent WAXD data were measured for the precipitated powder samples of P(HB-

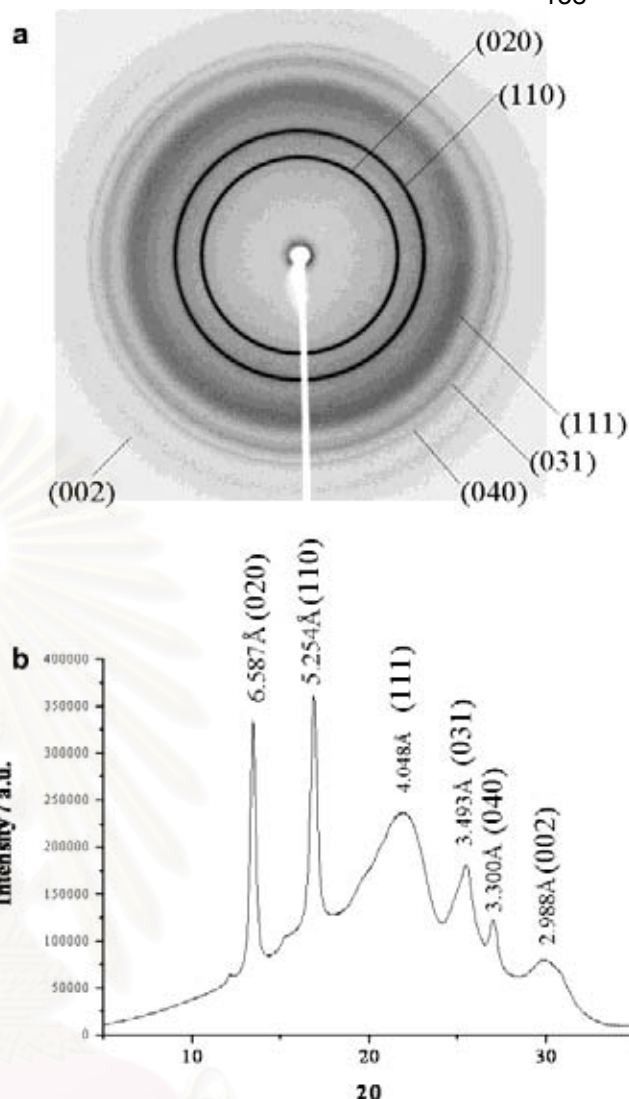


Figure 2. (a) An X-ray diffraction pattern of P(HB-*co*-HHx) (HHx = 12 mol %) powder sample at room temperature crystallized in the $P2_12_12_1$ orthorhombic system with the lattice parameters of $a = 5.76$ Å, $b = 13.20$ Å, $c = 5.96$ Å (fiber axis). (b) An X-ray diffraction trace of P(HB-*co*-HHx) (HHx = 12 mol %) powder sample at room temperature obtained by a radial microdensitometer scan of the powder diagram shown in (a).

co-HHx) over a temperature range from 25.0 to 110.0 °C in the scattering angle range of $2\theta = 5–13^\circ$ by using a two-circle Rigaku X-ray diffractometer equipped with a scintillation detector (RINT2000/PC). For comparison, the corresponding WAXD data were collected for the precipitated powder sample of PHB over a temperature range from 28.3 to 174.3 °C in the scattering angle range of $2\theta = 2–13^\circ$ by using the two-circle Rigaku X-ray diffractometer. Mo K α radiation (wavelength 0.710 69 Å) was used as an incident X-ray source (40 kV, 240 mA). The X-ray diffraction patterns of chloroform solution cast P(HB-*co*-HHx) were obtained with the two-circle Rigaku X-ray diffractometer and an imaging plate over a temperature range of 30.1–105.8 °C in the range of $2\theta = 2–30^\circ$. The silicone powder put in the samples was used for the calibration of the angle.

The observed X-ray diffraction intensity $I(2\theta)$ was assumed to consist of $I_{\text{peak}}(2\theta)$ and $I_{\text{BG}}(2\theta)$

$$I(2\theta) = I_{\text{peak}}(2\theta) + I_{\text{BG}}(2\theta) \quad (1)$$

where $I_{\text{peak}}(2\theta)$ and $I_{\text{BG}}(2\theta)$ are the diffraction peak intensities due to the crystalline and amorphous parts of the sample, respectively. The contributions from the crystalline ($I_{\text{peak}}(2\theta)$)

and amorphous ($I_{\text{BG}}(2\theta)$) parts to the X-ray scattering were estimated by computer fitting using a Gaussian function shown in eq 2 and a quadratic function shown in eq 3, respectively:

$$I_{\text{peak}}(2\theta) = \frac{A}{\sigma\sqrt{\pi/2}} \exp\left[-2\left(\frac{2\theta - 2\theta_0}{\sigma}\right)^2\right] \quad (2)$$

where A , σ , and $2\theta_0$ are a peak area, a full-width at half-maximum of the reflection peak, and a center point of the peak, respectively. The background peak $I_{\text{BG}}(2\theta)$ is calculated by the following equation:

$$I_{\text{BG}}(2\theta) = a(T)(2\theta)^2 + b(T)(2\theta) + c(T) \quad (3)$$

where $a(T)$, $b(T)$, and $c(T)$ are scaling and correction factors for the baseline. The values A , σ , $2\theta_0$, $a(T)$, $b(T)$, and $c(T)$ were determined together by a nonlinear least-squares fit to eq 1.

Differential Scanning Calorimetry (DSC). Differential scanning calorimetry (DSC) measurements of P(HB-co-HHx) copolymer were performed with a Seiko EXDSTAR6000 apparatus with a DSC6200 module over a temperature range from -50 to 140 °C at heating and cooling rates of 10 and 20 °C min^{-1} , respectively. The samples used for the DSC measurements were the same as those for the WAXD analysis.

Results and Discussion

WAXD. Parts a and b of Figure 2 show respectively a WAXD pattern and an X-ray diffraction trace of P(HB-co-HHx) powder sample at room temperature. P(HB-co-HHx) powder sample shows a high level of crystallinity.^{20,22} It was reported that the unit cells of PHB and poly(hydroxyvalerate) (PHV) belong to the orthorhombic system, $P2_12_12_1(D_2^4)$ ($\alpha = \beta = \gamma = 90^\circ$), with $a = 5.76$ Å, $b = 13.20$ Å, $c = 5.96$ Å (fiber repeat) and $a = 9.52$ Å, $b = 10.08$ Å, $c = 5.56$ Å (fiber repeat).^{14,15,25} The P(HB-co-HHx) (HHx = 12 mol %) also shows an orthorhombic system ($\alpha = \beta = \gamma = 90^\circ$) with $a = 5.76$ Å, $b = 13.20$ Å, $c = 5.96$ Å (fiber repeat), which is the same as the PHB crystal system.²⁰ The P(HB-co-HV) copolymers with the HV composition from 0 to 37 mol % crystallize in the PHB lattice, while those with the HV composition from 53 to 95 mol % crystallize in the PHV lattice.²³ The (110) d spacing of P(HB-co-HV) copolymer apparently increases as the HV content increases to 37 mol %, while the (020) and (002) d spacings remain unchanged, indicating that only the parameters of the unit cell change.^{18,23} As described above, P(HB-co-HHx) (HHx = 12 mol %) also shows only one crystalline form with the PHB lattice. It is reasonable to expect this result because the HHx content is 12 mol %. One may expect that the propyl side chains of HHx units expand the (110) d spacing of the PHB lattice in P(HB-co-HHx) even more so than that in P(HB-co-HV) due to the steric effects of the propyl side chains. However, as a matter of fact, the (110) d spacing of P(HB-co-HHx) is smaller than that of P(HB-co-HV).²³ It can be assumed that the propyl side chain of HHx has stronger inter- and intramolecular interactions than the ethyl side chain of HV, since the propyl side chain is located closer to the C=O group in the lattice constant a axis than the ethyl side chain. Another possibility is that the propyl side chains of HHx are protruded in the crystal structure, while the ethyl side chain of HV can be fixed in the crystal with PHB. Therefore, the (110) d spacing of P(HB-co-HHx) may show the proximity value with that of PHB.

Figure 3a shows a helical structure model of P(HB-co-HHx) copolymer proposed on the basis of the results

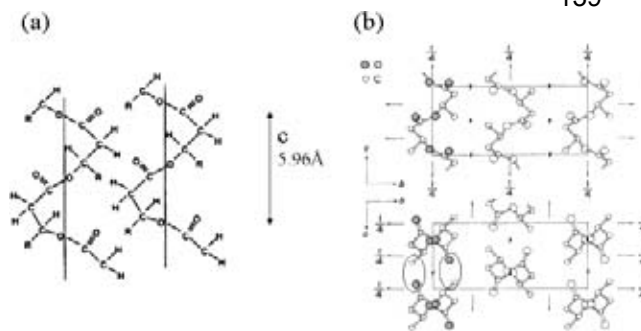


Figure 3. (a) Proposed helical structure model of P(HB-co-HHx) copolymer. (Reproduced from ref 27 with permission. Copyright 2001 John Wiley & Sons, Inc.) (b) Reported crystalline structure of PHB. The $P2_12_12_1$ orthorhombic system with the lattice parameters of $a = 5.76$ Å, $b = 13.20$ Å, $c = 5.96$ Å (fiber axis). (Reproduced from ref 14 with permission. Copyright 1973 Elsevier Science.)

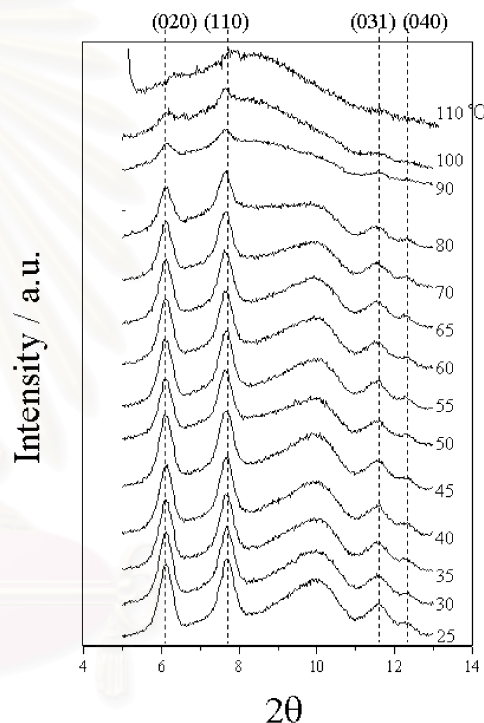


Figure 4. Temperature dependence of the X-ray diffraction of P(HB-co-HHx) powder sample measured over a temperature range from 25 to 110 °C.

of X-ray diffraction.^{14,15,26,27} The WAXD pattern shows that the crystalline structure of P(HB-co-HHx) is orthorhombic, $P2_12_12_1(D_2^4)$, with $a = 5.76$ Å, $b = 13.20$ Å, $c = 5.96$ Å (fiber repeat).²⁰ Figure 3b shows a structure of PHB studied by Yokouchi et al.¹⁴ Of note in Figure 3b is that the CH_3 group of PHB is close to the C=O group on the a axis.

Temperature-Dependent Variations in the WAXD of the Precipitated Sample. Figure 4 shows the temperature dependence of the WAXD pattern of the precipitated P(HB-co-HHx) sample. The WAXD patterns were measured over a temperature range from 25 to 110 °C in the scattering angle range of $2\theta = 5$ – 13° . It can be seen from Figure 4 that the (110) d spacing of P(HB-co-HHx) lattice expands as temperature increases. However, the (020), (040), and (031) d spacings of the sample do not change with temperature. The WAXD patterns in Figure 4 show that the peak due to the lattice constant a shifts to large value as temperature

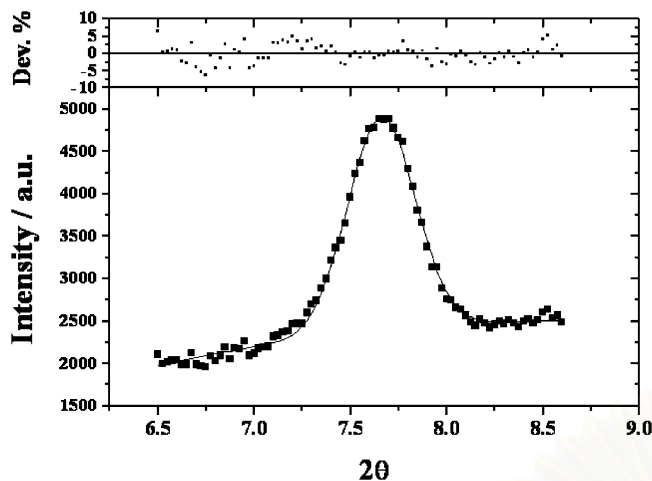


Figure 5. A representative (110) reflection of WAXD of P(HB-co-HHx) powder sample. The solid curve represents the one fitted by eq 1 with $A = 1102 \pm 22$, $\sigma = 0.350 \pm 0.005$, $2\theta_0 = 7.661 \pm 0.002$, $a(T) = -116.7 \pm 34.6$, $b(T) = 2013 \pm 524$, and $c(T) = -6178 \pm 1968$. Top panel: the relative errors of the fit.

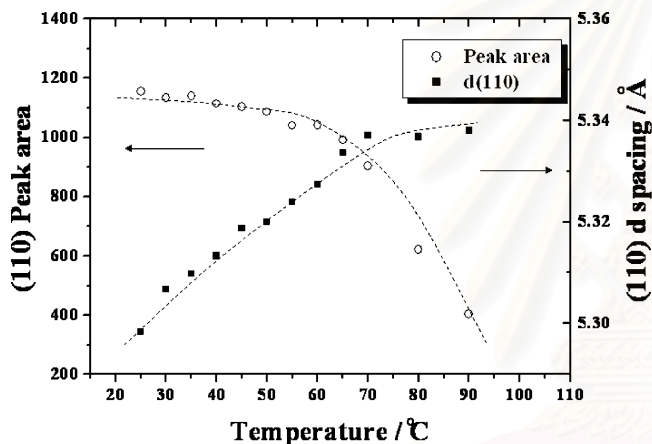


Figure 6. Temperature dependences of the peak area and d spacing of the (110) reflection of the P(HB-co-HHx) powder sample.

increases. In other words, only the lattice constant a of the unit cell changes with temperature in the P(HB-co-HHx) crystal. Referring to the crystalline structure of PHB (Figure 3),^{14,15} one can assume that there are intermolecular and intramolecular interactions between the C=O group and the CH₃ group also in the P(HB-co-HHx) copolymer.

Figure 5 shows a representative (110) reflection peak and the result of its nonlinear least-squares fitting (see Experimental Section) of the P(HB-co-HHx) powder sample. The solid curve represents the one fitted by eq 1 with $A = 1102 \pm 22$, $\sigma = 0.350 \pm 0.005$, $2\theta_0 = 7.661 \pm 0.002$, $a(T) = -116.7 \pm 34.6$, $b(T) = 2013 \pm 524$, and $c(T) = -6178 \pm 1968$. The fitting is quite satisfactory as shown in the deviations in Figure 5.

Figure 6 shows variations in the (110) peak area and the (110) d spacing vs temperature for the precipitated sample. The peak area and peak maximum position respectively indicate the crystallinity and the thermal expansion of the sample. It is noted that the (110) d spacing expands gradually with temperature, while the peak area changes little until around 50 °C and shows a gradual decrease above about 50 °C.

Figure 7 shows the temperature dependences of the (020) peak area and the (020) d spacing for the precipitated sample. Note that the thermal behavior of the

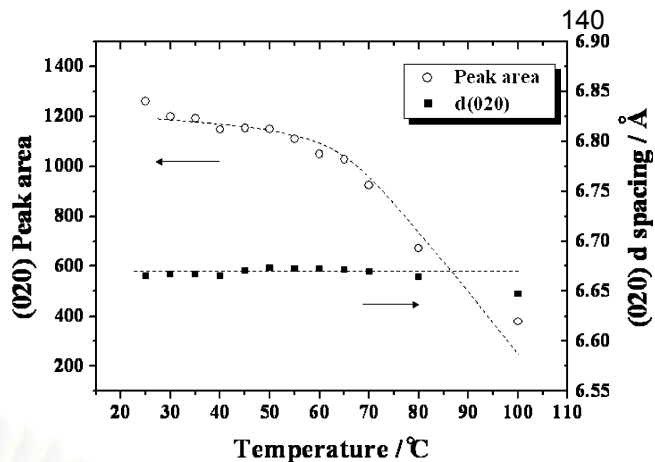


Figure 7. Temperature dependences of the peak area and spacing of the (020) reflection of the P(HB-co-HHx) powder sample.

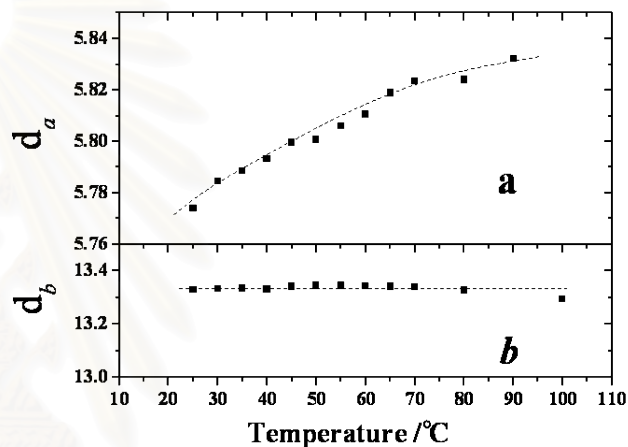


Figure 8. Changes in the lattice parameters, a and b , of the precipitated P(HB-co-HHx) sample vs temperature.

(020) peak area is similar to that of the (110) peak area. However, the (020) d spacing shows little thermal expansion compared to the (110) d spacing.

Figure 8 shows temperature-dependent variations in the lattice parameters, a and b , of the precipitated sample. It is clear from Figure 8 that the a lattice parameter increases gradually with the temperature increase while the b lattice parameter changes little. It is very likely that the increase in the a lattice parameter results from the decrease in the inter- and intramolecular interactions between the C=O group and the CH₃ group along the a axis of crystalline P(HB-co-HHx). The interaction is mainly concerned with the weak hydrogen bond between the C=O group and the CH₃ group, but there is the possibility that some C=O groups interact with the propyl group.

Temperature-Dependent Variations in WAXD of the Chloroform Solution Cast Film Sample. Figure 9 presents the temperature dependence of the (110) d spacing of the WAXD pattern of a P(HB-co-HHx) film cast from chloroform solution. Of note in Figure 9 is the thermal expansion of the (110) d spacing of P(HB-co-HHx). Variations in the (110) peak area and (110) d spacing vs temperature are shown in Figure 10 for the solution cast film sample. The temperature-dependent changes in the (110) peak area are quite different between the precipitated and solution cast samples (Figures 6 and 10). The peak area represents the crystallinity of the sample. The crystallinity of the

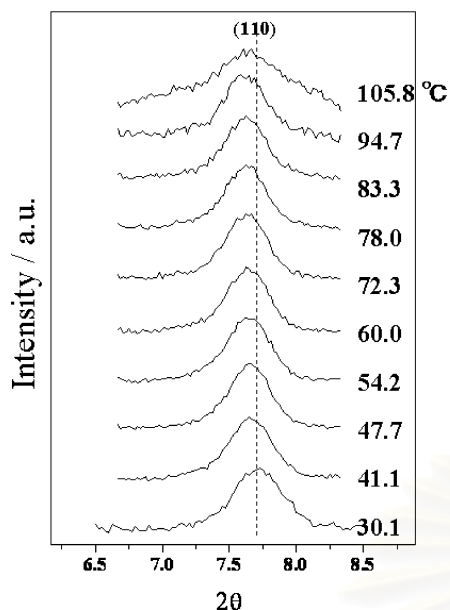


Figure 9. Temperature dependence of the X-ray diffraction of the P(HB-co-HHx) chloroform solution cast film sample over a temperature range from 30.1 to 105.8 °C.

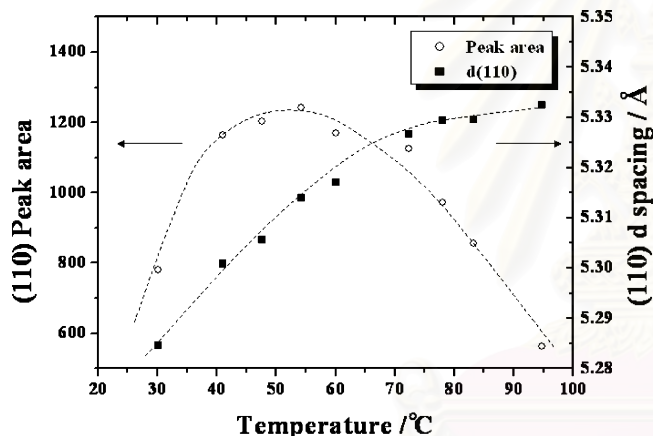


Figure 10. Temperature dependence of the peak area and d spacing of (110) reflection of P(HB-co-HHx) cast film sample from a chloroform solution.

precipitated sample changes little until about 50 °C while that of the solution cast sample increases until around 54 °C. Therefore, the maximum of the peak area around 54 °C suggests that a recrystallization of the chloroform solution cast P(HB-co-HHx) copolymer takes place around 54 °C.

Figure 11 shows effects of temperature on the lattice parameter a of the solution cast film sample. Changes in the lattice parameters of polymers can be observed under a variety of conditions.²⁸ Information about the changes in the lattice parameters provides insight into the forces that bind atoms and molecules in the crystal structure and the factors that determine the crystal structure. There is a slight difference in the shift of the lattice parameter a between the precipitated and solution cast samples (Figures 8 and 11). The change in the lattice parameter a of the chloroform solution cast sample is slightly larger than that of the precipitated sample. The slight difference in lattice parameter a comes from the difference in the crystallite size. The gradual peak shift of the WAXD pattern with temperature shows a thermal expansion of the crystalline structure of the sample. Therefore, it seems that the

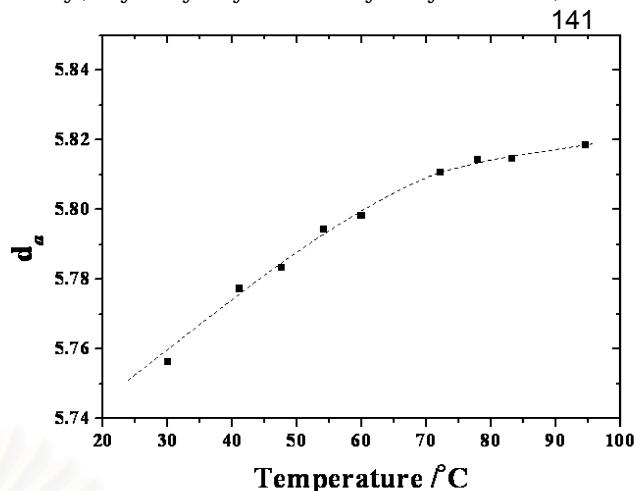


Figure 11. Temperature-dependent changes in the lattice parameter a of a chloroform solution cast film of P(HB-co-HHx).

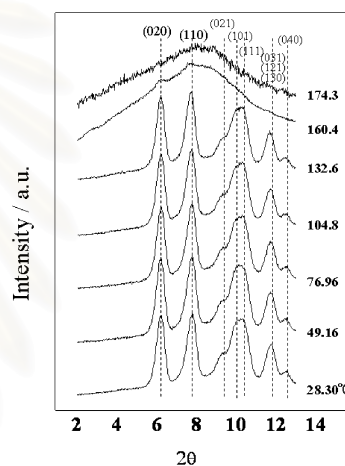


Figure 12. Temperature dependences of the X-ray diffraction of PHB homopolymer measured over a temperature range of 28.3–174.3 °C.

solution cast sample shows recrystallization process because the solution cast sample cannot assume the high-crystallinity structure and shows its own low crystallization rate.

Temperature-Dependent Variations in WAXD of PHB. Figure 12 presents a temperature dependence of the X-ray diffraction of PHB homopolymer. It shows clearly the (020), (110), (021), (101), (111), and (040) d spacings. Comparison of the result in Figure 12 with that in Figure 4 reveals that the crystallinity of PHB is higher than that of P(HB-co-HHx) precipitated sample.

Parts a and b of Figure 13 show respectively the temperature dependences of the (110) peak area and (110) d spacing and those of the (020) peak area and (020) d spacing of PHB. The melting temperature T_m of PHB was reported to be 178 °C.²² There is a drastic drop of the (110) and (020) peak areas around 160 °C. The (110) d spacing of PHB shows a gradual change with temperature as in the case of the P(HB-co-HHx) sample, while the (020) d spacing shows only a small shift different from that of the P(HB-co-HHx) sample. The (110) peak area of P(HB-co-HHx) decreases from around 50 °C while that of PHB changes little at least until 140 °C, indicating that the crystallinity of PHB remains nearly unchanged until 140 °C but that of P(HB-co-HHx) decreases gradually from fairly low temperature (~50 °C). The copolymerization of HHx units

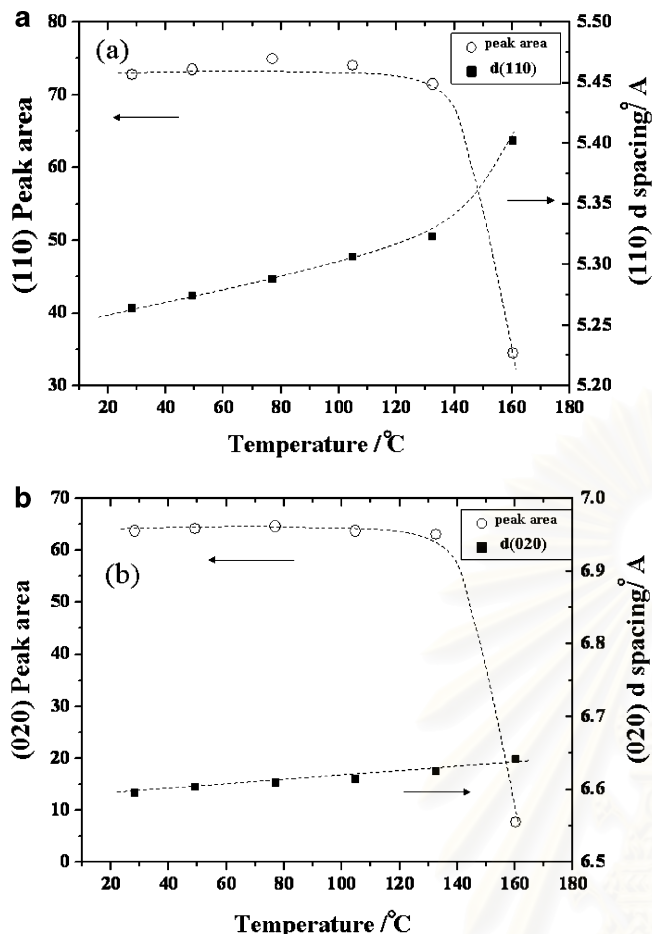


Figure 13. Temperature dependences of the peak area and d spacing of (a) (110) reflection and (b) (020) reflection of PHB homopolymer.

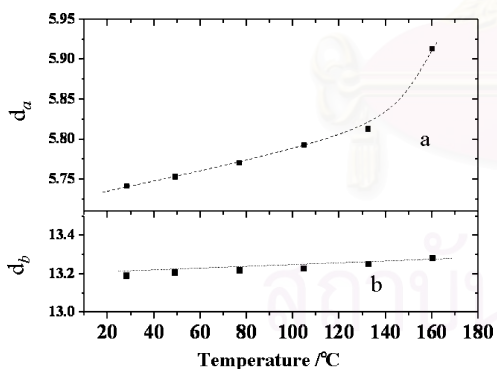


Figure 14. Changes in the lattice parameters, a and b , of the PHB homopolymer vs temperature.

in the molecular chain of PHB produces significant amounts of amorphous parts in P(HB-*co*-HHx), which change largely its thermal behavior from that of PHB.

Figure 14 shows effects of temperature on the lattice parameters of PHB. Both lattice parameters, a and b , show thermal expansion in the PHB sample. However, the thermal effects on the lattice parameters are significantly different between the lattice parameters, a and b , even in the PHB crystalline structure. P(HB-*co*-HHx) copolymer shows little expansion of the b axial length (Figure 8). However, PHB homopolymer shows a significant expansion of the b axial length, even though it is smaller than that of the a axial length (Figure 14), probably because the crystallinity of PHB is higher than that of P(HB-*co*-HHx) copolymer. Al-

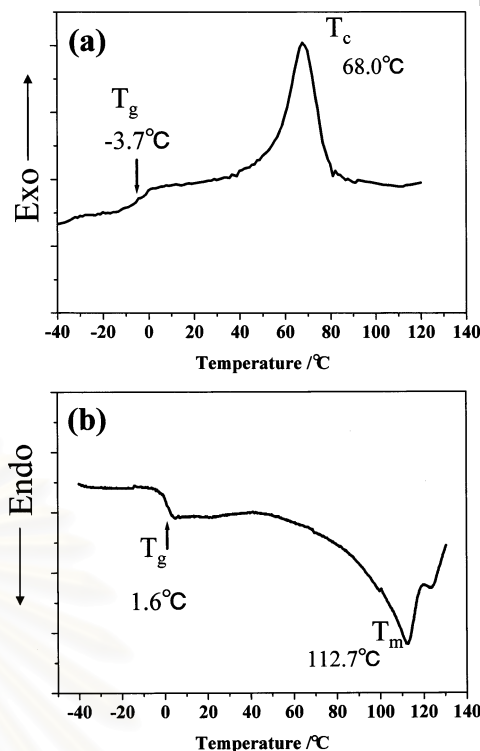


Figure 15. DSC curves of the (a) first cooling run and (b) second heating run of the precipitated P(HB-*co*-HHx) from -40 to 120 °C. Heating and cooling rates of the DSC measurements were 10 °C min^{-1} .

though our measurements were not made with high resolution, the results clearly point out the trend that the a axial length shows a much larger change than the b axial length in both P(HB-*co*-HHx) and PHB.

For both P(HB-*co*-HHx) and PHB, the lattice parameter a shows a significant variation by the temperature increase. This is an evidence showing that the inter- and intramolecular interactions are not so strong along the a axis in P(HB-*co*-HHx) and PHB crystallites. The variation of the lattice parameter a suggests that these interactions are those due to the C=O group and the CH₃ group, which are, in general, weak. The high crystallinity of P(HB-*co*-HHx) and PHB may be concerned with these interactions.

Thermal Analysis. Figure 15 shows the DSC curves of the (a) first cooling and (b) second heating of bulk sample of P(HB-*co*-HHx). The T_m and the glass transition temperature T_g respectively were determined from the DSC curves to be 112.7 and 1.6 °C. The appearance of intermediate states of P(HB-*co*-HV) (20.4% HV) and P(HB-*co*-HHx) (HHx = 10%) has been suggested from a small and wide endothermic premelting peak around 60 °C in the DSC measurement.^{26,27} Our result of the DSC measurement of P(HB-*co*-HHx) (HHx = 12 mol %) does not show any peak around 60 °C for the bulk sample. However, variations in FT-IR spectra of a cast film of P(HB-*co*-HHx) were observed around 60 °C. To check the possible development of a peak around 60 °C in the DSC measurement, we measured DSC curves of the chloroform cast sample. The cast sample was put in a small cup for the DSC measurement. Heating and cooling rates were 20 °C min^{-1} . Figure 16 shows the DSC curves of the (a) first cooling and (b) second heating for the cast sample of P(HB-*co*-HHx). The recrystallization temperature was determined to be 51.0 °C for the cast sample in the heating process. The result of

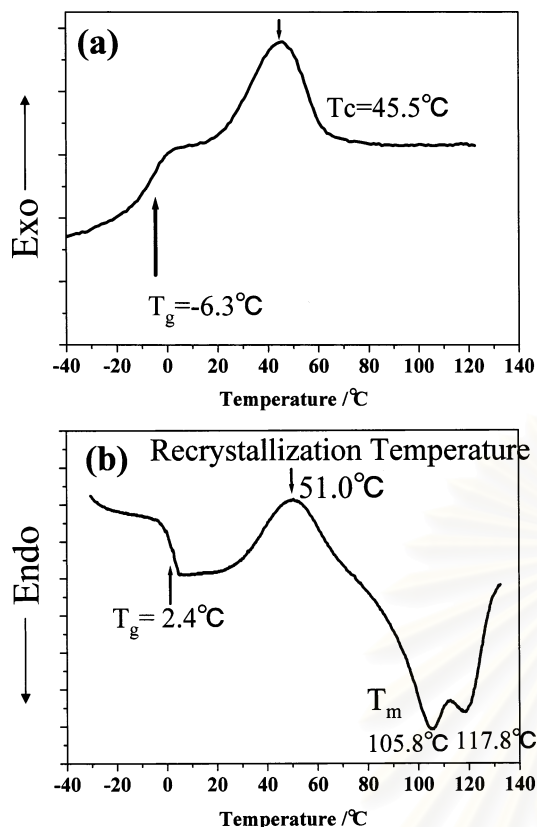


Figure 16. DSC curves of the (a) first cooling and (b) second heating run of the chloroform solution cast film sample of P(HB-co-HHx) from -40 to 120°C . Heating and cooling rates were $20^\circ\text{C min}^{-1}$.

the WAXD of the chloroform cast sample of P(HB-co-HHx) shows that the (110) peak area has a maximum value around 54°C . The maximum of the (110) peak area may be ascribed to the recrystallization process of the chloroform cast sample of P(HB-co-HHx) (Figure 10). It is in good agreement with the DSC results of the chloroform cast sample of P(HB-co-HHx). Furthermore, it is noted that two peaks of T_m appear in the DSC curve of the cast sample of P(HB-co-HHx) (105.8 and 117.8°C). There are two possibilities for the origin of the two peaks in the second heating cycle of DSC. One is melt and recrystallization of the sample. The other possibility is that there are two types of lamellae in the crystal.

Conclusion

The WAXD pattern of the P(HB-co-HHx) copolymer at room temperature shows that it has an orthorhombic system ($\alpha = \beta = \gamma = 90^\circ$) with $a = 5.76 \text{ \AA}$, $b = 13.20 \text{ \AA}$, $c = 5.96 \text{ \AA}$ (fiber repeat), which is identical to that of the PHB crystal system. The crystal structure and the thermal properties of precipitated and chloroform solution cast film samples of P(HB-co-HHx) copolymer have been investigated over the temperature range from 25 to 110°C in the scattering angle range of $2\theta = 5\text{--}13^\circ$. Measurements of the d spacing from WAXD have indicated an expansion of the (110) d spacing of P(HB-co-HHx) lattice as temperature increases. Only the a lattice parameter shows the thermal expansion, while the b lattice parameter shows very little in the P(HB-co-HHx) crystallites. This suggests that there are inter- and intramolecular interactions between the C=O group

and the CH_3 group because they are very closely located to each other along the a axis of P(HB-co-HHx) crystallites. The temperature-dependent variations in the (110) peak area for P(HB-co-HHx) and PHB have revealed that PHB keeps its high crystallinity at least until 140°C while that of P(HB-co-HHx) starts decreasing from 50°C . The copolymerization of HHx units in the molecular chain of PHB largely modifies the thermal behavior of PHB. The DSC measurements of the P(HB-co-HHx) between -40 and 120°C show a recrystallization peak around 51°C . This result is in a good agreement with the result of the WAXD of the chloroform cast sample of P(HB-co-HHx) that shows the maximum of the (110) peak area around 54°C .

Acknowledgment. We thank Dr. Mike Satkowski (The Procter and Gamble Co., Cincinnati, OH) for valuable discussions. A.P. thanks the Thailand Research Fund (TRF) for financial support (Grant contact number: PHD0066/2544).

References and Notes

- (1) Doi, Y. *Microbial Polyesters*; VCH Publishers: New York, 1990.
- (2) Anderson, A. J.; Dawes, E. A. *Microbiol. Rev.* **1990**, *54*, 450.
- (3) Lundgren, D. G.; Alper, R.; Schnaitman, C.; Marchessault, R. H. *J. Bacteriol.* **1965**, *89*, 245.
- (4) Dawes, E. A. *Novel Biodegradable Microbial Polymers*; Kluwer Academic: Dordrecht, 1990.
- (5) Lara, L. M.; Gjalt, W. H. *Microbiol. Mol. Biol. Rev.* **1991**, *63*, 21.
- (6) Iwata, T.; Doi, Y. *Macromol. Chem. Phys.* **1999**, *200*, 2429.
- (7) Barham, P. J.; Barker, P.; Organ, S. *FEMS Microbiol. Rev.* **1992**, *103*, 289.
- (8) Holmes, P. A. In *Developments in Crystalline Polymers*; Bassett, D. C., Ed.; Elsevier: London, 1987; Vol. 2, p 1.
- (9) Williams, S. F.; Martin, D. P. In *Biopolymers*; Doi, Y., Steinbüchel, A., Eds.; Wiley-VCH: Weinheim, 2001; Vol. 4, p 91.
- (10) Marchessault, R. H.; Coulombe, S.; Morikawa, H.; Okamura, K.; Revol, J. F. *Can. J. Chem.* **1981**, *59*, 38.
- (11) Barham, P. J.; Keller, A.; Otum, E. L.; Holmes, P. A. *J. Mater. Sci.* **1984**, *19*, 2781.
- (12) Barham, P. J. *J. Mater. Sci.* **1984**, *19*, 3826.
- (13) Satkowski, M. M.; Melik, D. H.; Autran, J.-P.; Green, P. R.; Noda, I.; Schechtman, L. A. In *Biopolymers*; Steinbüchel, A., Doi, Y., Eds.; Wiley-VCH: Weinheim, 2001; p 231.
- (14) Yokouchi, M.; Chatani, Y.; Tadokoro, H.; Teranishi, K.; Tani, H. *Polymer* **1973**, *14*, 267.
- (15) Cornibert, J.; Marchessault, R. H. *J. Mol. Biol.* **1972**, *71*, 735.
- (16) Yoshie, N.; Menju, H.; Sato, H.; Inoue, Y. *Macromolecules* **1995**, *28*, 6516.
- (17) Holmes, P. A. *Phys. Technol.* **1985**, *16*, 32.
- (18) Bluhm, T. L.; Hamer, G. K.; Marchessault, R. H.; Fyfe, C. A.; Veregin, R. P. *Macromolecules* **1986**, *19*, 2871.
- (19) Web site: www.nodax.com.
- (20) Doi, Y.; Kitamura, S.; Abe, H. *Macromolecules* **1995**, *28*, 4822.
- (21) Kobayashi, G.; Shiotani, T.; Shima, Y.; Doi, Y. In *Biodegradable Plastics and Polymers*; Doi, Y., Fukuda, K., Eds.; Elsevier: Amsterdam, 1994; p 410.
- (22) Abe, H.; Doi, Y.; Aoki, H.; Akehata, T. *Macromolecules* **1998**, *31*, 1791.
- (23) Kunioka, M.; Tamaki, A.; Doi, Y. *Macromolecules* **1989**, *22*, 694.
- (24) Sato, H.; Murakami, R.; Padermshoke, A.; Hirose, F.; Senda, K.; Noda, I.; Ozaki, Y., to be published.
- (25) Marchessault, R. H.; Morikawa, H.; Revol, F. J.; Bluhm, T. L. *Macromolecules* **1984**, *17*, 1882.
- (26) Wu, Q.; Tain, G.; Sun, S.; Noda, I.; Chen, G.-Q. *J. Appl. Polym. Sci.* **2001**, *82*, 934.
- (27) Tain, G.; Wu, Q.; Sun, S.; Noda, I.; Chen, G.-Q. *Appl. Spectrosc.* **2001**, *55*, 888.
- (28) Davis, G. T.; Eby, R. K.; Colson, J. P. *J. Appl. Phys.* **1970**, *41*, 4316.

CURRICULUM VITAE

Date of Birth: December 17, 1976 **Birth Place:** Bangkok, Thailand
Address: 23, Soi Shotiwat 18, Prachachuen Road, Bangsue, Bangkok 10800, Thailand

Educations:

Ph.D. /Petrochemistry	2004	Chulalongkorn University/Thailand
M.Sc./Petrochemistry and Polymer Science	1999	Chulalongkorn University/Thailand
B.Sc. /Chemistry	1997	Chulalongkorn University/Thailand

Research Publications:

1. S. Ekgasit and A. Padermshoke, Applied Spectroscopy, 55 (10), 1352-1359 (2001).
2. A. Padermshoke, H. Sato, Y. Katsumoto, S. Ekgasit, I. Noda, and Y. Ozaki, Vibrational Spectroscopy, 2004, in press.
3. A. Padermshoke, Y. Katsumoto, H. Sato, S. Ekgasit, I. Noda, and Y. Ozaki, Spectrochimica Acta Part A, 61, 541-550 (2005).
4. A. Padermshoke, Y. Katsumoto, H. Sato, S. Ekgasit, I. Noda, and Y. Ozaki, Polymer, 45 (19), 6547-6554.
5. A. Padermshoke, H. Sato, Y. Katsumoto, S. Ekgasit, I. Noda, and Y. Ozaki, Polymer, 45 (21), 7159-7165.
6. H. Sato, M. Nakamura, A. Padermshoke, H. Yamaguchi, H. Terauchi, S. Ekgasit, I. Noda, and Y. Ozaki, Macromolecules, 37, 3763-3769 (2004).
7. H. Sato, R. Murakami, A. Padermshoke, F. Hirose, K. Senda, I. Noda, and Y. Ozaki, Macromolecules, 37, 7203-7213 (2004).

International Conferences:

1. 2003/6 : 15th European Symposium on Polymer Spectroscopy, Crete, Greece.
2. 2002/12 : IUPAC Polymer Conference, Kyoto, Japan.
3. 2002/10 : Federation of Analytical and Chemical Societies of Spectroscopy, Rhode Island, USA.
4. 2000/3 : Post Eurasia Symposium, Bangkok, Thailand.

Scholarships and Awards:

2001-2004 : The Royal Golden Jubilee (RGJ) Ph.D. Scholarship/ The Thailand Research Fund.
 2002 : Award for the Outstanding Scientific Research on the P&G Biopolymers/ The Procter and Gamble Company, USA.

Current Professional:

From October, 2004: Postdoctoral research fellow at the Center for Quantum Life Sciences, Hiroshima University, Hiroshima, Japan.